University of Genoa
Doctoral school of Chemical and Materials Sciences and Technologies

Ph.D. degree in Chemical Sciences and Technologies

Ghent University
Doctoral school of Natural Sciences

Doctorate and doctoral training programme of Science: Chemistry

# Isotopic analysis of environmental samples using inductively coupled plasma mass spectrometry

Candidate:
Andrea Bazzano

Supervisors:
prof. dr. Marco Grotti
prof. dr. Frank Vanhaecke

Thesis submitted in March 2016

Typeset with LaTeX, using the suftesi class by Ivan Valbusa.

I travel not to go anywhere, but to go. I travel for travel's sake.
The great affair is to move.

*Robert Louis Stevenson*

Dedicato alla Nonna
(che non sapeva l'inglese).

# Acknowledgements

Science is collaborative for its own nature and during these three years many people contributed to this dissertation with their work and knowledge. Among them I want to thank Fiorenza and Nicole that helped with some of the sample preparation and measurements of Pb isotope ratios performed at the University of Genoa. A special thank is for Kris and Asha for their help with MC-ICP-MS measurements and the clean-lab facility at Ghent University.
My gratitude is also for my supervisors prof. Grotti and prof. Vanhaecke because of their guidance and the opportunity that they gave me to carry out this joint Ph.D.
This dissertation would not have been possible without the founding of the Italian Ministero dell'Istruzione, dell'Università e della Ricerca (MIUR).
Finally, above all I want to thank Alessandra and Buddy to look after my mental health.

# Preface

The work presented was conducted in the laboratory of analytical chemistry at the University of Genoa (IT) and in the laboratory of the A&MS group at Ghent University (BE). Experimental data were obtained and discussed by myself except when explicitly stated. The main text of the dissertation was written by me and edited by the supervisors prof. Grotti and prof. Vanhaecke.

A version of chapter 3 has been published in Journal of Analytical Atomic Spectrometry: Bazzano, A., and Grotti M., 2014. Determination of lead isotope ratios in environmental matrices by quadrupole ICP-MS working at low sample consumption rates. J. Anal. At. Spectrom. **29**, 926–933. doi: 10.1039/c3ja50388g.

A version of chapter 4 has been submitted to Atmospheric Environment: Bazzano, A., Cappelletti, D., Udisti R., and Grotti M. Long-range transport of atmospheric lead reaching Ny-Ålesund: inter-annual and seasonal variations of potential source areas. Atmos. Environ. *submitted* in December 2015. A part of the data reported in the chapter were previously published in Atmospheric Environment: Bazzano, A., Ardini, F., Becagli, S., Traversi, R., Udisti, R., Cappelletti, D., and Grotti M. 2015. Source assessment of atmospheric lead measured at Ny-Ålesund, Svalbard. Atmos. Environ. **113**, 20–26. doi: 10.1016/j.atmosenv.2015.04.053. Prof. Cappelletti provided and discussed most of the back-trajectory data reported in section 4.3.5 and, along with prof. Udisti, helped with the editing of the chapter.

A version of chapter 5 has been published in Marine Chemistry: Bazzano, A., Rivaro P., Soggia F., Ardini F., and Grotti M., 2014. Anthropogenic and natural sources of particulate trace elements in the coastal marine environment of Kongsfjorden, Svalbard. Mar. Chem. **163**, 28–35. doi: 10.1016/j.marchem.2014.04.001. Dr. Ardini collected the samples, dr. Soggia provided major element concentration data and prof. Rivaro provided and discussed the data about physical and biological characteristics of the water column reported in section 5.3.1 and helped with the editing of the chapter.

A version of chapter 6 has been published in Environmental Chemistry: Bazzano, A., Soggia F., and Grotti M., 2015. Source identification of atmospheric particle-bound metals at Terra Nova Bay, Antarctica. Environ. Chem. **12**, 245–252. doi: 10.1071/EN14185. Dr. Soggia provided major element concentration data.

A version of chapter 7 has been published in Journal of Analytical Atomic Spectrometry: Bazzano, A., Latruwe K., Grotti M., and Vanhaecke F., 2015. Lead isotopic analysis of antarctic snow using multi-collector ICP-mass spectrometry. J. Anal. At. Spectrom. **30**, 1322–1328. doi: 10.1039/C4JA00484A. Dr. Latruwe helped with the MC-ICP-MS measurements and with the editing of the chapter.

*Andrea Bazzano*
08 March 2016

# Abstract

In the context of environmental studies, isotope ratio measurements can help to discriminate between natural and anthropogenic inputs, as well as to identify their source regions and transport pathways. However, environmental samples can be characterised by a low amount of the target elements, thus hindering the measurement of precise and accurate isotope ratios.

During this doctoral study, research activity was carried out taking into account both analytical and environmental aspects related to the determination of isotope ratios in environmental matrices. On the analytical side, much effort was focused on obtaining precise and accurate isotope ratios at low amount of the target element, using single-collector and multi-collector inductively coupled plasma mass spectrometry (ICP-MS).

In particular, performances obtained measuring $^{208}Pb/^{207}Pb$ and $^{206}Pb/^{207}Pb$ ratios by single-collector ICP-MS at low sample consumption rates were investigated evaluating two micro-sample introduction systems: the PFA micro-nebuliser, working at 150 µL/min, and the torch integrated sample introduction system (TISIS), working at 20 µL/min. Under optimal conditions and using ammonia as damping gas, repeatability was $0.12 \pm 0.03$ and $0.17 \pm 0.04$ % RSD at 10 ng/mL of Pb, whereas the sample consumption was $<1.5$ and 0.2 mL. TISIS was also coupled with multi-collector ICP-MS achieving a repeatability of 0.16 ‰ consuming only 0.2 mL of sample solution. The coupling of the instrumental method with a pre-concentration step provided accurate ratios at Pb concentration levels down to 5 pg/g.

Finally, the use of multi-collector ICP-MS with a membrane nebuliser desolvating system was also investigated for the measurement of precise and accurate $^{87}Sr/^{86}Sr$ ratios, obtaining an intermediate precision of 0.19 ‰ at 0.4 ng/mL Sr concentration.

The developed methods were largely applied to various environmental studies in the framework of PNRA (Italian National Program for Antarctic Research) and RIS (Research in Svalbard) projects. Indeed, Pb isotope ratios were precisely and accurately measured in atmospheric particulate, surface snow, marine suspended particulate matter and sediment samples, collected from both the Arctic and Antarctica. Data were discussed in a multidisciplinary context and provided very useful information on sources and transport pathways of trace elements.

In particular, results for atmospheric particulate matter collected at Ny-Ålesund (Svalbard islands), showed a recurring seasonal transition with higher load of atmospheric Pb related to mining activities in Russia during spring, and inputs of anthropogenic Pb coming from eastern North America during summer. Similar measurements were also applied to suspend particulate matter collected from the marine environment of the Kongsfjorden (close to Ny-Ålesund) and distinguished between anthropogenic Pb associated to intruding Atlantic water, and crustal Pb associated to glacial run-off.

In the context of the Antarctic research, the chemical and isotopic characterisation of size-segregated atmospheric particulate collected at Terra Nova Bay (Northern Victoria

Land) revealed that both the crustal and anthropogenic elements were related to the air masses carried by the katabatic wind from the inland, whereas the marine input appeared to be higher in January when the sea-ice extent was reduced. Furthermore, the Pb isotope ratios pointed out that the anthropogenic input was likely related to the polluted aerosols from South America and Australia, representing the predominant fraction (50–70 %) of the Pb measured in the samples.

Finally, the precise measurement of Pb isotope ratios in surface snow from the Antarctic plateau enabled the identification of seasonal and inter-annual variations in the main sources of atmospheric Pb reaching Antarctica.

# Sommario

La misura dei rapporti isotopici può essere utile nel contesto delle scienze ambientali per discriminare tra apporti naturali ed antropogenici e per identificare la loro sorgente geografica ed i loro meccanismi di trasporto. Tuttavia, spesso i campioni ambientali sono caratterizzati da basse quantità degli elementi di interesse, condizione che rende complicata la misura precisa ed accurata dei rapporti isotopici.

La mia attività di ricerca durante il periodo del dottorato ha tenuto conto sia degli aspetti analitici, sia dei risultati ambientali relativi alla determinazione dei rapporti isotopici all'interno di matrici ambientali.

Per quanto riguarda l'aspetto analitico, gran parte del lavoro è stata focalizzata sull'ottenere rapporti isotopici precisi ed accurati analizzando piccole quantità degli elementi di interesse mediante la tecnica della spettrometria di massa con sorgente al plasma accoppiato induttivamente (ICP-MS), sia con rilevatore singolo che multiplo.

Per caratterizzare le prestazioni ottenibili dalla misura dei rapporti $^{208}Pb/^{207}Pb$ e $^{206}Pb/^{207}Pb$ impiegando la tecnica ICP-MS a rilevatore singolo in combinazione con basse portate del flusso di aspirazione del campione, si sono paragonati due sistemi di introduzione del campione: il micro-nebulizzatore PFA, operante a 150 µL/min ed un sistema di introduzione totale del campione denominato TISIS, operante a 20 µL/min. Dopo ottimizzazione del metodo, ed utilizzando ammoniaca per smorzare le fluttuazioni del fascio di ioni estratto dal plasma, la ripetibilità è risultata essere pari a $0.12 \pm 0.03$ e $0.17 \pm 0.04$ % RSD utilizzando $<1.5$ e 0.2 mL di una soluzione contenente 10 ng/mL di Pb. Il TISIS è stato anche impiegato in combinazione con la tecnica ICP-MS con rilevatore multiplo, ottenendo una ripetibilità dello 0.16 ‰ ed utilizzando solamente 0.2 mL di campione. Combinando tale metodo con una pre-concentrazione, si sono ottenuti rapporti isotopici del Pb accurati fino a concentrazioni di analita pari a 5 pg/g.

Infine, si sono valutate le prestazioni ottenibili dalla misura del rapporto $^{87}Sr/^{86}Sr$ utilizzando un sistema di desolvatazione del campione in combinazione con la tecnica ICP-MS con rilevatore multiplo. In condizioni di ripetibilità intermedia la precisione è risultata 0.19 ‰ impiegando una concentrazione di analita pari a 0.4 ng/mL.

I metodi sviluppati sono stati applicati all'interno di numerosi studi ambientali facenti parte dei progetti PNRA (Programma Nazionale per la Ricerca in Antartide) e RIS (*Research in Svalbard*). I rapporti isotopici del Pb sono stati determinati in modo preciso ed accurato all'interno di campioni di particolato atmosferico, neve superficiale, particolato e sedimento marino di provenienza sia Artica che Antartica. I dati sono stati discussi con un approccio multidisciplinare ed hanno prodotto informazioni molto utili per la comprensione delle sorgenti e dei meccanismi di trasporto degli elementi in tracce.

In particolare, i risultati relativi al particolato atmosferico campionato a Ny-Ålesund (arcipelago delle Svalbard), mostrano un andamento stagionale ricorrente, con maggiori quantità di Pb dovuto ad attività minerarie in territorio russo durante la primavera ed apporti antropogenici provenienti dal settore occidentale del Nord-America durante

l'estate. L'impiego di un approccio simile, ha anche permesso di identificare all'interno del Kongsfjorden (un fiordo in prossimità di Ny-Ålesund) la presenza di un apporto di Pb antropogenico, associato a masse d'acqua atlantiche ed un apporto crostale, dovuto all'attività di scioglimento dei ghiacciai.

Per quanto riguarda la ricerca in Antartide, la caratterizzazione chimica ed isotopica del particolato atmosferico campionato con differenti tagli dimensionali a Terra Nova Bay (nel settore settentrionale di Victoria Land) ha suggerito che sia gli elementi crostali, sia quelli antropogenici sono influenzati dalle masse d'aria trasportate dal vento catabatico proveniente dall'entroterra. L'apporto marino è risultato essere maggiore a gennaio, in concomitanza con la riduzione dell'estensione del ghiaccio marino. I rapporti isotopici del Pb hanno anche evidenziato come la maggior parte del Pb misurato nei campioni (50–70 %) sia probabilmente dovuto a particolato antropogenico proveniente da Sud America ed Australia.

Infine, la misura dei rapporti isotopici del Pb in campioni di neve superficiale proveniente dal plateau antartico ha permesso di identificare variazioni stagionali ed inter-annuali delle principali fonti di Pb atmosferico in Antartide.

# Abstract

In het kader van milieustudies kan de meting van isotopenverhoudingen helpen een onderscheid te maken tussen natuurlijke en antropogene bronnen, alsook om de bronregio's en transportroutes te identificeren. Maar, milieumonsters kunnen gekarakteriseerd zijn door lage gehaltes aan de analietelementen en dat kan een precieze en accurate bepaling van isotopenverhoudingen in de weg staan.

Gedurende dit doctoraat werd wetenschappelijk onderzoek doorgevoerd met betrekking tot de analytische en milieuaspecten gelinkt aan de bepaling van isotopenverhoudingen in milieustalen. Qua analytische aspecten werd veel aandacht besteed aan het realiseren van precieze en accurate metingen van isotopenverhoudingen met single-collector en multi-collector ICP-massaspectrometrie (ICP-MS) bij lage gehaltes aan het analietelement. De mogelijkheden van single-collector ICP-MS voor de bepaling van $^{208}Pb/^{207}Pb$ en $^{206}Pb/^{207}Pb$ isotopenverhoudingen bij laag monsterverbruik werden geëvalueerd bij gebruik van twee monsterintroductiesystemen, een PFA microverstuiver, werkend bij een debiet van 150 µL/min, en de "torch integrated sample introduction system" (TISIS), werkend bij een debiet van 20 µL/min. Na optimalisatie van de instrumentele condities en bij gebruik van ammoniak als dempingsgas, werd met deze systemen een herhaalbaarheid van respectievelijk $0.12 \pm 0.03$ en $0.17 \pm 0.04$ % RSD gerealiseerd bij een monsterverbruik dat beperkt was tot respectievelijk $<1.5$ en 0.2 mL. Het "TISIS" werd ook in combinatie met multi-collector ICP-MS gebruikt. Deze opstelling leverde accurate Pb-isotopenverhoudingen bij concentraties tot 5 pg/g.

Voor de bepaling van $^{87}Sr/^{86}Sr$ isotopenverhoudingen werd de combinatie van een membraandesolvatatie-eenheid en multi-collector ICP-MS onderzocht. Bij een Sr concentratie van 0.4 ng/mL werd een intermediaire precisie van 0.19 ‰ gerealiseerd.

De ontwikkelde methodes werden ingezet in verschillende milieustudies doorgevoerd in het kader van projecten van PNRA (het Italiaanse Nationale Programma voor Antarctisch Onderzoek) en PNR (Onderzoek in Svalbard). Pb-isotopenverhoudingen werden op accurate en precieze wijze bepaald in atmosferisch aerosol, oppervlaktesneeuw, in zeewater gesuspendeerde deeltjes en sedimentstalen, bemonsterd in zowel de Arctische omgeving als op Antarctica. De verkregen gegevens werden in een multidisciplinaire context geëvalueerd en leverden belangrijke informatie op met betrekking tot de bronnen en transportroutes van spoorelementen.

De resultaten behaald voor atmosferische aërosolen bemonsterd in Ny-Ålesund (Svalbard eilanden) brachten een weerkerende seizoensgebonden trend met een hogere Pb-belading gelinkt aan mijnacitiviteiten in Rusland gedurende de lente en aan antropogeen Pb komende van de oostzijde van Noord-Amerika tijdens de zomer aan het licht. Gelijkaardige metingen werden ook uitgevoerd voor gesuspendeerde deeltjes in het water in de Kongsfjorden (dicht bij Ny-Ålesund) en de resultaten lieten toe de antropogene input gelinkt aan het instromen van Atlantisch water en het van de aardkorst afkomstige Pb dat via smeltwater in de fjord terecht komt van elkaar te onderscheiden.

In de context van Antarctisch onderzoek, werd in de Terra Nova baai (Northern Victoria land) atmosferisch aerosol gecollecteerd, gescheiden naar partikelgrootte. Deze fracties werden onderzocht op chemische en isotopische samenstelling. De resultaten toonden aan dat zowel elementen afkomstig van de aardkorst als deze afkomstig van antropogene elementen gelinkt zijn aan de katabatische wind die uit het binnenland komt. De mariene input bleek hoger in januari wanneer de hoeveelheid zee-ijs vermindert. Pb-isotopenanalyse wees uit dat Pb aangevoerd met vervuilde aërosolen afkomstig van Zuid-Amerika en Australië de belangrijkste bijdrage tot het antropogene Pb (50–70 %) vormt.

De hoog-precieze bepaling van Pb-isotopenverhoudingen in oppervlaktesneeuw van het Antarctische plateau bracht tenslotte verschillen inzake de herkomst van het atmosferisch Pb dat Antarctica bereikt tussen de seizoenen en tussen verschillende jaren aan het licht.

# Contents

# List of Figures

# List of Tables

# Introduction

Isotope ratio measurement is considered a hot topic for both the analytical and geochemical scientific communities because of the unique information that they can reveal. Particularly, Pb and Sr isotopic systems are powerful tools for geochronologists aiming at finding information about the formation and transformation of ores and minerals, whereas in the context of environmental sciences, they can help to identify the different geographical sources related to anthropogenic and crustal inputs. However, such information is often difficult to obtain because of the low analyte concentration in the samples, thus the importance of developing sensitive analytical methods.

Inductively coupled plasma mass spectrometry (ICP-MS) is a powerful and versatile technique able to obtain information about the isotopic composition of virtually all the elements of the periodic table. However, the instrument sensitivity is limited by a low efficiency of the sample introduction system and of the transport of the analyte ions from the source to the detector. Reduced instrument sensitivity results in turn to poor precision and high uncertainty in the measured isotope ratios.

This Ph.D. dissertation discusses about isotope ratio measurements for environmental studies and focuses on the development and application of new analytical methods for the determination of Pb and Sr isotope ratios by ICP-MS in samples with a low amount of the target elements. Three different sample introduction systems were used in combination with single-collector and multi-collector ICP-MS in order to improve the instrumental sensitivity, and thus the isotope ratio precision.

The developed methods were then applied to the analysis of atmospheric particulate matter, marine suspended particulate matter, sediments and snow samples collected in the Arctic and Antarctica. Information provided by isotope ratio measurements not only helped to understand and justify the results obtained by chemical characterisations of the samples, but they were also useful to identify anthropogenic and natural inputs, elucidate their source regions and transport pathways, as well as to quantify their relative contributions.

These topics are discussed in nine chapters, as described below:

*Chapter 1* discusses the basic principles governing the variations in the isotopic composition of the elements, focusing mainly on the Pb and Sr isotopic systems and their use in the environmental sciences.

*Chapter 2* takes into account the fundamentals of isotope ratio measurements using single-collector and multi-collector ICP-MS.

*Chapter 3* compares the performances obtained using two different sample introduction systems combined with single-collector ICP-MS.

*Chapter 4* discusses the results obtained by the measurement of Pb isotope ratios in samples of atmospheric particulate matter collected in the Arctic.

*Chapter 5* examines the results provided by the Pb isotope ratio measurements and the

chemical characterisation of marine suspended particulate matter collected in an Arctic fjord.

*Chapter 6* considers the results of chemical characterisation and Pb isotope ratio measurements in size-segregated aerosol samples collected at a coastal Antarctic site.

*Chapter 7* reports the development of a method based on multi-collector ICP-MS for the determination of precise Pb isotope ratios in snow samples collected on the Antarctic plateau.

*Chapter 8* is about the development of a method for the determination of precise Sr isotope ratios by multi-collector ICP-MS using low amounts of the target element.

*Chapter 9* summarises the main findings and makes some considerations about future works.

# 1 The isotopic composition of the elements

## 1.1 *Introduction*

The chemical behaviour of an atom is *mainly* governed by its valence electrons, so that atoms with a different number of neutrons, but the same number of protons, display a very similar chemical behaviour. These atoms are called isotopes and are identified by their mass number ($A$), written as a superscript before the symbol of the chemical element. Therefore, the Pb nuclide with 82 protons and 126 neutrons is reported as $^{208}$Pb.

The relative abundance of the nuclide ${}^{i}X$ is calculated as the number of its moles $n$ (or atoms $N$), divided by the total amount (number of moles $n$ or atoms $N$) of the element $X$:

$$\theta({}^{1}X) = \frac{n({}^{1}X)}{\sum_{i=1}^{m} n({}^{i}X)} \tag{1.1}$$

The different binding energy per nucleon influenced the relative abundance of the isotopes at the moment of their formation by the different nucleosynthetic processes, so that higher binding energies correspond to higher abundances. As a result of the thorough mixing of most nuclides before the formation of the solar system (4.6 Gy ago, Faure and Mensing 2007), these "primitive" relative abundances were invariant in the whole solar system. However, at present, variations in the natural isotopic composition of many elements is well documented and can be attributed to various reasons such as

*Radioactive decay:* as a result of the decay of a naturally occurring and long-lived radionuclide, elements with one or more radiogenic nuclides have an isotopic composition which is subject to marked temporal variations. As a result of this time-dependent isotopic composition, isotopic systems affected by radioactive decay can be exploited for dating purposes. This group comprises well known isotopic systems, such as Pb and Sr, the analysis of which in different samples was the main aim of this work.

*Extraterrestrial material:* in some meteorites, elements may show different isotopic compositions in comparison to those measured in the terrestrial crust. This can be the result of the decay of some radionuclides with a short half-life in comparison to the age of the solar system. Such variations are rare for terrestrial materials, in large part because of the preferential sampling of the crust, whereas some extraterrestrial material, such as iron meteorites, resemble the Earth's core, in which parent to daughter element ratios may be much higher than in the crust (Vanhaecke and Degryse 2012).

*Interaction between cosmic rays and terrestrial matter:* the interaction between the Earth's atmosphere and highly energetic cosmic radiation results in the variation of the iso-

topic composition for some elements. A well known example of this phenomenon is the production of the radionuclide $^{14}C$ according to the reaction

$$^{1}n + {}^{14}N \longrightarrow {}^{14}C + {}^{1}p \tag{1.2}$$

in which thermal neutrons are produced by the interaction of cosmic rays with the upper layers of the troposphere. $^{14}C$ enters the food chain in the form of $CO_2$, affecting the C isotopic composition for all living organisms.

*Mass-dependent isotope fractionation:* the differences in mass between the isotopes of the same element influence their efficiency in participating to several reactions. Indeed, the different number of neutrons results in a difference in vibrational energy of reagents and products in an equilibrium process, or the differences in the vibrational energy levels of reagents and transition state in a unidirectional process. These two mechanisms are known as thermodynamic and kinetic effect, respectively, and together they are responsible for the mass-dependent isotope fractionation. The most studied isotopic systems subject to these kind of variations in their compositions are those of the lighter elements such as H, C, N and O. The relative differences in the mass of their isotopes is large (especially in the case of $^{2}H$ and $^{1}H$) and therefore, the fractionation effect is relatively easy to identify and measure. For metals and metalloids, the relative differences in mass among the isotopes is smaller and so is the extent of the isotope fractionation they undergo. However, thanks to the precision of powerful techniques such as thermal ionisation mass spectrometry (TIMS) or multi-collector inductively coupled plasma-mass spectrometry (MC-ICP-MS), mass-dependent isotope fractionation has been observed also for an element as heavy as U (Weyer et al. 2008).

*Mass-independent isotope fractionation:* for some elements, an isotope fractionation not linearly dependent on the difference in mass between the isotopes studied has been observed. The reasons for this phenomenon are currently attributed to differences in the interaction of the nucleus for such isotopes with the surrounding electron cloud. These in turn are related to slight differences in the volume of the nucleus or its magnetic properties.

*Anthropogenic effects:* variations in the isotopic composition of the elements can be artificially obtained by enhancing the extent of the naturally occurring fractionation or by production of specific isotopes. The production of enriched U for nuclear reactors and the preparation of enriched isotopic tracers for isotope dilution experiments belong to this group.

Given the variety of phenomena involved in the variation of the natural isotopic compositions of the elements, it is not surprising that the determination of the isotopic abundances can be an important tool to shed light on a number of topics spanning from the formation of the solar system (*e.g.* Halliday 2000) to the metabolic cycles of living organisms (*e.g.* Balcaen et al. 2008; Blanckenburg et al. 2014). However, in the following sections, the discussion will be limited to the Pb and Sr isotopic systems and their applications for environmental studies.

## 1.2 *The Pb isotopic system*

The isotopic composition of Pb is subject to temporal variations due to the radioactive decay of parent nuclides. Indeed, among the four stable isotopes of Pb, three are radiogenic. $^{206}Pb$, $^{207}Pb$ and $^{208}Pb$ are the end products of the decay chains of $^{238}U$ ($t_{1/2} = 4.468 \times 10^9$ y), $^{235}U$ ($t_{1/2} = 0.407 \times 10^{10}$ y) and $^{232}Th$ ($t_{1/2} = 14.010 \times 10^9$ y), respectively. On the other hand, $^{204}Pb$ is not radiogenic and its abundance is constant in time.

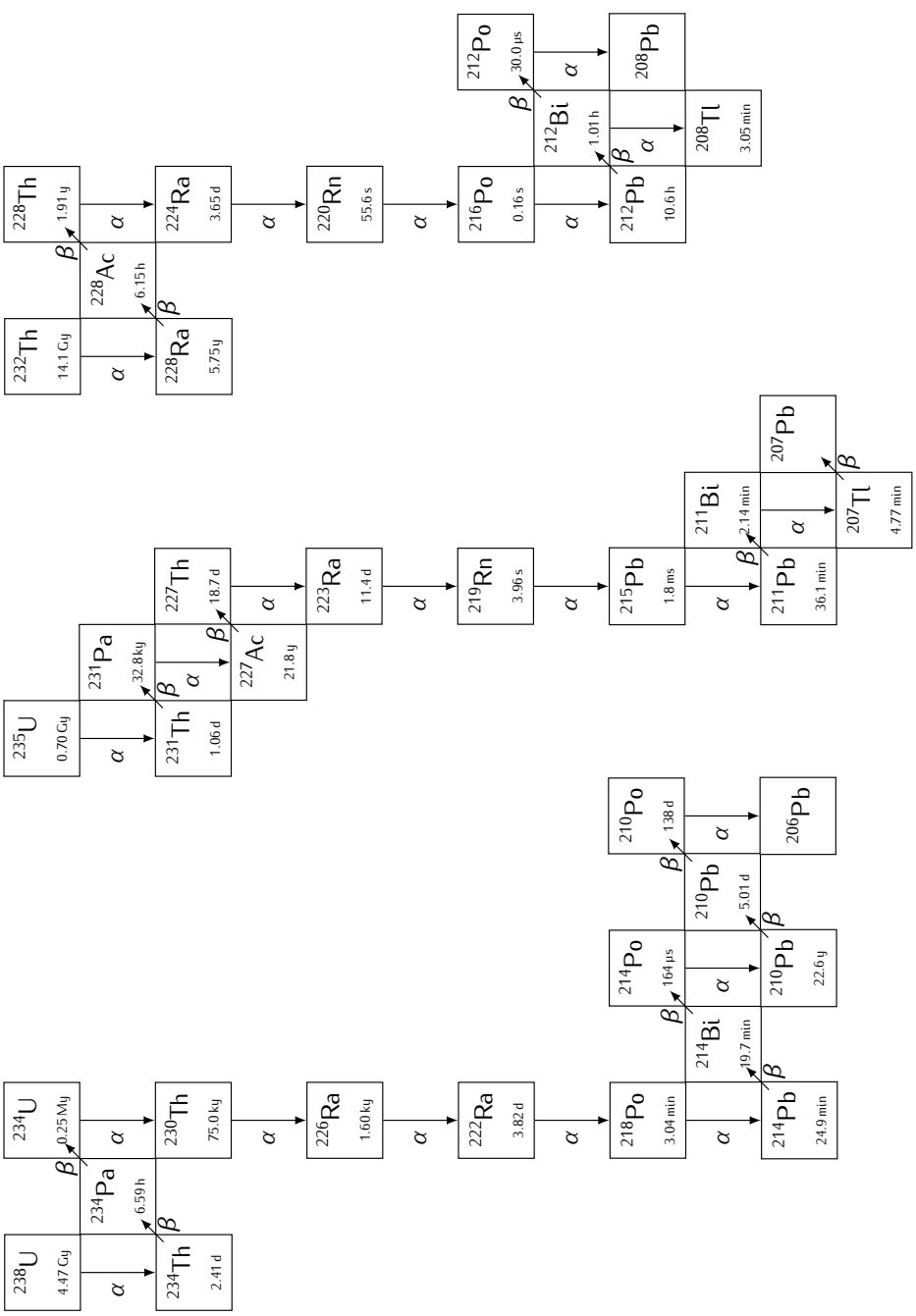


Figure 1.1. decay chains for $^{238}$U, $^{235}$U and $^{232}$Th, with $^{206}$Pb, $^{207}$Pb and $^{208}$Pb as stable end products. Half-lives are reported in small font (Bourdon et al. 2003).

At present, average abundances for the Pb isotopes are 52, 24, 23 and 1 % for $^{208}$Pb, $^{206}$Pb, $^{207}$Pb and $^{204}$Pb, respectively.

As shown in figure 1.1, the rate-determining step of the decay reactions is, by many orders of magnitude, the first. Therefore, the whole processes can be described as single step reactions, resulting in the abundance of Pb isotopes governed by time and the initial Pb, U and Th concentrations.

Considering time $= 0$ the moment in which a mineral crystallised, at time $= t$ the measured Pb will be the result of the initial Pb incorporated in the lattice and that produced over time by radioactive decay of the parent nuclide. For $^{206}$Pb this can be easily summarised using the following equation:

$$\left(\frac{^{206}\text{Pb}}{^{204}\text{Pb}}\right) = \left(\frac{^{206}\text{Pb}}{^{204}\text{Pb}}\right)_0 + \left(\frac{^{238}\text{U}}{^{204}\text{Pb}}\right)\left(e^{\lambda_{238}t} - 1\right) \tag{1.3}$$

where the 0 subscript indicates the ratio at the moment of crystallisation and $\lambda$ the decay constant of the parent nuclide.

Using a set of similar equations for the other radiogenic Pb isotopes, geochemists were able to determine the age of rocks (Schoene 2014), meteorites and Earth (Patterson 1956).

Equation (1.3) was expressed as a ratio between the abundance of the isotope of interest ($^{206}$Pb) and that of an isotope not subject to temporal variations ($^{204}$Pb). The use of ratios is more convenient than that of a single isotopic abundance because ratios can be determined with a much smaller uncertainty, without the need of calibration with a solution, the concentration of which can be affected by relatively large bias due to non-spectral interference.

Despite the wide use of $^{204}$Pb-normalised ratios in geochemical or Earth science contexts, the low abundance of $^{204}$Pb can result in values affected by relatively poor precision. This is especially relevant for samples with low Pb content and in this situation the ratios are often normalised against $^{207}$Pb. Indeed, due to its very long half-life, $^{238}$U still has a relatively high abundance on Earth, whereas most of $^{235}$U has already decayed (Erel et al. 2001). As a result, the abundance of $^{207}$Pb has changed very little with time compared with $^{206}$Pb and Pb isotope ratios reported as $^{206}$Pb/$^{207}$Pb can still provide some insights into the age of the rocks. Old formations are characterised by low values in the range 1.06–1.10, whereas recent ores show more radiogenic values, typically above 1.18 (Bacon 2002). However, when the geochronological information is not required, such as in environmental studies, $^{206}$Pb-normalised ratios can also be reported.

## 1.3 *The Sr isotopic system*

Sr has four stable isotopes: $^{84}$Sr, $^{86}$Sr, $^{87}$Sr and $^{88}$Sr. Among them, only $^{87}$Sr is radiogenic and produced via the $\beta^-$ decay of $^{87}$Rb ($t_{1/2} = 48.8 \times 10^9$ y). As a result the Sr isotopic composition is slowly being enriched in the radiogenic isotope and at present average relative abundances are 82.5, 7.0, 9.9 and 0.6 % for $^{88}$Sr, $^{87}$Sr, $^{86}$Sr and $^{84}$Sr, respectively.

Similarly to Pb, the measured $^{87}$Sr/$^{86}$Sr ratio is the result of its value at time $= 0$ plus that produced by radioactive decay so the following equation can be written:

$$\left(\frac{^{87}\text{Sr}}{^{86}\text{Sr}}\right) = \left(\frac{^{87}\text{Sr}}{^{86}\text{Sr}}\right)_0 + \left(\frac{^{87}\text{Rb}}{^{86}\text{Sr}}\right)\left(e^{\lambda_{87}t} - 1\right) \tag{1.4}$$

A direct consequence is that natural variations of $^{87}$Sr/$^{86}$Sr in rocks are the result of different crystallisation times and initial Rb/Sr ratios.

For minerals with different Rb/Sr ratios but that crystallised at the same time and shared the same initial $^{87}Sr/^{86}Sr$, the measured $^{87}Sr/^{86}Sr$ ratios lie on a line called isochron from which geochronological information can be obtained (Riley and Compston 1962).

Contrary to the $^{87}Sr/^{86}Sr$ ratio, the Sr isotope ratios not involving $^{88}Sr$ are not subjected to fractionation. Similarly, the ratio $^{87}Rb/^{85}Rb$ is thought to be the same for all the terrestrial material.

## 1.4 *Environmental applications*

Pb is a non-essential and toxic metal that had an important role throughout the human history. Significant production of Pb started about 5000 years ago with the smelting of Pb–Ag alloys from galena ores (PbS) and the cupelling of Ag for coinage (Nriagu 1983). The analysis of Greenland ice cores, revealed that during the Roman empire, the rate of Pb production reached 80 000 tonne/year, causing relevant pollution on a hemispheric scale (Hong et al. 1994).

In more recent times, the massive use of alkyl–Pb as anti-knocking additive for fuels caused a strong increase in the Pb concentration in the atmosphere, so that, during 1940–1970, 99 % of the concentration for this toxic metal was estimated to have originated from human activities in the Northen Hemisphere (Murozumi et al. 1969). The following decades were characterised by a constant decrease of the concentration of atmospheric Pb as a result of the phasing-out of the alkyl–Pb additives (Boutron et al. 1991) and more strict regulations for atmospheric emissions (von Storch et al. 2003).

In this context, the determination of Pb isotope ratios proved to be useful for the discrimination between natural and anthropogenic sources (Shirahata et al. 1980; Townsend and Snape 2008). Indeed, the Pb isotope ratios in the upper crust and those in ores mined for commercial purposes are usually different because of their different geological histories. A good example is provided by the Australian Broken Hill ore body, which is characterised by very low Pb isotope ratios $^{206}Pb/^{207}Pb$: $1.0407 \pm 0.0006$ and $^{208}Pb/^{207}Pb$: $2.3153 \pm 0.0013$ (Sangster et al. 2000). As most of the alkyl–Pb additive commercialised worldwide was prepared from this type of Pb ore, it was possible to identify the distinctive Pb isotopic signature for inputs related to automotive traffic by the analysis of atmospheric particulate samples (Bollhöfer and Rosman 2000).

After the phasing-out of alkyl–Pb in fossil fuels, the Pb isotopic composition of atmospheric particulate was more influenced by local industrial emissions (Simonetti et al. 2004), natural sources (Kylander et al. 2010) and long-range transport of pollutants (Sturges and Barrie 1987). The relative contributions of these sources provide a Pb isotopic fingerprint which is different for many areas across the globe (Bollhöfer and Rosman 2000; Bollhöfer and Rosman 2001a). In addition, Pb isotope ratios are not fractionated by normally occurring chemical or physical processes such as combustion, weathering or atmospheric transport. Therefore, they can be useful for tracking the production, dispersion and accumulation of pollutants in the environment by direct comparison of the values obtained by the analysis of different matrices of environmental relevance (Farmer et al. 2000). Notably, this feature was also exploited to trace regional and global patterns of atmospheric transport by the determination of the Pb isotope ratios in atmospheric samples or in paleo archives such as ice cores (De Deckker et al. 2010; Vallelonga et al. 2010).

Plots such as those reported in figure 1.2 can be useful for the identification of two possible sources affecting the Pb concentration in the samples. In figure 1.2 **(a)** the Pb isotope ratios values of the samples define a mixing line stretched between the Pb isotopic composition of the two sources (end-members). The points close to the lower left corner of the plot are more influenced by the end-member A than B and *vice versa*. In this

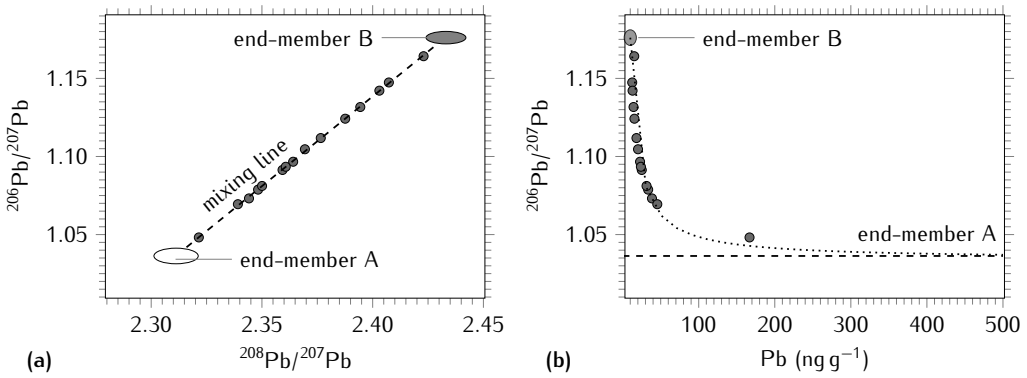


Figure 1.2. **(a)** three-isotope plot and **(b)** $^{206}Pb/^{207}Pb$ ratio as a function of Pb concentration for simulated data.

situation the relative contribution of the end-member A with Pb isotopic composition $(x_A, y_A)$ can be calculated for every sample $(x_i, y_i)$ using the equation:

$$\%A = 100\sqrt{\frac{(x_i - x_B)^2 + (y_i - y_B)^2}{(x_A - x_B)^2 + (y_A - y_B)^2}} \tag{1.5}$$

where $(x_B, y_B)$ is the isotopic composition of the end-member B.

In figure 1.2 **(b)** one Pb isotope ratio is plotted as function of the Pb concentration. The presence of mixing of two sources is evident from the hyperbolic curve which, for infinite Pb concentration, reaches the isotopic composition of the end-member A. The plot can be linearised using the inverse of the Pb concentration.

If three end-members contribute to the final isotope ratios measured in the samples, their values will plot in a triangular field. The contribution for each end-member A, B and C will be calculated solving a system of linear equations (equation 1.6) for each $(x_i, y_i)$ measured:

$$\begin{pmatrix} x_A & x_B & x_C \\ y_A & y_B & y_C \\ 1 & 1 & 1 \end{pmatrix} \begin{pmatrix} A \\ B \\ C \end{pmatrix} = \begin{pmatrix} x_i \\ y_i \\ 1 \end{pmatrix} \tag{1.6}$$

Contrary to Pb, the predominant source of Sr is the continental crust. Indeed, Sr is a relatively abundant element in rocks and soils, contributing to 316 ppm of the Earth's crust (Wedepohl 1995). Because of their similar atomic radii, $Sr^{2+}$ readily substitutes for $Ca^{2+}$ in minerals, resulting in a high content in basalts and carbonates, but low concentrations in sandstones and low-Ca granites. On the contrary, $Rb^+$ substitutes for $K^+$, resulting in relatively high Rb/Sr ratios in K-feldspars, micas and granites. Due to these geochemical differences, the Rb/Sr ratio in rocks can vary by several orders of magnitude, resulting in substantial variations in the $^{87}Sr/^{86}Sr$ ratio as a function of the different geological terrains. Typical $^{87}Sr/^{86}Sr$ ratios are in the range 0.710–0.740 for old basalts and 0.703–0.704 for younger granites, resulting in an overall variation from 0.702 to 0.750 for rocks of the continental crust (Bentley 2006).

Sr is released from rocks by weathering at rates that vary among the minerals present within the same rock, cycled through soil, vegetation and animals and eventually enters the ocean by river transport of sediments. The time scales of these processes are small compared to the decay rate of $^{87}Rb$, whereas mass-dependent fractionation phenomena are small compared to the variability of $^{87}Sr/^{86}Sr$ among the different Sr sources. As

a result, the ratio $^{87}Sr/^{86}Sr$ is conserved without important fractionation through the described steps, enabling its use for tracing purposes (Åberg 1995).

In this context, the large spatial variability of the $^{87}Sr/^{86}Sr$ ratio can be exploited in order to obtain a fingerprint for different geographical areas, enabling the identification of Sr inputs due to sea-spray, weathering of rocks or anthropogenic contributions, mainly related to the use of fertilizers (Négrel and Deschamps 1996).

In the context of atmospheric studies and Earth sciences, the determination of the Sr isotopic composition is useful in order to identify the geographical sources of mineral dust and thus, to infer patterns of atmospheric transport both at present or in past climate conditions (Basile et al. 1997; Bory et al. 2003; Grousset and Biscaye 2005). Care is however required when comparing $^{87}Sr/^{86}Sr$ values measured in fine windblown dust to values for whole rocks. Indeed, different Sr isotopic compositions can be found for different aerosol particle sizes that in turn are transported by wind with different efficiencies (Gaiero 2007).

Although not related to the main topic of the present text, fingerprint analysis based on $^{87}Sr/^{86}Sr$ was also extensively exploited in the context of archaeological sciences in order to provide some insights into human migrations. Indeed, the Sr isotopic composition of bones and teeth reflects that of Sr assimilated through diet, which in turn is determined by local geology (Degryse et al. 2012).

*References*

Åberg, G., 1995. The use of natural strontium isotopes as tracers in environmental studies. *Water, Air, and Soil Pollution*, **79**, 309–322. DOI: 10.1007/BF01100444

Bacon, J. R., 2002. Isotopic characterisation of lead deposited 1989–2001 at two upland Scottish locations. *Journal of Environmental Monitoring*, **4**, 291–299. DOI: 10.1039/b109731h

Balcaen, L. I. L., De Schamphelaere, K. A. C., Janssen, C. R., Moens, L., and Vanhaecke, F., 2008. Development of a method for assessing the relative contribution of waterborne and dietary exposure to zinc bioaccumulation in Daphnia magna by using isotopically enriched tracers and ICP-MS detection. *Analytical and Bioanalytical Chemistry*, **390**, 555–569. DOI: 10.1007/s00216-007-1620-5

Basile, I., Grousset, F. E., Revel, M., Petit, J. R., Biscaye, P. E., and Barkov, N. I., 1997. Patagonian origin of glacial dust deposited in East Antarctica (Vostok and Dome C) during glacial stages 2, 4 and 6. *Earth and Planetary Science Letters*, **146**, 573–589. DOI: 10.1016/S0012-821X(96)00255-5

Bentley, R. A., 2006. Strontium isotopes from the Earth to the archaeological skeleton: a review. *Journal of Archaeological Method and Theory*, **13**, 135–187. DOI: 10.1007/s10816-006-9009-x

Blanckenburg, F. v., Oelze, M., Schmid, D. G., Zuilen, K. v., Gschwind, H.-P., Slade, A. J., Stitah, S., Kaufmann, D., and Swart, P., 2014. An iron stable isotope comparison between human erythrocytes and plasma. *Metallomics*, **6**, 2052–2061. DOI: 10.1039/C4MT00124A

Bollhöfer, A. and Rosman, K. J. R., 2000. Isotopic source signatures for atmospheric lead: the Southern Hemisphere. *Geochimica et Cosmochimica Acta*, **64**, 3251–3262. DOI: 10.1016/S0016-7037(00)00436-1

Bollhöfer, A. and Rosman, K. J. R., 2001a. Isotopic source signatures for atmospheric lead: The Northern Hemisphere. *Geochimica et Cosmochimica Acta*, **65**, 1727–1740. DOI: 10.1016/S0016-7037(00)00630-X

Bory, A. J.-M., Biscaye, P. E., and Grousset, F. E., 2003. Two distinct seasonal Asian source regions for mineral dust deposited in Greenland (NorthGRIP). *Geophysical Research Letters*, **30**, 1167. DOI: 10.1029/2002GL016446

Bourdon, B., Turner, S., Henderson, G. M., and Lundstrom, C. C., 2003. Introduction to U-series Geochemistry. *Reviews in Mineralogy and Geochemistry*, **52**, 1–21. DOI: 10.2113/0520001

Boutron, C. F., Görlach, U., Candelone, J.-P. J. P., Bolshov, M. A., and Delmas, R. J., 1991. Decrease in anthropogenic lead, cadmium and zinc in Greenland snows since the late 1960s. *Nature*, **353**, 153–156

De Deckker, P., Norman, M., Goodwin, I. D., Wain, A., and Gingele, F. X., 2010. Lead isotopic evidence for an Australian source of aeolian dust to Antarctica at times over the last 170,000 years. *Palaeogeography, Palaeoclimatology, Palaeoecology*, **285**, 205–223. DOI: 10.1016/j.palaeo.2009.11.013

Degryse, P., Muynck, D. D., Delporte, S., Boyen, S., Jadoul, L., Winne, J. D., Ivaneanu, T., and Vanhaecke, F., 2012. Strontium isotopic analysis as an experimental auxiliary technique in forensic identification of human remains. *Analytical Methods*, **4**, 2674–2679. DOI: 10.1039/C2AY25035G

Erel, Y., Dubowski, Y., Halicz, L., Erez, J., and Kaufman, A., 2001. Lead concentrations and isotopic ratios in the sediments of the Sea of Galilee. *Environmental Science and Technology*, **35**, 292–299

Farmer, J. G., Eades, L. J., Graham, M. C., and Bacon, J. R., 2000. The changing nature of the $^{206}Pb/^{207}Pb$ isotopic ratio of lead in rainwater, atmospheric particulates, pine needles and leaded petrol in Scotland, 1982-1998. *Journal of Environmental Monitoring*, **2**, 49–57. DOI: 10.1039/a907558e

Faure, G. and Mensing, T. M., 2007. *Introduction to Planetary Science*. Dordrecht: Springer Netherlands

Gaiero, D. M., 2007. Dust provenance in Antarctic ice during glacial periods: From where in southern South America? *Geophysical Research Letters*, **34**, L17707. DOI: 10.1029/2007GL030520

Grousset, F. E. and Biscaye, P. E., 2005. Tracing dust sources and transport patterns using Sr, Nd and Pb isotopes. *Chemical Geology*, **222**, 149–167. DOI: 10.1016/j.chemgeo.2005.05.006

Halliday, A. N., 2000. Hf-W Chronometry and Inner Solar System Accretion Rates. *Space Science Reviews*, **92**, 355–370. DOI: 10.1023/A:1005280220751

Hong, S., Candelone, J.-P., Patterson, C. C., and Boutron, C. F., 1994. Greenland ice evidence of hemispheric lead pollution two millennia ago by Greek and Roman civilizations. *Science*, **265**, 1841–1843. DOI: 10.1126/science.265.5180.1841

Kylander, M. E., Klaminder, J., Bindler, R., and Weiss, D. J., 2010. Natural lead isotope variations in the atmosphere. *Earth and Planetary Science Letters*, **290**, 44–53. DOI: 10.1016/j.epsl.2009.11.055

Murozumi, M., Chow, T. J., and Patterson, C., 1969. Chemical concentrations of pollutant lead aerosols, terrestrial dusts and sea salts in Greenland and Antarctic snow strata. *Geochimica et Cosmochimica Acta*, **33**, 1247–1294. DOI: 10.1016/0016-7037(69)90045-3

Négrel, P. and Deschamps, P., 1996. Natural and anthropogenic budgets of a small watershed in the massif central (France): Chemical and strontium isotopic characterization of water and sediments. *Aquatic Geochemistry*, **2**, 1–27. DOI: 10.1007/BF00240851

Nriagu, J. O., 1983. Occupational exposure to lead in ancient times. *Science of the Total Environment*, **31**, 105–116. DOI: 10.1016/0048-9697(83)90063-3

Patterson, C., 1956. Age of meteorites and the earth. *Geochimica et Cosmochimica Acta*, **10**, 230–237. DOI: 10.1016/0016-7037(56)90036-9

Riley, G. H. and Compston, W., 1962. Theoretical and technical aspects of Rb-Sr geochronology. *Geochimica et Cosmochimica Acta*, **26**, 1255–1281. DOI: 10.1016/0016-7037(62)90055-8

Sangster, D. F., Outridge, P. M., and Davis, W. J., 2000. Stable lead isotope characteristics of lead ore deposits of environmental significance. *Environmental Reviews*, **8**, 115–147. DOI: 10.1139/a00-008

Schoene, B., 2014. U–Th–Pb Geochronology. *Treatise on Geochemistry*. Ed. by Karl K. Turekian and Holland, H. Second Edition. Vol. 4. The crust. 16 vols. Oxford: Elsevier, 341–378

Shirahata, H., Elias, R. W., Patterson, C. C., and Koide, M., 1980. Chronological variations in concentrations and isotopic compositions of anthropogenic atmospheric lead in sediments of a remote subalpine pond. *Geochimica et Cosmochimica Acta*, **44**, 149–162. DOI: 10.1016/0016-7037(80)90127-1

Simonetti, A., Gariépy, C., Banic, C. M., Tanabe, R., and Wong, H. K., 2004. Pb isotopic investigation of aircraft-sampled emissions from the Horne smelter (Rouyn, Québec): Implications for atmospheric pollution in northeastern North America1. *Geochimica et Cosmochimica Acta*, **68**, 3285–3294. DOI: 10.1016/j.gca.2004.02.008

Sturges, W. T. and Barrie, L. A., 1987. Lead 206/207 isotope ratios in the atmosphere of North America as tracers of US and Canadian emissions. *Nature*, **329**, 144–146. DOI: 10.1038/329144a0

Townsend, A. T. and Snape, I., 2008. Multiple Pb sources in marine sediments near the Australian Antarctic Station, Casey. *Science of the Total Environment*, **389**, 466–474. DOI: 10.1016/j.scitotenv.2007.09.022

Vallelonga, P., Gabrielli, P., Balliana, E., Wegner, A., Delmonte, B., Turetta, C., Burton, G., Vanhaecke, F., Rosman, K. J. R., Hong, S., Boutron, C. F., Cescon, P., and Barbante, C., 2010. Lead isotopic compositions in the EPICA Dome C ice core and Southern Hemisphere Potential Source Areas. *Quaternary Science Reviews*, **29**, 247–255. DOI: 10.1016/j.quascirev.2009.06.019

Vanhaecke, F. and Degryse, P., 2012. *Isotopic Analysis: Fundamentals and Applications Using ICP-MS*. Wiley

Von Storch, H., Costa-Cabral, M., Hagner, C., Feser, F., Pacyna, J., Pacyna, E., and Kolb, S., 2003. Four decades of gasoline lead emissions and control policies in Europe: a retrospective assessment. *Science of the Total Environment*, **311**, 151–176. DOI: 10.1016/S0048-9697(03)00051-2

Wedepohl, K. H., 1995. The composition of the continental crust. *Geochimica et Cosmochimica Acta*, **58A**, 959–960. DOI: 10.1180/minmag.1994.58A.2.234

Weyer, S., Anbar, A. D., Gerdes, A., Gordon, G. W., Algeo, T. J., and Boyle, E. A., 2008. Natural fractionation of 238U/235U. *Geochimica et Cosmochimica Acta*, **72**, 345–359. DOI: 10.1016/j.gca.2007.11.012

# 2 Isotope ratio measurements with ICP-MS

## 2.1 *Isotope ratio precision*

For many isotope ratio applications, very subtle variations in the isotopic composition of the target element need to be revealed and quantified. As a result, the measurement precision is often the most important parameter for the choice of a suitable method for the determination of isotope ratios.

In the context of isotope ratio measurements, the reported precision may refer to two different definitions.

*Repeatability:* also called internal precision or within-run precision, is expressed as relative standard deviation (RSD) calculated on $n$ successive replicates performed by the same operator, on the same measurement system, under the same operating conditions and at the same location (BIPM 2012).

*Reproducibility:* also called external precision, is the RSD calculated on $n$ measurements performed over an extended period of time or varying conditions (BIPM 2012).

When comparing such figures of merit, care is needed as sometimes the precision is reported as relative standard error (or percentage relative standard error of the mean). In this case the RSD can be obtained by multiplying the reported value by $\sqrt{n}$.

Repeatability is directly limited by Poisson counting statistics. Indeed when the variation in the arrival of ions at the detector can be considered as random, the standard deviation on a signal corresponding to $N$ counts is given by:

$$\sigma(N) = \sqrt{N} \tag{2.1}$$

Relying on the laws of uncertainty propagation, the standard deviation for an isotope ratio $N_1/N_2$ is then given by:

$$\sigma\left(\frac{N_1}{N_2}\right) = \frac{N_1}{N_2}\sqrt{\left[\frac{\sigma(N_1)}{N_1}\right]^2 + \left[\frac{\sigma(N_2)}{N_2}\right]^2 - 2\frac{\sigma^2(N_1,N_2)}{N_1 N_2}} \tag{2.2}$$

This equation is useful to predict the best precision attainable in isotope ratio measurements and it is a function of the absolute number of counted ions for both isotopes and their temporal correlation.

As a result of the role of the number of counts registered, the isotope ratio measurements are usually carried out at relatively high signal intensities, while using sufficiently long measurement times (Vanhaecke and Degryse 2012).

## 2.2 *Instrumental mass discrimination*

In ICP-MS instruments, different analyte masses are extracted from the ion source and transmitted to the detector with different efficiencies. Therefore the measured isotope

ratios may show a significant bias with respect to the corresponding true values. The extent of such error may amount to several % per mass unit, typically well above the expected significant natural variation of isotope ratios, and thus has to be corrected for.

In addition to its dependence to the analyte mass, instrumental mass discrimination is matrix-dependent (Ehrlich et al. 2001; Vanhaecke et al. 2003) and subject to small random fluctuations during the measurement session. The possibility to correct for the instrumental mass discrimination is related to the isotopic system under investigation, the method employed and the instrument capability.

Over the years, several methods have been proposed for calibrating isotope ratios (*e.g.* Albarède and Beard 2004; Baker et al. 2004; Baxter et al. 2006; Rehkämper and Halliday 1998; Woodhead 2002). A complete survey of these methods is beyond the scope of this work and only the principal approaches will be described. The terms *external* and *internal* are used synonymously with *sequential* and *simultaneous* procedures, in accordance to (Vanhaecke and Degryse 2012).

*External bracketing calibration:* the analysis of a standard solution with known isotope ratio for the target element is performed before and after the determination of the same isotope ratio in an unknown sample. The corrected isotope ratio for the sample is then obtained by applying the correction factor calculated for the standard solution measurements. This simple model does not account either for the different matrix between standard and sample, or for the fluctuations in the extent of mass discrimination within a single measurement. It is usually used for isotope ratio measurements by single collector ICP-MS instruments.

*Internal calibration with a calibrant element:* a calibrant element with a known or constant isotope ratio is added to the sample with unknown isotope ratio for the target element. The corrected isotope ratio of the target element is then obtained assuming the same mass discrimination for the calibrant element (Gallon et al. 2008; Longerich et al. 1987). Alternatively, the correlation between the mass discrimination for the calibrant and the target element can be determined empirically by regression analysis of the temporal variations in their measured isotope ratios (Baxter et al. 2006; Maréchal et al. 1999; White et al. 2000; Woodhead 2002). This approach compensates both for matrix effects and temporal variations in mass discrimination and is thus capable of very accurate isotope ratio data. In order to exploit the last advantage, simultaneous determination of the isotope ratios for the calibrant and target elements is required.

*Internal calibration with the target element:* if an element has more than two isotopes and at least one of the possible isotope ratios is well known and not subject to significant natural variations, it is possible to use this ratio to calibrate the isotope ratio of interest. This for example is the situation for Sr, for which the $^{87}Sr/^{86}Sr$ ratio can be calibrated by using the $^{88}Sr/^{86}Sr$ ratio. When a constant and well known ratio is not available, it is possible to modify one of the isotope ratios of the element by admixing of known amounts of a solution of the target element enriched in the two isotopes. The isotopic composition of the solution used for the "double spike" has to be carefully known (Baker et al. 2004; Rudge et al. 2009). This approach can correct for matrix-dependent mass discrimination and its temporal fluctuations. However, it is necessary to assume that both the calibrant and the target ratios undergo the same mass discrimination.

## 2.3 *Single-collector ICP-MS*

### 2.3.1 Overview

As discussed in the previous sections, the ability to acquire signals for different isotopes simultaneously has very significant benefits for the determination of precise and accurate isotope ratios. MC-ICP-MS instruments exploit these advantages.

However, most of the ICP-MS instruments are equipped with a single collector and therefore are just able of sequential monitoring of the target isotopes.

Five main components can be identified in single collector ICP-MS instruments:

1. the sample introduction system,
2. the ICP ion source,
3. the interface region,
4. the mass analyser and
5. the detection system.

Among the single-collector ICP-MS instruments, the main differences are situated in the mass analyser. Quadrupole mass analysers are the most widespread due to their simplicity. The optimum isotope ratio precision attainable with these instruments far exceeds the limiting value predicted on the basis of Poisson counting statistics and is usually $\geq$0.1 % RSD. This value can be lowered to approximately $\geq$0.05 % RSD using collisional damping in a collision/reaction cell pressurised with a non reactive gas. The collisions with the gas increase the temporal correlation between the ions extracted from the ICP at slightly different times, thus improving the internal precision (Bandura et al. 2000). However, preferential collisional losses of the lighter nuclides results in the increase of the extent of the instrument mass discrimination (Vanhaecke et al. 2003).

In ICP-MS instruments equipped with a time-of-flight mass analyser (TOF) all the ions within an ion package are extracted from the ion source and injected into the mass analyser at the same time. As a result, temporal correlations among ions in the same package is increased and an internal precision of about 0.05 % RSD can be obtained (Vanhaecke et al. 1999).

Sector field ICP-MS instruments operating at low mass resolution are able of isotope ratio precisions better than 0.05 % (Krachler et al. 2004; Vanhaecke et al. 1996). Under this condition, the signal transmission is enhanced in comparison with quadrupole-based ICP-MS instruments, resulting in better internal precision. Additionally, the beam diameter is smaller than the exit slit in front of the detector, therefore the resulting spectral peak is characterised by a flat-topped shape, thus avoiding the effect of mass calibration instability.

### 2.3.2 The sample introduction system

Samples are introduced into the ICP ion source as small particles carried by a gas flow, usually Ar. For solid samples this is accomplished by ablating the surface with a laser, whereas for solutions the sample is nebulised and introduced as an aerosol. The standard sample introduction system used for solutions usually consists of a pneumatic nebuliser fitted to a spray chamber (figure 2.1). The nebuliser is responsible for the generation of the primary aerosol through the interaction between an accelerated gas flow and a liquid surface (Vanhaecke and Degryse 2012).

The droplet size distribution of the aerosol delivered to the plasma is critical because large droplets are not efficiently handled by the ICP and have to be removed, decreasing the transport efficiency. The dimensions of the particles constituting the primary aerosol

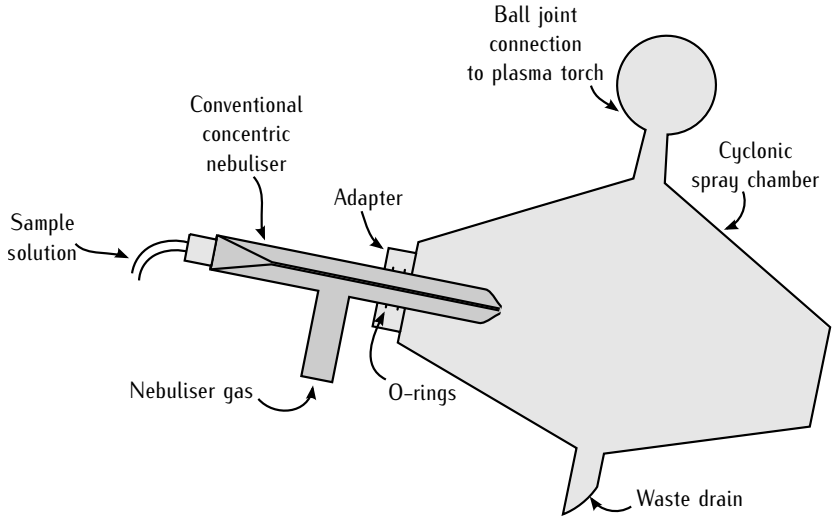


Figure 2.1. concentric nebuliser mounted on a cyclonic spray chamber.

can be described using the Sauter mean diameter ($d_s$). It is defined as the diameter of the primary aerosol droplets produced by the nebuliser whose volume-to-surface-area ratio is the mean of the distribution and it was found to be satisfactorily described by the Nukiyama-Tanasawa equation (Nukiyama and Tanasawa 1939):

$$d_s = \frac{585}{V}\left(\frac{\sigma}{\rho}\right)^{0.5} + 597\left[\frac{\eta}{(\sigma\rho)^{0.5}}\right]^{0.45}\left[\frac{10^3 Q_l}{Q_g}\right]^{1.5} \tag{2.3}$$

where $V$ is the velocity difference between the gas and liquid flows, $\sigma$ the surface tension of the liquid, $\rho$ the liquid density, $\eta$ the liquid viscosity and $Q_l$ and $Q_g$ the volume flow rates of liquid and gas, respectively.

From equation (2.3), given certain liquid characteristics, small particles can be obtained with high $V$ and $Q_g$ but small $Q_l$. As a result, in the nebuliser the interaction between gas and liquid should take place in a small region with high gas velocity and relatively low liquid velocity. Additionally, the liquid volume flow rate tend to be limited to a few hundreds of µL/min, as with these conditions, a lower amount of analyte introduced into the ICP ion-source is balanced by the higher amount of small particles and their enhanced transport efficiency.

The remaining fraction of large particles in the primary aerosol is then removed by impaction and gravitational settling using the spray chamber. Although this step is required in order to assure a stable plasma and guarantee efficient ionisation in the ICP, it leads to a drastic reduction in the sample introduction efficiency and degradation of the signal intensities and thus theoretical isotope ratio precision. The overall efficiency of the sample introduction system is generally below 3 % thus strongly limiting the instrument sensitivity and being considered the primary weakness of the technique (Browner and Boorn 1984).

A possible approach to overcome the low efficiency of the sample introduction system is to use a total consumption sample introduction system. Indeed, when working at very low liquid flow rates (a few tens of µL/min), the aerosol particle size distribution is mainly characterised by small particles and the transport efficiency is close to 100 %. An example of this kind of device is the Torch Integrated Sample Introduction System (TISIS) (Lagomarsino et al. 2007; Todolì and Mermet 2002a,b, 2003). It consists of a single-pass high-temperature evaporation chamber, with a lateral port to introduce a sheathing gas

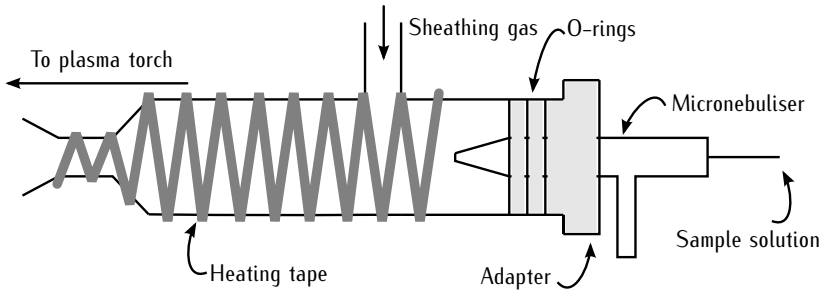


Figure 2.2. scheme of the microsample introduction system TISIS.

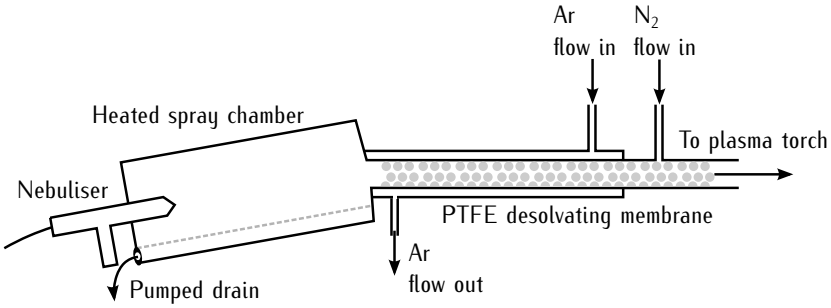


Figure 2.3. scheme of a desolvatation system (Aridus II) for the introduction of aqueous solutions in ICP-MS instruments.

stream, in a location close to the aerosol production point (figure 2.2). In this way, the aerosol solvent evaporation is enhanced and the impact of droplets against the cavity walls reduced.

The relatively high sensitivity and the very limited sample consumption of the TISIS, renders this system particularly useful for the analysis of microsamples (Grotti et al. 2008, 2013a).

An alternative approach to increase the signal intensity, and thus the instrument sensitivity and isotope ratio precision, is to increase the analyte-to-solvent ratio introduced into the ICP ion-source. This can be achieved using a desolvation system (figure 2.3). It basically consists of a tube manufactured from a semi-permeable porous membrane, around which heated Ar gas is flowing in the opposite direction to the sample aerosol flow. The solvent is vaporised and selectively leaves the central tube via the pores, carried off by the heated Ar flow (Vanhaecke and Degryse 2012).

### 2.3.3 The inductively coupled plasma ion source

The Ar ICP is a plasma ion source. The plasma is one of the four fundamental states of the matter and is defined as a gas mixture at high temperature in which ions and free electrons are present. The presence of the charged particles allows energy transfer into the plasma via induction.

The main advantage of using an ICP over other ion sources is the almost quantitative ionisation for most of the elements. Indeed the ionisation efficiency can be estimated using the Saha equation (Saha 1920):

$$K_i = \frac{n_i n_e}{n_a} = \left(\frac{2\pi m_e k T_i}{h^2}\right)^{\frac{3}{2}} \frac{2Z_i}{Z_a} e^{-\frac{E}{kT_i}} \tag{2.4}$$

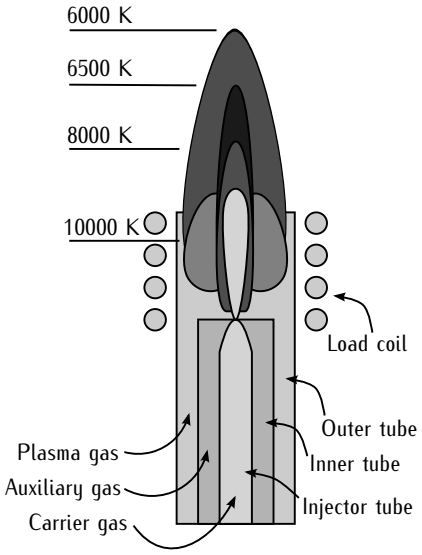


Figure 2.4. scheme of torch and ICP. Typical ionisation temperatures for different plasma regions are reported.

where $K_i$ is the ionisation equilibrium constant, $n_i$, $n_e$ and $n_a$ are the number densities of ions, electrons, and atoms, respectively, $m_e$ the mass of the electron, k the Boltzmann constant, $T_i$ the ionisation temperature, h the Planck's constant, $Z_i$ and $Z_a$ the partition functions for the ionic and atomic state, respectively, and $E$ the ionisation energy for the element considered. From $K_i$ the degree of ionisation ($\alpha$) can be deduced using the following equation:

$$\alpha = \frac{K_i}{n_e + K_i} \tag{2.5}$$

Taking into account a typical $T_i$ = 7500 K and $n_e$ = $10^{15}/cm^3$, it was computed that $\alpha \geq 0.9$ up to $E$ = 8 eV, which is the case for most of the metals; $0.3 \geq \alpha \geq 0.8$ for all the metalloids, whereas $0.01 \geq \alpha \geq 0.3$ for non-metals only (Mermet 2006).

The ionisation of the elements in the ICP is achieved by, at least, three different processes

$$Ar^+ + M \longrightarrow Ar + M^+ \tag{2.6}$$

$$M + e^- \longrightarrow M^+ + 2e^- \tag{2.7}$$

$$Ar^m + M \longrightarrow Ar + M^+ + e^- \tag{2.8}$$

In the first mechanism, the ionisation of the analyte (M) is achieved by charge transfer from $Ar^+$, an abundant species in the plasma. The second mechanism is the ionisation by electron impact in which an electron accelerated by the electromagnetic field generated in the load coil (see the text below), collides with a neutral atom of the analyte. In the collision, part of the kinetic energy of the electron is transferred to the electrons of the analyte's outer shell. If the amount of transferred energy is above the first ionisation energy of the analyte, the process produces an ion.

The third process represents the Penning ionisation. In this process, a metastable Ar atom ($Ar^m$) transfers part of its energy to the analyte, producing an ion and an electron. Metastable Ar is very abundant in the plasma and it is produced by ionisation and recombination processes:

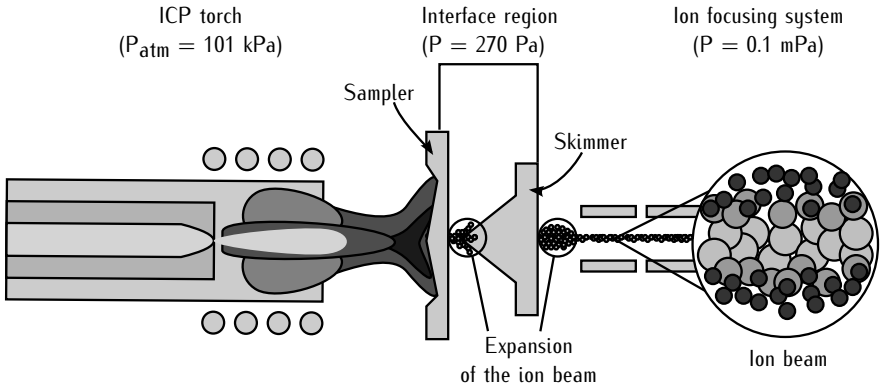


Figure 2.5. scheme of the ICP torch with the interface region and the ion focusing system. The space charge effects in the ion beam (in the magnifier glass) are strongly emphasised.

$$Ar + e^- \longrightarrow Ar^+ + 2\,e^- \tag{2.9}$$

$$Ar^+ + e^- \longrightarrow Ar^m + h^\circ \tag{2.10}$$

The ICP is generated at the end of a quartz torch, consisting of three concentric tubes, the top of which is surrounded by a water- or gas-cooled load coil (figure 2.4).

The plasma generation starts with the production of seed electrons by the Tesla generator; then a time-dependent magnetic field is obtained by sending a radio-frequency electrical current through the coil. The interaction between the magnetic field and the constant downstream flow of Ar, forces the electron to move along spiralling paths, producing other electrons through the processes described above. The plasma is then sustained as long as Ar is provided and the current is maintained in the load coil.

Once the sample aerosol is introduced into the ICP through the injector tube, the droplets are desolvated, the molecules atomised and atoms thus formed ionised.

### 2.3.4 Interface region

The ICP and the mass analyser operate under very different conditions: the first one works at atmospheric pressure and reaches an ionisation temperature of 7500 K, whereas the second one needs high-vacuum conditions (1.0–0.1 mPa). The role of the interface region is to transport the ions efficiently from the plasma to the mass spectrometer, without altering their electrical properties.

The interface consists of two (or three) water-cooled metallic cones with small orifices. The region between the two cones is maintained at ∼270 Pa with a mechanical roughing pump (figure2.5).

After the ions and electrons are generated in the ICP, they pass through the first cone (sampler cone) and, travelling to the skimmer cone, they experience an adiabatic expansion due to lower pressure in the interface region in comparison to the ICP torch. The aliquot of the plasma passing through the orifice of the second cone (skimmer cone) is expected to be slightly depleted in lighter ions as a result of the nozzle separation effect accompanying the expansion of plasma (Heumann et al. 1998). This phenomenon is one of the two resulting in the high mass discrimination experimentally observed for isotope ratios determined by ICP-MS.

The overall efficiency of the ion-transfer process from the ICP torch to the ion optics is of about 1 %. Therefore, the interface region is considered a critical part of the ICP-MS instrument.

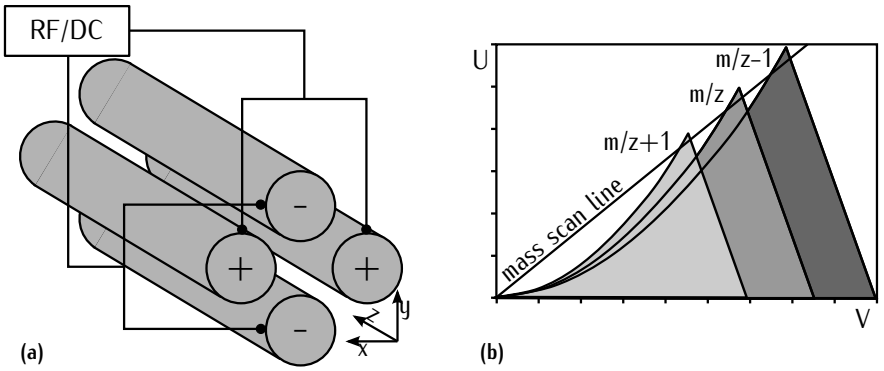


Figure 2.6. **(a)** scheme of a quadrupole mass analyser; **(b)** simplified Mathieu stability diagram of a quadrupole mass filter: the three shapes represent the stability regions for three mass-to-charge ratios, whereas the dashed line is the mass scan line performed by the quadrupole mass analyser.

Noteworthy, the electrical properties of the plasma are unaffected by the expansion and transit through the orifices, as the diameters of these are much larger than the mean free paths of ions and electrons in the conditions typical of the interface region.

### 2.3.5 Ion focusing system

Under high-vacuum conditions, the free electrons of the plasma diffuse much more rapidly than the ions so that the plasma electric neutrality is lost. The result is an ion beam of positive particles subjected to electrostatic repulsions. Due to the repulsions and the different expansion speeds for ions with different masses, the outer part of the ion beam is slightly enriched in lighter ions, whereas the inner part is dominated by heavier ions (magnifier glass in figure 2.5), resulting in preferential transmission of the latter and increasing the extent of mass discrimination.

The ion focusing system (i) counteracts the repulsion between ions, (ii) and removes photons or neutral species from the ion beam. Both these goals are achieved using electrostatic lenses with slightly different shapes and complexity depending on the commercial solutions adopted.

### 2.3.6 The quadrupole mass analyser

The final aim of every mass spectrometer is to separate different ions according to their mass-to-charge ratios ($m/z$). This is achieved using several devices based on some basic principles. In this section, only the quadrupole mass analyser will be discussed.

The quadrupole mass analyser consists of four parallel cylindrical or hyperbolic rods manufactured from, or coated by, conducting material (figure 2.6 **a**). The diametrically opposite rods are electrically connected, forming two electrode pairs. To both pairs, a voltage consisting of a DC ($U$) and an AC component ($V$) is applied. For the first pair the DC component is $+U$ and the AC component is $V\sin(\omega t)$ where $\omega$ is the angular frequency and $t$ the time.

The ions moving along the $z$ axis will be focused towards the centre of the quadrupole assembly by the DC component. A similar effect will be also observed during the positive half period of the AC component, whereas the ions will be defocused during the negative half period. Due to their high mobility, lighter ions will be removed from the beam by the AC component more efficiently than heavier ions. This pair of electrodes thus acts as a high-mass filter. The DC and AC components applied to the second pair of electrodes are $-U$ and $V\sin(\omega t + \pi)$, respectively. The average potential is now

negative so that heavier ions, less influenced by the AC component, are progressively defocused and removed from the beam. This pair of electrodes thus acts as a low-mass filter. Considering both pairs of electrodes, the quadrupole acts as a bandpass filter, so that at given $U$ and $V$ a narrow mass window (one mass unit wide) is defined.

A more quantitative approach can be obtained by solving the Mathieu function:

$$\frac{\mathrm{d}^2 u}{\mathrm{d}\,\xi^2} + [a + 2q\cos(2\xi)]u = 0 \tag{2.11}$$

where $u$ is a variable representing the position of the ion inside the quadrupole assembly and

$$\xi = \frac{t}{2} \tag{2.12}$$

$$a = \frac{4zeU}{m\omega^2 r^2} \tag{2.13}$$

$$q = \frac{2zeV}{m\omega^2 r^2} \tag{2.14}$$

with $r$ defined as the distance from the electrode surface to the $z$ axis. The result is that for each $m/z$, a well-defined stability area can be identified in the $U$,$V$ space, as shown in figure 2.6 **(b)**. In the same plot a line can be defined by a constant $2U/V$ ratio, so that for different DC and AC potentials the transit of different $m/z$ is achieved.

The time spent by the mass analyser on a single $m/z$ is called dwell time, whereas the time required by the mass analyser to move from $m/z$ to $m/z + 1$ is the settling time. In order to increase the temporal correlation between the isotopes of interest, and thus improve the internal precision, it is important to reduce the dwell time (Gray et al. 1994; Monna et al. 1998; Quétel et al. 1997). Additionally, a compromise value of the dwell time should be chosen, in order to combine fast scanning with an acceptable duty cycle.

The principal limitation of the quadrupole mass analyser is the limited resolution (±1 amu), resulting in possible spectral interferences by polyatomic and isobaric species. On the other hand, the fast scanning speed (3000 amu/s) and the relatively low purchase cost are the main advantages offered by this mass analyser.

### 2.3.7 Electron multiplier

In most of the single-collector ICP-MS devices the ion detection is carried out by an electron multiplier. In its basic principle, it is constituted by a tube coated with a semiconducting material. Typically, voltages from −2.6 to −3.0 kV are applied to the front of the multiplier, whereby ions coming from the mass analyser are attracted. The collision of the ion with the surface of the detector results in the ejection of secondary electrons. As the back of the detector is held at ground potential, secondary electrons are accelerated down the tube, producing more secondary electrons by successive collisions and resulting in a overall amplification ($10^7$–$10^8$ fold) of the initial ion signal (Prohaska et al. 2014). The electron pulses representing single incident ions are then recorded.

Nowadays, this is achieved in practice by using discrete dynodes secondary electron multipliers (SEMs). SEMs typically consist of 12 to 24 dynodes assembled into an array (figure 2.7). The dynodes are made of layered metals and are constructed in a curved shape in order to focus the electrons onto the subsequent dynode. With this approach the multiplication of the secondary electrons is more efficient, resulting in SEMs being particularly useful for the measurement of small ion currents.

The dead time ($\tau$) is the time required by an electron multiplier and its associated electronics to count and record a single pulse. During this time, which is of the order

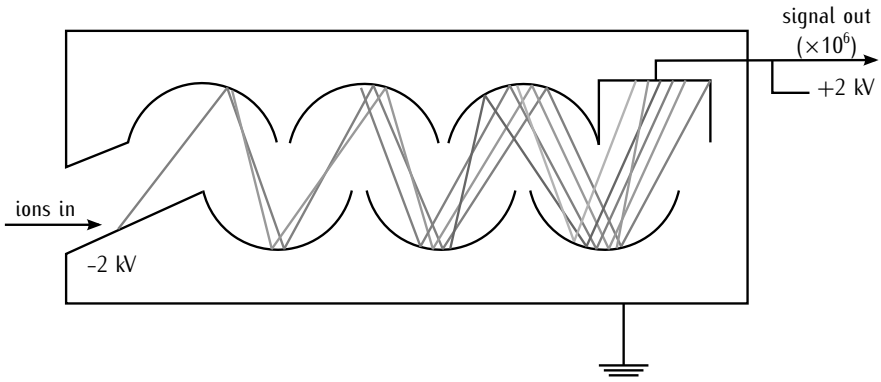


Figure 2.7. discrete dynode secondary electron multiplier.

of 5–100 ns (Vanhaecke and Degryse 2012), the detector is incapable of determining a subsequent pulse and its signal will not be counted. The fraction of ions which is not detected increases with the count rates, so that for measuring an isotope ratio differing from 1, a bias dependent on the analyte concentration is observed.

The effect of the dead time is usually corrected using the equation:

$$I_t = \frac{I_o}{1 - (I_o \tau)} \tag{2.15}$$

where $I_t$ and $I_o$ are the true and observed count rates, respectively. When the correct value is used, the measured isotope ratios are not affected by systematic variations as a function of the element concentration.

The determination of the dead time can be accomplished experimentally by the analysis of a series of standard solutions of a given element, spanning a sufficiently wide concentration range. The signal intensities are then corrected assuming different dead times and the resulting isotope ratios are calculated.

The actual dead time value can then be obtained by plotting the isotope ratios value as a function of the assumed dead time (figure 2.8 **a**) (Russ III 1989), or as a function of the element concentration (figure 2.8 **b**) (Nelms et al. 2001). In the first case $\tau$ would correspond to the intersection of the lines, whereas in the latter case the dead time value should result in a line with zero slope.

## 2.4 *Multi-collector ICP-MS*

### 2.4.1 Introduction

The first prototype MC-ICP-MS was built by VG Elemental in 1990 and provided results comparable to TIMS data for the determination of U, Pb and Sr isotope ratios (Walder and Freedman 1992). Since then, the MC-ICP-MS technique has opened up several research field previously considered intractable in earth sciences, cosmochemistry, oceanography and life sciences (Halliday et al. 1998).

In MC-ICP-MS the high ionisation efficiency of the ICP is combined with a mass spectrometer able to monitor different isotopes simultaneously. This approach permits the determination of isotope ratios with repeatability as low as 0.001 % RSD even for elements with high first-ionisation potential (Yang 2009).

The instrument is basically constituted by an ICP ion source fitted to a double focusing mass spectrometer (figure 2.9). The simultaneous detection of the signals is typically

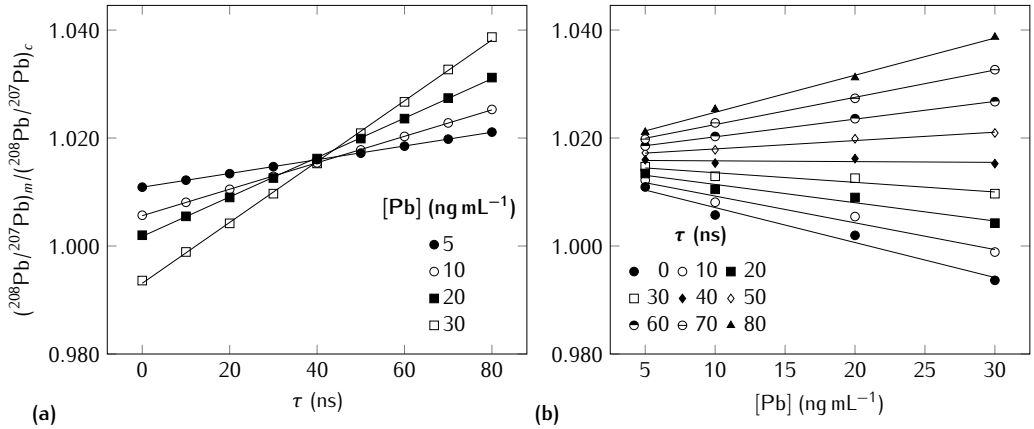


Figure 2.8. experimental determination of the dead time. **(a)** The actual dead time should be at the intersection of lines corresponding to various analyte concentration levels. **(b)** The actual dead time corresponds to a horizontal line.

accomplished by an array of Faraday cups and signals are usually monitored on flat-topped peak to further enhance the repeatability of the measurement.

In comparison with TIMS, MC-ICP-MS can provide much higher throughput and it is becoming the instrument of choice for the determination of isotope ratios of heavy elements (Albarède and Beard 2004). An additional advantage of MC-ICP-MS is the possible use of laser ablation (LA) for direct determination of precise isotope ratios in solid samples with high spatial resolution (*e.g.* Iizuka and Hirata 2005).

A major limitation of MC-ICP-MS is the presence of spectral interferences. Indeed, isotope ratio measurements typically aim to resolve very small differences in isotopic composition and are therefore, very vulnerable to such analytical artefacts (Rehkämper et al. 2001). When interferences are due to isobaric overlap with isotopes of another element, the bias can be corrected for by measuring an other isotope of the interfering element free from interferences and applying a suitable mathematical correction for the interfered isotope. Alternatively, the sample solution can be purified and the target analyte isolated by column chemistry. All sample and standard solutions to be measured are then present in the same matrix and are typically concentration-matched within 30 %. Under these conditions, matrix effects are identical for all solutions and mass discrimination can be reliably corrected for. On the other hand, if the interference is due to polyatomic species such as $^{40}Ar^{16}O^+$, which is isobaric with $^{56}Fe^+$ and very abundant in the ICP, the most elegant strategies available are based on high resolution.

When the mass difference between the analyte and the interfering species is large enough, only the part of the peak corresponding to the analyte can be monitored using a narrow entrance slit and a wide exit slit. In this way the ion signal is still measured on a flat-topped peak and the interference is filtered out (Vanhaecke and Moens 2003; Weyer and Schwieters 2003).

Other robust approaches consist of the use of a cell pressurised with a collision gas in order to dissociate the polyatomic species (Beard et al. 2003), or in using an instrument with a large mass dispersion that can provide both high mass resolution for multiple Faraday cups and the flat-topped peaks necessary for high-precision isotopic measurements (Williams et al. 2005).

In the following sections, the mass analyser and the multi-collection system will be described in some detail, as they are the main characterising components of an MC-ICP-MS instrument.

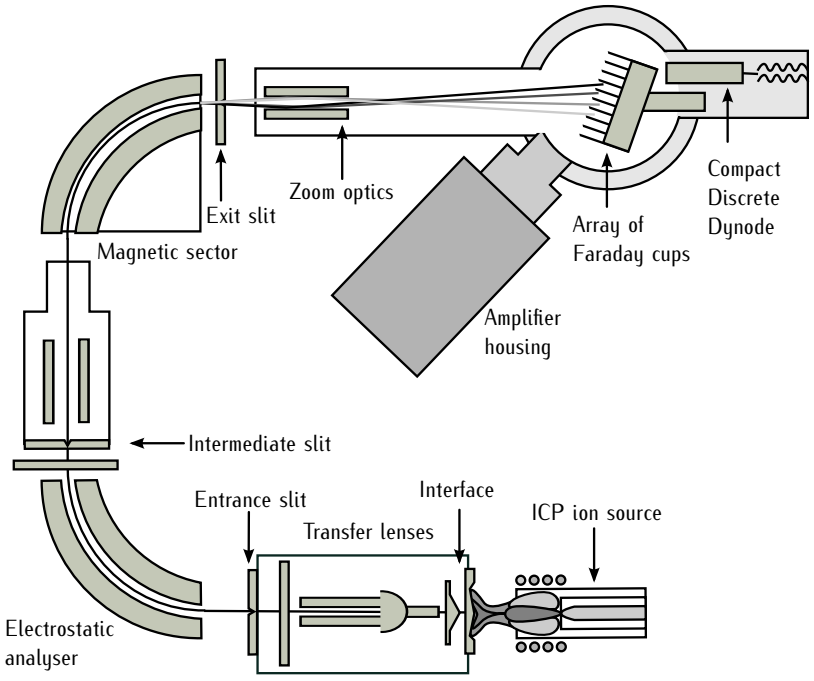


Figure 2.9. scheme of a multi-collector ICP-MS instrument (Neptune by Thermo Scientific).

### 2.4.2 The mass analyser

In magnetic sectors, ions are separated from one other in space depending on their momentum ($p = mv$, where $v$ is the velocity for an ion) and charge ($q = z\mathrm{e}$, where e is the charge of the electron) following the equation:

$$r = \frac{mv}{z\mathrm{e}B} \tag{2.16}$$

so that for a given magnetic field $B$ perpendicular to the ion motion, ions with different $m/z$ , but same velocity, will move along circular paths of different radii $r$.

Ions extracted from the ICP have a relatively wide range of kinetic energies resulting from their thermal energy spread and the plasma potential. Self-evidently, the spread in kinetic energies results in different ion velocities, so that a single sector field cannot provide high resolution for ions produced by an ICP. On the other hand, TIMS instruments produce ions with a narrow range of kinetic energies so that a magnetic sector suffices.

In ICP-MS instruments, the magnetic sector has to be combined with an electrostatic sector to provide high mass resolution. The result is a double-focusing setup. As the ions move between the positively and negatively charged bent plates of the electrostatic sector, they are forced to move along a circular path. For singly charged ions, the radius of the path is determined by their kinetic energy ($E_\mathrm{k}$) and the electrical field applied ($E$), following the equation:

$$r = \frac{2E_\mathrm{k}}{z\mathrm{e}E} \tag{2.17}$$

when a plate with a narrow slit is placed behind the electrostatic analyser, only ions with energies within an acceptable range are transmitted, whereas ions showing either too high or too low energies are removed from the beam (Vanhaecke and Degryse 2012).

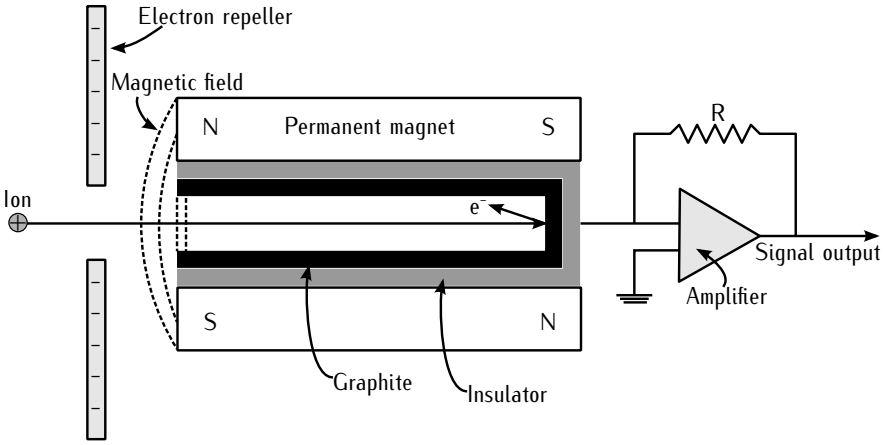


Figure 2.10. schematic diagram of a Faraday cup and its amplifier circuit.

With this approach, narrowing the slit corresponds to increasing the resolution but also to lowering the transmission efficiency and hence instrument sensitivity.

In double-focusing setups the dispersion created by the first sector is exactly compensated for by the other sector. Consequently, a wider intermediate slit aperture can be used, preserving both high mass resolution and beam transmission efficiency.

In multi-collector devices, the different isotopes must reach the detector assembly separated in space, therefore ions extracted from the ICP enter the electrostatic analyser *before* the magnetic sector. This arrangement is known as Nier-Johnson geometry and permits the double focusing of ions within a mass range from $m$ to 1.3 $m$. For isotopes meeting this requisite, their ion signals can be monitored in static conditions, without the need to vary either the magnetic field ($B$-scanning), or the electrostatic field ($E$-scanning). Under static conditions, the total time for the analysis is divided between baseline and peak measurement. The first is usually carried out at the beginning of the analysis monitoring by the signal at both sides of the peaks of interest, whereas the remaining time is then spent to continuously acquire the signals for the peaks (Gill 2014).

Measurements on flat-topped peaks, free of interferences and using static conditions are mandatory requirements to obtain high precision isotope ratios using MC-ICP-MS.

### 2.4.3 The multi-collector assembly

The simultaneous measurement of the different $m/z$ ratios is carried out by an array of detectors. The position of each detector on the array is adjusted via motorised stages with a precision better than a few micrometers, ensuring the accommodation of several isotopic systems and the sampling of a signal free of interference.

The most used detector in multi-collector instruments is the Faraday cup. Despite being less sensitive and displaying a slower response in comparison to electron multipliers, Faraday cups offer a number of advantages:

- the measured and amplified ion currents are proportional to the number of ions;
- there is no significant mass discrimination caused by differences in the mass of entering ions;
- the response of this detector is constant over a long period of time;
- the ionic current is continuously measured, thus no correction for the dead time is required.

In practice a Faraday cup is a relatively deep bucket machined from a graphite sheet (figure 2.10). When the ions impinge the internal surface of the cup their charge is neutralised by electrons flowing from the ground through a high-ohmic resistor, and the potential difference thus created is measured.

In order to measure a current which is finely proportional to the number of ions impinging the cup, it is necessary that no charges produced inside the cup (electrons and secondary ions) leave the bucket before being measured. This is achieved in practice by a combination of different approaches. The use of graphite for the internal surface of the cup is very important, as carbon produces very few positive secondary ions but significantly more negative secondary ions. As a consequence, the use of a negatively charged repeller placed over the detector aperture can avoid them from being lost (Vanhaecke and Degryse 2012). The use of small permanent magnets further minimise the escape of secondary electrons and prevent free electrons, coming from other sections of the instruments, to collide with the inner surface of bucket (Prohaska et al. 2014).

The Faraday cup is then connected to a current amplifier with high-ohmic feedback resistors housed in an evacuated and temperature stabilised environment. Under these conditions, the main source of noise is the random thermal motion of electrons inside the resistors, so-called Johnson noise (Vanhaecke and Degryse 2012). The magnitude of the Johnson noise ($\Delta V$) is given by the equation:

$$\Delta V = \sqrt{\frac{4\mathrm{k}RT}{t}} \tag{2.18}$$

where k is the Boltzmann's constant, $R$ is the value of the resistor, $T$ is the temperature and $t$ the integration time of the measurement. Self-evidently the noise magnitude scales with the square root of the integration time, so that quadrupling the measurement time will result in half of the noise. Concerning the effect of the feedback resistor, increasing $R$ from $10^{10}$ to $10^{12}\,\Omega$, will result in a 10-fold increase of the noise. However, the gain of the amplifier increases linearly with $R$, resulting in a 100-fold enhanced signal. The overall signal-to-noise will be improved 10-fold. For this reasons higher values of feedback resistors are particularly suitable for measuring low signal intensities.

The sensitivity of the instrument can be further extended by using electron multipliers instead of Faraday cups. However, under these conditions, counting statistics and dead time can significantly limit the precision and accuracy of the measured isotope ratio values.

*References*

Albarède, F. and Beard, B., 2004. Analytical methods for non-traditional isotopes. *Reviews in Mineralogy and Geochemistry*, **55**, 113–152. DOI: 10.2138/gsrmg.55.1.113

Baker, J., Peate, D., Waight, T., and Meyzen, C., 2004. Pb isotopic analysis of standards and samples using a $^{207}$Pb-$^{204}$Pb double spike and thallium to correct for mass bias with a double-focusing MC-ICP-MS. *Chemical Geology*, **211**, 275–303. DOI: 10.1016/j.chemgeo.2004.06.030

Bandura, D. R., Baranov, V. I., and Tanner, S. D., 2000. Effect of collisional damping and reactions in a dynamic reaction cell on the precision of isotope ratio measurements. *Journal of Analytical Atomic Spectrometry*, **15**, 921–928. DOI: 10.1039/B000285M

Baxter, D. C., Rodushkin, I., Engström, E., and Malinovsky, D., 2006. Revised exponential model for mass bias correction using an internal standard for isotope abundance ratio measurements by multi-collector inductively coupled plasma mass spectrometry. *Journal of Analytical Atomic Spectrometry*, **21**, 427–430. DOI: 10.1039/b517457k

Beard, B., Johnson, C. M., Skulan, J. L., Nealson, K. H., Cox, L., and Sun, H., 2003. Application of Fe isotopes to tracing the geochemical and biological cycling of Fe. *Chemical Geology*, Isotopic records of microbially mediated processes **195**, 87–117. DOI: 10.1016/S0009-2541(02)00390-X

BIPM, 2012. International Vocabulary of Metrology - Basic and general concept and associated terms (VIM)

Browner, R. F. and Boorn, A. W., 1984. Sample Introduction: The Achilles' Heel of Atomic Spectroscopy? *Analytical Chemistry*, **56**, 786A–798A. DOI: 10.1021/ac00271a718

Ehrlich, S., Gavrieli, I., Dor, L.-B., and Halicz, L., 2001. Direct high-precision measurements of the $^{87}Sr/^{86}Sr$ isotope ratio in natural water, carbonates and related materials by multiple collector inductively coupled plasma mass spectrometry (MC-ICP-MS). *Journal of Analytical Atomic Spectrometry*, **16**, 1389–1392. DOI: 10.1039/B107996B

Gallon, C., Aggarwal, J., and Flegal, A. R., 2008. Comparison of mass discrimination correction methods and sample introduction systems for the determination of lead isotopic composition using a Multicollector Inductively Coupled Plasma Mass Spectrometer. *Analytical Chemistry*, **80**, 8355–8363. DOI: 10.1021/ac800554k

Gill, R., 2014. *Modern Analytical Geochemistry: An Introduction to Quantitative Chemical Analysis Techniques for Earth, Environmental and Materials Scientists*. Routledge. 342 pp.

Gray, A. L., Williams, J. G., Ince, A. T., and Liezers, M., 1994. Communication. Noise sources in inductively coupled plasma mass spectrometry: an investigation of their importance to the precision of isotope ratio measurements. *Journal of Analytical Atomic Spectrometry*, **9**, 1179–1181. DOI: 10.1039/ja9940901179

Grotti, M., Soggia, F., and Luis Todolì, J.-L., 2008. Ultratrace analysis of Antarctic snow samples by reaction cell inductively coupled plasma mass spectrometry using a total-consumption micro-sample-introduction system. *Analyst*, **133**, 1388–1394. DOI: 10.1039/b804043e

Grotti, M., Ardini, F., and Todolì, J.-L., 2013a. Total introduction of microsamples in inductively coupled plasma mass spectrometry by high-temperature evaporation chamber with a sheathing gas stream. *Analytica Chimica Acta*, **767**, 14–20. DOI: 10.1016/j.aca.2013.01.017

Halliday, A. N., Lee, D.-C., Christensen, J. N., Rehkämper, M., Yi, W., Luo, X., Hall, C. M., Ballentine, C. J., Pettke, T., and Stirling, C., 1998. Applications of Multiple Collector-ICPMS to cosmochemistry, geochemistry, and paleoceanography. *Geochimica et Cosmochimica Acta*, **62**, 919–940. DOI: 10.1016/S0016-7037(98)00057-X

Heumann, K. G., Gallus, S. M., Rädlinger, G., and Vogl, J., 1998. Precision and accuracy in isotope ratio measurements by plasma source mass spectrometry. *Journal of Analytical Atomic Spectrometry*, **13**, 1001–1008. DOI: 10.1039/A801965G

Iizuka, T. and Hirata, T., 2005. Improvements of precision and accuracy in in situ Hf isotope microanalysis of zircon using the laser ablation-MC-ICPMS technique. *Chemical Geology*, **220**, 121–137. DOI: 10.1016/j.chemgeo.2005.03.010

Krachler, M., Le Roux, G., Kober, B., and Shotyk, W., 2004. Optimising accuracy and precision of lead isotope measurement ($^{206}Pb$, $^{207}Pb$, $^{208}Pb$) in acid digests of peat with ICP-SMS using individual mass discrimination correction. *Journal of Analytical Atomic Spectrometry*, **19**, 354–361. DOI: 10.1039/b314956k

Lagomarsino, C., Grotti, M., Todolì, J.-L., and Mermet, J.-M., 2007. Study of the absence of recondensation with low liquid delivery rates by using a cavity sheathing gas in inductively coupled plasma-atomic emission spectrometry. *Journal of Analytical Atomic Spectrometry*, **22**, 523. DOI: 10.1039/b618487a

Longerich, H. P., Fryer, B. J., and Strong, D. F., 1987. Determination of lead isotope ratios by inductively coupled plasma-mass spectrometry (ICP-MS). *Spectrochimica Acta, Part B: Atomic Spectroscopy*, **42**, 39–48. DOI: 10.1016/0584-8547(87)80048-4

Maréchal, C. N., Télouk, P., and Albarède, F., 1999. Precise analysis of copper and zinc isotopic compositions by plasma-source mass spectrometry. *Chemical Geology*, **156**, 251–273. DOI: 10.1016/S0009-2541(98)00191-0

Mermet, J.-M., 2006. Fundamental Principles of Inductively Coupled Plasmas. *Inductively Coupled Plasma Spectrometry and its Applications*. Ed. by Hill, S. J. Blackwell Publishing Ltd, 27–60

Monna, F., Loizeau, J.-L., Thomas, B. A., Guéguen, C., and Favarger, P.-Y., 1998. Pb and Sr isotope measurements by inductively coupled plasma–mass spectrometer: efficient time management for precision improvement. *Spectrochimica Acta, Part B: Atomic Spectroscopy*, **53**, 1317–1333. DOI: 10.1016/S0584-8547(98)00164-5

Nelms, S. M., Quétel, C. R., Prohaska, T., Vogl, J., and Taylor, P. D. P., 2001. Evaluation of detector dead time calculation models for ICP-MS. *Journal of Analytical Atomic Spectrometry*, **16**, 333–338. DOI: 10.1039/b007913h

Nukiyama, S. and Tanasawa, Y., 1939. Experiments on the atomization of liquids in an air stream. *Japanese Society of Mechanical Engineering*, **5**, 68–75

Prohaska, T., Irrgeher, J., Zitek, A., and Jakubowski, N., 2014. *Sector Field Mass Spectometry for Elemental and Isotopic Analysis*. Royal Society of Chemistry. 666 pp.

Quétel, C. R., Thomas, B., Donard, O. F., and Grousset, F. E., 1997. Factorial optimization of data acquisition factors for lead isotope ratio determination by inductively coupled plasma mass spectrometry. *Spectrochimica Acta, Part B: Atomic Spectroscopy*, **52**, 177–187. DOI: 10.1016/S0584-8547(96)01587-X

Rehkämper, M. and Halliday, A. N., 1998. Accuracy and long-term reproducibility of lead isotopic measurements by multiple-collector inductively coupled plasma mass spectrometry using an external method for correction of mass discrimination. *International Journal of Mass Spectrometry*, **181**, 123–133. DOI: 10.1016/S1387-3806(98)14170-2

Rehkämper, M., Schönbächler, M., and Stirling, C. H., 2001. Multiple Collector ICP-MS: introduction to instrumentation, measurement techniques and analytical capabilities. *Geostandards Newsletter: The Journal of Geostandards and Geoanalysis*, **25**, 23–40. DOI: 10.1111/j.1751-908X.2001.tb00785.x

Rudge, J. F., Reynolds, B. C., and Bourdon, B., 2009. The double spike toolbox. *Chemical Geology*, **265**, 420–431. DOI: 10.1016/j.chemgeo.2009.05.010

Russ III, G. P., 1989. Isotope ratio measurements using ICP-MS. *Applications of inductively coupled plasma mass spectrometry*

Saha, M. N., 1920. Ionization in the solar chromosphere. *Philosophical Magazine A*, **40**, 472–488. DOI: 10.1080/14786441008636148

Todolì, J.-L. and Mermet, J.-M., 2002a. New torch design with an in-built chamber for liquid sample analysis by ICP-AES. *Journal of Analytical Atomic Spectrometry*, **17**, 345–351. DOI: 10.1039/b111416f

Todolì, J.-L. and Mermet, J.-M., 2002b. Study of matrix effects using an adjustable chamber volume in a torch-integrated sample introduction system (TISIS) in ICP-AES. *Journal of Analytical Atomic Spectrometry*, **17**, 913–921. DOI: 10.1039/b201881k

Todolì, J.-L. and Mermet, J.-M., 2003. Optimization of the evaporation cavity in a torch integrated sample introduction system based ICP-AES system. Applications to matrix and transient effects, analysis of microsamples and analysis of certified solid samples. *Journal of Analytical Atomic Spectrometry*, **18**, 1185–1191. DOI: 10.1039/b212698b

Vanhaecke, F., Moens, L., Dams, R., and Taylor, P., 1996. Precise seasurement of isotope ratios with a double-focusing magnetic sector ICP mass spectrometer. *Analytical Chemistry*, **68**, 567–569. DOI: 10.1021/ac9507247

Vanhaecke, F., Moens, L., Dams, R., Allen, L., and Georgitis, S., 1999. Evaluation of the isotope ratio performance of an axial time-of-flight ICP mass spectrometer. *Analytical Chemistry*, **71**, 3297–3303. DOI: 10.1021/ac990016b

Vanhaecke, F., Balcaen, L., Deconinck, I., De Schrijver, I., Marisa Almeida, C., and Moens, L., 2003. Mass discrimination in dynamic reaction cell (DRC)-ICP-mass spectrometry. *Journal of Analytical Atomic Spectrometry*, **18**, 1060–1065. DOI: 10.1039/b303528j

Vanhaecke, F. and Moens, L., 2003. Overcoming spectral overlap in isotopic analysis via single- and multi-collector ICP–mass spectrometry. *Analytical and Bioanalytical Chemistry*, **378**, 232–240. DOI: 10.1007/s00216-003-2175-8

Vanhaecke, F. and Degryse, P., 2012. *Isotopic Analysis: Fundamentals and Applications Using ICP-MS*. Wiley

Walder, A. J. and Freedman, P. A., 1992. Communication. Isotopic ratio measurement using a double focusing magnetic sector mass analyser with an inductively coupled plasma as an ion source. *Journal of Analytical Atomic Spectrometry*, **7**, 571–575. DOI: 10.1039/JA9920700571

Weyer, S. and Schwieters, J. B., 2003. High precision Fe isotope measurements with high mass resolution MC-ICPMS. *International Journal of Mass Spectrometry*, **226**, 355–368. DOI: 10.1016/S1387-3806(03)00078-2

White, W. M., Albarède, F., and Télouk, P., 2000. High-precision analysis of Pb isotope ratios by multi-collector ICP-MS. *Chemical Geology*, **167**, 257–270. DOI: 10.1016/S0009-2541(99)00182-5

Williams, H. M., Peslier, A. H., McCammon, C., Halliday, A. N., Levasseur, S., Teutsch, N., and Burg, J.-P., 2005. Systematic iron isotope variations in mantle rocks and minerals: The effects of partial melting and oxygen fugacity. *Earth and Planetary Science Letters*, **235**, 435–452. DOI: 10.1016/j.epsl.2005.04.020

Woodhead, J., 2002. A simple method for obtaining highly accurate Pb isotope data by MC-ICP-MS. *Journal of Analytical Atomic Spectrometry*, **17**, 1381–1385. DOI: 10.1039/b205045e

Yang, L., 2009. Accurate and precise determination of isotopic ratios by MC-ICP-MS: A review. *Mass Spectrometry Reviews*, **28**, 990–1011. DOI: 10.1002/mas.20251

# 3 Determination of Pb isotope ratios in environmental matrices by single-collector ICP-MS

## 3.1 *Introduction*

In order to obtain information on the provenance of Pb in a large number of environmental samples, a method for the determination of Pb isotope ratios by quadrupole ICP-MS was developed.

As already mentioned in section 2.3, quadrupole-based ICP-MS is only capable of sequential acquisition of the signals for the monitored isotopes. As a result, the fluctuations of the ion density in the beam extracted from the ICP may limit the achievable precision to values above 0.10 % RSD. However, for instruments equipped with a collision/reaction cell, this value can be lowered to 0.05 % by method optimisation and collisional damping (section 2.1).

Under these conditions, the internal precision is limited by the counting statistics and hence by the number of counts detected. This constitutes a problem for the analysis of samples with low Pb concentrations, such as those collected in pristine areas. The insufficient sample volume (*e.g.* snow, brine, pore water) may constitute a further problem, due to the long acquisition time usually required for the isotope ratio measurements. In this case, reduction of the sample uptake rate or sample dilution would result in a degradation of the signal intensity and, hence, of the internal precision.

Minimization of the sample consumption without a significant decrease in sensitivity can be obtained using the micro-sample introduction system TISIS (section 2.3.2).

The aim of this chapter was thus to optimize the measurement of Pb isotope ratios in environmental matrices using ICP-MS at low sample consumption rates. In particular, two micro-sample introduction systems were evaluated: the PFA micro-nebuliser working at 150 µL/min, mounted onto a low-volume spray chamber, and the total-consumption sample introduction system TISIS, working at 20 µL/min.

The study was performed according to the empirical modelling and experimental design concepts (Box et al. 2005), in order to maximize the information and take into account the possible interactions between the instrumental parameters. Then, the optimised method was validated and applied to several environmental samples collected from polar regions, including atmospheric aerosol, marine particulate, sediment and snow samples with a very low Pb content (20–30 pg/g).

## 3.2 *Experimental*

### 3.2.1 Instrumentation

The ICP-MS system used was a PerkinElmer (Waltham, MA, USA) Elan DRC II. The instrument is equipped with the dynamic reaction cell (DRC) (Tanner and Baranov 1999), which consists of a bandpass quadrupole, located in a reaction chamber situated between

the single lens ion optics and the analyser quadrupole. When operated in standard mode, no gas is added and the reaction cell is evacuated through additional apertures (cell vent). The quadrupole inside the dynamic reaction cell then acts as an RF-only ion guide. In the DRC mode, the cell vent is closed and the chamber is pressurized with a suitable reaction gas through a transfer line. The reaction gas flow rate is regulated using a mass-flow controller. A potential bias is applied to the entrance and exit aperture (Cell Path Voltage, CPV), the reaction cell quadrupole rods (Cell Rod Offset, CRO) and the analyser quadrupole rods (Quadrupole Rod Offset, QRO). An additional axial field (AFT) (Bandura et al. 2002) can be applied to the reaction cell, which constantly accelerates the ions towards the exit aperture of the cell.

The main operating parameters are summarised in tables 3.1 and 3.2. Two sample introduction systems were considered: (i) a PFA-ST micro-concentric pneumatic nebuliser (Elemental Scientific, Omaha, NE, USA) mounted onto a cinnabar spray chamber (Glass Expansion, Melbourne, Australia) and (ii) the total-consumption micro-sample-introduction system TISIS, used under the operating conditions previously optimized for ICP-MS analyses (Grotti et al. 2013a). The detector dead time and its uncertainty were measured every two weeks according to the methods reported in section 2.3.7, obtaining a value of $52 \pm 4$ ns.

### 3.2.2 Reagents and material

Ultrapure water was obtained from the Milli-Q four-column ion-exchange system fed by the reverse osmosis system Elix 3, both from Millipore (El Paso, TX, USA). Suprapur 65 % nitric acid from Merck (Darmstadt, Germany) was used for the cleaning of materials, while Trace Select Ultra 65 % nitric acid from Sigma-Aldrich (St. Louis, MO, USA) was used for the final stage of the cleaning procedure of materials and for the preparation of standards and samples. Suprapur 30 % hydrogen peroxide, Suprapur 40% hydrofluoric acid and Suprapur 99.9999 % boric acid from Merck were used for the sample digestion procedures. Materials for sample collection and treatment, and the cleaning procedures have been previously described (Grotti et al. 2001, 2008).

1000 µg/mL single-element standard solutions for the interference study were prepared using the following reagent-grade quality oxides: La, Pr, Sm, Gd, Tb, Dy, Ho, Er and Yb from the American Potash & Chemical Corporation (West Chicago, ILL, USA); Nd from BDH (London, UK); Eu from Sigma-Aldrich and Tm from Janssen (Beerse, Belgium). In addition, 1000 µg/mL standard solutions were purchased from Sigma-Aldrich (Ce and Lu) and Janssen (Ir).

Ammonia gas (99.9995 %) from Siad (Bergamo, Italy) was used as the damping gas.

### 3.2.3 Standard reference materials

The Pb isotopic reference material SRM 981 from NIST (Gaithersburg, MD, USA) was used to compute the instrumental mass discrimination and to determine the detector dead time. The stock solution was prepared by dissolving 0.6 g (±0.1 mg) of the Pb wire with 10 mL of nitric acid in a pre-cleaned 50 mL volumetric flask and filling it to the mark with ultrapure water. Finally, the stock solution was transferred into an acid-cleaned 50 mL PP graduated conical test tube (Kartell, Milan, Italy) and stored at 4 °C.

Daily standards (0.5–50 ng/mL) were prepared by serial dilution of the stock solution with 0.1 % nitric acid.

The lichen reference material CRM 482 provided from IRMM (Geel, Belgium) with reference values for Pb isotope ratios by Cloquet et al. (2006) and De Muynck et al. (2008) was used for the method validation. The sample was digested as described in the papers cited above, and diluted to a final Pb concentration of about 10 ng/mL.

Table 3.1. instrumental characteristics and operating parameters used for the determination of Pb isotope ratio measurements by ICP-MS.

| Instrument | PerkinElmer-Sciex Elan DRC II |
|---|---|
| Sample introduction system I | |
| Nebuliser | PFA-ST micro-concentric |
| Spray chamber | Mini-cyclonic (inner volume: 20 mL) |
| Nebuliser gas flow rate | 1.02 L/min |
| Sample uptake rate | 150 µL/min |
| Sample introduction system II | TISIS |
| Nebuliser | PFA-ST micro-concentric |
| Evaporation chamber | Single pass |
| Chamber temperature | 150 °C |
| Nebuliser gas flow rate | 0.70 L/min |
| Sheathing gas flow rate | 0.35 L/min |
| Sample uptake rate | 20 µL/min |
| Plasma source | Free-running (nominal 40 MHz) ICP |
| RF power | 1500 W |
| Plasma gas flow rate | 14.5 L/min |
| Auxiliary gas flow rate | 1.65 L/min |
| Interface | |
| Sampler | 1.1 mm diameter Pt |
| Skimmer | 0.9 mm diameter Pt |
| Ion optics | Stop disk and single cylinder lens |
| Lens voltage | 11.8 V |
| Detector | Dual analog/digital discrete dynode electron multiplier |
| Analog stage voltage | −2250 V |
| Pulse stage voltage | 1250 V |
| Signal measurement | |
| Acquisition mode | Peak-hopping |
| Integration time | 10 s |
| Replicates | 10 |
| Nuclides monitored | $^{206}$Pb, $^{207}$Pb, $^{208}$Pb |

Table 3.2. variation ranges and optimal values of the investigated parameters for Pb isotope ratio measurements by ICP-MS.

| Parameter | Minimum | Maximum | Optimal |
|---|---|---|---|
| Cell path voltage (V) | −40 | −20 | −35 |
| Reaction cell rod offset (V) | −5 | 2 | 2 |
| Quadrupole rod offset (V) | −10 | 0 | −6 |
| Axial field voltage (V) | −400 | 400 | 0 |
| $NH_3$ flow rate (mL/min) | 0.10 | 0.40 | 0.10 |
| RPq | 0.05 | 0.70 | 0.05 |
| Sweeps | 100 | 1000 | 1000 |
| Dwell time (ms) | 1 | 10 | 1 |
| Settling time (ms) | 0.2 | 4.0 | 0.2 |

### 3.2.4 Sample collection and analysis

*Atmospheric particulate.* Size-fractionated aerosol samples were collected at Terra Nova Bay (Northern Victoria Land, Antarctica) from November 2010 to January 2011, with 10 days resolution, using a Tisch (Cleves, OH, USA) TE-6070V-BL sampler, equipped with a Tisch TE 235 six-stage cascade impactor (cut-off at 10.0, 3.0, 1.5, 0.95 and 0.49 µm). The sampler was provided with cellulose filters (Whatman 41) and operated at a flow rate of 1130 L/min. After the sampling, the filters were placed in acid-cleaned plastic Petri dishes, sealed in double polyethylene bags and stored at −20 °C until analysis.

Sub-samples (⅛ of each filter) were transferred into the acid-cleaned Teflon vessels of the MARS-5 microwave-assisted digestion system (CEM, Matthews, NC, USA) and 5 mL of nitric acid, 2 mL of hydrogen peroxide, 2 mL of ultrapure water and 1 mL of hydrofluoric acid were added. Digestion was conducted for 50 min at 220 °C. After cooling, 5 mL of saturated boric acid solution (3 g in 50 mL) were added and the heating program repeated for 20 min. Finally, the samples were transferred into 15 mL PP graduated tubes and analysed by ICP-MS for Pb content and Pb isotope ratios.

$PM_{10}$ sampling at Ny-Ålesund (Svalbard islands, Norwegian Arctic) was carried out from April to September 2012, with 4 days resolution, using a Tecora (Paris, France) ECHO PM sampler, equipped with Teflon filters and operated at a flow rate of 200 L/min. After the sampling, the filters were placed in acid-cleaned plastic Petri dishes, sealed in double polyethylene bags and stored at −20 °C until analysis.

Sub-samples (¼ of each filter) were dissolved with 2 mL of nitric acid and 0.5 mL of hydrogen peroxide, using the MARS-5 microwave-assisted digestion system. Digestion was conducted according to the current legislation of the European Community in the field of air quality monitoring (UNI 14902 2005). Digested samples were then diluted to 10 mL with ultrapure water and analysed by ICP-MS.

*Snow.* Antarctic snow samples were collected at Terra Nova Bay during the Austral summer 2010/2011. In order to prevent contamination during sampling, operators wore clean room garment and approached the sampling site upwind. The samples were collected in acid-cleaned 50 mL PP graduated tubes (Kartell), sealed inside double polyethylene bags and stored at −20 °C until analysis. Following a previously developed procedure (Grotti et al. 2008), 12 samples were allowed to melt under a laminar flow hood. Subsequently, 20 mL aliquots were transferred into acid-cleaned 50 mL PP graduated tubes, acidified with 100 µL of nitric acid and refrozen. Then, the samples were freeze-dried, re-dissolved in 200 µL of 0.05 % nitric acid solution and analysed by ICP-MS.

*Marine particulate and sediment.* Suspended particulate matter (SPM) and sediment samples were collected in Kongsfiorden (Svalbard islands) during the summer 2011. Seawater samples were collected aboard the oceanographic boat Teisten (Kings Bay AS, Norway) by using 10 L Niskin bottles. SPM was obtained by filtration through 0.4 µm polycarbonate filters (Millipore, 47 mm diameter), as previously reported (Grotti et al. 2001). The filters were placed in plastic Petri dishes, sealed in double polyethylene bags and stored at −20 °C until analysis. Sediment samples were collected using a stainless steel Van Veen grab, placed in polycarbonate containers and stored at −20 °C until analysis. The sediment samples were sieved at <63 µm, oven-dried at 40 °C and homogenized with an automatic agate grinder. Filters with SPM and sediment sub-samples (ca. 100 mg) were dissolved following the same procedure as for the atmospheric particulate collected at Ny-Ålesund and analysed by ICP-MS. Digests from sediment samples were filtered through 0.45 µm Teflon filters and ten-fold diluted with ultrapure water prior to the analysis.

### 3.2.5 Data processing

In the optimization study, Placket–Burman and central composite designs were sequentially applied, allowing the estimation of linear effects, quadratic effects and two-term interactions. Multiple linear regression analysis was performed using the free software environment for statistical computing and graphics R (R Core Team 2015). The models were validated by applying the leave-one-out cross-validation procedure and by performing a 15-points validation set.

## 3.3 *Results and discussion*

### 3.3.1 Optimisation of the instrumental parameters

Several instrumental parameters may affect the precision and accuracy of the Pb isotope ratio measurements by ICP-DRC-MS, likely in a complex inter-related way. Therefore, the optimisation study was performed according to the empirical modelling and experimental design approach (using the system I).

The variables investigated, their variation range and the optimal values obtained are reported in table 3.2. The quadrupole rod offset (QRO), cell rod offset (CRO), ammonia flow rate and the Mathieu stability parameter of the cell's quadrupole (RPq) significantly affected the measurement at the 95 % probability level. The combined effects of the QRO, CRO and ammonia flow rate on the internal precision (RSD) and the systematic error (departure from the certified value, as $\delta$‰) of $^{208}Pb/^{207}Pb$ data are illustrated in figure 3.1 (similar results were obtained for $^{206}Pb/^{207}Pb$, but are not reported). The CRO showed a negative effect on RSD, meaning that an increase of this parameter improves the precision. Moreover, a significant interaction between CRO and QRO was found, meaning that the precision can be further improved using a low value of QRO along with a high value of CRO (and *vice versa*). Finally, the damping gas flow rate displayed a positive linear effect on RSD and a significant interaction with QRO.

Remembering the dependence of the counting statistics limit of the precision on the signal intensity, a possible explanation for the observed effects can be obtained. QRO acts as a potential barrier at the entrance of the analyser quadrupole, thus affecting the ion transmission efficiency. Therefore, a decrease of this parameter towards negative values improves the ion intensity and, hence, the achievable precision. A positive CRO value focuses the ions onto the cell's longitudinal axis, thus preserving their kinetic energy and improving the ion transmission. Consequently, precision is improved by increasing the CRO voltage, as observed in this study. Moreover, according to this explanation, it is expected that the beneficial effect of CRO on the precision increases with increasing QRO value and that the detrimental effect of QRO may be mitigated by an increase in the CRO voltage. Hence, the mutual interaction between these parameters.

In this context, also the effect of the damping gas and its interaction with QRO can be explained. In fact, by increasing the gas flow rate, the ion kinetic energy decreases, due to collisions with the gas molecules, reducing the ion transmission efficiency. Again, the effect is expected to increase with increasing QRO voltage (*i.e.* the energy required to enter into the analyser quadrupole) that would explain the significant interaction between the ammonia flow rate and the QRO. This explanation was also supported by the results obtained for the systematic error (figure 3.1 **b**). In fact, an increase of the ion kinetic energy reduces the residence time of the ions within the cell, thus decreasing the space-charge effects. Accordingly, the systematic error decreased by lowering the gas flow rate and the QRO voltage.

Concerning RPq, the best precision was achieved by setting this parameter at 0.05, that it is lower than that usually applied (0.6 in DRC mode, according to Tanner et al.

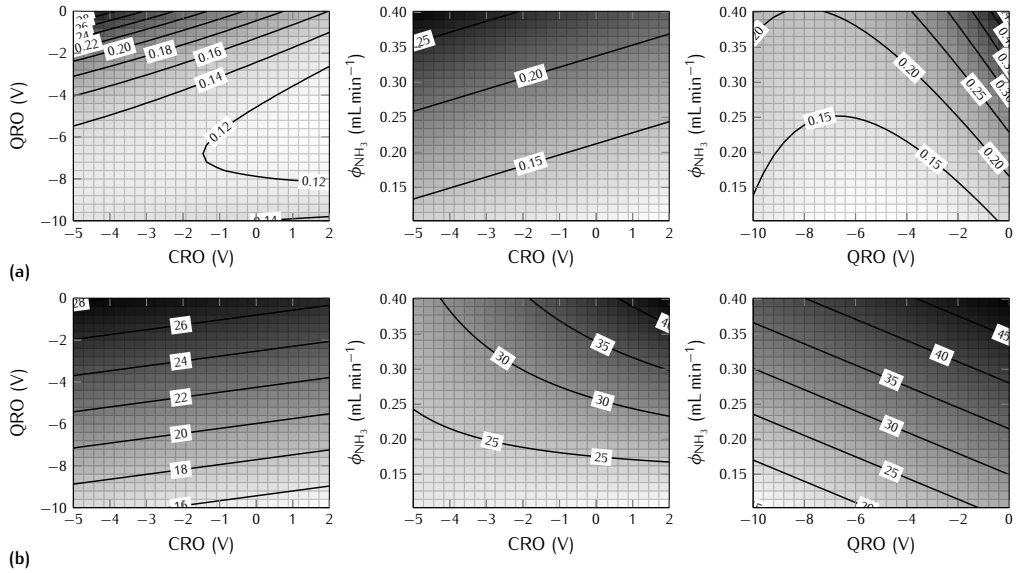


Figure 3.1. response surfaces showing the combined effect of QRO, CRO and the ammonia flow rate on **(a)** internal precision (% RSD) and **(b)** systematic error (departure from the certified value, as $\delta$‰) of $^{208}Pb/^{207}Pb$ measurement data. Slices at CPV = −35 V; Φ $NH_3$ = 0.14 mL/min; QRO = −5.5 V; CRO = 2.0 V.

2000). In fact, by decreasing RPq from 0.6 to 0.05, the internal precision improved by a factor of 2, despite a 25 %-decrease in the ion intensity.

Finally, the remaining parameters did not show any significant effect on the measurement (at 95 % confidence level), and they were set at the most convenient value (*e.g.* the minimum settling time to reduce the measurement time and AFT switched off).

### 3.3.2 Analytical figures of merit

Under the optimized conditions, the analytical performances using both micro-sample introduction systems were evaluated in terms of the working range, in-cell interference and precision achievable. Concerning the analytical working range, the lowest limit may be defined as the concentration at which the precision reaches a given threshold value. In fact, as stated in section 2.1, the achievable precision is limited by counting statistics and, hence, by the signal intensities.

By combining equations (2.1) and (2.2), and assuming to be negligible the contribution due to the covariation of the measured signals, the theoretical relative standard deviation can be estimated using the equation:

$$\%RSD_t = 100\sqrt{\frac{1}{I_1} + \frac{1}{I_2}} \tag{3.1}$$

where $I_1$ and $I_2$ are the ion intensities of the two isotopes monitored. Therefore, according to equation 3.1, the relative standard deviation steeply increases by lowering the concentration. The effect of the analytical concentration on the internal precision was evaluated for the two sample introduction systems. Considering a threshold of 0.50 % as the lowest useful precision, the concentration limits were 0.5 ng/mL and 1.0 ng/mL, working at 150 and 20 µL/min, respectively. The upper concentration, delimited by the sag effect, was evaluated during the detector dead time measurements to be 50 ng/mL.

Table 3.3. comparison of the precision for Pb isotope ratio measurements ($n = 10$) by ICP-MS. UR is short for uptake rate, system I refers to the PFA micro-nebuliser with Cinnabar chamber and system II to the total-consumption micro-sample-introduction system TISIS.

| System | UR | $^{208}Pb/^{207}Pb$ | | $^{206}Pb/^{207}Pb$ | |
|---|---|---|---|---|---|
| | (µL/min) | %RSD $t = 10$ s | %RSD $t = 30$ s | %RSD $t = 10$ s | %RSD $t = 30$ s |
| I | 150 | $0.12 \pm 0.03$ | $0.09 \pm 0.03$ | $0.13 \pm 0.05$ | $0.11 \pm 0.02$ |
| II | 20 | $0.17 \pm 0.04$ | $0.11 \pm 0.03$ | $0.18 \pm 0.03$ | $0.14 \pm 0.04$ |

Table 3.4. Pb isotope analysis of CRM 482 lichen. System I and II refer to the PFA micro-nebuliser with Cinnabar chamber, and the total-consumption micro-sample-introduction system TISIS, respectively.

| Instrument set-up | $n$ | $^{208}Pb/^{207}Pb$ (mean $\pm 2s$) | $^{206}Pb/^{207}Pb$ (mean $\pm 2s$) |
|---|---|---|---|
| ICP-DRC-MS – System I | 4 | $2.4093 \pm 0.0034$ | $1.1308 \pm 0.0010$ |
| ICP-DRC-MS – System II | 4 | $2.4085 \pm 0.0044$ | $1.1307 \pm 0.0015$ |
| ICP-DRC-MS[a] | 3 | $2.4085 \pm 0.0047$ | $1.1310 \pm 0.0024$ |
| MC-ICP-MS[b] | 4 | $2.4078 \pm 0.0004$ | $1.1311 \pm 0.0001$ |

[a] De Muynck et al. (2008)
[b] Cloquet et al. (2006)

These working ranges proved to be adequate for the analysis of various environmental matrices, as shown below.

Using the DRC, the generation of new interfering species within the cell is another important issue, especially at the very low RPq value (0.05) found to be the optimal condition. Using ammonia as the damping gas, the possible interference arising during the analysis of environmental matrices could be due to the polyatomic species $^{191}Ir^{14}N^{1}H^{+}$ and $^{193}Ir^{14}N^{1}H^{+}$, having the same nominal mass of $^{206}Pb^{+}$ and $^{208}Pb^{+}$ isotopes, respectively. Therefore, the occurrence of this interference was tested by analysing the standard reference material SRM 981 at a concentration of 10 ng/mL with and without the addition of 0.1 ng/mL Ir standard solution (the Ir/Pb ratio in the terrestrial crust is about $10^{-6}$). Since no significant variation was found in the Pb isotope ratios, it was concluded that the isotopes monitored are not interfered. Moreover, various high-order cluster ions between ammonia and rare earth elements may be formed, such as $Yb(NH_3)_2^{+}$, $Gd(NH_3)_3^{+}$ and $Ce(NH_3)_4^{+}$, potentially affecting the measurement of Pb isotopes (Woods and McCurdy 2013). However, with similar experiments to those for Ir, it was verified that lanthanides do not significantly affect the measurement of the Pb isotope ratios, up to the concentration of 100 ng/mL (10 ng/mL for Lu).

The precision was evaluated by replicated analysis of the standard reference material SRM 981 at a concentration of 10 ng/mL. The results are reported in table 3.3. Using an integration time of 30 s, an internal precision as low as 0.09–0.11 % and 0.11–0.14 % ($n = 10$) can be achieved for the two sample introduction systems. These figures are comparable with the precision reported in the previous studies using ICP-DRC-MS (Bandura et al. 2000; De Muynck et al. 2008; Jackson et al. 2004; Resano et al. 2008), but were obtained here at a much lower sample uptake rate.

The precision was about two-fold better than that observed in standard mode (*i.e.* without the damping gas). This improvement is similar to that previously reported using neon as the damping gas (De Muynck et al. 2008; Resano et al. 2008). The precision obtained with an integration time of 10 s was slightly worse, but it can be considered

adequate for the analytical task. For example, the natural variation of $^{208}Pb/^{207}Pb$ and $^{206}Pb/^{207}Pb$ in the atmospheric particulate is 4 and 8 %, respectively (Bollhöfer and Rosman 2001a,b). Hence, an integration time of 10 s was used for the rest of the work, allowing minimization of the analysis time and sample consumption.

Finally, the reliability of the method for the analysis of real samples was tested on CRM 482 lichen reference material CRM 482, previously analysed *via* ICP-DRC-MS after extraction chromatographic separation (De Muynck et al. 2008) and MC-ICP-MS (Cloquet et al. 2006). As can be seen from table 3.4, there is excellent agreement between the values obtained in this chapter and literature data. Also the precision obtained *via* the single-collector instruments was similar.

### 3.3.3 Uncertainty estimation

In environmental studies, Pb isotope ratio data are very useful for identifying pollution sources and tracing transport pathways. However, in order to discriminate different isotope ratios in a statistically significant way, a careful estimation of uncertainty is needed. According to the GUM guideline (BIPM et al. 1995), the uncertainty sources were identified and then their contribution calculated.

The uncertainty sources in isotope ratio determination are related to the correction for detector dead time and its determination, the correction for the instrumental mass discrimination and the contribution of the blank, $u(b)$. Particularly, the dead-time-dependent uncertainty $u(R_\tau)$ is a function of the internal precision $s(R_e)$, the standard deviation of the dead time $s(\tau)$ and the standard deviation of the measured $^{207}Pb$ signal intensity $s(I_e)$ (in counts per second). The contributions for these terms are expressed by the following equations (Encinar et al. 2001):

$$u(I_e) = s(I_e)\frac{I_e\tau(R_e - 1)}{(1 - \tau I_e)(1 - \tau R_e I_e)} \tag{3.2}$$

$$u(\tau) = s(\tau)\frac{I_e\tau(R_e - 1)}{(1 - \tau I_e)(1 - \tau R_e I_e)} \tag{3.3}$$

$$u(R_e) = \frac{s(R_e)}{\sqrt{n}}\frac{1}{1 - \tau R_e I_e} \tag{3.4}$$

It should be noted that the standard deviation of the ratio is divided by the square root of the number of replicates $n$, so that it can be considered as the standard deviation of the mean isotope ratio. The uncertainty associated with the correction for the instrumental mass discrimination can be divided into three terms: the uncertainty related to the isotope ratios $R_{s1}$ and $R_{s2}$ of the bracketing standards $s(R_s)$, the uncertainty of the certified ratios $s(R_c)$ and a second uncertainty contribution due to precision of measuring the isotope ratios in the samples $s(R_e)$. Their contributions are expressed by the following equations:

$$u(R_e) = \frac{s(R_e)}{\sqrt{n}}\frac{2R_e}{R_{s1} + R_{s2}} \tag{3.5}$$

$$u(R_s) = \frac{s(R_{s1}) + s(R_{s2})}{\sqrt{n}}\frac{2R_e R_c}{R_{s1} + R_{s2}} \tag{3.6}$$

$$u(R_c) = s(R_c)\frac{2R_e}{R_{s1} + R_{s2}} \tag{3.7}$$

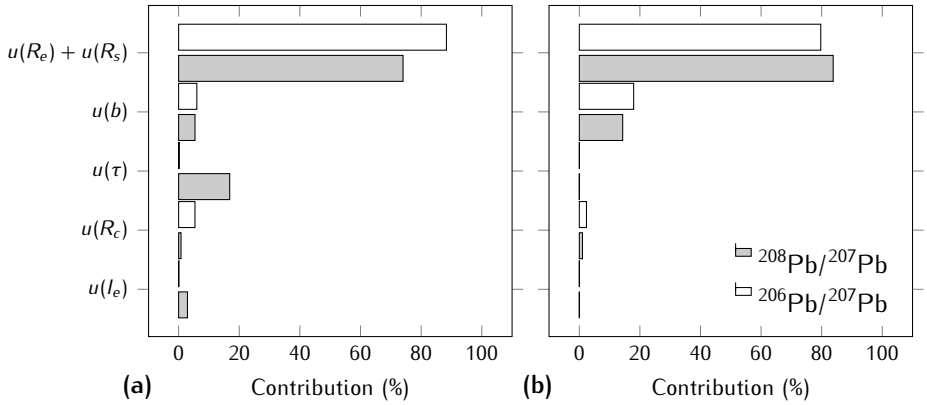


Figure 3.2. extended uncertainty budget for Pb isotope ratios measured by ICP-MS: **(a)** high count rates; and **(b)** low count rates.

When precision of the each measured ratio is similar to that predicted by counting statistics, the relative standard deviation of the ratios can be approximated according to equation (2.2):

$$\left[\frac{s(R)}{R}\right]^2 = \left[\frac{s(I_1)}{I_1}\right]^2 + \left[\frac{s(I_2)}{I_2}\right]^2 \tag{3.8}$$

In order to take into account the effect of the blank subtraction on the uncertainty of measurement, the terms $s(I_1)$ and $s(I_2)$ can be further decomposed into the separate contributions of the standard deviations of the sample ($I_s$) and blank signal ($I_b$):

$$s^2(I) = s^2(I_s) + s^2(I_b) \tag{3.9}$$

The total extended uncertainty was finally obtained by computing the square root sum of squares of every single contribution and multiplying by a coverage factor $k = 2$.

The uncertainty was calculated on the basis of 20 isotope ratio measurements of SRM 981 at a concentration of 10 ng/mL. The mean uncertainty for $^{208}Pb/^{207}Pb$ and $^{206}Pb/^{207}Pb$ was 0.005 and 0.002, respectively, in good agreement with that obtained using Monte-Carlo simulation (0.005 and 0.002) and the dispersion of the measured ratios (0.004 and 0.001). The percentage contributions of each term to the total uncertainty are shown in figure 3.2, considering two cases: **(a)** high count rates (at Pb concentration of 20 ng/mL) and **(b)** low count rates (at Pb concentration of 1 ng/mL). The terms $u(R_e)$ and $u(R_s)$ were summed and reported as a single contribution because both are expressions of the precision of the measurement. It can be seen that the internal precision was by far the most important contribution to the total uncertainty. Dead time uncertainty showed an effect only for the measurement of $^{208}Pb/^{207}Pb$, whose value is different from one, and only at high count rates. The contribution of the blank to the total uncertainty was about 20 % at low count rates, and less than 10 % at high count rates.

### 3.3.4 Analysis of Antarctic snow samples

Since the concentration of heavy metals in polar ice and snow samples is extremely low, typically at the pg/g level, accurate and precise measurement of Pb isotope ratios in these samples is highly challenging. Nevertheless, good results were obtained by combining the use of TISIS with the application of a simple and clean pre-concentration procedure

Table 3.5. Pb isotope ratio measured by ICP-MS in environmental samples from polar areas. Values are reported as mean value and uncertainties as 95 % confidence level.

| Matrix | Sampling site | $n$ | $^{208}Pb/^{207}Pb$ | $^{206}Pb/^{207}Pb$ |
|---|---|---|---|---|
| Atmospheric particulate | Ny-Ålesund (The Arctic) | 31 | $2.442 \pm 0.009$ | $1.165 \pm 0.005$ |
| Marine SPM | Ny-Ålesund (The Arctic) | 28 | $2.448 \pm 0.005$ | $1.176 \pm 0.003$ |
| Marine sediment | Ny-Ålesund (The Arctic) | 4 | $2.481 \pm 0.004$ | $1.206 \pm 0.002$ |
| Atmospheric particulate | Terra Nova Bay (Antarctica) | 26 | $2.423 \pm 0.015$ | $1.150 \pm 0.009$ |

by sample volume reduction (Grotti et al. 2008). In fact, by working at 20 µL/min under the optimal operating conditions, precise measurements of $^{208}Pb/^{207}Pb$ and $^{206}Pb/^{207}Pb$ were accomplished while consuming less than 200 µL of sample. This allowed a pre-concentration factor of 100, using only 20 mL of the sample (as water equivalent).

The procedure was applied to the analysis of two surface snow samples from Antarctica, having a Pb concentration of 18 and 30 pg/g. The measured $^{208}Pb/^{207}Pb$ and $^{206}Pb/^{207}Pb$ ratios were $2.456 \pm 0.006$ and $1.183 \pm 0.004$ for the first sample, whereas $2.450 \pm 0.008$ and $1.185 \pm 0.003$ for the second one (uncertainties are 95 % confidence intervals). These data are in good agreement with the Pb isotopic composition measured by TIMS in firn core samples from the Styx glacier in Victoria Land, dating 1948–1978 AD (Van de Velde et al. 2005). Uncertainties were in the 0.24–0.34 % range, which is quite similar to those reported for the analysis of the firn core samples (0.12–0.53 %).

### 3.3.5 Application to other environmental matrices

The analytical procedure developed was further applied to other environmental samples, in the context of national research programs in the polar regions. The matrix types considered included atmospheric particulate, marine SPM and sediment. Instrumental mass discrimination was corrected for by external calibration using a matrix-matched isotopic standard (Vanhaecke et al. 2003), prepared with the same mixture of acids used for the sample digestion. The application of the external correction method instead of internal correction also minimized the number of measured isotopes and, hence, the analysis time and sample consumption. For sample-standard bracketing purposes, the isotopic reference material (NIST SRM 981, 10 ng/mL) was measured every four samples.

The results are summarized in table 3.5 with as purpose showing the suitability of the proposed method for the analysis of real samples, while a deeper discussion based on the whole dataset is presented in chapters 4, 5 and 6. The values obtained for the aerosol collected at Ny-Ålesund are consistent with previous investigations of atmospheric Pb pollution in Northern Europe (Bindler 2011; Bollhöfer and Rosman 2001b) and the Canadian Arctic (Sturges and Barrie 1989). The uncertainties obtained were quite small, confirming that the precision achieved *via* the optimized analytical method was adequate for the analytical task. Finally, it is noteworthy that the analysis of each sample, performed at 150 µL/min, required only 1.5 mL of solution and it was accomplished in 8 min, corresponding to a throughput of 5 samples/h (including the analysis of the standards).

## 3.4 *Conclusions*

The application of ICP-DRC-MS for the accurate and precise measurement of Pb isotope ratios in environmental matrices at low sample consumption rates was demonstrated.

Under the optimal operating conditions, the sample introduction systems investigated provided fit-for-purpose performance, enabling Pb isotopic analysis of micro-samples, such as limited-sized samples and pre-concentrates. The main contribution (∼80 %) to the total uncertainty of the measurements came from the internal precision, that was reduced down to (∼0.1 % RSD) by the optimization of the instrumental parameters and using ammonia for collisional damping. The contribution of the blank to the total uncertainty was about 20% at low count rates, and less than 10 % at high count rates.

The simple method based on the use of a PFA micro-nebuliser for sample introduction, allowed the fast determination of Pb isotope ratios in a number of samples of environmental relevance from the Arctic and Antarctica, as shown in chapters 4, 5 and 6.

The application of TISIS in combination with an ultra-clean pre-concentration procedure allowed the precise determination of Pb isotope ratios in Antarctic snow samples (Pb concentration: 20–30 pg/g), using only 20 mL of sample (as water equivalent). This result opens interesting perspectives for the isotopic analysis of snow and ice core samples with high vertical resolution, which would be useful in the context of various polar research programs. The use of this sample introduction system was further investigated, as described in chapter 7, for the high-precision determination of Pb isotope ratios in Antarctic snow in combination with MC-ICP-MS.

*References*

Bandura, D. R., Baranov, V. I., and Tanner, S. D., 2000. Effect of collisional damping and reactions in a dynamic reaction cell on the precision of isotope ratio measurements. *Journal of Analytical Atomic Spectrometry*, **15**, 921–928. DOI: 10.1039/B000285M

Bandura, D. R., Baranov, V. I., and Tanner, S. D., 2002. Inductively coupled plasma mass spectrometer with axial field in a quadrupole reaction cell. *Journal of American Society for Mass Spectrometry*, **13**, 1176–1185. DOI: 10.1016/S1044-0305(02)00435-X

Bindler, R., 2011. Contaminated lead environments of man: Reviewing the lead isotopic evidence in sediments, peat, and soils for the temporal and spatial patterns of atmospheric lead pollution in Sweden. *Environmental Geochemistry and Health*, **33**, 311–329. DOI: 10.1007/s10653-011-9381-7

BIPM, IEC, IFCC, ISO, IUPAC, IUPAP, and OIML, 1995. *Guide to the expression of uncertainty in measurement*. Joint Committee for Guides in Metrology (JCGM)

Bollhöfer, A. and Rosman, K. J. R., 2001a. Isotopic source signatures for atmospheric lead: The Northern Hemisphere. *Geochimica et Cosmochimica Acta*, **65**, 1727–1740. DOI: 10.1016/S0016-7037(00)00630-X

Bollhöfer, A. and Rosman, K. J. R., 2001b. Lead isotopic ratios in European atmospheric aerosols. *Physics and Chemistry of the Earth, Part B: Hydrology, Oceans and Atmosphere*, **26**, 835–838. DOI: 10.1016/S1464-1909(01)00094-6

Box, G. E. P., Hunter, J. S., and Hunter, W. G., 2005. *Statistics for experimenters: design, innovation, and discovery*. Wiley series in probability and statistics. Wiley-Interscience

Cloquet, C., Carignan, J., and Libourel, G., 2006. Atmospheric pollutant dispersion around an urban area using trace metal concentrations and Pb isotopic compositions in epiphytic lichens. *Atmospheric Environment*, **40**, 574–587. DOI: 10.1016/j.atmosenv.2005.09.073

De Muynck, D., Cloquet, C., and Vanhaecke, F., 2008. Development of a new method for Pb isotopic analysis of archaeological artefacts using single-collector ICP-dynamic reaction cell-MS. *Journal of Analytical Atomic Spectrometry*, **23**, 62–71. DOI: 10.1039/b709461b

Encinar, J. R., Garcia Alonso, J. I., Sanz-Medel, A., Main, S., and Turner, P. J., 2001. A comparison between quadrupole, double focusing and multicollector ICP-MS. Part II. Evaluation of total combined uncertainty in the determination of lead in biological

matrices by isotope dilution. *Journal of Analytical Atomic Spectrometry*, **16**, 322–326. DOI: 10.1039/b006147f

Grotti, M., Soggia, F., Abelmoschi, M. L., Rivaro, P., Magi, E., and Frache, R., 2001. Temporal distribution of trace metals in Antarctic coastal waters. *Marine Chemistry*, **76**, 189–209. DOI: 10.1016/S0304-4203(01)00063-9

Grotti, M., Soggia, F., and Luis Todolì, J.-L., 2008. Ultratrace analysis of Antarctic snow samples by reaction cell inductively coupled plasma mass spectrometry using a total-consumption micro-sample-introduction system. *Analyst*, **133**, 1388–1394. DOI: 10.1039/b804043e

Grotti, M., Ardini, F., and Todolì, J.-L., 2013a. Total introduction of microsamples in inductively coupled plasma mass spectrometry by high-temperature evaporation chamber with a sheathing gas stream. *Analytica Chimica Acta*, **767**, 14–20. DOI: 10.1016/j.aca.2013.01.017

Jackson, B. P., Winger, P. V., and Lasier, P. J., 2004. Atmospheric lead deposition to Okefenokee Swamp, Georgia, USA. *Environmental Pollution*, **130**, 445–451. DOI: 10.1016/j.envpol.2003.12.019

R Core Team, 2015. *R: A Language and Environment for Statistical Computing*. URL: http://www.r-project.org/ (visited on 03/03/2016)

Resano, M., Marzo, P., Pérez-Arantegui, J., Aramendía, M., Cloquet, C., and Vanhaecke, F., 2008. Laser ablation-inductively coupled plasma-dynamic reaction cell-mass spectrometry for the determination of lead isotope ratios in ancient glazed ceramics for discriminating purposes. *Journal of Analytical Atomic Spectrometry*, **23**, 1182–1191. DOI: 10.1039/b802266f

Sturges, W. T. and Barrie, L. A., 1989. Stable lead isotope ratios in arctic aerosols: evidence for the origin of arctic air pollution. *Atmospheric Environment*, **23**, 2513–2519. DOI: 10.1016/0004-6981(89)90263-1

Tanner, S. D. and Baranov, V. I., 1999. Theory, design, and operation of a dynamic reaction cell for ICP-MS. *Atomic Spectroscopy*, **20**, 45–52

Tanner, S. D., Baranov, V. I., and Vollkopf, U., 2000. A dynamic reaction cell for inductively coupled plasma mass spectrometry (ICP-DRC-MS). Part III. Optimization and analytical performance. *Journal of Analytical Atomic Spectrometry*, **15**, 1261–1269. DOI: 10.1039/B002604M

UNI 14902, 2005. *Ambient air quality-Standard method for the measurement of Pb, Cd, As and Ni in the $PM_{10}$ fraction of suspended particulate matter*

Van de Velde, K., Vallelonga, P., Candelone, J. P., Rosman, K. J. R., Gaspari, V., Cozzi, G., Barbante, C., Udisti, R., Cescon, P., and Boutron, C. F., 2005. Pb isotope record over one century in snow from Victoria Land, Antarctica. *Earth and Planetary Science Letters*, **232**, 95–108. DOI: 10.1016/j.epsl.2005.01.007

Vanhaecke, F., Balcaen, L., Deconinck, I., De Schrijver, I., Marisa Almeida, C., and Moens, L., 2003. Mass discrimination in dynamic reaction cell (DRC)-ICP-mass spectrometry. *Journal of Analytical Atomic Spectrometry*, **18**, 1060–1065. DOI: 10.1039/b303528j

Woods, G. and McCurdy, E., 2013. Triple-quadrupole ICP-MS provides improved performance for difficult polyatomic and isobaric overlaps on lead isotopes. *Spectroscopy*, **28**, s28–s34

# 4 Pb isotopic analysis of atmospheric particulate in the Arctic region

## 4.1 *Introduction*

The scarcity of local sources makes the long-range transport of pollutants from mid-latitudes a major source of atmospheric particulate matter in the Arctic (Fisher et al. 2011). This mechanism can be very effective in spring, causing a marked increase in the number of particles in the accumulation mode, and resulting in the so called "Arctic haze" phenomenon. The particles of this haze mainly consists of anthropogenic sulphate and particulate organic matter, but can also include various amount of dust, black carbon (BC) and heavy metals (Quinn et al. 2007). On the other hand, during summer, the number of particles in the accumulation mode is low and the particle size distribution is dominated by Aitken nuclei (Engvall et al. 2007; Tunved et al. 2013).

The reason for this seasonality resides in the particular meteorology of the Arctic air mass that, in spring, is characterised by fast transport from mid-latitudes, reduced vertical mixing and lack of precipitation (Barrie 1986; Fisher et al. 2011; Quinn et al. 2007). On the contrary, during summer, the transport from mid-latitudes is slow, the vertical stratification is weaker than in winter (Stohl 2006) and wet scavenging is enhanced (Garrett et al. 2010).

Along with the transport and removal efficiency, also the source areas of the aerosols reaching the Arctic is subjected to seasonal variation. Indeed, high inputs of pollutants, such as anthropogenic sulphates and BC, are related to air masses reaching the Arctic from northern Eurasia in spring (Barrie 1986; Law and Stohl 2007), whereas local sources and marine inputs appear to affect NO, BC and aerosol number concentration in summer (Geng et al. 2010; Stohl 2006; Tunved et al. 2013).

In this context, the use of the Pb isotope ratios has proven to be very useful for the identification of the source areas of atmospheric Pb reaching the Arctic (Bazzano et al. 2015; Sturges and Barrie 1989; Sturges et al. 1993). Indeed, as explained in section 1.2, different ores can have different Pb isotope ratios, depending on the time of their formation and their initial chemical composition. The combination of weathering processes and human activities has introduced terrigenous and anthropogenic Pb into the atmosphere, resulting in a distinctive Pb isotopic fingerprint for atmospheric particulate matter originating from different geographical areas (Bollhöfer and Rosman 2000; Bollhöfer and Rosman 2001a,b; Hopper et al. 1991).

In this chapter, Pb isotope ratios have been used in order to identify the source areas of the pollutants reaching Ny-Ålesund during spring-summer campaigns, over a five-year period (2010–2014). For this purpose atmospheric particulate matter with aerodynamic equivalent diameter below 10 µm ($PM_{10}$) were collected and analysed. Additionally, the results have been corroborated by back-trajectory analysis.

Table 4.1. ICP-AES instrumental parameters used for the determination of Al concentration in $PM_{10}$ samples.

| Instrument | Varian Vista PRO |
|---|---|
| Sample introduction system | |
| Nebulizer | Concentric |
| Spray chamber | Cyclonic |
| Nebulizer gas flow rate | 0.75 L/min |
| Sample uptake rate | 0.78 mL/min |
| Internal standard uptake rate | 0.22 mL/min |
| Plasma source | |
| RF Power | 1400 W |
| Plasma gas flow rate | 15.0 L/min |
| Auxiliary gas flow rate | 1.50 L/min |
| Signal measurement | |
| Integration | 15 s |
| Replicates | 7 |
| Selected wavelengths (nm) | Al (236.705; 237.312; 396.152)<br>Lu (291.139) |

## 4.2 *Experimental*

### 4.2.1 Sampling

The sampling of $PM_{10}$ was carried out during five spring-summer (April-September) campaigns, from 2010 to 2014, on the roof of the Gruvebadet (GVB) observatory at Ny-Ålesund, Svalbard Islands (78.918 °N, 11.895 °E). The atmospheric particulate was collected, with a 4-day resolution, by a low-volume sampler (Tecora ECHO PM), operating at the constant flow rate of 200 L/min (actual conditions), on 90-mm hydrophilic PTFE membrane filters (H100A090C by Advantec MFS, Dublin, CA, USA); the filter efficiency was >99 % for 0.3 µm particles.

The GVB observatory was located in a clean area, about 800 m south-west of the Ny-Ålesund village. Anthropic activities, including snowmobile traffic, were forbidden at a distance up to 500 m from the sampling site. Because of the particular orography of the Kongsfjorden, the dominant winds follow the North-West – South-East direction, preventing the sampling site to be affected by air masses coming from Ny-Ålesund. In addition, a meteo-trigger system switched off the sampling devices when the wind was absent (<0.5 m/s) or coming from the village. After the sampling, the filters were placed in polystyrene Petri dishes, sealed in polyethylene bags and stored at −20 °C until analysis.

### 4.2.2 Sample analysis

A quarter of each filter was dissolved with 2 mL of Trace Select Ultra 65 % nitric acid from Sigma-Aldrich (St. Louis, MO, USA) and 0.5 mL of Suprapur 30 % hydrogen peroxide from Merck (Darmstadt, Germany), using a MARS-5 microwave digestion system (CEM, Matthews, NC, USA). After digestion, the samples were diluted to 10 mL with ultrapure water (Milli-Q water purification system from Merck Millipore, Darmstadt, Germany) and analysed by ICP-MS (Elan DRCII by Perkin-Elmer, Waltham, MA, USA) for the determination of Pb content and isotope ratios. Procedural blank corresponded to $2.6 \pm 1.5\,pg/m^3$ and the resulting limit of detection (3 s) was $4.5\,pg/m^3$.

$^{208}Pb/^{206}Pb$ and $^{207}Pb/^{206}Pb$ were measured according to the method described in chapter 3 and in Bazzano and Grotti (2014). The internal precision was 0.12 % RSD ($n = 4$, $C = 10\,ng/mL$) and the accuracy was verified during each measurement session by the analysis of BCR CRM 482 certified reference material, previously characterised by MC-ICP-MS (Cloquet et al. 2006). The values obtained ($^{208}Pb/^{206}Pb$= 2.1283 ± 0.0017 and $^{207}Pb/^{206}Pb$= 0.8844 ± 0.0005, $n = 20$), were in good agreement with the reference values ($^{208}Pb/^{206}Pb$= 2.1288 ± 0.0002 and $^{207}Pb/^{206}Pb$= 0.8841 ± 0.0005).

The concentration of Al was determined by inductively coupled plasma-atomic emission spectrometry (ICP-AES, Vista PRO by Varian, Springvale, Australia), using Lu as an internal standard to correct for non-spectral interferences and instrumental drift. Further instrumental parameters are reported in table 4.1. Data are reported as mean ± 95 %-confidence interval throughout this chapter.

### 4.2.3 Back-trajectory analysis

The trajectory of an infinitesimal air parcel is defined by the equation:

$$\frac{\mathrm{d}\,\mathbf{x}}{\mathrm{d}\,t} = \mathbf{v} \tag{4.1}$$

where $\mathbf{x}$ is the position vector, $t$ is the time and $\mathbf{v}$ the wind velocity vector. Given an initial $\mathbf{x}_0$ position at time $t_0$ for the parcel, then it is possible to calculate its path at each $t_i \neq t_0$. Similarly, given the position $\mathbf{x}_i$ of the parcel at time $t$, its trajectory can be followed backwards and its initial position $\mathbf{x}_0$ calculated (Stohl 1998).

Information about the path followed by the air parcels arriving at $\mathbf{x}$ at different times can be obtained by calculating several back-trajectories (BTs) at regular time intervals. Individual flow patterns can then be identified using cluster analysis.

In the clustering process, the spatial variance (SV) is computed between each endpoint ($k$) along trajectory ($j$) within its cluster ($i$):

$$\mathrm{SV}_{i,j} = \sum_k (\mathbf{x}_{j,k} - \mathbf{c}_{i,k})^2 \tag{4.2}$$

where $\mathbf{c}$ is the position vector for the cluster mean trajectory. The cluster spatial variance (CSV) is then just the sum of the spatial variance of all trajectories within its cluster:

$$\mathrm{CSV}_i = \sum_j \mathrm{SV}_{i,j} \tag{4.3}$$

and the total spatial variance (TSV) is the sum of the CSV over all clusters:

$$\mathrm{TSV} = \sum_i \mathrm{CSV}_i \tag{4.4}$$

Clustering starts by assigning each trajectory to its own cluster, so that there are $i$ clusters with $j = 1$ trajectories in each cluster. In each iteration the cluster number is reduced by one as two clusters are merged together. This process continues until only one cluster remains. With each iteration, the TSV is computed for each cluster combination and that with the minimum TSV is passed on to the next iteration. The optimal number of clusters to be considered is that giving the last largest change in the TSV.

To corroborate the findings obtained by chemical and isotopic analysis, air mass back-trajectories were calculated using the HYSPLIT 4.9 transport model (Draxler and Rolph 2014). Meteorological data fields were supplied by the ARL (Air Resources Lab, http://ready.arl.noaa.gov/gdas1.php) archiving programs input data. This program produces a 3 hourly, global, 1° latitude/longitude dataset on pressure surfaces. 6-day

back-trajectories (BT) were run every six hours at the Ny-Ålesund endpoint (at the altitude of 500, 1000 and 1500 m a.g.l.)

Each ensemble of monthly BTs was characterized by cluster analysis (package included in the 4.9 version of HYSPLIT). Typical number of monthly clusters range between 7 and 12. The air mass origin was identified by calculating the fraction of BT originating from specific continental sectors (northern Europe, Eurasia, northern America, Greenland, Arctic sea and local), as discussed below.

The uncertainty associated with such a procedure was estimated with a further series of calculations. First, the spatial variability has been checked by calculating and clustering BTs for a given month for five different endpoints, one centred in Ny-Ålesund and the other four placed on the corners of a $1° \times 1°$ cell around Ny-Ålesund. Second, the dependence on the endpoint altitude has been checked with calculations carried out for 500, 1000, 1500, 2000 and 2500 m a.g.l. Overall, the evaluation of the contribution from the potential source area (PSA) varied less than ±20 % of the final figures discussed in section 4.3.5.

## 4.3 *Results and discussion*

### 4.3.1 Pb concentration, enrichment and isotope ratios

The Pb concentration, the $^{208}Pb/^{206}Pb$ and $^{207}Pb/^{206}Pb$ ratios are reported in table 4.2. The average Pb concentration was $59.2 \pm 17.8\,pg/m^3$ and its origin was investigated by the calculation of the Pb enrichment factors (EFs), defined as:

$$EF(Pb/Al) = \frac{(Pb/Al)_s}{(Pb/Al)_c} \tag{4.5}$$

where $(Pb/Al)_s$ and $(Pb/Al)_c$ are the ratio measured in the sample and in the upper continental crust (UCC), respectively. The latter is $2.194 \times 10^{-4}$ (Wedepohl 1995). The resulting average $EF(Pb/Al)$ was $65 \pm 11$, thus indicating a predominant anthropogenic origin of the atmospheric particulate. Moreover, no significant inter-annual variations of Pb concentration and EFs were detected (ANOVA, $p$-value$>0.1$). This stationary trend is in contrast to the strong decrease of Pb concentration observed from 1977 to 2005 (Steinnes et al. 2011), thereby suggesting that no further reduction in the amount of atmospheric Pb reaching the Arctic recently occurred.

Pb isotope ratios were scattered in the range from 2.0493 to 2.1161 and from 0.8371 to 0.8733 for $^{208}Pb/^{206}Pb$ and $^{207}Pb/^{206}Pb$, respectively. Inter-annual differences were found not significant (ANOVA, $p$-value$>0.1$), indicating that the atmospheric Pb reaching Ny-Ålesund was probably emitted by the same sources.

Table 4.2. Pb concentration, enrichment factors and isotope ratios in $PM_{10}$ collected at Ny-Ålesund from 2010 to 2014 (4-days of integration time).

| Date | Pb ($pg/m^3$) | EF(Pb/Al) | $^{208}Pb/^{206}Pb$ | Uncertainty | $^{207}Pb/^{206}Pb$ | Uncertainty |
|---|---|---|---|---|---|---|
| 2010-03-16 | 122 | 370 | 2.106 | 0.006 | 0.862 | 0.002 |
| 2010-03-20 | 8.90 | 63 | 2.108 | 0.008 | 0.869 | 0.003 |
| 2010-03-23 | 442 | 255 | 2.102 | 0.005 | 0.864 | 0.002 |
| 2010-03-27 | 174 | 82 | 2.106 | 0.005 | 0.865 | 0.002 |
| 2010-03-31 | 1428 | 183 | 2.097 | 0.006 | 0.863 | 0.002 |
| 2010-04-08 | 151 | 53 | 2.104 | 0.005 | 0.865 | 0.002 |

*Continued on next page*

*Continued from previous page*

| Date | Pb ($pg/m^3$) | EF(Pb/Al) | $^{208}Pb/^{206}Pb$ | Uncertainty | $^{207}Pb/^{206}Pb$ | Uncertainty |
|---|---|---|---|---|---|---|
| 2010-04-12 | 59.4 | 19 | 2.103 | 0.005 | 0.862 | 0.001 |
| 2010-04-16 | 71.8 | 21 | 2.105 | 0.004 | 0.863 | 0.001 |
| 2010-04-22 | 44.9 | 32 | 2.087 | 0.008 | 0.863 | 0.003 |
| 2010-04-24 | 38.3 | 60 | 2.100 | 0.008 | 0.864 | 0.004 |
| 2010-04-28 | 68.2 | 34 | 2.101 | 0.006 | 0.864 | 0.002 |
| 2010-05-02 | 101 | 31 | 2.101 | 0.004 | 0.863 | 0.002 |
| 2010-05-10 | 42.4 | 38 | 2.105 | 0.006 | 0.863 | 0.001 |
| 2010-05-18 | 98.8 | 41 | 2.110 | 0.004 | 0.863 | 0.002 |
| 2010-06-17 | <4.50 | – | – | – | – | – |
| 2010-06-22 | <4.50 | – | – | – | – | – |
| 2010-06-26 | 17.3 | 7.2 | 2.086 | 0.007 | 0.860 | 0.005 |
| 2010-06-30 | 84.3 | 9.0 | 2.095 | 0.006 | 0.853 | 0.003 |
| 2010-07-04 | 13.5 | 2.0 | 2.078 | 0.009 | 0.851 | 0.004 |
| 2010-07-09 | 6.08 | 11 | 2.084 | 0.012 | 0.859 | 0.003 |
| 2010-07-14 | 10.7 | 2.2 | 2.061 | 0.008 | 0.845 | 0.003 |
| 2010-07-19 | 52.8 | 174 | 2.092 | 0.007 | 0.853 | 0.002 |
| 2010-07-24 | 17.6 | 24 | 2.076 | 0.004 | 0.856 | 0.001 |
| 2010-07-29 | <4.50 | – | – | – | – | – |
| 2010-08-02 | 31.6 | 17 | 2.078 | 0.012 | 0.852 | 0.004 |
| 2010-08-08 | 5.34 | 4.2 | 2.085 | 0.005 | 0.859 | 0.003 |
| 2010-08-14 | 17.3 | 26 | 2.092 | 0.005 | 0.860 | 0.003 |
| 2010-08-19 | 62.5 | 27 | 2.057 | 0.008 | 0.842 | 0.002 |
| 2010-08-24 | 14.0 | 13 | 2.079 | 0.007 | 0.857 | 0.004 |
| 2010-08-28 | <4.50 | – | – | – | – | – |
| 2010-09-05 | <4.50 | – | – | – | – | – |
| 2010-09-13 | 43.5 | 23 | 2.101 | 0.006 | 0.859 | 0.004 |
| 2011-03-29 | 555 | 183 | 2.109 | 0.003 | 0.865 | 0.001 |
| 2011-04-03 | 163 | 60 | 2.103 | 0.008 | 0.864 | 0.003 |
| 2011-04-07 | 126 | 63 | 2.116 | 0.005 | 0.870 | 0.002 |
| 2011-04-11 | 55.5 | 71 | 2.098 | 0.005 | 0.860 | 0.002 |
| 2011-05-01 | 88.1 | 81 | 2.099 | 0.004 | 0.862 | 0.002 |
| 2011-05-05 | 114 | 54 | 2.102 | 0.004 | 0.865 | 0.001 |
| 2011-05-09 | 44.1 | 39 | 2.097 | 0.005 | 0.863 | 0.003 |
| 2011-05-13 | 95.4 | 46 | 2.107 | 0.007 | 0.864 | 0.003 |
| 2011-05-17 | 74.6 | 16 | 2.109 | 0.008 | 0.863 | 0.003 |
| 2011-05-21 | 60.4 | 24 | 2.105 | 0.007 | 0.861 | 0.003 |
| 2011-05-25 | 42.3 | 27 | 2.094 | 0.006 | 0.865 | 0.003 |
| 2011-05-29 | 27.3 | 16 | 2.097 | 0.006 | 0.870 | 0.002 |
| 2011-06-05 | 21.4 | 43 | 2.088 | 0.011 | 0.866 | 0.003 |
| 2011-06-09 | 18.8 | 13 | 2.099 | 0.008 | 0.862 | 0.005 |
| 2011-06-13 | 91.9 | 20 | 2.102 | 0.006 | 0.864 | 0.003 |
| 2011-06-21 | <4.50 | – | – | – | – | – |
| 2011-07-03 | 11.1 | 18 | 2.098 | 0.007 | 0.860 | 0.003 |
| 2011-07-07 | 22.8 | 22 | 2.093 | 0.008 | 0.860 | 0.003 |
| 2011-07-10 | <4.50 | – | – | – | – | – |
| 2011-07-15 | <4.50 | – | – | – | – | – |
| 2011-07-23 | 26.8 | 43 | 2.098 | 0.008 | 0.862 | 0.003 |
| 2012-04-21 | 52.0 | 80 | 2.108 | 0.005 | 0.864 | 0.003 |
| 2012-04-25 | 65.8 | 95 | 2.106 | 0.006 | 0.863 | 0.004 |
| 2012-04-29 | 61.0 | 73 | 2.103 | 0.005 | 0.864 | 0.003 |
| 2012-05-03 | 50.6 | 82 | 2.113 | 0.007 | 0.863 | 0.005 |

*Continued on next page*

*Continued from previous page*

| Date | Pb (pg/m$^3$) | EF(Pb/Al) | $^{208}$Pb/$^{206}$Pb | Uncertainty | $^{207}$Pb/$^{206}$Pb | Uncertainty |
|---|---|---|---|---|---|---|
| 2012-05-07 | 51.3 | 47 | 2.113 | 0.005 | 0.864 | 0.005 |
| 2012-05-15 | 121 | 36 | 2.102 | 0.006 | 0.859 | 0.003 |
| 2012-05-19 | 71.4 | 33 | 2.107 | 0.004 | 0.861 | 0.004 |
| 2012-05-23 | 72.3 | 52 | 2.099 | 0.006 | 0.860 | 0.004 |
| 2012-05-27 | 29.3 | 27 | 2.107 | 0.008 | 0.860 | 0.005 |
| 2012-05-31 | 39.9 | 23 | 2.109 | 0.009 | 0.864 | 0.005 |
| 2012-06-04 | 45.4 | 39 | 2.106 | 0.007 | 0.861 | 0.003 |
| 2012-06-08 | 22.8 | 41 | 2.107 | 0.009 | 0.863 | 0.005 |
| 2012-06-12 | 26.1 | 32 | 2.108 | 0.008 | 0.863 | 0.005 |
| 2012-06-16 | 30.8 | 124 | 2.110 | 0.008 | 0.865 | 0.006 |
| 2012-06-20 | 7.05 | 33 | 2.107 | 0.012 | 0.865 | 0.005 |
| 2012-06-24 | <4.50 | – | – | – | – | – |
| 2012-06-28 | 14.9 | 130 | 2.094 | 0.013 | 0.859 | 0.008 |
| 2012-07-02 | 29.9 | 57 | 2.092 | 0.007 | 0.856 | 0.005 |
| 2012-07-06 | 5.30 | 5.4 | 2.091 | 0.027 | 0.852 | 0.010 |
| 2012-07-10 | 118 | 73 | 2.078 | 0.005 | 0.851 | 0.003 |
| 2012-07-14 | 28.8 | 49 | 2.092 | 0.005 | 0.857 | 0.004 |
| 2012-07-18 | 15.4 | 11 | 2.099 | 0.011 | 0.860 | 0.005 |
| 2012-07-22 | 35.5 | 71 | 2.077 | 0.005 | 0.851 | 0.005 |
| 2012-07-26 | 24.0 | 15 | 2.099 | 0.008 | 0.860 | 0.007 |
| 2012-07-30 | 44.2 | 67 | 2.098 | 0.004 | 0.860 | 0.003 |
| 2012-08-03 | 32.7 | – | 2.102 | 0.007 | 0.865 | 0.002 |
| 2012-08-07 | 45.8 | 115 | 2.090 | 0.007 | 0.857 | 0.003 |
| 2012-08-11 | <4.50 | – | – | – | – | – |
| 2012-08-15 | 24.5 | 54 | 2.071 | 0.010 | 0.852 | 0.005 |
| 2012-08-23 | <4.50 | – | – | – | – | – |
| 2012-08-27 | 41.4 | 141 | 2.090 | 0.011 | 0.858 | 0.005 |
| 2012-08-31 | 11.1 | 37 | 2.082 | 0.022 | 0.857 | 0.010 |
| 2012-09-04 | <4.50 | – | – | – | – | – |
| 2013-05-01 | 42.6 | 51 | 2.105 | 0.007 | 0.863 | 0.002 |
| 2013-05-05 | 82.8 | 63 | 2.107 | 0.003 | 0.863 | 0.002 |
| 2013-05-09 | 6.72 | – | 2.084 | 0.011 | 0.863 | 0.009 |
| 2013-05-13 | 19.8 | 31 | 2.099 | 0.010 | 0.860 | 0.003 |
| 2013-05-17 | 24.3 | 23 | 2.095 | 0.009 | 0.862 | 0.003 |
| 2013-05-21 | 21.8 | 42 | 2.106 | 0.004 | 0.866 | 0.002 |
| 2013-05-25 | 26.0 | 17 | 2.106 | 0.006 | 0.862 | 0.003 |
| 2013-05-29 | 20.1 | 55 | 2.099 | 0.006 | 0.866 | 0.002 |
| 2013-06-02 | – | – | – | – | – | – |
| 2013-06-06 | 26.3 | 9.9 | 2.092 | 0.008 | 0.857 | 0.001 |
| 2013-06-10 | 15.6 | 26 | 2.104 | 0.009 | 0.865 | 0.004 |
| 2013-06-14 | <4.50 | – | – | – | – | – |
| 2013-06-18 | 32.1 | 200 | 2.072 | 0.003 | 0.845 | 0.002 |
| 2013-06-22 | 6.22 | – | 2.101 | 0.004 | 0.873 | 0.008 |
| 2013-06-26 | 16.8 | 40 | 2.107 | 0.005 | 0.865 | 0.004 |
| 2013-06-30 | 30.7 | 145 | 2.101 | 0.006 | 0.866 | 0.004 |
| 2013-07-04 | 32.4 | 91 | 2.090 | 0.007 | 0.856 | 0.003 |
| 2013-07-08 | <4.50 | – | – | – | – | – |
| 2013-07-12 | 25.2 | 8.3 | 2.094 | 0.006 | 0.860 | 0.003 |
| 2013-07-16 | 14.5 | 2.7 | 2.098 | 0.007 | 0.864 | 0.005 |
| 2013-07-20 | 6.73 | 27 | 2.095 | 0.011 | 0.864 | 0.006 |
| 2013-07-24 | <4.50 | – | – | – | – | – |

*Continued on next page*

*Continued from previous page*

| Date | Pb ($pg/m^3$) | EF(Pb/Al) | $^{208}Pb/^{206}Pb$ | Uncertainty | $^{207}Pb/^{206}Pb$ | Uncertainty |
|---|---|---|---|---|---|---|
| 2013-08-05 | 6.96 | 28 | 2.062 | 0.009 | 0.847 | 0.003 |
| 2013-08-13 | <4.50 | – | – | – | – | – |
| 2013-08-17 | 87.0 | 443 | 2.107 | 0.004 | 0.873 | 0.002 |
| 2013-08-21 | <4.50 | – | – | – | – | – |
| 2013-08-29 | <4.50 | – | – | – | – | – |
| 2013-09-02 | 14.9 | 26 | 2.103 | 0.009 | 0.869 | 0.004 |
| 2013-09-06 | 6.25 | 3.9 | 2.101 | 0.012 | 0.866 | 0.004 |
| 2013-09-10 | 24.0 | – | 2.057 | 0.007 | 0.839 | 0.002 |
| 2014-03-31 | 88.5 | 68 | 2.105 | 0.005 | 0.864 | 0.002 |
| 2014-04-04 | 72.1 | 111 | 2.105 | 0.002 | 0.863 | 0.001 |
| 2014-04-08 | 572 | 160 | 2.103 | 0.004 | 0.863 | 0.002 |
| 2014-04-12 | 85.8 | 97 | 2.109 | 0.003 | 0.863 | 0.002 |
| 2014-04-16 | 188 | – | 2.113 | 0.004 | 0.866 | 0.002 |
| 2014-04-20 | 307 | 135 | 2.107 | 0.003 | 0.865 | 0.002 |
| 2014-04-24 | 110 | 135 | 2.102 | 0.007 | 0.863 | 0.002 |
| 2014-04-28 | 81.3 | 53 | 2.102 | 0.005 | 0.861 | 0.002 |
| 2014-05-02 | 62.9 | 195 | 2.104 | 0.004 | 0.864 | 0.003 |
| 2014-05-07 | 51.6 | 29 | 2.100 | 0.006 | 0.861 | 0.003 |
| 2014-05-11 | 41.0 | 56 | 2.115 | 0.005 | 0.870 | 0.002 |
| 2014-05-15 | 68.7 | 44 | 2.106 | 0.004 | 0.863 | 0.001 |
| 2014-05-19 | 36.6 | 6.6 | 2.103 | 0.008 | 0.868 | 0.003 |
| 2014-05-23 | 65.3 | 6.7 | 2.100 | 0.005 | 0.854 | 0.003 |
| 2014-05-27 | 30.3 | 35 | 2.098 | 0.012 | 0.857 | 0.006 |
| 2014-05-31 | 12.6 | 62 | 2.110 | 0.009 | 0.864 | 0.003 |
| 2014-06-04 | 75.1 | 156 | 2.107 | 0.003 | 0.867 | 0.002 |
| 2014-06-08 | 17.0 | 47 | 2.091 | 0.009 | 0.864 | 0.004 |
| 2014-06-16 | 11.1 | – | 2.114 | 0.006 | 0.867 | 0.002 |
| 2014-06-20 | 34.9 | 9.9 | 2.101 | 0.009 | 0.871 | 0.004 |
| 2014-06-24 | <4.50 | – | – | – | – | – |
| 2014-06-28 | 26.6 | 3.2 | 2.049 | 0.008 | 0.837 | 0.003 |
| 2014-07-03 | 11.0 | 14 | 2.092 | 0.010 | 0.855 | 0.005 |
| 2014-07-07 | 24.5 | 16 | 2.072 | 0.010 | 0.852 | 0.006 |
| 2014-07-12 | 66.9 | 476 | 2.072 | 0.008 | 0.850 | 0.004 |
| 2014-07-17 | 43.2 | 415 | 2.110 | 0.005 | 0.868 | 0.003 |
| 2014-07-21 | 18.3 | 18 | 2.099 | 0.007 | 0.863 | 0.004 |
| 2014-07-25 | <4.50 | – | – | – | – | – |
| 2014-07-29 | <4.50 | – | – | – | – | – |
| 2014-08-02 | 8.66 | 25 | 2.095 | 0.018 | 0.860 | 0.007 |
| 2014-08-06 | 14.1 | 19 | 2.075 | 0.014 | 0.848 | 0.005 |
| 2014-08-10 | 13.6 | 13 | 2.081 | 0.010 | 0.854 | 0.005 |
| 2014-08-18 | <4.50 | – | – | – | – | – |
| 2014-08-22 | 12.5 | 48 | 2.081 | 0.009 | 0.856 | 0.005 |
| 2014-08-26 | 23.5 | 24 | 2.097 | 0.010 | 0.860 | 0.005 |
| 2014-08-30 | 61.5 | 134 | 2.095 | 0.005 | 0.860 | 0.002 |
| 2014-09-03 | <4.50 | – | – | – | – | – |
| 2014-09-07 | <4.50 | – | – | – | – | – |

### 4.3.2 Seasonal variations

Boxplots in figure 4.1 **(a)** show the presence of a sharp seasonal pattern in the $PM_{10}$ Pb concentration, which was characterised by significantly ($p$-value$<0.001$) higher con-

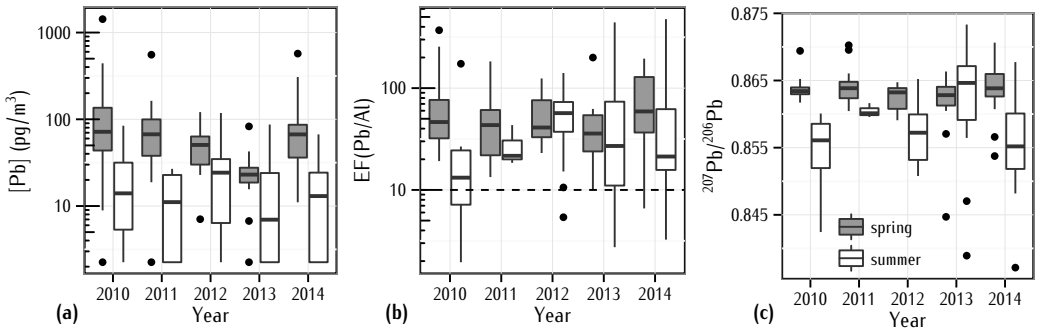


Figure 4.1. boxplot presentation for **(a)** Pb concentration; **(b)** $EF(Pb/Al)$ and **(c)** $^{207}Pb/^{206}Pb$ measured in $PM_{10}$ samples collected at Ny-Ålesund.

centrations during spring ($96.3 \pm 34.7\,pg/m^3$) compared to summer ($20.7 \pm 4.4\,pg/m^3$). Such a seasonal variation is not apparent in the boxplots for $EF(Pb/Al)$ reported in figure 4.1 **(b)** showing that most of the atmospheric Pb reaching Ny-Ålesund was anthropogenic in both seasons.

The $^{208}Pb/^{206}Pb$ and $^{207}Pb/^{206}Pb$ ratios were $2.1030 \pm 0.0014$ and $0.8632 \pm 0.0007$ in spring, and $2.0878 \pm 0.0031$ and $0.8572 \pm 0.0017$ in summer. This variation was significant ($p$-value$<0.001$) throughout the studied period (figure 4.1 **c**) and it was interpreted as a seasonal shift in the source area of the atmospheric particulate matter reaching Ny-Ålesund. Noteworthy this shift regularly occurred in late June and typically no sample with intermediate Pb isotopic composition between the two seasonal averages was recorded. This finding seems to indicate a fast transition in the atmospheric transport processes, and agrees with the abrupt seasonal change in particle number concentration observed by Tunved et al. (2013).

In 2013, both Pb content and Pb ratios showed similar values in the two seasons. However, as discussed in section 4.3.4, this year has to be considered as anomalous.

### 4.3.3 Atmospheric Pb source areas identification

The potential source areas (PSAs) of the atmospheric Pb reaching Ny-Ålesund were investigated by comparing the measured values to literature data (Bollhöfer and Rosman 2001a, 2002; Carignan et al. 2002; Mukai et al. 2001a,b) using the three-isotope plot reported in figure 4.2. In the plot, spring and summer data are differentiated, the isotope mixing line is showed and the signature of a possible local end-member of natural origin (diamictite debris) is also reported (section 5.3.3 and Bazzano et al. 2014).

In agreement with previous findings (Bazzano et al. 2015), the measured ratios were scattered along a mixing line ($R^2 = 0.760$) and far from the signature of the local diamictite; therefore, local natural sources were likely negligible. Spring data showed an isotopic composition compatible with Russian emissions, whereas in summer the influence of multiple sources, comprising Canada and US, was probable. PSAs were then further constrained by comparing the separated seasonal signatures with more specific literature data (figure 4.3).

Spring data showed a small spread only and no significant mixing line was found, indicating the dominance of a single source area with a well-defined Pb isotopic composition. The latter coincides with values measured in Russian urban aerosol (Bollhöfer and Rosman 2001b; Mukai et al. 2001a) and in emissions from mining areas in Russia and north-eastern Kazakhstan (Mukai et al. 2001a).

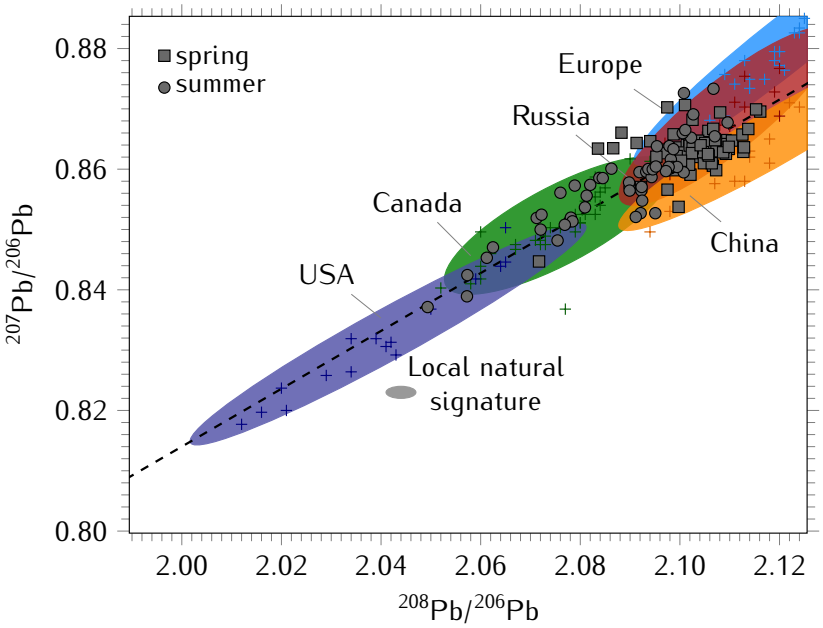


Figure 4.2. three-isotope plot Pb isotope ratios measured in $PM_{10}$ samples collected at Ny-Ålesund with values reported in literature. Ellipses represent the joint-distribution (95 % confidence level) of literature data (Canada and USA: Bollhöfer and Rosman 2001a; Carignan et al. 2002; Europe: Bollhöfer and Rosman 2001a,b, 2002; Russia: Bollhöfer and Rosman 2001b; Mukai et al. 2001a; China: Bollhöfer and Rosman 2001a; Mukai et al. 2001b). (■) Spring samples. (●) summer samples. (−−) mixing line.

In addition, the spring Pb isotopic composition is in agreement with the values measured in ice cores, dated from 1935 to 1990, collected in the Rudny Altai region, at the Russian border with Kazakhstan and Mongolia (weighted average $^{208}Pb/^{206}Pb = 2.1082 \pm 0.0045$ and $0.8674 \pm 0.0020$). The atmospheric Pb in the Altai region is mainly ($86 \pm 6$ %) affected by the intensive mining activities in the area (Eichler et al. 2012), which is responsible for most of the Pb ores processed in both Kazakhstan and Russia. In accordance, the possible Russian end-member was identified as the average of both ice cores and Pb ores collected in the Altai region, resulting in $2.1020 \pm 0.0079$ and $0.8642 \pm 0.0047$ for $^{208}Pb/^{206}Pb$ and $^{207}Pb/^{206}Pb$, respectively.

Summer data were scattered along a mixing line ($R^2 = 0.817$), suggesting the presence of two end-members. Moreover, the measured values covered a range of Pb isotopic compositions very similar to that found in lichens (Carignan et al. 2002), snowpack (Simonetti et al. 2000) and precipitation samples collected in north-eastern North America (Sherman et al. 2015). The end-members were associated to Canadian and northern USA emissions, according to the values reported by Carignan and Gariépy (1995) and Carignan et al. (2002), respectively.

The similar Pb isotopic composition for the Russian and Canadian end-members did not allow an accurate estimate of their relative contribution in spring. However, based on the above discussion and results from BT analysis (see section 4.3.5), Russian inputs likely dominated in spring. On the other hand, the very different Pb isotopic signatures of the Canadian and USA end-members enabled an estimate of their relative contribution, resulting in $66 \pm 5$ % and $34 \pm 5$ %, respectively.

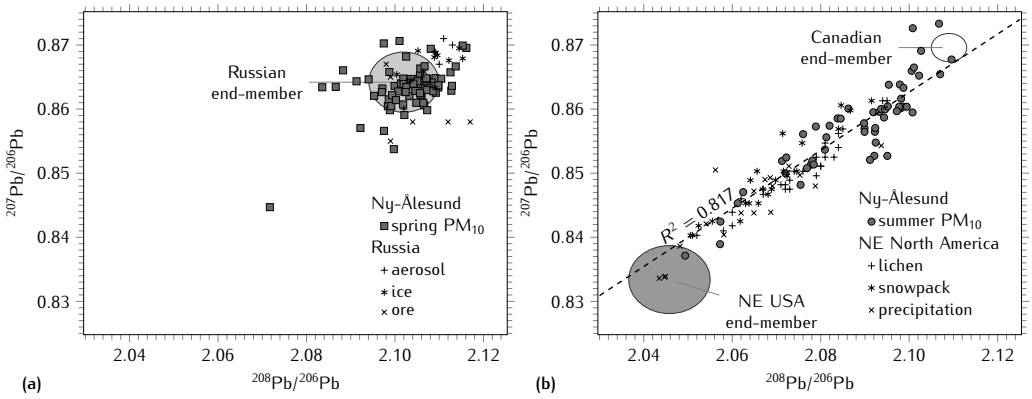


Figure 4.3. three-isotope plot for **(a)** spring and **(b)** summer $PM_{10}$ samples collected at Ny-Ålesund. References are reported in the text.

### 4.3.4 The anomaly in 2013

The 2013 samples showed significant differences in the seasonal pattern of the Pb concentration and in the impact of European and North American source areas. Indeed, during this year, the differences in Pb concentration and Pb isotopic composition between the two seasons were not significant ($p$-value$>$0.1).

During spring 2013, the average Pb concentration was $26.7 \pm 10.2\,pg/m^3$, a result that is significantly lower than the $109 \pm 39\,pg/m^3$ average measured during same season of the other years ($p$-value$<$0.001). In summer, no such significant difference was observed and the average Pb concentration was $16.6 \pm 7.9$ and $21.9 \pm 5.0\,pg/m^3$ for 2013 and the other years, respectively.

The Pb isotopic composition in the 2013 samples ($^{208}Pb/^{206}Pb = 2.0949 \pm 0.0040$, $^{207}Pb/^{206}Pb = 0.8615 \pm 0.0024$) was not significantly different in comparison with the other years ($p$-value$>$0.1) and was compatible with a Russian origin in both seasons. These results may be interpreted as a less effective transport of the particulate matter from the Russian source area during spring and a persistent influence of the same source during summer.

### 4.3.5 Back-trajectory analysis

Pb source areas were further investigated using back-trajectory analysis. Several authors (*e.g.* Klonecki et al. 2003; Law and Stohl 2007) reported the presence of a cold polar dome that generally prevents air masses to reach the lower atmosphere over the Arctic. Cold and relatively fast air masses usually arrive from Eurasia during spring, whereas slower air masses coming from west and south-west sectors, including northern America, are observed during summer.

The results of the cluster analysis of monthly BTs (cluster means), reported in table 4.3, confirmed this pattern. For each month, the analysis provided a cluster weight expressed as a percentage of BTs represented by the cluster. Only the contributions from continental areas are reported. The remaining BTs have been assigned to air masses coming from north eastern and western sectors of the Arctic Ocean and from marine areas around Svalbard Islands (Short Range atmospheric transport). The cluster analysis indicated a significantly higher contribution for air masses coming from northern Eurasia during spring 2010, 2012 and 2014 in comparison with the summer period of the same years ($p$-value $= 0.004$), when air masses from North America were shown to have a more significant impact ($p$-value $= 0.006$).

Table 4.3. results of cluster analysis of monthly back-trajectories (BTs) for air masses reaching Ny-Ålesund. Values are the percentage of BTs represented by the cluster.

| Period | North Europe | Eurasia | North America | Greenland Iceland | Arctic Ocean | Short range |
|---|---|---|---|---|---|---|
| April 2010 | 16 | 19 | 14 | 9 | 25 | 18 |
| May 2010 | 11 | 28 | 0 | 18 | 19 | 24 |
| June 2010 | 2 | 26 | 22 | 14 | 4 | 32 |
| July 2010 | 11 | 2 | 19 | 28 | 18 | 22 |
| August 2010 | 0 | 9 | 40 | 14 | 22 | 14 |
| April 2011 | 18 | 18 | 34 | 19 | 11 | 0 |
| May 2011 | 9 | 24 | 39 | 1 | 27 | 0 |
| June 2011 | 4 | 9 | 11 | 13 | 43 | 20 |
| July 2011 | 0 | 33 | 5 | 28 | 14 | 20 |
| August 2011 | 9 | 34 | 10 | 24 | 0 | 23 |
| April 2012 | 0 | 42 | 4 | 6 | 20 | 28 |
| May 2012 | 9 | 20 | 3 | 20 | 29 | 18 |
| June 2012 | 5 | 19 | 9 | 13 | 32 | 23 |
| July 2012 | 5 | 12 | 18 | 26 | 24 | 15 |
| August 2012 | 7 | 10 | 20 | 34 | 8 | 21 |
| April 2013 | 11 | 37 | 15 | 12 | 22 | 6 |
| May 2013 | 11 | 12 | 4 | 35 | 9 | 28 |
| June 2013 | 14 | 18 | 10 | 36 | 13 | 8 |
| July 2013 | 18 | 13 | 8 | 19 | 19 | 23 |
| August 2013 | 28 | 6 | 5 | 33 | 26 | 4 |
| April 2014 | 0 | 34 | 4 | 24 | 29 | 9 |
| May 2014 | 0 | 24 | 11 | 26 | 12 | 27 |
| June 2014 | 4 | 0 | 4 | 45 | 15 | 32 |
| July 2014 | 10 | 0 | 20 | 26 | 24 | 20 |
| August 2014 | 0 | 13 | 19 | 20 | 32 | 16 |
| Average (2010-2012-2014) | | | | | | |
| April | 5.3 | 32 | 7.3 | 13 | 25 | 18 |
| May | 6.7 | 24 | 4.7 | 21 | 20 | 23 |
| June | 3.7 | 15 | 12 | 24 | 17 | 29 |
| July | 8.7 | 4.7 | 19 | 27 | 22 | 19 |
| August | 2.3 | 11 | 26 | 23 | 21 | 17 |
| Average (2011-2013) | | | | | | |
| April | 15 | 28 | 25 | 16 | 17 | 3.0 |
| May | 10 | 18 | 22 | 18 | 18 | 14 |
| June | 9.0 | 14 | 11 | 25 | 28 | 14 |
| July | 9.0 | 23 | 6.5 | 24 | 17 | 22 |
| August | 19 | 20 | 7.5 | 29 | 13 | 14 |

On the contrary, during 2013, a different pattern was observed with a slightly higher influence of the North American sector in spring and a higher percentage of Eurasian air masses during summer. However, such seasonal differences did not result significant ($p$-value$>$0.1).

The seasonal trends spotlighted by BT analysis for the Eurasia and North America advection routes are in good agreement with the marked seasonal differences recorded for both Pb concentration and Pb isotopic composition measured in the samples. The only exception is observed for the 2011 samples, for which a significant seasonal difference was highlighted by Pb concentration and isotopic composition. However, due to sampling difficulties, only three samples were collected during summer 2011 and their representativeness for the whole season is hence questionable.

Finally, in every case, air masses from other locations, including Northern Europe, were not subjected to significant seasonal variations and therefore appeared to not significantly influence the above scenario.

## 4.4 *Conclusions*

The determination of Pb concentrations showed that most of the atmospheric Pb reaching Ny-Ålesund was of anthropogenic origin and its average value was not subjected to significant inter-annual variations over a 5-years period (2010–2014). Similarly, the average Pb isotopic composition was similar throughout the period studied, indicating that the main source areas for atmospheric Pb were not affected by inter-annual variations.

On the other hand, a sharp recurring transition was observed between spring and summer. Indeed, spring seasons were characterised by a higher load of atmospheric Pb than summer. In agreement with a different pattern in BTs for the two seasons, the Pb isotopic composition was compatible with smelting activities in the Rudny Altay region during spring and inputs from north-eastern North America during summer. Particularly in this season, Canadian emissions were estimated to account for $66 \pm 5$ % of the Pb reaching Ny-Ålesund, whereas US inputs accounted for the remaining Pb.

During 2013, a different situation occurred: the spring Pb load was significantly lower than that observed in the other years and the difference between the two seasons was not relevant for both Pb concentration and isotopic composition. Indeed, BTs and the Pb isotopic composition were compatible with Russian inputs in both seasons. BT analysis also detected similar conditions during 2011, but the scarcity of summer samples did not allow comparison of these finding with results obtained by chemical analysis.

The presence of these anomalous years highlights the need of extending the present dataset to a longer period, in order to investigate reasons and possible trends for these variations. In addition, to further constrain and validate the possible source areas for atmospheric Pb reaching the Arctic, an extensive chemical characterisation of the particulate matter is mandatory.

*References*

Barrie, L. A., 1986. Arctic air pollution: An overview of current knowledge. *Atmospheric Environment*, **20**, 643–663. DOI: 10.1016/0004-6981(86)90180-0

Bazzano, A. and Grotti, M., 2014. Determination of lead isotope ratios in environmental matrices by quadrupole ICP-MS working at low sample consumption rates. *Journal of Analytical Atomic Spectrometry*, **29**, 926–933. DOI: 10.1039/c3ja50388g

Bazzano, A., Rivaro, P., Soggia, F., Ardini, F., and Grotti, M., 2014. Anthropogenic and natural sources of particulate trace elements in the coastal marine environment of Kongsfjorden, Svalbard. *Marine Chemistry*, **163**, 28–35. DOI: 10.1016/j.marchem.2014.04.001

Bazzano, A., Ardini, F., Becagli, S., Traversi, R., Udisti, R., Cappelletti, D., and Grotti, M., 2015. Source assessment of atmospheric lead measured at Ny-Ålesund, Svalbard. *Atmospheric Environment*, **113**, 20–26. DOI: 10.1016/j.atmosenv.2015.04.053

Bollhöfer, A. and Rosman, K. J. R., 2000. Isotopic source signatures for atmospheric lead: the Southern Hemisphere. *Geochimica et Cosmochimica Acta*, **64**, 3251–3262. DOI: 10.1016/S0016-7037(00)00436-1

Bollhöfer, A. and Rosman, K. J. R., 2001a. Isotopic source signatures for atmospheric lead: The Northern Hemisphere. *Geochimica et Cosmochimica Acta*, **65**, 1727–1740. DOI: 10.1016/S0016-7037(00)00630-X

Bollhöfer, A. and Rosman, K. J. R., 2001b. Lead isotopic ratios in European atmospheric aerosols. *Physics and Chemistry of the Earth, Part B: Hydrology, Oceans and Atmosphere*, **26**, 835–838. DOI: 10.1016/S1464-1909(01)00094-6

Bollhöfer, A. and Rosman, K. J. R., 2002. The temporal stability in lead isotopic signatures at selected sites in the Southern and Northern Hemispheres. *Geochimica et Cosmochimica Acta*, **66**, 1375–1386. DOI: 10.1016/S0016-7037(01)00862-6

Carignan, J. and Gariépy, C., 1995. Isotopic composition of epiphytic lichens as a tracer of the sources of atmospheric lead emissions in southern Québec, Canada. *Geochimica et Cosmochimica Acta*, **59**, 4427–4433. DOI: 10.1016/0016-7037(95)00302-G

Carignan, J., Simonetti, A., and Gariépy, C., 2002. Dispersal of atmospheric lead in northeastern North America as recorded by epiphytic lichens. *Atmospheric Environment*, **36**, 3759–3766. DOI: 10.1016/S1352-2310(02)00294-7

Cloquet, C., Carignan, J., and Libourel, G., 2006. Atmospheric pollutant dispersion around an urban area using trace metal concentrations and Pb isotopic compositions in epiphytic lichens. *Atmospheric Environment*, **40**, 574–587. DOI: 10.1016/j.atmosenv.2005.09.073

Draxler, R. and Rolph, G., 2014. *HYSPLIT (HYbrid Single-Particle Lagrangian Integrated Trajectory) Model access via NOAA ARL READY Website.* URL: http://ready.arl.noaa.gov/HYSPLIT_ash.php (visited on 03/03/2016)

Eichler, A., Tobler, L., Eyrikh, S., Gramlich, G., Malygina, N., Papina, T., and Schwikowski, M., 2012. Three centuries of Eastern European and Altai lead emissions recorded in a Belukha ice core. *Environmental Science and Technology*, **46**, 4323–4330. DOI: 10.1021/es2039954

Engvall, A.-C., Krejci, R., Ström, J., Treffeisen, R., Scheele, R., Hermansen, O., and Paatero, J., 2007. Changes in aerosol properties during spring-summer period in the Arctic troposphere. *Atmospheric Chemistry and Physics Discussions*, **7**, 1215–1260. DOI: 10.5194/acpd-7-1215-2007

Fisher, J. A., Jacob, D. J., Wang, Q., Bahreini, R., Carouge, C. C., Cubison, M. J., Dibb, J. E., Diehl, T., Jimenez, J. L., Leibensperger, E. M., Lu, Z., Meinders, M. B., Pye, H. O., Quinn, P. K., Sharma, S., Streets, D. G., van Donkelaar, A., and Yantosca, R. M., 2011. Sources, distribution, and acidity of sulfate–ammonium aerosol in the Arctic in winter–spring. *Atmospheric Environment*, **45**, 7301–7318. DOI: 10.1016/j.atmosenv.2011.08.030

Garrett, T. J., Zhao, C., and Novelli, P. C., 2010. Assessing the relative contributions of transport efficiency and scavenging to seasonal variability in Arctic aerosol. *Tellus Series B*, **62**, 190–196. DOI: 10.1111/j.1600-0889.2010.00453.x

Geng, H., Ryu, J., Jung, H. J., Chung, H., Ahn, K. H. O., and Ro, C. U. N., 2010. Single-particle characterization of summertime arctic aerosols collected at Ny-Ålesund, Svalbard. *Environmental Science and Technology*, **44**, 2348–2353. DOI: 10.1021/es903268j

Hopper, J. F., Ross, H. B., Sturges, W. T., and A., B. L., 1991. Regional source discrimination of atmospheric aerosols in Europe using the isotopic composition of lead. *Tellus Series B*, **43**, 45–60. DOI: 10.1034/j.1600-0889.1991.00004.x

Klonecki, A., Hess, P., Emmons, L., Smith, L., Orlando, J., and Blake, D., 2003. Seasonal changes in the transport of pollutants into the Arctic troposphere-model study. *Journal of Geophysical Research, D: Atmospheres*, **108** (D4), 8367. DOI: 10.1029/2002JD002199

Law, K. S. and Stohl, A., 2007. Arctic Air Pollution: Origins and Impacts. *Science*, **315**, 1537–1540. DOI: 10.1126/science.1137695

Mukai, H., Machida, T., Tanaka, A., Vera, Y. P., and Uematsu, M., 2001a. Lead isotope ratios in the urban air of eastern and central Russia. *Atmospheric Environment*, **35**, 2783–2793. DOI: 10.1016/S1352-2310(00)00341-1

Mukai, H., Tanaka, A., Fujii, T., Zeng, Y., Hong, Y., Tang, J., Guo, S., Xue, H., Sun, Z., Zhou, J., Xue, D., Zhao, J., Zhai, G., Gu, J., and Zhai, P., 2001b. Regional characteristics of sulfur and lead isotope ratios in the atmosphere at several Chinese urban sites. *Environmental Science and Technology*, **35**, 1064–1071. DOI: 10.1021/es001399u

Quinn, P. K., Shaw, G., Andrews, E., Dutton, E. G., Ruoho-Airola, T., and Gong, S. L., 2007. Arctic haze: Current trends and knowledge gaps. *Tellus Series B*, **59**, 99–114. DOI: 10.1111/j.1600-0889.2006.00238.x

Sherman, L. S., Blum, J. D., Dvonch, J. T., Gratz, L. E., and Landis, M. S., 2015. The use of Pb, Sr, and Hg isotopes in Great Lakes precipitation as a tool for pollution source attribution. *Science of the Total Environment*, **502**, 362–374. DOI: 10.1016/j.scitotenv.2014.09.034

Simonetti, A., Gariépy, C., and Carignan, J., 2000. Pb and Sr isotopic compositions of snowpack from québec, canada: inferences on the sources and deposition budgets of atmospheric heavy metals. *Geochimica et Cosmochimica Acta*, **64**, 5–20. DOI: 10.1016/S0016-7037(99)00207-0

Steinnes, E., Berg, T., and Uggerud, H. T., 2011. Three decades of atmospheric metal deposition in Norway as evident from analysis of moss samples. *Science of the Total Environment*, **412-413**, 351–8. DOI: 10.1016/j.scitotenv.2011.09.086

Stohl, A., 1998. Computation, accuracy and applications of trajectories - a review and bibliography. *Atmospheric Environment*, Developments in Environmental Science **32**, 947–966. DOI: 10.1016/S1474-8177(02)80024-9

Stohl, A., 2006. Characteristics of atmospheric transport into the Arctic troposphere. *Journal of Geophysical Research, D: Atmospheres*, **111** (D11), D11306. DOI: 10.1029/2005JD006888

Sturges, W. T. and Barrie, L. A., 1989. Stable lead isotope ratios in arctic aerosols: evidence for the origin of arctic air pollution. *Atmospheric Environment*, **23**, 2513–2519. DOI: 10.1016/0004-6981(89)90263-1

Sturges, W. T., Hopper, J. F., Barrie, L. A., and Schnell, R. C., 1993. Stable lead isotope ratios in Alaskan arctic aerosols. *Atmospheric EnvironmentPart A General Topics*, **27**, 2865–2871. DOI: 10.1016/0960-1686(93)90317-R

Tunved, P., Ström, J., and Krejci, R., 2013. Arctic aerosol life cycle: linking aerosol size distributions observed between 2000 and 2010 with air mass transport and precipitation at Zeppelin station, Ny-Ålesund, Svalbard. *Atmospheric Chemistry and Physics*, **13**, 3643–3660. DOI: 10.5194/acp-13-3643-2013

Wedepohl, K. H., 1995. The composition of the continental crust. *Geochimica et Cosmochimica Acta*, **58A**, 959–960. DOI: 10.1180/minmag.1994.58A.2.234

# 5 Pb isotopic analysis of marine particulate in the Arctic region

## 5.1 *Introduction*

In chapter 4, it was described how Pb isotope ratio measurements can help to understand how the Arctic atmosphere is connected to the rest of the world, and how it receives contaminants from sources far outside the Arctic region.

Similar influences, from pollution sources at lower latitudes, have also been clearly demonstrated for the Arctic marine environment (AMAP 2005; Macdonald et al. 2000; Muir et al. 1992, 1999). The pathways by which these contaminants are delivered to the Arctic are complex and strongly influenced by climate variability and global climate change. In particular, the distribution of heavy metals among the various environmental compartments is dynamic and apparently driven by multiple processes, both natural and anthropogenic (AMAP 2005). Suspended particulate matter (SPM) is a carrier of metals in the marine ecosystem and plays a fundamental role in many global processes. Therefore, the study of metals associated to SPM and the assessment of their origin can provide important information for the correct interpretation of their biogeochemical cycles.

Kongsfjorden (79 °N, 12–13 °E) is a glacial fjord located on the north-west coast of Spitsbergen, the largest of Svalbard Islands, and it has been regarded as a very suitable site to investigate the effects of the climate change (Svendsen et al. 2002). Here, the concentration of SPM is strongly influenced by the activity of five glaciers (Beszczynska-Moller et al. 1997), as well as by long-range transport processes driven by oceanic and atmospheric circulation (AMAP 2005).

The hydrographic and oceanographic features of Kongsfjorden have been described in detail by Svendsen et al. (2002) and by Cottier et al. (2005). The distribution of the water masses results from interactions between forces governing the fjord circulation, coupled with the complex bottom topography and coastline. Generally, the fjord has a maximum content of Atlantic Water (AW) from the West Spitsbergen Current (WSC) in late summer, while through the fall and winter, the fjord water masses are gradually replaced by fresher and cold Arctic water (Cottier et al. 2005). The Transformed Atlantic Water (TAW) obtains its properties on the way into the fjord, as a result of mixing of AW with Arctic Water and outflows from the fjords transported by coastal currents flowing northward around southern and western Spitsbergen.

Water circulation in the outer part of the fjord is typical of broad fjords (Aliani et al. 2004; Svendsen et al. 2002), depending on the morphology, offshore geostrophic circulation and wind patterns. In the inner Kongsfjord, warmer surface waters from the WSC enter across the southern passage of the moraine, flow northward along the glaciers' fronts, getting colder and fresher, and exit across the passage between Blømstrandbreen glacier and the island of Blømstrand (Aliani et al. 2004). Therefore, in the summer period,

the water column is well stratified with cold lenses of freshwater outflowing from the glaciers at the surface.

The SPM composition, particle dynamics and sedimentation processes in this area have been deeply investigated, with particular interest devoted to the particles exported by glaciers (Aliani et al. 2004; Svendsen et al. 2002; Zaborska et al. 2006). Most of the solid material derived from the glaciers is accumulated on the seafloor within the fjord: the coarser grains are deposited close to the glacier front, whereas the finer fractions are transported by the surface waters to the central and outer parts of the fjord (Zajaczkowski 2008). In fact, as reported by Svendsen et al. (2002), the sediment accumulation rate decreases by one order of magnitude from the glaciers fronts ($>1.8\,g/cm^2/y$) to the secondary sill in the central part of the fjord (0.2–0.4 $g/cm^2/y$), and by another order of magnitude toward the outer fjord on the continental shelf (0.02 $g/cm^2/y$). Concerning the composition of SPM, the particulate inorganic matter (PIM) results one order of magnitude higher than the particulate organic matter (POM) during summer. Moreover, PIM decreases moving far from the glacier front (Svendsen et al. 2002).

The input of particles into the fjord and their transport through the local circulation and sedimentation processes also condition the distribution of particulate trace elements in the water column, where they can display either toxic (*e.g.* Pb) or biological (*e.g.* Fe) effects (Nies 1999). However, though there have been recently published studies on the distribution of trace metals in Kongsfjorden sediments (Grotti et al. 2013b; Lu et al. 2013), no reports on trace element distribution in SPM are available.

In 2012, we were able to obtain measurements of the Kongsfjorden's bio-geochemical features (nutrients, phytoplankton pigments and SPM) for the sea surface and water column during the summer season within the context of the Italian ARCTICA (ARCTic research on the Inter-connections between Climate and Atmosphere) project activities.

This chapter presents first data on trace element distribution in SPM that aid in understanding its elemental composition and the possible sources of the particulate metals into the marine environment of Kongsfjorden.

After a description of the distribution of the parameters analysed together with the physical description of the main water masses, the sources of SPM were evaluated by measuring $^{208}Pb/^{207}Pb$ and $^{206}Pb/^{207}Pb$ isotope ratios, together with crustal enrichment factors, and comparing them with the isotopic signature of the atmospheric particulate and marine sediments collected in the same area.

## 5.2 *Materials and methods*

### 5.2.1 Sample collection pre-treatment and storage

The area investigated and the sampling stations are shown in figure 5.1. Two surveys were carried out in late spring 2012 (1–4 Jun) and in late summer 2012 (30 Aug–6 Sept) on board of the research vessel Teisten (Kings Bay AS, Norway). In that period, Kongsfjorden was clear from sea ice.

The sampling stations were chosen to be representative of different glacial runoff and anthropogenic impacts. Station A, near the Ny-Ålesund pier, is not directly affected by the glacial runoff and it could be locally influenced by the anthropogenic activities. Station B, at the inlet of the fjord, is scarcely affected by both runoff and anthropic sources. Station C and Station D are very close to melt-water runoff sources.

The sampling depths were chosen according to the CTD profiles. Seawater samples were collected in 10 L-Niskin bottles, at various depths corresponding to surface, fluorescence maximum (indicative of biological activity), intermediate and deep waters. The location of sampling stations and the samples collected are listed in table 5.1.

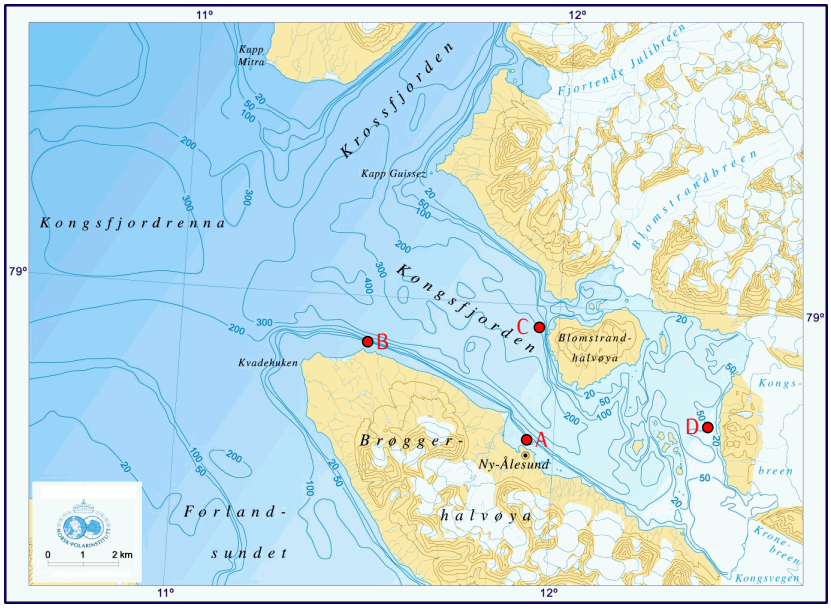


Figure 5.1. map of Kongsfjorden and position of the sampling stations.

Table 5.1. sampling stations and collected samples in the Kongsfjorden.

| Station | Latitude (N) | Longitude (E) | Bottom depth (m) | Sampling date | Sampling depth (m) |
|---|---|---|---|---|---|
| A | 78°55.920 | 11°56.696 | 45 | 04/06/2012<br>30/08/2012 | 3, 20, 35<br>5, 22, 40 |
| B | 78°58.474 | 11°35.271 | 150 | 01/06/2012<br>04/09/2012 | 5, 20, 50, 140<br>5, 50, 100, 140 |
| C | 78°59.304 | 11°56.805 | 200 | 01/06/2012<br>04/09/2012 | 5, 35, 60, 180<br>5, 30, 70, 170 |
| D | 78°56.236 | 12°23.670 | 45 | 04/06/2012<br>06/09/2012 | 3, 15, 35<br>4, 15, 35 |

SPM was obtained by filtration through 0.4 µm polycarbonate filters (Millipore, 47 mm diameter), as previously reported (Grotti et al. 2001). For each sample, two filters were obtained (2 L each one), for the determination of trace elements and phytoplankton pigments, respectively. Filters were placed in Petri dishes, sealed in double polyethylene bags and stored at −30 °C until analysis.

Sub-samples of filtered seawater for the determination of nutrients ($NO_3^-$, $NO_2^-$, $NH_4^+$, $Si(OH)_4$ and $PO_4^{3-}$) were collected in 50 mL polypropylene graduated conical test tubes (Kartell, Milan, Italy), sealed in double polyethylene bags and stored at −30 °C until analysis.

### 5.2.2 Sample preparation and analysis

*Nutrients and phytoplankton pigments.* The nutrients were determined using a five-channel continuous flow Technicon Autoanalyzer II, according to the method described by Hansen and Koroleff (1999), which was adapted to our instrumentation. The accuracy and the precision of the method were checked by using Certified Ref-

erence Material (CRM) MOOS-2 (Seawater CRM for Nutrients provided by the National Research Council of Canada). The precision of the method was estimated by analysing five homogeneous aliquots of the CRM with the following results: ±0.10 µM for $NO_3^-$, ±0.01 µM for $NO_2^-$, ±0.10 µM for $NH_4^+$, ±0.30 µM for $Si(OH)_4$ and ±0.07 µM for $PO_4^{3-}$. The measured nutrients in the CRM MOOS-2 were not significantly different ($p$-value$<0.05$) from the certified values.

Phytoplankton chlorophyll-*a* (Chl-*a*) and pheopigments (Pheo) were determined *via* spectrophotometric analysis, according to Lorenzen (1967).

*Particulate elements.* Before and after SPM collection, filters were weighed with a precision of ±0.01 mg (Sartorius BP 210 D). SPM samples were dissolved following the procedure described in section 3.2.4 and analysed using ICP-AES and ICP-MS. Selected elements and main instrumental conditions are summarized in tables 5.2 and 5.3. Accuracy and precision of the analytical procedure were verified by using the certified reference material CRM-414 (marine plankton) provided by the Institute for Reference Materials and Measurements of the European Commission. The results are summarized in table 5.4.

*Pb isotope ratio measurements.* Aliquots of the dissolved SPM samples were analysed for their $^{208}Pb/^{207}Pb$ and $^{206}Pb/^{207}Pb$ isotope ratios following the method described in chapter 3.

### 5.2.3 Data processing

The data matrix, constituted of 28 rows (samples) and 31 columns (physical, biological and chemical parameters), was processed by principal component analysis (PCA), using the open-source software environment for statistical computing and graphics "R" (R Core Team 2015).

Visualization of the data has been realised using the "Ocean Data View" software, developed by Schlitzer (2015).

## 5.3 *Results and discussion*

### 5.3.1 Physical and biological characteristics of the water column

Figure 5.2 shows a diagram in which potential temperature ($\theta$) and salinity (S) are reported for the stations sampled in both surveys. Using this kind of diagram, it is possible to identify different water masses by their physical characteristics.

According to the definitions given by Cottier et al. (2005) four water masses were identified in the area studied:

- the Surface Water (SW) characterised by a temperature higher than 1.0 °C and a salinity lower than 34.00;
- the Intermediate Water (IW), defined by a temperature higher than 1.0 °C and a salinity ranging from 34.00 to 34.65;
- the Transformed Atlantic Water (TAW), defined by a temperature ranging from 1.0 to 3.0 °C, a salinity higher than 34.65 and potential density ($\sigma_\theta$) lower than 27.92 kg/m$^3$ and
- the Atlantic Water (AW), defined by temperature higher than 3 °C, a salinity higher than 34.65 and $\sigma_\theta$ lower than 27.92 kg/m$^3$.

Table 5.5 summarizes the values of the hydrographic (temperature, salinity, fluorescence, turbidity, potential density) and bio-geochemical variables of the samples collected during the June and September surveys.

Table 5.2. ICP-AES instrumental parameters for the determination of major elements in marine suspended particulate matter.

| Instrument | Varian Inc (Palo Alto, CA, USA) Vista PRO |
|---|---|
| Nebuliser | Pneumatic concentric (K-style) |
| Spray chamber | Cyclonic |
| Plasma source configuration | Axial |
| RF Power | 1100 W |
| Plasma gas flow rate | 15.0 L/min |
| Auxiliary gas flow rate | 1.5 L/min |
| Nebuliser gas flow rate | 0.75 L/min |
| Sample uptake rate | 0.78 mL/min |
| Internal standard uptake rate | 0.22 mL/min |
| Integration time | 15 s |
| Replicates | 7 |
| Analytes and wavelengths (nm) | Al (236.705; 237.312; 396.152) |
| | Ba (233.527; 455.403; 493.408) |
| | Ca (315.887; 370.602; 373.690) |
| | Cr (205.560; 206.158; 267.716) |
| | Fe (234.350; 240.489; 258.588) |
| | K (404.721) |
| | Lu (291.139)[a] |
| | Mg (279.800; 285.213; 293.651) |
| | Mn (257.610; 293.305; 294.921) |
| | Na (568.821; 588.995; 589.592) |
| | P (213.618; 214.914) |
| | Sr (346.445; 407.771; 421.552) |
| | Ti (334.941; 336.122; 337.280) |
| | V (289.164; 289.265; 292.401) |
| | Zn (202.548; 206.200; 213.857) |

[a] Internal standard

Table 5.3. ICP-MS instrumental parameters used for trace element determinations in marine suspended particulate matter.

| Instrument | Perkin-Elmer (Waltham, MA, USA) Elan DRC II |
|---|---|
| Nebuliser | PFA-ST microconcentric |
| Spray chamber | Low-volume cyclonic (cinnabar) |
| RF Power | 1500 W |
| Plasma gas flow rate | 14.5 L/min |
| Auxiliary gas flow rate | 1.65 L/min |
| Nebuliser gas flow rate | 0.95 L/min |
| Sample uptake rate | 150 µL/min |
| RF amplitude | 150 V |
| Axial field voltage | 300 V |
| Cell path voltage | −28 V |
| Cell rod offset | −8.0 V |
| Mass analyser rod offset | 0.0 V |
| Stability parameters[a] | RPa = 0.0; RPq = 0.25 |
| Dwell time | 50 ms |
| Sweeps | 20 |
| Replicates | 5 |
| Nuclides monitored | $^{59}Co^{+}$, $^{60}Ni^{+}$, $^{63}Cu^{+}$, $^{98}Mo^{+}$, $^{111}Cd^{+}$, $^{208}Pb^{+}$, $^{115}In^{+}$[b] |

[a] Mathieu stability parameters of the cell's quadrupole: $a = 1.9 \times \mathrm{RPa}$; $q = 0.95 \times \mathrm{RPq}$
[b] Internal standard

Table 5.4. analysis of major and trace elements in BCR CRM 414 (marine plankton). Data are reported as mean ± 95 %-confidence interval. Indicative values are reported within parentheses.

| Element | Unit | Measured | Certified |
|---|---|---|---|
| Al | mg/g | $2.3 \pm 0.1$ | $(1.8 \pm 0.3)$ |
| Ba | µg/g | $30 \pm 1$ | $(31 \pm 2)$ |
| Ca | mg/g | $69 \pm 2$ | $(65 \pm 2)$ |
| Cd | µg/g | $0.436 \pm 0.021$ | $0.383 \pm 0.014$ |
| Co | µg/g | $1.55 \pm 0.06$ | $(1.43 \pm 0.06)$ |
| Cr | µg/g | $23.6 \pm 2.3$ | $23.8 \pm 1.2$ |
| Cu | µg/g | $30.7 \pm 1.1$ | $29.5 \pm 1.3$ |
| Fe | mg/g | $1.3 \pm 0.1$ | $(1.9 \pm 0.2)$ |
| K | mg/g | $8.3 \pm 0.4$ | $(7.6 \pm 0.2)$ |
| Mg | mg/g | $2.2 \pm 0.1$ | $(2.4 \pm 0.1)$ |
| Mn | µg/g | $282 \pm 9$ | $299 \pm 13$ |
| Mo | µg/g | $1.6 \pm 0.2$ | $(1.4 \pm 0.2)$ |
| Na | mg/g | $7.9 \pm 0.3$ | $(8.3 \pm 0.4)$ |
| Ni | µg/g | $18.0 \pm 0.9$ | $18.8 \pm 0.8$ |
| P | mg/g | $13.2 \pm 0.5$ | $(12.3 \pm 0.6)$ |
| Pb | µg/g | $3.62 \pm 0.19$ | $3.97 \pm 0.19$ |
| Sr | µg/g | $238 \pm 8$ | $(261 \pm 25)$ |
| Ti | mg/g | $0.04 \pm 0.01$ | $(48 \pm 5)$ |
| V | µg/g | $9.08 \pm 0.63$ | $8.10 \pm 0.18$ |
| Zn | µg/g | $109.3 \pm 3.8$ | $111.6 \pm 2.5$ |

Table 5.5. temperature (T), salinity (S), fluorescence (F), turbidity (Tb), potential density ($\sigma_\theta$), nutrients ($NH_4^+$, $NO_3^-$, $NO_2^-$, $Si(OH)_4$, $PO_4^{3-}$, chlorophyll-*a* (Chl-*a*), phaeopigments (Phaeo) and suspended particulate matter (SPM) measured along the water column in the Kongsfjorden.

| Station | Depth (m) | T (°C) | S | F (µg/L) | Tb (FTU) | $\sigma_\theta$ (kg/m$^3$) | $NH_4^+$ (µM) | $NO_2^-$ (µM) | $NO_3^-$ (µM) | $Si(OH)_4$ (µM) | $PO_4^{3-}$ (µM) | Chl-*a* (µg/L) | Phaeo (µg/L) | SPM (mg/L) |
|---|---|---|---|---|---|---|---|---|---|---|---|---|---|---|
| June survey | | | | | | | | | | | | | | |
| A | 3 | 4.56 | 34.86 | 0.12 | 0.98 | 27.61 | <0.01 | 0.04 | 0.04 | 0.43 | 0.15 | 0.04 | 0.49 | 0.50 |
| | 20 | 3.69 | 34.98 | 1.44 | 0.76 | 27.80 | 0.15 | 0.03 | 0.35 | 0.45 | 0.19 | 0.65 | 0.68 | 0.53 |
| | 35 | 3.15 | 35.01 | 0.77 | 0.63 | 27.88 | 0.46 | 0.06 | 0.65 | 0.70 | 0.21 | 0.31 | 0.21 | 0.32 |
| B | 5 | 3.06 | 34.94 | 0.11 | 1.18 | 27.84 | 0.30 | 0.04 | 0.55 | 0.35 | 0.16 | 0.13 | 0.42 | 0.38 |
| | 20 | 3.01 | 34.98 | 1.14 | 1.01 | 27.87 | 0.46 | 0.10 | 0.65 | 0.40 | 0.19 | 0.17 | <0.06 | 0.73 |
| | 50 | 3.01 | 35.04 | 0.15 | 0.30 | 27.92 | 0.15 | 0.17 | – | 2.35 | 0.66 | <0.04 | 0.37 | 0.16 |
| | 140 | – | – | – | – | – | <0.01 | 0.26 | 5.15 | 3.10 | 0.57 | 0.15 | 0.30 | 0.14 |
| C | 5 | 2.59 | 34.68 | 0.09 | 1.93 | 27.67 | <0.01 | 0.09 | 0.35 | 0.30 | 0.24 | 0.27 | 0.28 | 0.80 |
| | 35 | 2.84 | 34.96 | 0.56 | 1.24 | 27.87 | 0.30 | 0.07 | 0.85 | 0.40 | 0.19 | 0.31 | 0.41 | 0.57 |
| | 60 | 2.89 | 34.97 | 1.66 | 0.94 | 27.87 | 0.25 | 0.08 | 1.05 | 0.25 | 0.23 | 0.69 | 0.26 | 0.41 |
| | 180 | 2.73 | 35.06 | 0.42 | 0.32 | 27.96 | 0.20 | 0.15 | 3.95 | 3.20 | 0.63 | 0.27 | 0.07 | 0.21 |
| D | 3 | 3.35 | 34.22 | 0.03 | 4.27 | 27.23 | 0.10 | 0.04 | 0.75 | 0.40 | 0.12 | 0.25 | 0.25 | 1.27 |
| | 15 | 2.63 | 34.81 | 0.11 | 1.79 | 27.77 | 0.05 | 0.03 | 0.45 | 0.20 | 0.15 | 0.12 | 0.13 | 0.75 |
| | 35 | 2.25 | 34.86 | 0.34 | 1.75 | 27.84 | 0.15 | 0.12 | 1.60 | 0.23 | 0.22 | 0.23 | 0.45 | 0.91 |
| September survey | | | | | | | | | | | | | | |
| A | 5 | 4.15 | 33.51 | – | – | 26.59 | 0.08 | 0.11 | 0.10 | 0.30 | 0.21 | 0.89 | 1.38 | 0.82 |
| | 22 | 4.60 | 34.21 | – | – | 27.10 | 0.43 | 0.04 | <0.01 | 0.80 | <0.01 | 0.64 | 0.48 | 0.35 |
| | 40 | 4.69 | 34.31 | – | – | 27.17 | 0.25 | <0.01 | 0.15 | 0.83 | 0.13 | 0.59 | 0.29 | 0.39 |
| B | 5 | 4.45 | 33.48 | 0.89 | 1.77 | 26.54 | 0.08 | 0.08 | <0.01 | 0.65 | 0.09 | 0.41 | 0.63 | 0.63 |
| | 50 | 4.45 | 34.29 | 0.23 | 0.28 | 27.18 | 0.51 | 0.05 | 0.30 | 0.65 | 0.27 | 0.16 | 0.22 | 0.18 |
| | 100 | 3.16 | 34.81 | 0.05 | 0.22 | 27.72 | 1.02 | 0.11 | 2.50 | 2.60 | 0.57 | 0.12 | 0.22 | 0.14 |
| | 140 | 2.97 | 34.87 | 0.03 | 0.25 | 27.78 | 0.51 | 0.08 | 3.60 | 2.75 | 0.56 | 0.05 | 0.08 | 0.16 |
| C | 5 | 3.29 | 32.70 | 1.30 | 5.12 | 26.03 | 0.35 | 0.17 | 0.40 | 0.50 | 0.13 | 1.16 | 0.25 | 1.96 |
| | 30 | 4.55 | 33.95 | 0.36 | 0.82 | 26.89 | 0.35 | <0.01 | <0.01 | 0.90 | 0.10 | – | – | 0.40 |
| | 70 | 3.77 | 34.52 | 0.11 | 0.64 | 27.43 | 0.61 | 0.30 | 1.50 | 1.95 | 0.38 | 0.09 | <0.06 | 0.30 |
| | 170 | 3.32 | 34.91 | 0.04 | 0.50 | 27.78 | <0.01 | 0.07 | 4.40 | 3.60 | 0.64 | <0.04 | <0.06 | 0.17 |
| D | 4 | 2.89 | 32.35 | 0.68 | 7.17 | 25.78 | 0.52 | 0.23 | 0.75 | 2.10 | 0.20 | 0.36 | 0.07 | 2.92 |
| | 15 | 2.95 | 33.34 | 0.42 | 6.47 | 26.56 | 0.26 | 0.26 | 0.73 | 1.30 | 0.10 | 0.52 | 0.32 | 1.70 |
| | 35 | 3.16 | 34.12 | 0.14 | 3.64 | 27.17 | 0.43 | 0.28 | 1.10 | 1.85 | 0.37 | 0.28 | <0.06 | 1.18 |

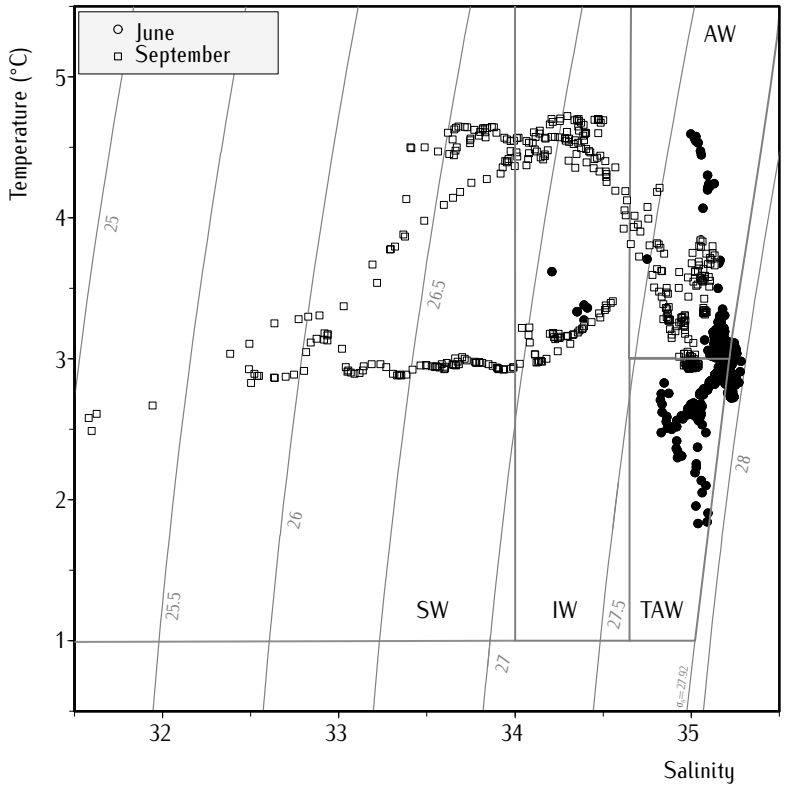


Figure 5.2. $\theta$/S diagram of the stations sampled in Kongsfjorden during June (•) and September (□) surveys. AW = Atlantic Water; IW = Intermediate Water; SW = Surface Water; TAW = Transformed Atlantic Water.

At Kongsfjorden, solar heating reaches the top 20–30 m of the water column in early June every year (Hegseth and Tverberg 2013). As a consequence of the increasing incident solar radiation, warm surface temperature (from 2.65 to 4.60 °C) and low salinity (34.19 to 34.99) were recorded during the June survey. The range of the surface temperature remained almost the same in September (from 2.44 to 4.49 °C), while a decrease of the surface salinity was observed (range from 29.67 to 33.33). In particular, the lowest salinity was measured at the surface in station D, located near the Kongsbreen glacier. Therefore, SW was found during the September survey only, occupying the top 20–30 m of the water column.

SW formed from glacial melt is dominant in summer in a layer that generally decreases from the inner part toward the fjord mouth (Svendsen et al. 2002). The freshwater input of melting ice and the solar heating determine the strength of the surface stratification.

In this study, an increase of in situ density $>0.05\,kg/m^3$ over a 5 m depth interval was the criterion used to establish the depth of the upper mixed layer (UML) in the surface and sub-surface layer (Mitchell and Holm-Hansen 1991). A thin UML was found in stations A and D (6 m) in the June survey, whereas it became deeper in the other stations, ranging from 11 m (station C) to 27 m (station B). The UML became shallowest and comparable in all of the stations (6 m) in September, consistent with surface salinity values lower than those measured in June, since salinity, at cold temperatures, contributes more than temperature in determining density.

IW was found at the top 0–6 m at station D in June (therefore it coincided with the UML); it occupied the whole water column below the surface water at stations A and

D and the intermediate layer down to about 70 m at stations B and C in September. As regards the deeper layer, intruding AW was revealed in station A in June only and in stations B and C in both surveys. Moreover, at station B, AW was shallower than 54 m in June and displayed a layer between 66 and 107 m in September, whereas at station C, it was deeper than 75 m in both surveys.

The nutrient concentration ranges were quite similar in both surveys, with the highest values at the bottom layer of stations B and C, as a consequence of the Atlantic water intrusion (table 5.5). Phosphate positively and significantly co-varied with nitrate ($R^2 = 0.83$).

An important factor controlling nutrient utilization in surface waters is the Redfield ratio, which describes the stoichiometric relationship between phytoplankton cellular C and major inorganic nutrients (N and P) that are required for phytoplankton growth. A number of studies have shown that the drawdown of C, N and P deviates substantially from Redfield ratios (106:16:1), suggesting an important role played by phytoplankton taxonomic variation. For instance when diatoms dominate the phytoplankton bloom the ratio decreases (Massolo et al. 2009). In this study, N/P disappearance ratio was calculated from the slope of $NO_3{}^-$ plotted against $PO_4{}^{3-}$ for the whole dataset and it was lower than the Redfield value (7.56), suggesting that diatom bloom occurred prior to our surveys. This finding is consistent with previous studies carried out in the Kongsfjorden area, reporting diatoms as the dominating species in the spring bloom (Degerlund and Eilertsen 2009).

The silicate concentration followed partly the same patterns as shown by nitrate and phosphate, exhibiting the lowest values (0.3–0.7 µM) in the upper 20 m of the entire fjord and the highest in deeper layers. The only exception was observed in the September survey in station D, where it had a concentration as high as 2.1 µM at the surface, consistent with the input of glacial ice melting. Differently from nitrate, silicate was never exhausted.

Our data are significantly lower than those already reported for the Kongsfjorden area by Hegseth and Tverberg (2013) (3–10 µM and 1–6 µM for nitrate and silicate, respectively), referring to spring sampling, when nutrients in upper layer become already reduced to about half of the winter values (Svendsen et al. 2002). However, it is important to note that, in this study, the sampling occurred in late spring–late summer, when nutrients had been consumed by photosynthetic activities.

Similarly to nutrients, low levels of Chl-*a* were measured in our samples, ranging from <0.04–0.69 µg/L and from <0.04–1.16 µg/L in June and September, respectively. These data are lower than values previously reported for the Kongsfjorden area, consistent with the fact that April is the normal time for the spring bloom in fjords in Svalbard (Hegseth and Tverberg 2013). Therefore, these environmental conditions appeared favorable to investigate sources and physical transport of particulate elements, without the overlapping of biological activity.

Concerning the SPM, the observed ranges were 0.14–1.27 mg/L and 0.14–2.92 mg/L, in June and September, respectively (table 5.5) with the highest values recorded at the surface, particularly in station D, which is close to the inter-moraine depression area where preferential sediment accumulation occurs. This result is in agreement with the spatial distribution of PIM previously reported (Svendsen et al. 2002). The intruding Atlantic waters were characterised by a relatively low content of SPM in both surveys (∼0.2 mg/L), with the lowest values in the deep waters of stations B and C.

### 5.3.2 Trace elements associated to SPM

The concentrations of trace metals associated to SPM, expressed in terms of both water volume and SPM mass, are reported in tables 5.6 and 5.7. The concentration ranges of

Table 5.6. particulate trace elements concentration (moles of element per seawater volume) measured in the Kongsfjorden.

| Station | Depth | Al | Ca | Fe | K | Mg | Na | Ba | Cr | Cu | Mn | Ni | P | Sr | Ti | V | Zn | Cd | Co | Mo | Pb |
|---|---|---|---|---|---|---|---|---|---|---|---|---|---|---|---|---|---|---|---|---|---|
| | (m) | (μM) | | | | | | (nM) | | | | | | | | | | (pM) | | | |
| June survey | | | | | | | | | | | | | | | | | | | | | |
| A | 3 | 0.47 | 0.74 | 0.16 | 0.09 | 0.43 | 0.09 | 0.91 | 0.42 | 0.69 | 3.31 | 0.36 | 116 | 0.75 | 8.18 | 0.57 | 0.89 | 3 | 43 | 36 | 50 |
| | 20 | 0.34 | 0.38 | 0.13 | 0.08 | 0.29 | 0.44 | 0.57 | 0.60 | 0.62 | 4.49 | 0.36 | 114 | 0.67 | 7.08 | 0.56 | 0.87 | 3 | 40 | 38 | 85 |
| | 35 | 0.32 | 0.27 | 0.11 | 0.05 | 0.17 | 0.09 | 0.59 | 0.33 | 0.55 | 6.32 | 0.20 | 67.7 | 0.55 | 7.22 | 0.41 | 0.63 | 3 | 39 | 21 | 67 |
| B | 5 | 0.55 | 0.52 | 0.18 | 0.10 | 0.28 | 0.09 | 0.88 | 0.33 | 0.81 | 5.35 | 0.17 | 60.9 | 0.63 | 10.5 | 0.58 | 1.35 | 3 | 53 | 7 | 93 |
| | 20 | 0.13 | 0.25 | 0.04 | 0.16 | 0.75 | 6.50 | 0.87 | 0.52 | 0.31 | 2.19 | 0.17 | 20.6 | 1.43 | 4.20 | 0.19 | 0.76 | 123 | 14 | 3 | 20 |
| | 50 | 0.14 | 0.09 | 0.04 | 0.03 | 0.10 | 0.38 | 0.51 | 0.12 | 0.18 | 2.53 | 0.05 | 19.9 | 0.29 | 5.64 | 0.18 | 0.31 | 11 | 15 | 3 | 26 |
| | 140 | 0.13 | 0.04 | 0.04 | 0.02 | 0.05 | 0.08 | 0.61 | 0.11 | 0.42 | 2.01 | 0.10 | 20.8 | 0.22 | 5.39 | 0.21 | 0.35 | 4 | 11 | 28 | 25 |
| C | 5 | 1.55 | 0.75 | 0.55 | 0.31 | 0.55 | 0.09 | 4.48 | 1.08 | 0.51 | 13.0 | 0.43 | 65.4 | 0.84 | 36.1 | 1.52 | 2.64 | 4 | 176 | 16 | 176 |
| | 35 | 0.73 | 0.53 | 0.26 | 0.13 | 0.39 | 0.63 | 2.21 | 1.08 | 1.34 | 7.66 | 0.78 | 62.4 | 0.67 | 1.47 | 0.73 | 2.82 | 18 | 81 | 26 | 83 |
| | 60 | 0.62 | 0.36 | 0.22 | 0.11 | 0.27 | 0.09 | 1.29 | 0.37 | 0.32 | 7.41 | 0.20 | 54.9 | 0.47 | 13.4 | 0.69 | 1.28 | 4 | 68 | 11 | 51 |
| | 180 | 0.26 | 0.15 | 0.11 | 0.04 | 0.12 | 0.09 | 0.87 | 0.66 | 0.31 | 2.69 | 0.26 | 24.2 | 0.26 | 6.59 | 0.41 | 1.27 | 4 | 32 | 22 | 65 |
| D | 3 | 2.74 | 1.64 | 0.94 | 0.58 | 1.00 | 0.09 | 2.98 | 1.68 | 1.20 | 20.8 | 0.83 | 104 | 1.39 | 56.1 | 2.48 | 2.56 | 42 | 349 | 27 | 143 |
| | 15 | 1.43 | 0.91 | 0.49 | 0.29 | 0.61 | 0.58 | 1.77 | 1.13 | 0.61 | 17.6 | 0.52 | 61.0 | 0.90 | 27.6 | 1.39 | 1.50 | 19 | 170 | 33 | 161 |
| | 35 | 1.55 | 1.04 | 0.53 | 0.33 | 0.71 | 1.23 | 1.93 | 0.97 | 0.73 | 28.1 | 0.76 | 67.2 | 1.44 | 30.1 | 1.54 | 3.31 | 141 | 187 | 23 | 128 |
| September survey | | | | | | | | | | | | | | | | | | | | | |
| A | 5 | 1.25 | 0.50 | 0.45 | 0.30 | 0.56 | 1.72 | 1.85 | 0.95 | 2.30 | 10.2 | 0.58 | 83.0 | 1.36 | 25.9 | 1.24 | 4.40 | 4 | 166 | 33 | 133 |
| | 22 | 0.35 | 0.20 | 0.11 | 0.06 | 0.15 | 0.11 | 0.60 | 0.25 | 0.56 | 7.13 | 0.16 | 49.7 | 0.91 | 7.47 | 0.40 | 1.41 | 4 | 44 | 12 | 43 |
| | 40 | 0.40 | 0.25 | 0.14 | 0.10 | 0.29 | 1.30 | 0.58 | 0.20 | 0.49 | 5.67 | 0.10 | 35.9 | 0.64 | 9.29 | 0.44 | 0.86 | 4 | 45 | 16 | 42 |
| B | 5 | 1.23 | 0.38 | 0.43 | 0.24 | 0.42 | 0.09 | 1.78 | 0.76 | 1.15 | 13.2 | 0.40 | 67.8 | 1.69 | 21.6 | 1.20 | 2.19 | 4 | 162 | 96 | 81 |
| | 50 | 0.22 | 0.11 | 0.07 | 0.04 | 0.12 | 0.31 | 0.50 | 0.28 | 0.45 | 8.36 | 0.14 | 23.1 | 0.41 | 5.98 | 0.28 | 0.85 | 22 | 33 | 94 | 28 |
| | 100 | 0.14 | 0.08 | 0.06 | 0.03 | 0.10 | 0.46 | 0.62 | 0.41 | 1.34 | 6.65 | 0.16 | 8.50 | 0.28 | 4.49 | 0.25 | 1.97 | 4 | 23 | 84 | 65 |
| | 140 | 0.23 | 0.12 | 0.09 | 0.04 | 0.12 | 0.33 | 0.57 | 0.58 | 1.48 | 7.37 | 0.41 | 9.19 | 0.38 | 5.81 | 0.35 | 1.58 | 4 | 31 | 55 | 165 |
| C | 5 | 4.36 | 1.96 | 1.60 | 1.05 | 1.51 | 1.04 | 4.66 | 3.51 | 4.07 | 27.1 | 1.29 | 122 | 4.35 | 111 | 4.12 | 5.64 | 18 | 568 | 69 | 266 |
| | 30 | 0.45 | 0.25 | 0.17 | 0.12 | 0.29 | 1.32 | 0.86 | 0.50 | 2.57 | 11.0 | 0.74 | 33.8 | 0.60 | 14.6 | 0.50 | 2.57 | 30 | 71 | 25 | 220 |
| | 70 | 0.59 | 0.31 | 0.23 | 0.12 | 0.24 | 0.33 | 0.89 | 0.72 | 1.55 | 7.94 | 0.47 | 17.0 | 0.44 | 15.3 | 0.65 | 2.78 | 4 | 75 | 63 | 179 |
| | 170 | 0.24 | 0.15 | 0.10 | 0.04 | 0.12 | 0.19 | 0.56 | 0.75 | 1.44 | 5.36 | 0.38 | 11.4 | 0.38 | 6.72 | 0.36 | 3.11 | 4 | 34 | 35 | 135 |
| D | 4 | 7.70 | 2.95 | 2.80 | 1.82 | 2.31 | 1.03 | 7.89 | 4.83 | 1.96 | 37.6 | 2.00 | 85.3 | 3.10 | 176 | 6.82 | 7.10 | 12 | 996 | 29 | 536 |
| | 15 | 4.43 | 1.86 | 1.54 | 0.99 | 1.34 | 0.09 | 4.86 | 2.81 | 1.22 | 25.0 | 1.11 | 69.9 | 1.73 | 95.1 | 3.85 | 3.86 | 4 | 537 | 20 | 232 |
| | 35 | 3.12 | 1.37 | 1.09 | 0.66 | 0.99 | 0.09 | 3.24 | 1.96 | 1.96 | 18.2 | 0.81 | 40.6 | 1.23 | 67.1 | 2.77 | 2.73 | 4 | 369 | 19 | 162 |

Table 5.7. particulate trace elements concentration (moles of element per mass of SPM) measured in the Kongsfjorden.

| Station | Depth | Al | Ca | Fe | K | Mg | Na | Ba | Cr | Cu | Mn | Ni | P | Sr | Ti | V | Zn | Cd | Co | Mo | Pb |
|---|---|---|---|---|---|---|---|---|---|---|---|---|---|---|---|---|---|---|---|---|---|
| | (m) | (mmol/g) | | | | | | (µmol/g) | | | | | | | | | | (nmol/g) | | | |
| June survey | | | | | | | | | | | | | | | | | | | | | |
| A | 3 | 0.94 | 1.48 | 0.32 | 0.18 | 0.86 | 0.17 | 1.81 | 0.85 | 1.38 | 6.61 | 0.72 | 231 | 1.50 | 16.4 | 1.15 | 1.79 | 7 | 85 | 73 | 100 |
| | 20 | 0.64 | 0.71 | 0.24 | 0.15 | 0.55 | 0.84 | 1.08 | 1.13 | 1.16 | 8.47 | 0.68 | 215 | 1.27 | 13.4 | 1.05 | 1.64 | 6 | 76 | 72 | 160 |
| | 35 | 1.00 | 0.86 | 0.35 | 0.17 | 0.54 | 0.27 | 1.85 | 1.05 | 1.73 | 19.9 | 0.63 | 213 | 1.72 | 22.8 | 1.29 | 2.00 | 10 | 122 | 66 | 211 |
| B | 5 | 1.44 | 1.35 | 0.48 | 0.26 | 0.74 | 0.23 | 2.30 | 0.87 | 2.13 | 14.0 | 0.45 | 159 | 1.64 | 27.4 | 1.51 | 3.52 | 9 | 139 | 19 | 244 |
| | 20 | 0.18 | 0.34 | 0.06 | 0.22 | 1.02 | 8.90 | 1.19 | 0.71 | 0.42 | 3.00 | 0.23 | 28.2 | 1.97 | 5.75 | 0.26 | 1.04 | 169 | 20 | 4 | 27 |
| | 50 | 0.87 | 0.55 | 0.27 | 0.19 | 0.61 | 2.35 | 3.17 | 0.72 | 1.15 | 15.8 | 0.32 | 124 | 1.82 | 35.2 | 1.13 | 1.91 | 67 | 92 | 20 | 164 |
| | 140 | 0.90 | 0.31 | 0.29 | 0.14 | 0.37 | 0.56 | 4.25 | 0.76 | 2.95 | 14.1 | 0.73 | 146 | 1.56 | 37.8 | 1.47 | 2.45 | 25 | 78 | 196 | 174 |
| C | 5 | 1.95 | 0.94 | 0.70 | 0.39 | 0.69 | 0.11 | 5.64 | 1.36 | 0.64 | 16.4 | 0.54 | 82.2 | 1.05 | 45.4 | 1.92 | 3.32 | 4 | 222 | 20 | 222 |
| | 35 | 1.29 | 0.94 | 0.45 | 0.23 | 0.69 | 1.11 | 3.92 | 1.92 | 2.37 | 13.6 | 1.39 | 110 | 1.19 | 2.60 | 1.30 | 5.00 | 32 | 143 | 46 | 147 |
| | 60 | 1.51 | 0.89 | 0.53 | 0.28 | 0.65 | 0.21 | 3.15 | 0.90 | 0.78 | 18.1 | 0.49 | 134 | 1.15 | 32.6 | 1.67 | 3.13 | 9 | 167 | 28 | 124 |
| | 180 | 1.28 | 0.73 | 0.55 | 0.21 | 0.58 | 0.46 | 4.26 | 3.23 | 1.53 | 13.1 | 1.27 | 118 | 1.28 | 32.1 | 1.99 | 6.21 | 17 | 155 | 105 | 317 |
| D | 3 | 2.15 | 1.29 | 0.74 | 0.45 | 0.79 | 0.07 | 2.34 | 1.32 | 0.94 | 16.3 | 0.65 | 81.9 | 1.09 | 44.1 | 1.95 | 2.01 | 33 | 274 | 22 | 112 |
| | 15 | 1.90 | 1.21 | 0.65 | 0.39 | 0.81 | 0.77 | 2.36 | 1.50 | 0.81 | 23.4 | 0.69 | 81.1 | 1.20 | 36.7 | 1.84 | 1.99 | 25 | 227 | 44 | 214 |
| | 35 | 1.70 | 1.13 | 0.58 | 0.37 | 0.78 | 1.35 | 2.11 | 1.06 | 0.80 | 30.8 | 0.84 | 73.7 | 1.58 | 32.9 | 1.68 | 3.63 | 154 | 205 | 25 | 140 |
| September survey | | | | | | | | | | | | | | | | | | | | | |
| A | 5 | 1.52 | 0.61 | 0.55 | 0.37 | 0.69 | 2.09 | 2.26 | 1.16 | 2.81 | 12.4 | 0.71 | 101 | 1.65 | 31.6 | 1.51 | 5.37 | 4 | 202 | 41 | 162 |
| | 22 | 1.00 | 0.56 | 0.32 | 0.18 | 0.44 | 0.32 | 1.71 | 0.71 | 1.61 | 20.4 | 0.45 | 142 | 2.60 | 21.4 | 1.14 | 4.02 | 10 | 125 | 35 | 123 |
| | 40 | 1.02 | 0.63 | 0.36 | 0.26 | 0.76 | 3.36 | 1.49 | 0.53 | 1.25 | 14.6 | 0.26 | 93 | 1.64 | 24.0 | 1.14 | 2.22 | 9 | 115 | 41 | 107 |
| B | 5 | 1.96 | 0.61 | 0.69 | 0.38 | 0.67 | 0.14 | 2.83 | 1.21 | 1.82 | 20.9 | 0.63 | 108 | 2.69 | 34.3 | 1.91 | 3.48 | 6 | 257 | 153 | 129 |
| | 50 | 1.20 | 0.63 | 0.41 | 0.24 | 0.65 | 1.70 | 2.73 | 1.51 | 2.46 | 45.8 | 0.77 | 127 | 2.26 | 32.7 | 1.54 | 4.64 | 120 | 180 | 513 | 155 |
| | 100 | 0.97 | 0.60 | 0.41 | 0.21 | 0.73 | 3.26 | 4.44 | 2.96 | 9.59 | 47.5 | 1.11 | 60.7 | 2.00 | 32.1 | 1.78 | 14.1 | 25 | 167 | 603 | 462 |
| | 140 | 1.40 | 0.71 | 0.54 | 0.27 | 0.72 | 2.03 | 3.49 | 3.57 | 9.10 | 45.3 | 2.52 | 56.6 | 2.32 | 35.8 | 2.14 | 9.69 | 22 | 190 | 339 | 1016 |
| C | 5 | 2.23 | 1.00 | 0.82 | 0.54 | 0.77 | 0.53 | 2.38 | 1.80 | 2.08 | 13.9 | 0.66 | 62.6 | 2.23 | 56.6 | 2.11 | 2.89 | 9 | 290 | 35 | 136 |
| | 30 | 1.14 | 0.63 | 0.43 | 0.30 | 0.74 | 3.32 | 2.15 | 1.27 | 6.48 | 27.7 | 1.87 | 85.1 | 1.50 | 36.8 | 1.27 | 6.47 | 75 | 178 | 63 | 554 |
| | 70 | 1.99 | 1.04 | 0.76 | 0.40 | 0.80 | 1.13 | 3.01 | 2.44 | 5.27 | 26.9 | 1.59 | 57.7 | 1.49 | 51.9 | 2.19 | 9.41 | 12 | 255 | 215 | 608 |
| | 170 | 1.45 | 0.88 | 0.58 | 0.27 | 0.72 | 1.13 | 3.34 | 4.49 | 8.59 | 32.0 | 2.26 | 67.8 | 2.26 | 40.1 | 2.17 | 18.6 | 21 | 203 | 209 | 804 |
| D | 4 | 2.64 | 1.01 | 0.96 | 0.62 | 0.79 | 0.35 | 2.70 | 1.65 | 0.67 | 12.9 | 0.68 | 29.2 | 1.06 | 60.2 | 2.34 | 2.43 | 4 | 341 | 10 | 184 |
| | 15 | 2.61 | 1.10 | 0.91 | 0.59 | 0.79 | 0.05 | 2.87 | 1.65 | 0.72 | 14.8 | 0.66 | 41.3 | 1.02 | 56.1 | 2.27 | 2.27 | 2 | 317 | 12 | 137 |
| | 35 | 2.65 | 1.17 | 0.93 | 0.56 | 0.84 | 0.07 | 2.76 | 1.66 | 1.67 | 15.4 | 0.69 | 34.5 | 1.05 | 57.0 | 2.35 | 2.32 | 3 | 314 | 16 | 138 |

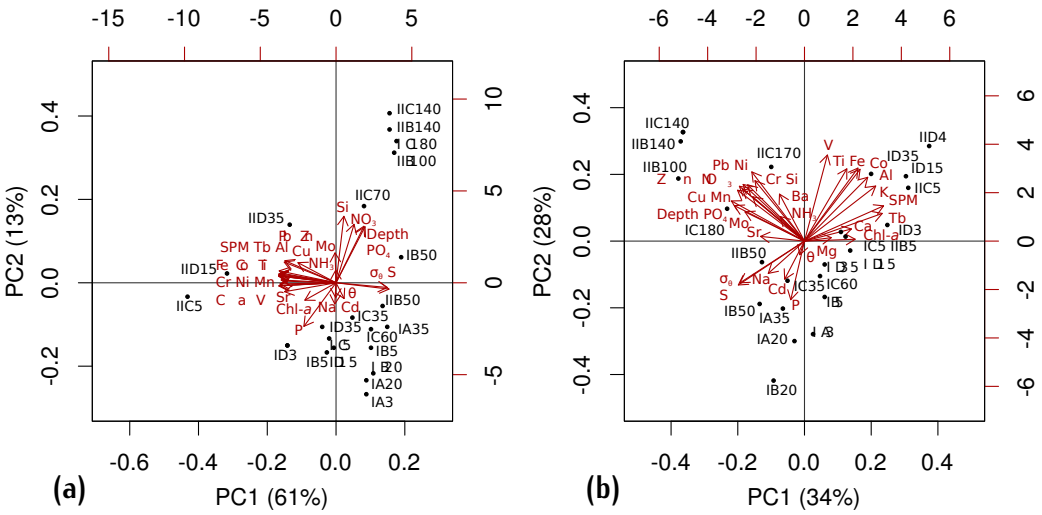


Figure 5.3. principal component analysis results for samples of suspended particulate matter collected in the Kongsfjorden. Particulate metal concentrations expressed in terms of water volume **(a)** or SPM mass **(b)**. The score label includes the sampling period (I = June; II = September), the site (stations A–D, see figure 5.1) and the sampling depth.

Cd, Cu, Fe, Mn, Pb and Zn were similar to those reported by Ahn et al. (2004) for Marian Cove (Maxwell Bay, King George Island, Antarctica), a fjord affected by glacier-melt water during the austral summer. In order to explore possible correlations among trace elements and other physical (salinity, density, temperature) and biological (chlorophyll-*a*, nutrients) parameters, and to identify similarities among the samples, PCA was applied to the dataset, providing the results displayed in figure 5.3.

Figure 5.3 **(a)** shows the bi-plot (score and loadings plots overlapped) obtained by expressing particulate metal concentrations in terms of water volume. After auto-scaling of the data, two principal components were identified, collectively explaining 74 % of the total variance of the data. The loadings of the variables that constitutes these components showed that the concentration of SPM and associated elements is negatively correlated with salinity and density, highlighting the influence of the freshwater outflowing from the glaciers in determining the amount of SPM and trace metals in the water column. Differences in the elemental composition of SPM were emphasized by performing PCA on the data expressing the metal concentration in terms of SPM mass. The result is shown in figure 5.3 **(b)**. The loadings of the variables on the first two principal components (which collectively explain 62 % of the total variance) clearly divided the variables into two groups, almost uncorrelated to each other. The first one comprises SPM and a number of associated metals, such as Al, Co, Fe, K, Ti and V, which are negatively and significantly ($p$-value$<0.05$) correlated with salinity. The second group is strongly related to the sampling depth and it comprises nutrients and the remaining trace elements, namely Ba, Cr, Cu, Mn, Mo, Ni, Pb and Zn. This result could suggest two different sources of particulate trace elements: those metals comprised in the first group are related to inputs of particulate matter from the fresher runoff waters of the glaciers, whereas the elements of the second group could enter the fjord by the intrusion of Atlantic water, characterised by a relatively high nutrient and low SPM content, as well (see section 5.3.1).

This finding is also supported by the PCA scores of the samples. These are plotted in figure 5.3 **(b)** using a three-term label, which indicates the sampling period (I = June; II = September), the site (stations A–D, see figure 5.1) and the sampling depth. The

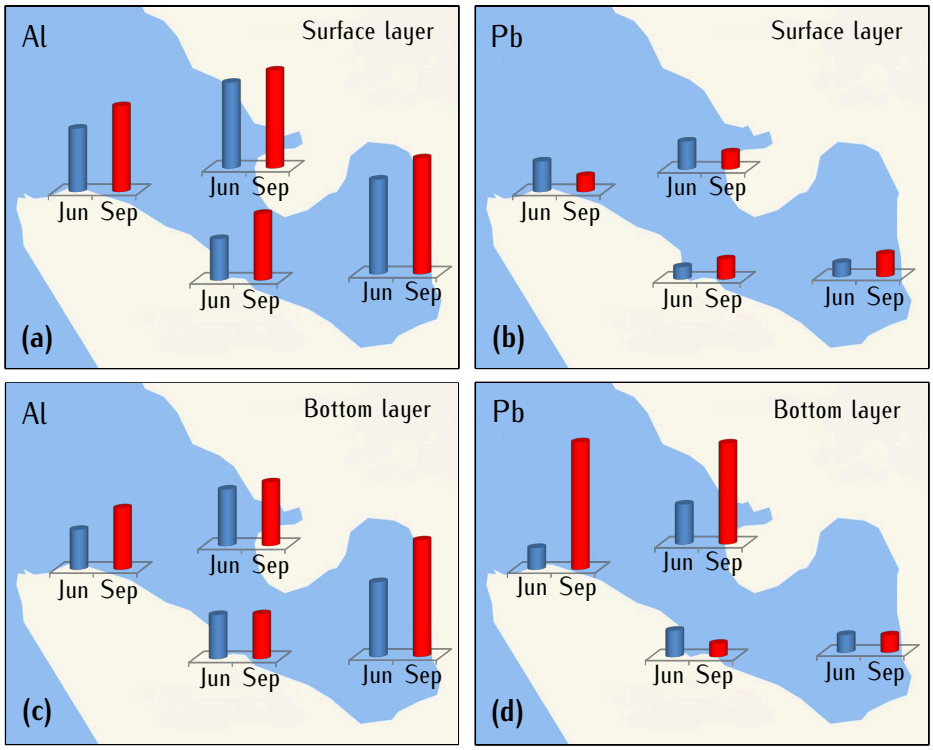


Figure 5.4. concentrations of Al **(a, b)** and Pb **(c, d)** in surface **(a, c)** and bottom **(b, d)** layers in Kongsfjorden.

samples collected in June were separated from those collected in September on PC2. The concentration of terrigenous elements (*e.g.* Al, Fe, Ti), higher in September than in June, can be attributed to a more relevant input of glacial freshwater, as suggested by the loading of the salinity on this PC. Similarly, their concentrations increased moving toward the Kongsbreen (from stations B to D) and to the water surface, reaching a maximum for the sample IID4. Conversely, metals such as Cr and Pb showed higher concentrations in deep seawater samples collected at the outer fjord (stations B and C), where the in-flow of water masses of Atlantic origin was evidenced by the hydrographic properties and nutrient concentration. This result is also consistent with the spatial distribution of Pb in surface sediments from Kongsfjorden as described by Lu et al. (2013) and Grotti et al. (2013b), who attributed its higher average concentration in the outer fjord to the influence of the WSC.

The findings from PCA are well illustrated in figure 5.4, where concentrations of Al (chosen as representative for the elements of the first PCA group) and Pb (chosen as representative for the elements of the second PCA group) in surface and bottom layers are displayed.

### 5.3.3 Sources of trace elements inferred from Pb isotope ratios and enrichment factors

The possible sources of the particulate metals introduced into the marine environment of Kongsfjorden were investigated measuring $^{208}Pb/^{207}Pb$ and $^{206}Pb/^{207}Pb$ isotope ratios and comparing them with the isotopic signature of the atmospheric particulate and marine sediments collected in the same area. The values (table 5.8) are represented

in figure 5.5, where SPM samples are arranged in a straight line, with the samples collected above 40 m depth (*i.e.* surely not influenced by Atlantic waters) lying above those collected in the deepest layer of the water column. This alignment would suggest that the Pb occurring in the samples is the result of the mixing of two end-members. The possible origin of Pb from two different sources was further verified by calculating the Pb enrichment factors EF(Pb/Al), according to equation (4.5) at page 46.

Finally, the Pb isotope ratios were plotted against the calculated enrichment factors, obtaining the following relationships:

$$^{208}\mathrm{Pb}/^{207}\mathrm{Pb} = 2.445 + 0.050 \times \frac{1}{\mathrm{EF(Pb/Al)}} \tag{5.1}$$

$$^{206}\mathrm{Pb}/^{207}\mathrm{Pb} = 1.162 + 0.054 \times \frac{1}{\mathrm{EF(Pb/Al)}} \tag{5.2}$$

The best-fitting straight line through the data fitted the experimental data with an $R^2$ of 0.67 and 0.91, respectively. Therefore, a natural source of Pb, characterised by the highest isotope ratios and EF(Pb/Al) close to 1, can be distinguished from an anthropogenic source characterised by the lowest isotopic ratios and high EF(Pb/Al). From equations (5.1) and (5.2), the isotopic composition of the natural ($^{208}\mathrm{Pb}/^{207}\mathrm{Pb} = 2.496$, $^{208}\mathrm{Pb}/^{207}\mathrm{Pb} = 1.216$) and the anthropogenic ($^{208}\mathrm{Pb}/^{207}\mathrm{Pb} = 2.445$, $^{208}\mathrm{Pb}/^{207}\mathrm{Pb} = 1.162$) end-members was estimated by considering $\mathrm{EF(Pb/Al)} = 1$ and $\mathrm{EF(Pb/Al)} = \infty$, respectively.

The first isotopic signature was close to the Pb isotope ratios measured in the marine sediments collected at the four sites considered ($^{208}\mathrm{Pb}/^{207}\mathrm{Pb} = 2.481 \pm 0.004$; $^{206}\mathrm{Pb}/^{207}\mathrm{Pb} = 1.206 \pm 0.002$). Moreover, the natural ratio estimated for $^{206}\mathrm{Pb}/^{207}\mathrm{Pb}$ (1.216) was in good agreement with the background value (1.220) recorded by Liu et al. (2012) in lake sediment cores collected at Ny-Ålesund and dated from 1000 BC to 1400 AD. The other end-member showed isotope ratios similar to the atmospheric particulate collected at Ny-Ålesund from March to September of that very year ($^{208}\mathrm{Pb}/^{207}\mathrm{Pb} = 2.442 \pm 0.009$; $^{206}\mathrm{Pb}/^{207}\mathrm{Pb} = 1.165 \pm 0.005$; $n = 31$) (Bazzano et al. 2015). A similar Pb isotopic composition was also obtained considering the weighted average for the particulate matter collected at the same sampling site from 2010 to 2014 ($^{208}\mathrm{Pb}/^{207}\mathrm{Pb} = 2.4360 \pm 0.0003$; $^{206}\mathrm{Pb}/^{207}\mathrm{Pb} = 1.1597 \pm 0.0003$, $n = 129$; mean ±95 %-confidence interval, table 4.2). Hence, anthropogenic Pb is likely introduced into Kongsfjorden by atmospheric particulate, either by direct deposition inside the fjord basin or, indirectly, through the Atlantic waters entering the fjord. Accordingly, Véron et al. (1999) reported $^{206}\mathrm{Pb}/^{207}\mathrm{Pb}$ values of 1.165, 1.167 and 1.169 for superficial Atlantic waters collected between the Iceland–Scotland Ridge and Denmark Straits, attributing these results to inputs of atmospheric particulate from Eurasia.

The relative importance of both natural and anthropogenic sources showed differences due to the sampling period and spatial trends. The samples collected in September had a quite uniform isotopic signature at stations B, C and D, but low isotope ratio values at station A. Moreover, the surface samples collected in the inner basin were characterised by lower isotope ratios in September than in June, despite the greater extent of the freshwater input from the glacier occurring in late summer. Further investigation is needed to explain this result.

Concerning the spatial trend, Pb isotope ratios in surface waters collected in June decreased by moving from the inner to the outer fjord, tracking the decreasing influence of the continental inputs through the melting of the glaciers. In addition, the outer basin is more influenced by the Atlantic water, which can introduce Pb of anthropogenic origin, characterised by lower isotope ratios. Accordingly, Pb isotope ratios correlated

Table 5.8. Pb isotope ratios (mean values and uncertainties at 95 % confidence level) measured in suspended particulate matter from the Kongsfjorden.

| Station | Depth (m) | $^{208}Pb/^{207}Pb$ | Uncertainty | $^{206}Pb/^{207}Pb$ | Uncertainty |
|---|---|---|---|---|---|
| June survey | | | | | |
| A | 3 | 2.459 | 0.006 | 1.182 | 0.003 |
| | 20 | 2.459 | 0.006 | 1.174 | 0.003 |
| | 35 | 2.453 | 0.007 | 1.170 | 0.003 |
| B | 5 | 2.456 | 0.003 | 1.173 | 0.003 |
| | 20 | 2.461 | 0.007 | 1.175 | 0.004 |
| | 50 | 2.449 | 0.007 | 1.169 | 0.005 |
| | 140 | 2.452 | 0.005 | 1.169 | 0.002 |
| C | 5 | 2.463 | 0.004 | 1.178 | 0.003 |
| | 35 | 2.466 | 0.004 | 1.174 | 0.003 |
| | 60 | 2.470 | 0.003 | 1.180 | 0.004 |
| | 180 | 2.450 | 0.004 | 1.163 | 0.003 |
| D | 3 | 2.479 | 0.005 | 1.191 | 0.003 |
| | 15 | 2.462 | 0.005 | 1.177 | 0.002 |
| | 35 | 2.466 | 0.005 | 1.183 | 0.003 |
| September survey | | | | | |
| A | 5 | 2.449 | 0.003 | 1.176 | 0.001 |
| | 22 | 2.456 | 0.006 | 1.174 | 0.004 |
| | 40 | 2.458 | 0.005 | 1.180 | 0.002 |
| B | 5 | 2.469 | 0.003 | 1.187 | 0.002 |
| | 50 | 2.455 | 0.006 | 1.170 | 0.003 |
| | 100 | 2.449 | 0.005 | 1.163 | 0.003 |
| | 140 | 2.442 | 0.005 | 1.163 | 0.002 |
| C | 5 | 2.458 | 0.003 | 1.184 | 0.002 |
| | 30 | 2.443 | 0.004 | 1.165 | 0.002 |
| | 70 | 2.446 | 0.004 | 1.164 | 0.002 |
| | 140 | – | – | – | – |
| D | 4 | 2.447 | 0.004 | 1.182 | 0.002 |
| | 15 | 2.469 | 0.004 | 1.190 | 0.002 |
| | 35 | 2.468 | 0.003 | 1.192 | 0.002 |

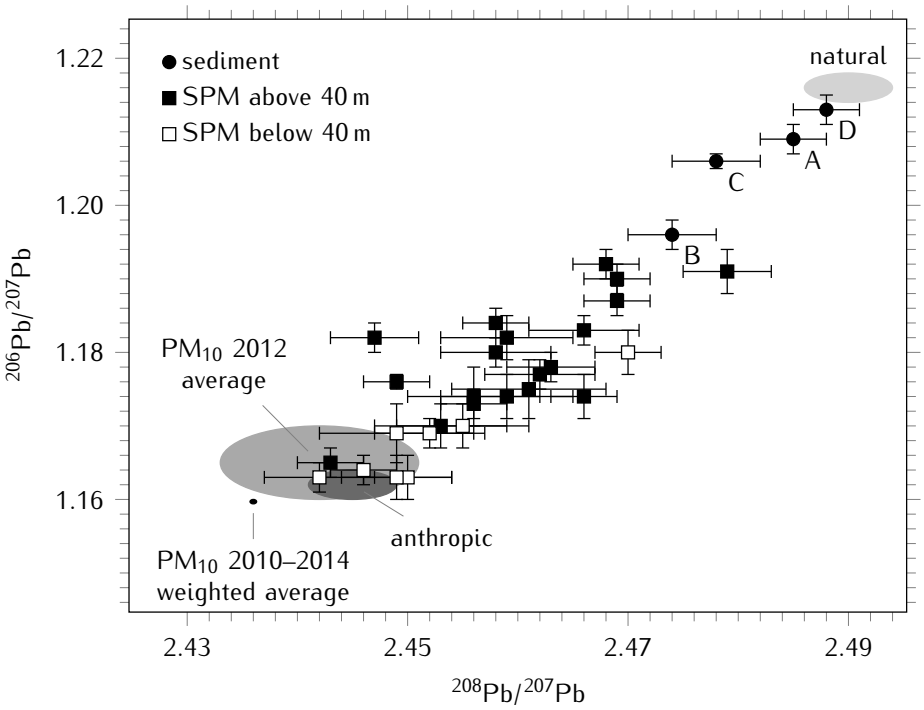


Figure 5.5. Pb isotopic signature of SPM above 40 m (■), SPM below 40 m (□) and sediment (•) samples collected in Kongsfjorden. Ranges for atmospheric particulate (table 4.2) and end-members for natural and anthropogenic sources are also showed.

positively with the elements associated with the glacial runoff (PCA first group), and negatively with those elements introduced by the intrusion of the Atlantic water (PCA second group). This assumption is also supported by the Pb isotope ratios measured in the sediments, which significantly increased from the outer station B toward the central (stations A–C) and inner (station D) parts of the fjord (figure 5.1 ). Moreover, the different isotopic signatures between the sediment samples and the SPM collected in the deep waters allow to exclude any significant contribution to SPM due to sediment re-suspension.

## 5.4 *Conclusions*

The sources of particulate trace elements in the coastal marine environment of Kongsfjorden have been assessed. Natural input from the glacial runoff is the main source for Al, Co, Fe, K, Ti and V, whereas the intrusion of Atlantic waters is a major pathway to introduce Ba, Cr, Cu, Mn, Mo, Ni, Pb and Zn of anthropogenic origin from low and middle latitudes to this Arctic fjord. The relevance of these sources depend on both the sampling site and period. In particular, the influence of the natural source decreased by moving far from the front of the glaciers, while the effect of the Atlantic waters was more relevant at the mouth of the fjord compared to the inner basin. Finally, the effect of both sources was higher at the end of the summer season than in late spring.

*References*

Ahn, I. Y., Chung, K. H., and Choi, H. J., 2004. Influence of glacial runoff on baseline metal accumulation in the Antarctic limpet Nacella concinna from King George Island. *Marine Pollution Bulletin*, **49**, 119–127. DOI: 10.1016/j.marpolbul.2004.03.008

Aliani, S., Bartholini, G., Degl'innocenti, F., Delfanti, R., Galli, C., Lazzoni, E., Lorenzelli, R., Malaguti, A., Meloni, R., Papucci, C., Salvi, S., and Zaborska, A., 2004. Multidisciplinary investigations in the marine environment of the inner Kongsfiord, Svalbard islands (September 2000 and 2001). *Chemistry and Ecology*, **20** (sup1), S19–S28. DOI: 10.1080/02757540410001655396

AMAP, 2005. *AMAP Assessment 2002: Heavy Metals in the Arctic*. Oslo, Norway: Arctic Monitoring and Assessment Programme, xvi + 265 pp.

Bazzano, A., Ardini, F., Becagli, S., Traversi, R., Udisti, R., Cappelletti, D., and Grotti, M., 2015. Source assessment of atmospheric lead measured at Ny-Ålesund, Svalbard. *Atmospheric Environment*, **113**, 20–26. DOI: 10.1016/j.atmosenv.2015.04.053

Beszczynska-Moller, A., Weslawski, J. M., Walczowski, W., and Zajaczkowski, M., 1997. Estimation of glacial meltwater discharge into Svalbard coastal waters. *Oceanologia*, **39**, 289–298

Cottier, F., Tverberg, V., Inall, M., Svendsen, H., Nilsen, F., and Griffiths, C., 2005. Water mass modification in an Arctic fjord through cross-shelf exchange: The seasonal hydrography of Kongsfjorden, Svalbard. *Journal of Geophysical Research, C: Oceans*, **110** (C12), 1–18. DOI: 10.1029/2004JC002757

Degerlund, M. and Eilertsen, H. C., 2009. Main species characteristics of phytoplankton spring blooms in NE Atlantic and Arctic waters (68–80 °N). *Estuaries and Coasts*, **33**, 242–269. DOI: 10.1007/s12237-009-9167-7

Grotti, M., Soggia, F., Abelmoschi, M. L., Rivaro, P., Magi, E., and Frache, R., 2001. Temporal distribution of trace metals in Antarctic coastal waters. *Marine Chemistry*, **76**, 189–209. DOI: 10.1016/S0304-4203(01)00063-9

Grotti, M., Soggia, F., Ianni, C., Magi, E., and Udisti, R., 2013b. Bioavailability of trace elements in surface sediments from Kongsfjorden, Svalbard. *Marine Pollution Bulletin*, **77**, 367–374. DOI: 10.1016/j.marpolbul.2013.10.010

Hansen, H. P. and Koroleff, F., 1999. Determination of nutrients. *Methods of Seawater Analysis*. Ed. by Grasshoff, K., Kremling, K., and Ehrhardt, n. Wiley-VCH Verlag GmbH, 159–228

Hegseth, E. N. and Tverberg, V., 2013. Effect of Atlantic water inflow on timing of the phytoplankton spring bloom in a high Arctic fjord (Kongsfjorden, Svalbard). *Journal of Marine Systems*, **113–114**, 94–105. DOI: 10.1016/j.jmarsys.2013.01.003

Liu, X., Jiang, S., Zhang, P., and Xu, L., 2012. Effect of recent climate change on Arctic Pb pollution: A comparative study of historical records in lake and peat sediments. *Environmental Pollution*, **160**, 161–168. DOI: 10.1016/j.envpol.2011.09.019

Lorenzen, C. J., 1967. Determination of Chlorophyll and Pheo-Pigments: Spectrophotometric Equations1. *Limnology and Oceanography*, **12**, 343–346. DOI: 10.4319/lo.1967.12.2.0343

Lu, Z., Cai, M., Wang, J., Yin, Z., and Yang, H., 2013. Levels and distribution of trace metals in surface sediments from Kongsfjorden, Svalbard, Norwegian Arctic. *Environmental Geochemistry and Health*, **35**, 257–269. DOI: 10.1007/s10653-012-9481-z

Macdonald, R. W., Barrie, L. A., Bidleman, T. F., Diamond, M. L., Gregor, D. J., Semkin, R. G., Strachan, W. M. J., Li, Y. F., Wania, F., Alaee, M., Alexeeva, L. B., Backus, S. M., Bailey, R., Bewers, J. M., Gobeil, C., Halsall, C. J., Harner, T., Hoff, J. T., Jantunen, L. M. M., Lockhart, W. L., Mackay, D., Muir, D. C. G., Pudykiewicz, J., Reimer, K. J., Smith, J. N., Stern, G. A., Schroeder, W. H., Wagemann, R., and Yunker, M. B., 2000. Contaminants in the Canadian Arctic: 5 years of progress in

understanding sources, occurrence and pathways. *Science of the Total Environment*, **254**, 93–234. DOI: 10.1016/S0048-9697(00)00434-4

Massolo, S., Messa, R., Rivaro, P., and Leardi, R., 2009. Annual and spatial variations of chemical and physical properties in the Ross Sea surface waters (Antarctica). *Continental Shelf Research*, **29**, 2333–2344. DOI: 10.1016/j.csr.2009.10.003

Mitchell, B. G. and Holm-Hansen, O., 1991. Observations of modeling of the Antartic phytoplankton crop in relation to mixing depth. *Deep Sea Research Part A: Oceanographic Research Papers*, **38**, 981–1007. DOI: 10.1016/0198-0149(91)90093-U

Muir, D. C. G., Wagemann, R., Hargrave, B. T., Thomas, D. J., Peakall, D. B., and Norstrom, R. J., 1992. Arctic marine ecosystem contamination. *Science of the Total Environment*, **122**, 75–134. DOI: 10.1016/0048-9697(92)90246-O

Muir, D. C. G., Braune, B., DeMarch, B., Norstrom, R., Wagemann, R., Lockhart, L., Hargrave, B., Bright, D., Addison, R., Payne, J., and Reimer, K., 1999. Spatial and temporal trends and effects of contaminants in the Canadian Arctic marine ecosystem: a review. *Science of the Total Environment*, **230**, 83–144. DOI: 10.1016/S0048-9697(99)00037-6

Nies, D. H., 1999. Microbial heavy-metal resistance. *Applied Microbiology and Biotechnology*, **51**, 730–750

R Core Team, 2015. *R: A Language and Environment for Statistical Computing*. URL: http://www.r-project.org/ (visited on 03/03/2016)

Schlitzer, R., 2015. *Ocean Data View*. URL: http://odv.awi.de (visited on 03/03/2016)

Svendsen, H., Beszczynska-Møller, A., Hagen, J. O., Lefauconnier, B., Tverberg, V., Gerland, S., Ørbøk, J. B., Bischof, K., Papucci, C., Zajaczkowski, M., Azzolini, R., Bruland, O., Wiencke, C., Winther, J. G., and Dallmann, W., 2002. The physical environment of Kongsfjorden-Krossfjorden, and Arctic fjord system in Svalbard. *Polar Research*, **21**, 133–166. DOI: 10.1111/j.1751-8369.2002.tb00072.x

Véron, A. J., Church, T. M., Rivera-Duarte, I., and Flegal, A. R., 1999. Stable lead isotopic ratios trace thermohaline circulation in the subarctic North Atlantic. *Deep Sea Research Part II: Topical Studies in Oceanography*, **46**, 919–935. DOI: 10.1016/S0967-0645(99)00009-0

Zaborska, A., Pempkowiak, J., and Papucci, C., 2006. Some sediment characteristics and sedimentation rates in an Arctic Fjord (Kongsfjorden, Svalbard). *Annual Environmental Protection*, **8**, 79–96

Zajaczkowski, M., 2008. Sediment supply and fluxes in glacial and outwash fjords, Kongsfjorden and Adventfjorden, Svalbard. *Polish Polar Research*, **29**, 59–72

# 6 Pb isotopic analysis of atmospheric particulate in Antarctica

## 6.1 *Introduction*

Due to a different atmospheric pattern and a greater distance from industrialised areas, Antarctica is characterised by a reduced anthropogenic impact in comparison to the Arctic. Moreover, the thick ice sheet covering most of the continent constitutes a unique archive of the past atmospheric conditions. As a result of these two facts, the southernmost continent is a valuable laboratory for monitoring and understanding the state of the global environment (Bodhaine et al. 1992).

The chemical characterisation of size-segregated aerosol can provide useful information to understand the main processes to which the particulate is subjected during its permanence in the atmosphere, whereas the determination of specific metals associated to the particulate matter, such as Al, Na or Pb, can help to identify the possible sources. Indeed, the origin of major and trace elements occurring in the Antarctic aerosols can be related to both natural and anthropogenic sources. Possible natural sources include continental dust (Gaiero 2007; Gassó et al. 2010; Revel-Rolland et al. 2006; Vallelonga et al. 2010), volcanic emissions (Matsumoto and Hinkley 2001; Zreda-Gostynska et al. 1997) and sea-salt (Jourdain et al. 2008; Udisti et al. 2012). Anthropogenic contributions can be related to emissions to the atmosphere from metal production activities in the Southern Hemisphere (J. Pacyna and E. Pacyna 2001) or local emissions from research stations (Mazzera et al. 2001).

At present, such studies regarding atmospheric particulate matter reaching Antarctica have been mainly focused on the study of major ionic compounds (Becagli et al. 2012; Fattori et al. 2005; Jourdain et al. 2008; Udisti et al. 2012), whereas just few data are available for trace metals (Maenhaut et al. 1979; Mazzera et al. 2001; Toscano et al. 2005).

In this study, chemical characterisation of size-segregated aerosol reaching Terra Nova Bay, in East Antarctica, have been combined with calculation of EFs to discriminate among crustal, marine and anthropogenic inputs. Moreover, Pb isotope ratio determinations were used to obtain information on the possible geographical sources of the particulate matter. To the best of my knowledge, this is the first study to provide data of Pb isotopic composition measured in size-segregated Antarctic aerosol.

## 6.2 *Materials and method*

### 6.2.1 Sample collection and storage

The aerosol sampling was carried out from 29 November 2010 to 23 January 2011, with a 10-day resolution, using a Tisch (Cleves, OH, US) six-stage cascade impactor with 10.0, 7.2, 3.0, 1.5, 0.95 and 0.49 µm particle cut-off diameters, placed at Campo Faraglione

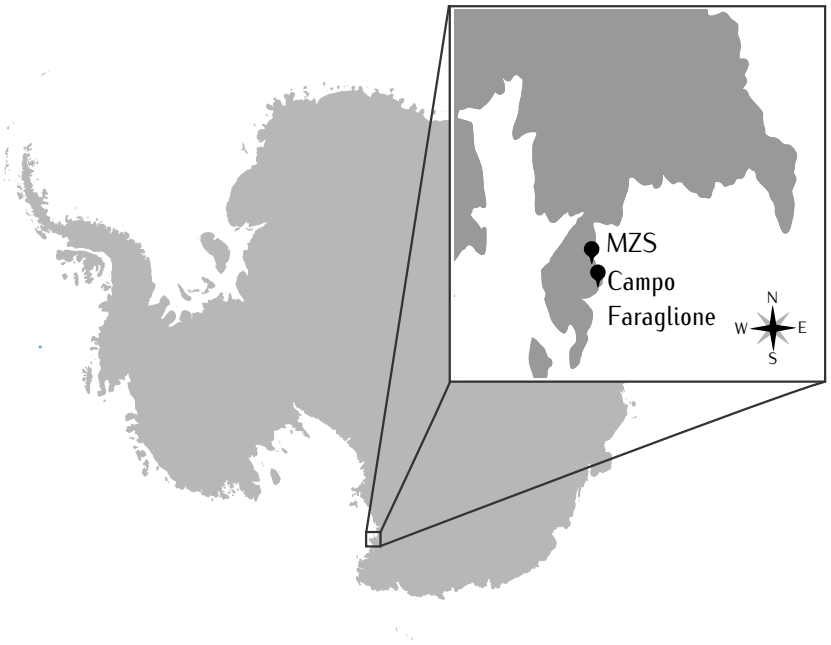


Figure 6.1. location of the sampling site (Campo Faraglione) and Mario Zucchelli Station (MZS) at Terra Nova Bay on Antarctica.

(74°42′58″ S, 164°6′54″ E; figure 6.1), 3 km south of the "Mario Zucchelli" Italian Station (formerly Terra Nova Bay Station).

The device employed cellulose filters and operated at a flow rate of 1130 L/min. After sampling, the filters were placed in acid-cleaned plastic Petri dishes, sealed in double polyethylene bags and stored at −20 °C until analysis. Three field blanks for every cut-size were concomitantly prepared by installing the filters in the switched-off sampler for a few tens of minutes and then following the same procedure used for the sample filters.

### 6.2.2 Meteorological data

Hourly measurements of wind speed ($W_s$, m/s), wind direction ($W_d$, compass degrees), relative humidity (RH, percentages) and atmospheric temperature ($T$, °C) at the Eneide meteorological station (74°42′0″ S, 164°5′24″ E) were obtained from the Meteo-Climatological Observatory of the Italian National Program for Research in Antarctica (PNRA, www.climantartide.it). The average wind directions were computed by averaging the north–south ($\sin W_d$) and east–west ($\cos W_d$) component of the wind.

### 6.2.3 Determination of particulate metals and Pb isotope ratios

Sub-samples (1/10 of each filter) were mineralised using a MARS-5 microwave digestion system (CEM, Matthews, NC, USA), according to a two-step procedure:

1. addition of 5 mL of 65 % nitric acid (Suprapur from Sigma–Aldrich, St Louis, MO, USA), 2 mL of 30 % hydrogen peroxide (Suprapur from Merck, Darmstadt, Germany), 1 mL of hydrofluoric acid (Suprapur from Sigma–Aldrich), 2 mL of ultrapure water (Milli-Q from Merck Millipore, Darmstadt, Germany) and heating at 220 °C for 50 min;
2. addition of 5 mL of a saturated boric acid solution (Suprapur from Merck) and repeating the heating procedure for 20 min.

The resulting solutions were then analysed by ICP-AES and ICP-MS using the operating conditions reported in tables 5.2 and 5.3.

The elemental concentrations of the field blanks are reported in table 6.1. These values took into account every possible contamination during the complete process of sampling, sample treatment and analysis, and were hence subtracted from the sample concentrations. Field blanks were also used to calculate the limits of detections (LoDs), according to the 3*s*-criterion. LODs (reported in table 6.1) proved to be adequate for >90 % of determinations.

The accuracy of the procedure was verified by the analysis of the certified reference material MURST-ISS-A1 from PNRA–Istituto Superiore di Sanità, Rome (table 6.2). The values found were not significantly different from the certified values ($p$-value>0.1), with recoveries ranging from 96 to 111 %.

The determination of $^{208}Pb/^{207}Pb$ and $^{206}Pb/^{207}Pb$ ratios was carried out by ICP-MS according to the method described in chapter 3.

### 6.2.4 Data processing

In the dataset for statistical analysis, the concentration values below the LoD were substituted by ½LoD and only variables or samples with more than 50 % of the data above the LoD were considered. Principal component analysis (PCA) was performed on the auto-scaled data matrix, constituted by 22 rows (samples) and 19 columns (meteorological and chemical parameters), using the open-source software environment for statistical computing and graphics 'R' (R Core Team 2015).

Positive matrix factorisation (PMF) was applied to the chemical data matrix, using the software of the United States Environmental Protection Agency (Norris et al. 2015). This statistical analysis is a specialised version of factor analysis used in receptor modelling and thus it aims to solve the equation:

$$x_{ij} = \sum_{k=1}^{p} f_{ik} g_{kj} \tag{6.1}$$

where $x_{ij}$ is the elemental concentration measured in the $j^{th}$ sample, $f_{ik}$ is the gravimetric concentration (ng/mg) of the $i^{th}$ element in material from the $k^{th}$ source, and $g_{kj}$ is the airborne mass concentration (mg/m$^3$) of material from the $k^{th}$ source contributing to the $j^{th}$ sample. Differently from PCA analysis or simple factor analysis where auto-scaling is often the best choice for the pretreatment of concentration data, in PMF each value of the dataset is scaled taking into account its uncertainty. In addition, the possible solutions are constrained taking into account fundamental physical requirements such as:

- original data must be explained by the model as much as possible;
- the predicted source compositions ($f_{ik}$) must be non-negative;
- the predicted source contribution to the aerosol ($g_{kj}$) must be non negative;
- the sum of the predicted elemental mass contribution for each source must be less than or equal to the total measured mass for each element (Paatero and Tapper 1994).

Results obtained using this approach are useful to identify possible sources based on their chemical profiles, as well as their relative contribution to the aerosol reaching the receptor site.

Table 6.1. field blanks and limits of detection for the measurement of major and trace elements in size-segregated atmosperic particulate matter.

| Stage | Al | Fe | Mg | Na | Co | Cu | Li | Mn | Mo | Pb | Rb | Y | Cr | V |
|---|---|---|---|---|---|---|---|---|---|---|---|---|---|---|
| (µm) | ($ng/m^3$) | | | | ($pg/m^3$) | | | | | | | | | |
| Field blanks | | | | | | | | | | | | | | |
| 10 – 7.2 | 1.3 | 0.2 | 0.05 | 43 | 0.34 | 2.2 | 0.08 | 2.4 | 0.48 | 1.5 | 0.26 | 0.44 | 14 | 0.50 |
| 7.2 – 3.0 | 1.2 | 0.2 | 0.05 | 43 | 0.38 | 2.6 | 0.06 | 3.5 | 0.41 | 0.65 | 0.31 | 0.47 | 18 | 0.35 |
| 3.0 – 1.5 | 1.2 | 0.17 | 0.06 | 44 | 0.36 | 3.1 | 0.08 | 2.8 | 0.61 | 0.62 | 0.23 | 0.47 | 17 | 0.43 |
| 1.5 – 0.95 | 1.2 | 0.17 | 0.07 | 44 | 0.39 | 2.6 | 0.10 | 3.1 | 0.41 | 0.73 | 0.29 | 0.46 | 14 | 0.36 |
| 0.95 – 0.49 | 1.4 | 0.17 | 0.09 | 43 | 0.38 | 3.0 | 0.17 | 2.4 | 0.40 | 0.48 | 0.28 | 0.49 | 17 | 0.38 |
| Limits of detection | | | | | | | | | | | | | | |
| 10 – 7.2 | 0.17 | 0.30 | 0.22 | 2.1 | 0.05 | 0.20 | 0.05 | 1.5 | 0.10 | 0.20 | 0.10 | 0.03 | 2.9 | 0.34 |
| 7.2 – 3.0 | 0.04 | 0.30 | 0.22 | 2.1 | 0.01 | 2.7 | 0.03 | 4.6 | 0.08 | 0.15 | 0.09 | 0.05 | 6.9 | 0.04 |
| 3.0 – 1.5 | 0.08 | 0.30 | 0.22 | 2.0 | 0.25 | 6.3 | 0.04 | 4.2 | 0.50 | 0.26 | 0.18 | 0.22 | 2.2 | 0.11 |
| 1.5 – 0.95 | 0.01 | 0.30 | 0.21 | 2.0 | 0.01 | 2.2 | 0.04 | 4.5 | 0.03 | 0.29 | 0.10 | 0.01 | 0.76 | 0.04 |
| 0.95 – 0.49 | 0.04 | 0.29 | 0.20 | 2.1 | 0.05 | 1.3 | 0.25 | 1.7 | 0.03 | 0.10 | 0.05 | 0.01 | 1.7 | 0.15 |

Table 6.2. Major and trace elements measured in the CRM-MURST-ISS-A1 (Antarctic sediment). Values are averages and 95 %-confidence intervals, indicative values are reported within parentheses.

| Element | Unit | Measured | Certified |
|---|---|---|---|
| Al | % | $6.45 \pm 0.08$ | $6.71 \pm 0.33$ |
| Co | µg/g | $6.76 \pm 0.76$ | $6.87 \pm 0.31$ |
| Cr | µg/g | $46.9 \pm 3.5$ | $42.1 \pm 3.4$ |
| Cu | µg/g | $5.97 \pm 1.01$ | $(5.79 \pm 1.59)$ |
| Fe | % | $2.34 \pm 0.13$ | $2.44 \pm 0.07$ |
| Mg | % | $0.96 \pm 0.04$ | $(1.52 \pm 0.13)$ |
| Mn | µg/g | $437 \pm 43$ | $446 \pm 19$ |
| Mo | µg/g | $0.9 \pm 0.7$ | $(1.1 \pm 0.6)$ |
| Na | % | $2.20 \pm 0.16$ | $(2.27 \pm 0.06)$ |
| Pb | µg/g | $20.5 \pm 1.7$ | $21.0 \pm 2.9$ |
| Rb | µg/g | $123.4 \pm 9.2$ | $(124.8 \pm 5.1)$ |
| Y | µg/g | $18.5 \pm 2.4$ | $(19.1 \pm 2.5)$ |
| V | µg/g | $51.6 \pm 9.9$ | $(51.8 \pm 2.2)$ |

## 6.3 *Results and discussion*

### 6.3.1 Concentration levels, correlations and EFs

The concentrations of major and trace metals associated to the size-segregated aerosol are gathered in table 6.3. The median concentrations in the integrated $<10\,\mu m$ ($PM_{10}$) fraction was similar to that reported by Toscano et al. (2005) for samples collected from the same sampling site during the austral summers of 2000–2001 and 2001–2002. The only exception is Cu, the concentration of which was almost 50 times higher in the samples analysed by Toscano et al. (2005).

In order to explore possible correlations between variables and similarities among samples, the dataset was merged with meteorological variables and subjected to PCA, obtaining the biplot (loadings and score plots overlaid) displayed in figure 6.2. The first two principal components explained 76 % of the total variance of the data. Loadings of the variables appeared to be separated into three groups: the first one comprised Al, Fe, Mn and Y and was positively correlated with the PC1, the second one comprised Co, Li, Mg, Na, Rb and V and showed a positive correlation with both the PCs, and the third one was formed by Cr, Cu, Mo and Pb and the result was negatively correlated with the PC2. Even at this exploratory stage, the nature of the elements in each group could suggest different sources of the particulates. Indeed, the first group comprised elements that are typically associated to terrigenous inputs, the second one was mainly related to sea-salt, whereas the third group could be indicative of anthropogenic activities, as discussed below. It is worth noting that the concentrations of the elements in the last group were also influenced by the meteorological variables. Indeed, a strong positive correlation to wind velocity, and a negative correlation with both relative humidity and temperature were detected. Differently, elements of the first group appeared to be correlated positively with the N–S component of the wind ($\sin W_d$), and negatively with the E–W component ($\cos W_d$), thus pointing out a possible inland source.

In the same plot, the scores of the samples are shown as filled dots with a two-term label indicating the sampling period (progressive number) and the particle size range (a = 10–7.2, b = 7.2–3.0, c = 3.0–1.5, d = 1.5–0.95, and e = 0.95–0.49 µm). Most of the samples were dispersed close to the origin without any particular trend. The only two exceptions were: (1) the samples collected during the first period (from 29 November

Table 6.3. concentrations of major and trace metals associated to size-segregated aerosols at Terra Nova Bay.

| Sampling period | Stage (μm) | Al (ng/m$^3$) | Fe | Mg | Na | Co (pg/m$^3$) | Cu | Li | Mn | Mo | Pb | Rb | Y | Cr | V |
|---|---|---|---|---|---|---|---|---|---|---|---|---|---|---|---|
| 2010-11-29 2010-12-09 | 10–7.2 | 0.46 | <0.30 | <0.22 | <2.06 | 0.83 | 19.9 | 0.42 | 11.1 | 0.85 | 6.15 | 1.09 | 1.00 | 32.0 | 1.27 |
| | 7.2–3.0 | 1.12 | 1.05 | 2.08 | 14.3 | 1.14 | 17.7 | 1.29 | 24.9 | 0.77 | 6.42 | 3.04 | 1.44 | 31.9 | 2.50 |
| | 3.0–1.5 | 1.35 | 1.34 | 2.36 | 16.8 | 1.33 | 11.9 | 1.66 | 31.6 | 0.76 | 5.89 | 3.74 | 1.47 | 27.4 | 2.67 |
| | 1.5–0.95 | 1.37 | <0.30 | 3.04 | 21.3 | 1.49 | 11.0 | 2.10 | 35.6 | 0.81 | 7.06 | 4.39 | 1.60 | 29.9 | 3.07 |
| | 0.95–0.49 | 1.16 | 1.15 | 2.43 | 20.6 | 1.35 | 13.4 | 1.53 | 28.2 | 0.85 | 7.80 | 3.43 | 1.46 | 28.4 | 2.51 |
| 2010-12-09 2010-12-19 | 10–7.2 | 0.89 | 0.73 | 2.16 | 11.7 | 1.38 | 7.61 | 1.27 | 12.7 | 0.70 | 4.67 | 2.65 | 1.27 | 11.3 | 4.06 |
| | 7.2–3.0 | 1.74 | 1.61 | 7.58 | 59.4 | 1.90 | 5.96 | 2.67 | 26.0 | 0.68 | 8.19 | 5.11 | 1.60 | 10.8 | 6.53 |
| | 3.0–1.5 | 1.48 | 1.26 | 3.81 | 24.8 | 1.66 | <6.34 | 1.94 | 21.3 | <0.50 | 5.34 | 4.04 | 1.49 | 7.72 | 5.96 |
| | 1.5–0.95 | – | – | – | – | – | – | – | – | – | – | – | – | – | – |
| | 0.95–0.49 | 0.97 | 0.72 | 1.30 | <2.08 | 1.35 | 5.49 | 0.88 | 11.5 | 0.52 | 4.17 | 2.58 | 1.20 | 7.06 | 3.67 |
| 2010-12-19 2010-12-29 | 10–7.2 | 0.58 | 0.48 | 1.48 | 7.00 | 1.12 | 7.02 | 0.50 | 7.01 | 0.68 | 4.10 | 1.18 | 0.94 | 9.20 | 3.26 |
| | 7.2–3.0 | – | – | – | – | – | – | – | – | – | – | – | – | – | – |
| | 3.0–1.5 | – | – | – | – | – | – | – | – | – | – | – | – | – | – |
| | 1.5–0.95 | 0.11 | <0.30 | <0.22 | <1.96 | 0.94 | 2.01 | <0.04 | <4.17 | 0.50 | 7.20 | 0.52 | 0.85 | 5.18 | 1.07 |
| | 0.95–0.49 | <0.04 | <0.29 | 1.70 | 6.12 | 1.20 | 3.17 | <0.25 | 9.35 | 0.59 | 0.05 | 1.83 | 1.11 | <1.68 | 4.57 |
| 2010-12-29 2011-01-08 | 10–7.2 | 0.09 | <0.30 | 1.61 | <2.06 | 1.05 | 8.52 | 0.70 | 7.67 | 0.63 | 5.65 | 1.62 | 1.00 | 7.15 | 2.78 |
| | 7.2–3.0 | 1.08 | 0.82 | 7.22 | 62.7 | 1.31 | <2.70 | 1.46 | 11.3 | 0.53 | 5.34 | 2.53 | 1.09 | <6.86 | 3.17 |
| | 3.0–1.5 | 0.71 | 0.52 | 2.91 | 21.7 | 1.18 | <6.34 | 0.74 | 7.26 | <0.50 | 4.52 | 1.66 | 1.03 | <2.15 | 2.56 |
| | 1.5–0.95 | 0.88 | 0.56 | 1.53 | 8.22 | 1.12 | <2.23 | 0.79 | 7.56 | 0.68 | 4.73 | 1.51 | 0.92 | 10.8 | 2.45 |
| | 0.95–0.49 | 0.72 | <0.29 | 0.63 | <2.08 | 1.12 | 8.19 | 0.52 | 5.59 | 0.53 | 5.73 | 1.27 | 0.87 | 7.50 | 2.10 |
| 2011-01-08 2011-01-23 | 10–7.2 | 0.90 | 0.91 | 20.4 | 167 | 1.47 | 9.96 | 4.56 | 19.5 | 0.61 | 3.50 | 4.68 | 1.12 | 3.79 | 4.62 |
| | 7.2–3.0 | 1.85 | 1.94 | 44.3 | 406 | 2.29 | 13.2 | 9.91 | 35.8 | 0.66 | 4.16 | 10.2 | 1.59 | <6.86 | 9.10 |
| | 3.0–1.5 | 0.97 | 0.92 | 11.7 | 98.7 | 1.54 | 7.30 | 3.07 | 21.1 | 0.54 | 3.68 | 3.77 | 1.03 | 3.65 | 4.61 |
| | 1.5–0.95 | 0.89 | 0.81 | 7.65 | 60.3 | 1.43 | 6.23 | 2.18 | 17.9 | 0.55 | 3.86 | 3.06 | 0.96 | 5.11 | 4.12 |
| | 0.95–0.49 | 0.61 | 0.58 | 3.64 | 26.0 | 1.30 | 7.07 | 1.17 | 15.0 | 0.52 | 4.27 | 2.20 | 0.81 | 4.92 | 3.54 |
| Median as $PM_{10}$ | | 5.08 | 3.54 | 13.9 | 92.6 | 6.14 | 19.1 | 6.77 | 71.5 | 2.38 | 22.4 | 14.4 | 5.51 | 25.4 | 13.1 |
| Mean as $PM_{10}$ | | 3.98 | 3.08 | 25.9 | 207 | 5.90 | 32.5 | 7.87 | 73.6 | 2.59 | 22.5 | 13.2 | 5.17 | 48.8 | 16.0 |

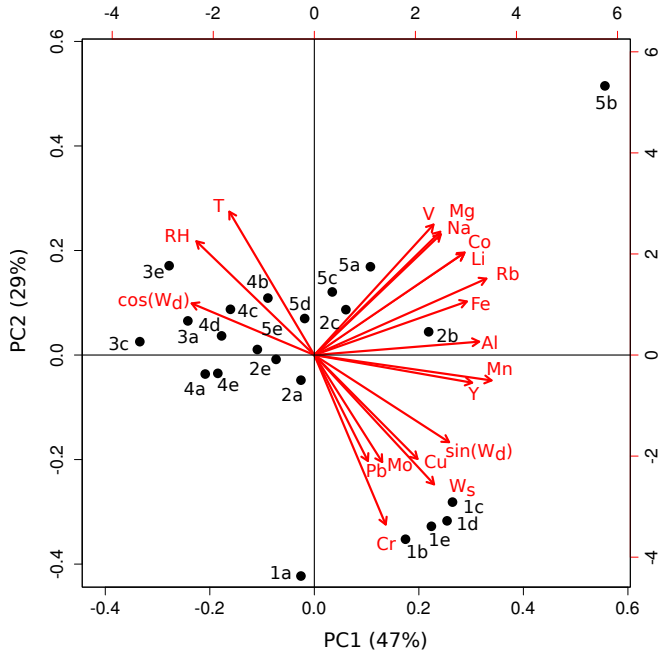


Figure 6.2. principal component analysis results for size-segregated atmospheric particulate matter collected at Terra Nova Bay. The scores label includes a progressive number for the sampling period (see table 6.3) and a progressive letter for the cut-off size (a = 10–7.2, b = 7.2–3.0, c = 3.0–1.5, d = 1.5–0.95, and e = 0.95–0.49 µm). $W_s$, wind speed; $W_d$ , wind direction; RH, relative humidity; $T$, temperature.

2010 to 29 December 2010), characterised by higher concentrations of Cr, Cu, Mo and Pb than the remaining samples and high wind velocity values, and (2) the sample 5b collected during the last period (from 8 January 2011 to 23 January 2011) with a particle size of 7.2–3.0 µm, which showed the highest concentrations of the elements related to sea-salt.

EFs were calculated for all the elements in the dataset considering the average element-to-Al ratio in the UCC (Wedepohl 1995) and the element-to-Na ratio in the superficial sea-water (Turekian 1968). The results are shown in figure 6.3. According to the results, Co, Fe, Mn, Y and V may be associated with terrigenous inputs, whereas Mg with the contribution of sea-salt particles. EFs for Li and Rb are compatible with both sources. Finally, Cr, Cu, Mo and Pb showed high marine and crustal EFs, revealing their anthropogenic origin. The results are in good agreement with previous investigations on trace metals in Antarctic aerosols (Toscano et al. 2005) and surface snow (Grotti et al. 2011, 2015), collectively indicating the dominant anthropogenic origin of Cd, Cr, Cu, Pb and Zn. Evidence of the anthropogenic origin for Cr, Cu, and Pb was also pointed out by the analysis of dated snow samples collected at Coats Land from 1834 to 1990 (Planchon et al. 2002a).

### 6.3.2 Size-resolved and temporal distributions

Size-resolved chemical distributions of Al, Na and Cr are reported in figure 6.4. These elements have been selected as representative of metals having crustal, marine and anthropogenic origin, respectively. The size distribution of Al appeared to be bimodal with a first maximum in the 7.2–3.0 µm bin (coarse mode) and a second one centred in the 1.5–0.95 µm range. The distribution of Na was uni-modal with the maximum

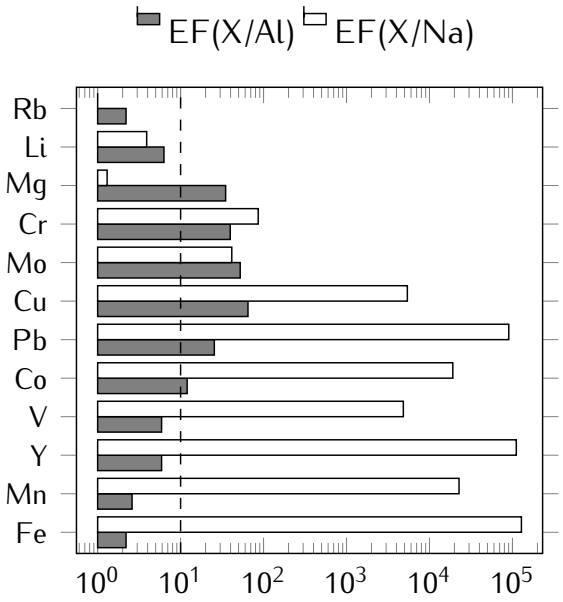


Figure 6.3. average enrichment factors for size-segregated atmospheric particulate matter collected at Terra Nova Bay.

in the coarse mode between 7.2 and 3.0 µm, in agreement with a previous study in coastal Antarctica (Jourdain and Legrand 2002). It is worth noting that, during the first ten days of the aerosol collection, both elements showed a very similar bell-shaped size-distribution, with maximum concentrations between 1.5 and 0.95 µm. The size-distribution for Cr was bimodal with the absolute maximum in the 1.5–0.95 µm range but also high concentrations in the coarse mode between 10 and 3.0 µm. Moreover, the same size-distribution was found throughout the sampling period.

The temporal trends of the average concentration of Al, Na and Cr are reported in figure 6.5, along with the temporal evolution of the meteorological parameters $T$, $W_s$ and $W_d$. The first two periods (from 29 November to 19 December) experienced a strong, cold wind coming mainly from the inland (west) and referred to as a katabatic wind (Bromwich 1989). The temporal distribution of Al was characterised by two periods of relatively high concentrations separated by a sharp decline from 19 to 29 December. The Na concentration considerably increased during the last period, whereas the opposite trend was found for Cr, the concentration of which in the first sampling period was approximately five times higher than that measured afterwards. Cr concentration correlated positively with the wind speed ($R = 0.856$; $p$-value $<0.0001$) and negatively with the temperature ($R = 0.885$; $p$-value $<0.0001$).

### 6.3.3 Pb isotopic composition

Table 6.4 shows the $^{208}Pb/^{207}Pb$ and $^{206}Pb/^{207}Pb$ ratios, along with their 95 %-level uncertainties. The mean values were $2.423 \pm 0.006$ and $1.148 \pm 0.006$ for $^{208}Pb/^{207}Pb$ and $^{206}Pb/^{207}Pb$, respectively. No significant difference was detected either among the different size bins or the sampling periods.

The isotopic signature of the atmospheric particulate samples were represented and compared to literature data by using the three-isotope plot reported in figure 6.6. In figure 6.6, the isotopic signature found by Van de Velde et al. (2005) for snow samples

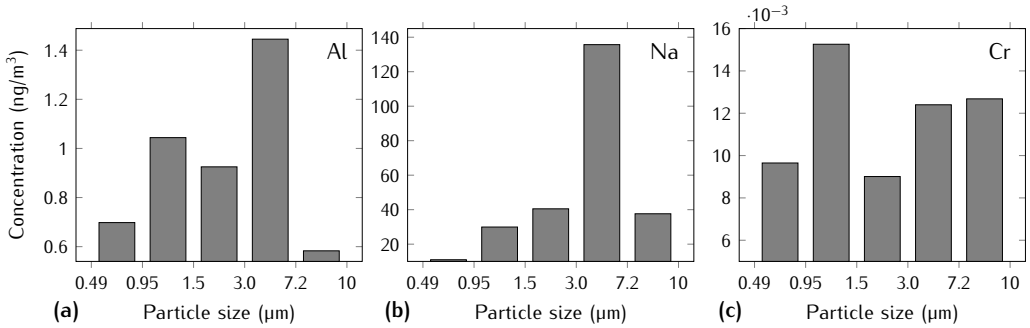


Figure 6.4. size-resolved chemical distribution of Al, Na and Cr for atmospheric particulate matter collected at Terra Nova Bay.

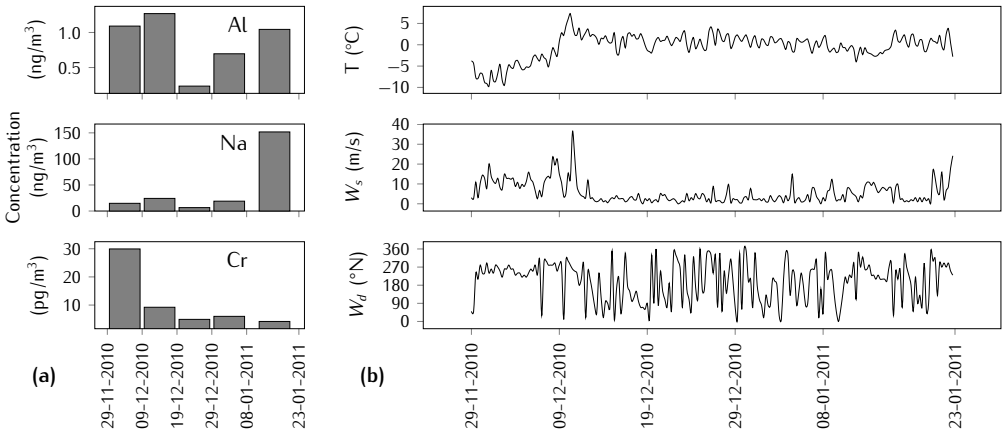


Figure 6.5. temporal distribution of **(a)** average concentrations of Al, Na and Cr and **(b)** meteorological parameters $T$ (temperature), $W_s$ (wind speed) and $W_d$ (wind direction).

collected at the Hercules Névé (Victoria Land, Antarctica) are also shown, as well as the Pb isotope ratios for the basaltinoids of Ross Island (representative of volcanic inputs) and for sediments collected at the South Sandwich Islands and in the South Atlantic Ocean (representative of crustal inputs).The isotope ratios found in our samples matched those reported for the Hercules Névé samples (dated 1986–1994) very well and are spread between two end-members, which represent the isotopic signatures of the natural and anthropogenic sources, as discussed below.

### 6.3.4 Anthropogenic and natural sources of metals

In order to assess the sources of metals in aerosols, chemical tracers such as Al (crustal marker) and Na (marine marker) may be used to evaluate possible enrichment of elements compared to natural levels. According to this approach, several elements (Co, Fe, Mn, Y and V) were found to have a predominant crustal origin and their concentration in aerosols was hence highly correlated (PCA, figure 6.2). Similarly, Mg, Li and Rb appeared to have a common marine origin and were also highly correlated. PCA also showed that the marine and crustal sources were, to some extent, correlated to one another, suggesting the presence of internally mixed particles, as previously observed by Biancato et al. (2006). Evidence of internally mixed particles also came from the bell-shaped size distribution found for both Al and Na during the first ten days of the

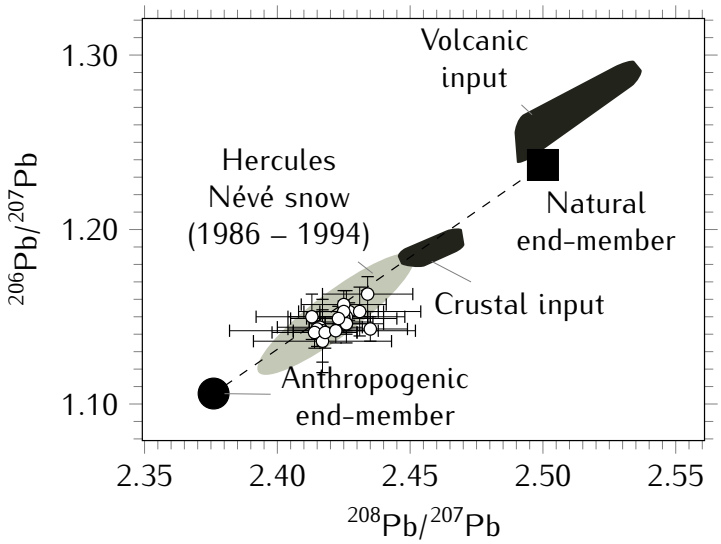


Figure 6.6. Pb three-isotope plot for the aerosol samples collected at Terra Nova Bay. Uncertainties are 95 %-confidence intervals. Reference values are from Van de Velde et al. (2005).

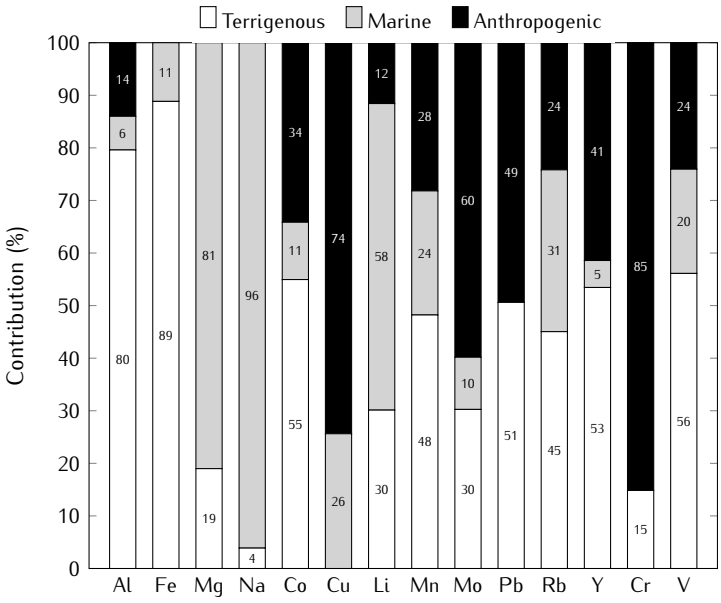


Figure 6.7. factor profiles from positive matrix factorisation (PMF) analysis for aerosol samples collected at Terra Nova Bay. Values are percentage contribution of each factor.

Table 6.4. Pb isotope ratios in size-segregated aerosols at Terra Nova Bay. Uncertainties are expressed as 95 %-confidence levels.

| Sampling period | Stage | $^{208}Pb/^{207}Pb$ | Uncertainty | $^{206}Pb/^{207}Pb$ | Uncertainty |
|---|---|---|---|---|---|
| 2010-11-29 2010-12-09 | 10 – 7.2 | 2.416 | 0.016 | 1.144 | 0.006 |
| | 7.2 – 3.0 | 2.427 | 0.011 | 1.153 | 0.005 |
| | 3.0 – 1.5 | 2.424 | 0.012 | 1.147 | 0.004 |
| | 1.5 – 0.95 | 2.425 | 0.016 | 1.157 | 0.008 |
| | 0.95 – 0.49 | 2.426 | 0.008 | 1.146 | 0.004 |
| 2010-12-09 2010-12-19 | 10 – 7.2 | 2.417 | 0.026 | 1.136 | 0.018 |
| | 7.2 – 3.0 | 2.413 | 0.021 | 1.150 | 0.013 |
| | 3.0 – 1.5 | 2.426 | 0.022 | 1.150 | 0.015 |
| | 1.5 – 0.95 | – | – | – | – |
| | 0.95 – 0.49 | 2.417 | 0.035 | 1.142 | 0.018 |
| 2010-12-19 2010-12-29 | 10 – 7.2 | 2.415 | 0.011 | 1.143 | 0.010 |
| | 7.2 – 3.0 | – | – | – | – |
| | 3.0 – 1.5 | – | – | – | – |
| | 1.5 – 0.95 | 2.425 | 0.009 | 1.150 | 0.005 |
| | 0.95 – 0.49 | – | – | – | – |
| 2010-12-29 2011-01-08 | 10 – 7.2 | 2.414 | 0.016 | 1.141 | 0.009 |
| | 7.2 – 3.0 | 2.425 | 0.020 | 1.149 | 0.008 |
| | 3.0 – 1.5 | 2.418 | 0.012 | 1.141 | 0.009 |
| | 1.5 – 0.95 | 2.422 | 0.016 | 1.142 | 0.007 |
| | 0.95 – 0.49 | 2.425 | 0.015 | 1.153 | 0.006 |
| 2011-01-08 2011-01-23 | 10 – 7.2 | 2.426 | 0.014 | 1.146 | 0.006 |
| | 7.2 – 3.0 | 2.431 | 0.023 | 1.153 | 0.014 |
| | 3.0 – 1.5 | 2.435 | 0.014 | 1.143 | 0.007 |
| | 1.5 – 0.95 | 2.423 | 0.012 | 1.149 | 0.007 |
| | 0.95 – 0.49 | 2.434 | 0.017 | 1.163 | 0.010 |
| Average ± st. dev. | | $2.423 \pm 0.006$ | | $1.148 \pm 0.006$ | |

aerosol collection, in conjunction with the katabatic wind conditions occurring in those days (figure 6.5 **b**).

Finally, several heavy metals (Cr, Cu, Mo and Pb) were clearly shown to have a significant additional source, likely anthropogenic. In fact, these elements displayed high crustal and marine EFs (figure 6.4) and different dimensional (figure 6.4) and temporal (figure 6.5) distributions. Consequently, they grouped differently from the remaining metals in the PCA plot, because of the lack of correlation with the other elements.

The apportionment of these sources was then evaluated with receptor modelling based on PMF (Chavent et al. 2009; Paatero and Tapper 1994). Three main factors were found, accounting for the marine, crustal and anthropogenic inputs. The factor profiles are shown in figure 6.7. The contribution of the marine source was predominant for Na (96 %), Mg (81 %) and Li (58 %), whereas the crustal contribution was important for Fe (89 %), Al (80 %), Co (55 %), V (56 %), Y (53 %) and Mn (48 %). Finally, the anthropogenic source was relevant for Cr (85 %), Cu (74 %), Mo (60 %) and Pb (49 %). Although these values should be considered as estimates because of the limited number of samples, PMF analysis substantially confirmed the source assessment based on PCA and EF values.In order to further estimate the relative contributions of the anthropogenic and natural sources and to identify the source area of the anthropogenic elements, the Pb isotope

ratios were measured and compared with reference values (figure 6.6). Van de Velde et al. (2005) calculated the Pb isotopic composition of the anthropogenic end-member by averaging the values of Pb isotope ratios measured in the biggest cities of the Southern Hemisphere (Bollhöfer and Rosman 2000; Bollhöfer and Rosman 2002), obtaining $^{206}Pb/^{207}Pb = 1.10$ and $^{208}Pb/^{207}Pb = 2.37$. The hypothesis of the combined influence of several urban emissions coming from a wide range of latitudes in the Southern Hemisphere was also reported by Bollhöfer et al. (2005) for the interpretation of aerosol samples approaching Cape Grim (Tasmania, Australia) from the open ocean. In particular, a prominent role of South American and Australian emissions was pointed out by Planchon et al. (2003). The natural end-member was identified by the Pb background level in Victoria Land during the Holocene and was found to have average values for $^{206}Pb/^{207}Pb = 1.237 \pm 0.005$ and $^{208}Pb/^{207}Pb = 2.500 \pm 0.030$ (almost equal contributions from crustal and volcanic inputs) (Van de Velde et al. 2005). Hence, the Pb isotope ratios measured in the aerosols at Terra Nova Bay may be interpreted as the mixing of particles from natural sources and anthropogenic emissions of South American and Australian polluted aerosols thoroughly mixed into the atmosphere. Finally, according to a two-terms mixing model, the Pb isotopic composition of the two end-members was used to calculate the anthropogenic contribution, resulting in the average value of $61 \pm 5$ % (range from 52 to 69 %).

### 6.3.5 Influence of the meteorological conditions

PCA and temporal trends of chemical and meteorological parameters clearly indicated a strong influence of the weather conditions on the metal concentrations in aerosols. This dependence was not the same, however, for all the elements. Metals having a predominant crustal origin significantly correlated with the wind direction, showing an increase attributable to the katabatic wind. This wind originates on the Antarctic plateau from the strong radiative cooling of the sloping ice field, gains very high velocity close to the steep terminus of the coastal ice slopes and is usually associated with low temperature and relative humidity (Argentini et al. 1995; Bromwich 1989; Parish and Bromwich 1991). Therefore, under the katabatic wind regime experienced at the beginning of the aerosol sampling (figure 6.5), an increase in the concentrations of terrigenous elements was observed. The katabatic wind also affected the size-distribution of these elements, leading to the already mentioned bell-shaped distribution centred at 1.5–0.95 µm. The disappearance of the coarse mode (7.2–3.0 µm bin) under the katabatic wind regime could be ascribed to a larger contribution of fine dust coming from the inland areas, and characterised by internally mixed particles.

The katabatic wind appeared to also play an important role in the transport of anthropogenic elements, as suggested by the significant correlation between Cr concentration and the wind speed. On the Antarctic plateau, where the katabatic wind originates, higher EFs of anthropogenic elements in surface snow were found compared to the coastal areas (Grotti et al. 2011; Ikegawa et al. 1999). Hence, we can suppose that the greater inputs of heavy metals from the inland under the katabatic wind regime could increase their concentration in the aerosol collected at the coastal areas.

Finally, it was noted that the concentrations of metals with crustal and marine origin increased in the last period of aerosol collection (figure 6.5 **a**). This result could be attributed to the reduction of the snow coverage and the melting of the sea-ice occurring with the proceeding of the season, as supported by observations on site and the above-zero temperature registered in the previous sampling periods (figure 6.5 **b**).

## 6.4 *Conclusions*

The different sources of metals associated to the atmospheric particulate collected at Terra Nova Bay have been assessed. The results showed the presence of a dominant crustal input for Al, Co, Fe, Li, Mn, Rb, Y and V, a significant marine contribution for Li, Mg, Na and Rb, and an additional anthropogenic source influencing the concentration of Cr, Cu, Mo and Pb. Moreover, the elements associated to the crustal and the marine inputs showed the highest concentrations in the coarse mode (7.2–3.0 µm bin), whereas most of the anthropogenic elements presented a bi-modal distribution with a second peak at lower aerodynamic diameters (1.5–0.95 µm).

The temporal trends revealed that both the crustal and anthropogenic inputs were influenced by the katabatic wind flowing from the inland, whereas the marine input appeared to increase in January when the sea was clear from sea-ice.

Finally, the determination of Pb isotope ratios confirmed that the samples were influenced by both natural and anthropogenic inputs, with significant contribution (50–70 % for Pb) of polluted aerosols from South America and Australia.

Increasing the sampling resolution would provide a better understanding of the role of the meteorological variables. Moreover, further improvements in the analytical procedure for the determination of the Pb isotope ratios could be helpful to resolve small differences in the isotope ratios among the aerodynamic diameters.

*References*

Argentini, S., Del Buono, P., Della Vedova, A., and Mastrantonio, G., 1995. A statistical analysis of wind in Terra Nova Bay, Antarctica, for the austral summers 1988 and 1989. *Atmospheric Research*, **39**, 145–156. DOI: 10.1016/0169-8095(95)00009-G

Becagli, S., Scarchilli, C., Traversi, R., Dayan, U., Severi, M., Frosini, D., Vitale, V., Mazzola, M., Lupi, A., Nava, S., and Udisti, R., 2012. Study of present-day sources and transport processes affecting oxidised sulphur compounds in atmospheric aerosols at Dome C (Antarctica) from year-round sampling campaigns. *Atmospheric Environment*, **52**, 98–108. DOI: 10.1016/j.atmosenv.2011.07.053

Biancato, D., Ceccato, D., Chiminello, F., and Mittner, P., 2006. Micro-PIXE and principal component analysis in a study of internal mixing phenomena in Antarctic coastal aerosol. *Nuclear Instruments and Methods in Physics Research Section B: Beam Interactions with Materials and Atoms*, **249**, 561–565. DOI: 10.1016/j.nimb.2006.03.053

Bodhaine, B. A., Barrie, L. A., Schnell, R. C., Shaw, G. E., and Mckie, J. K., 1992. Symposium on the tropospheric chemistry of the Antarctic Region. *Tellus B*. Vol. 44, 250–251. DOI: 10.1034/j.1600-0889.1992.t01-3-00002.x

Bollhöfer, A. and Rosman, K. J. R., 2000. Isotopic source signatures for atmospheric lead: the Southern Hemisphere. *Geochimica et Cosmochimica Acta*, **64**, 3251–3262. DOI: 10.1016/S0016-7037(00)00436-1

Bollhöfer, A. and Rosman, K. J. R., 2002. The temporal stability in lead isotopic signatures at selected sites in the Southern and Northern Hemispheres. *Geochimica et Cosmochimica Acta*, **66**, 1375–1386. DOI: 10.1016/S0016-7037(01)00862-6

Bollhöfer, A., Rosman, K. J. R., Dick, A. L., Chisholm, W., Burton, G. R., Loss, R. D., and Zahorowski, W., 2005. Concentration, isotopic composition, and sources of lead in Southern Ocean air during 1999/2000, measured at the Cape Grim Baseline Air Pollution Station, Tasmania. *Geochimica et Cosmochimica Acta*, **69**, 4747–4757. DOI: 10.1016/j.gca.2005.06.024

Bromwich, D. H., 1989. Satellite analyses of Antarctic katabatic wind behavior. *Bulletin American Meteorological Society*, **70**, 738–749. DOI: 10.1175/1520-0477(1989)070<0738:SAOAKW>2.0.CO;2

Chavent, M., Guégan, H., Kuentz, V., Patouille, B., and Saracco, J., 2009. PCA- and PMF-based methodology for air pollution sources identification and apportionment. *Environmetrics*, **20**, 928–942. DOI: 10.1002/env.963

Fattori, I., Becagli, S., Bellandi, S., Castellano, E., Innocenti, M., Mannini, A., Severi, M., Vitale, V., and Udisti, R., 2005. Chemical composition and physical features of summer aerosol at Terra Nova Bay and Dome C, Antarctica. *Journal of Environmental Monitoring*, **7**, 1265–1274. DOI: 10.1039/b507327h

Gaiero, D. M., 2007. Dust provenance in Antarctic ice during glacial periods: From where in southern South America? *Geophysical Research Letters*, **34**, L17707. DOI: 10.1029/2007GL030520

Gassó, S., Stein, A., Marino, F., Castellano, E., Udisti, R., and Ceratto, J., 2010. A combined observational and modeling approach to study modern dust transport from the Patagonia desert to East Antarctica. *Atmospheric Chemistry and Physics*, **10**, 8287–8303. DOI: 10.5194/acp-10-8287-2010

Grotti, M., Soggia, F., Ardini, F., and Magi, E., 2011. Major and trace element partitioning between dissolved and particulate phases in Antarctic surface snow. *Journal of Environmental Monitoring*, **13**, 2511–2520. DOI: 10.1039/c1em10215j

Grotti, M., Soggia, F., Ardini, F., Magi, E., Becagli, S., Traversi, R., and Udisti, R., 2015. Year-round record of dissolved and particulate metals in surface snow at Dome Concordia (East Antarctica). *Chemosphere*, **138**, 916–923. DOI: 10.1016/j.chemosphere.2014.10.094

Ikegawa, M., Kimura, M., Honda, K., Akabane, I., Makita, K., Motoyama, H., Fujii, Y., and Itokawa, Y., 1999. Geographical variations of major and trace elements in East Antarctica. *Atmospheric Environment*, **33**, 1457–1467. DOI: 10.1016/S1352-2310(98)00243-X

Jourdain, B. and Legrand, M., 2002. Year-round records of bulk and size-segregated aerosol composition and HCl and $HNO_3$ levels in the Dumont d'Urville (coastal Antarctica) atmosphere: Implications for sea-salt aerosol fractionation in the winter and summer. *Journal of Geophysical Research, D: Atmospheres*, **107** (D22), 4645. DOI: 10.1029/2002JD002471

Jourdain, B., Preunkert, S., Cerri, O., Castebrunet, H., Udisti, R., and Legrand, M., 2008. Year-round record of size-segregated aerosol composition in central Antarctica (Concordia station): Implications for the degree of fractionation of sea-salt particles. *Journal of Geophysical Research, D: Atmospheres*, **113** (D14), D14308. DOI: 10.1029/2007JD009584

Maenhaut, W., Zoller, W. H., Duce, R. A., and Hoffman, G. L., 1979. Concentration and size distribution of particulate trace elements in the south polar atmosphere. *Journal of Geophysical Research, D: Atmospheres*, **84** (C5), 2421. DOI: 10.1029/JC084iC05p02421

Matsumoto, A. and Hinkley, T. K., 2001. Trace metal suites in Antarctic pre-industrial ice are consistent with emissions from quiescent degassing of volcanoes worldwide. *Earth and Planetary Science Letters*, **186**, 33–43. DOI: 10.1016/S0012-821X(01)00228-X

Mazzera, D. M., Lowenthal, D. H., Chow, J. C., Watson, J. G., and Grubisíc, V., 2001. PM10 measurements at McMurdo Station, Antarctica. *Atmospheric Environment*, **35**, 1891–1902. DOI: 10.1016/S1352-2310(00)00409-X

Norris, G., Duvall, R., Brown, S., and Bai, S., 2015. *EPA Positive Matrix Factorization (PMF) 5.0 Fundamentals and User Guide*. Version 5.0. URL: http://www.epa.gov/heasd/documents/PMF_5.0_User_Guide.pdf (visited on 03/03/2016)

Paatero, P. and Tapper, U., 1994. Positive matrix factorization: A non-negative factor model with optimal utilization of error estimates of data values. *Environmetrics*, **5**, 111–126. DOI: 10.1002/env.3170050203

Pacyna, J. and Pacyna, E., 2001. An assessment of global and regional emissions of trace metals to the atmosphere from anthropogenic sources worldwide. *Environmental Reviews*, **9**, 269–298. DOI: 10.1139/er-9-4-269

Parish, T. R. and Bromwich, D. H., 1991. Continental-scale simulation of the Antarctic katabatic wind regime. *Journal of Climate*, **4**, 135–146. DOI: 10.1175/1520-0442(1991)004<0135:CSSOTA>2.0.CO;2

Planchon, F. A. M., Boutron, C. F., Barbante, C., Cozzi, G., Gaspari, V., Wolff, E. W., Ferrari, C. P., and Cescon, P., 2002a. Changes in heavy metals in Antarctic snow from Coats Land since the mid-19th to the late-20th century. *Earth and Planetary Science Letters*, **200**, 207–222. DOI: 10.1016/S0012-821X(02)00612-X

Planchon, F. A. M., van de Velde, K., Rosman, K. J. R., Wolff, E. W., Ferrari, C. P., and Boutron, C. F., 2003. One hundred fifty–year record of lead isotopes in Antarctic snow from Coats Land. *Geochimica et Cosmochimica Acta*, **67**, 693–708. DOI: 10.1016/S0016-7037(02)01136-5

R Core Team, 2015. *R: A Language and Environment for Statistical Computing*. URL: http://www.r-project.org/ (visited on 03/03/2016)

Revel-Rolland, M., De Deckker, P., Delmonte, B., Hesse, P., Magee, J., Basile-Doelsch, I., Grousset, F., and Bosch, D., 2006. Eastern Australia: A possible source of dust in East Antarctica interglacial ice. *Earth and Planetary Science Letters*, **249**, 1–13. DOI: 10.1016/j.epsl.2006.06.028

Toscano, G., Gambaro, A., Moret, I., Capodaglio, G., Turetta, C., and Cescon, P., 2005. Trace metals in aerosol at Terra Nova Bay, Antarctica. *Journal of Environmental Monitoring*, **7**, 1275–1280. DOI: 10.1039/b507337p

Turekian, K. K., 1968. *Oceans*. Ed. by Prentice-Hall. 2nd editio. Englewood Cliffs, NJ. 120 pp.

Udisti, R., Dayan, U., Becagli, S., Busetto, M., Frosini, D., Legrand, M., Lucarelli, F., Preunkert, S., Severi, M., Traversi, R., and Vitale, V., 2012. Sea spray aerosol in central Antarctica. Present atmospheric behaviour and implications for paleoclimatic reconstructions. *Atmospheric Environment*, **52**, 109–120. DOI: 10.1016/j.atmosenv.2011.10.018

Vallelonga, P., Gabrielli, P., Balliana, E., Wegner, A., Delmonte, B., Turetta, C., Burton, G., Vanhaecke, F., Rosman, K. J. R., Hong, S., Boutron, C. F., Cescon, P., and Barbante, C., 2010. Lead isotopic compositions in the EPICA Dome C ice core and Southern Hemisphere Potential Source Areas. *Quaternary Science Reviews*, **29**, 247–255. DOI: 10.1016/j.quascirev.2009.06.019

Van de Velde, K., Vallelonga, P., Candelone, J. P., Rosman, K. J. R., Gaspari, V., Cozzi, G., Barbante, C., Udisti, R., Cescon, P., and Boutron, C. F., 2005. Pb isotope record over one century in snow from Victoria Land, Antarctica. *Earth and Planetary Science Letters*, **232**, 95–108. DOI: 10.1016/j.epsl.2005.01.007

Wedepohl, K. H., 1995. The composition of the continental crust. *Geochimica et Cosmochimica Acta*, **58A**, 959–960. DOI: 10.1180/minmag.1994.58A.2.234

Zreda-Gostynska, G., Kyle, P. R., Finnegan, D., and Prestbo, K. M., 1997. Volcanic gas emissions from Mount Erebus and their impact on the Antarctic environment. *Journal of Geophysical Research, D: Atmospheres*, **102** (B7), 15039–15055. DOI: 10.1029/97JB00155

# 7 Determination of Pb isotope ratios in Antarctic snow by multi-collector ICP-MS

## 7.1 *Introduction*

The determination of isotope ratios in polar atmospheric particulate collected on filters can help to identify the dominant sources of particulate at the moment of the air sampling. In contrast, the analysis of snow and ice can help to reconstruct how those sources, their transport routes, and their relative contributions changed over time (Rosman et al. 1998; Vallelonga et al. 2005, 2010). The accurate measurement of these isotope ratios can, however, be quite challenging. Indeed, the Pb concentration in polar snow and ice is extremely low, typically at or below the pg/g level (Rosman et al. 1994), therefore requiring the application of ultraclean procedures for sampling, sample storage and treatment, as well as very high instrument sensitivities.

Isotope dilution-TIMS (ID-TIMS) is capable of the simultaneous determination of the concentration of Pb and its isotopic composition and therefore appears to be the method of choice for the analysis of snow and ice samples of limited size (Chisholm et al. 1995; Vallelonga et al. 2002). MC-ICP-MS, described in section 2.4, can be considered a strong competitor of TIMS for many applications, but so far, it has not been employed for the determination of Pb isotope ratios in snow samples from polar areas. In MC-ICP-MS, the low analyte transport efficiency from the sample solution to the detectors and the modest sensitivity of the Faraday cups used for ion monitoring can limit the isotope ratio precision achievable at low concentration of the target element. For many sample types, this problem can be circumvented via an analyte pre-concentration step, but this approach requires relatively large sample amounts, thus reducing the spatial/temporal resolution of the information provided in the specific case of Pb isotopic analysis of snow samples. A way to increase the instrument sensitivity, while adhering to a low sample consumption, is the use of so-called "total consumption" sample introduction systems. Among these devices, the TISIS (see section 2.3.2) proved to efficiently introduce microsamples into an ICP source, in ICP-AES (Ardini et al. 2012; Lagomarsino et al. 2007) and ICP-MS (Grotti et al. 2013a; Paredes et al. 2009).

Paredes et al. investigated the performance of a TISIS coupled with MC-ICP-MS for the determination of Pb (Paredes et al. 2011) and Sr (Paredes et al. 2013a,b) isotope ratios. Accurate data were obtained at a very low sample uptake rate (5–30 µL/min), consuming less than 0.3 mL of solution. However, in these works, relatively high element concentrations were considered, resulting in a signal strength of about 1 V for the most abundant isotope monitored. The low concentration levels of Pb in snow from remote areas brings us far away from these ideal conditions.

In this chapter, snow samples were first submitted to analyte pre-concentration, based on sample volume reduction by freeze-drying (Bazzano and Grotti 2014). The solutions thus obtained were introduced into an MC-ICP-MS instrument for Pb isotopic analysis

using a TISIS. This analytical protocol was optimised, characterised in terms of precision and accuracy at ultra-trace concentration level, and, finally, applied to the analysis of recent snow collected from Antarctica during two year-round expeditions.

## 7.2 *Materials and method*

### 7.2.1 Reagents

All solutions were prepared with ultrapure water (resistivity $\geq$18.2 MΩ cm), obtained from a Milli-Q Element water purification system (Millipore, Mollsheim, France). Suprapur 65 % $HNO_3$ from Merck (Darmstadt, Germany) was used for the cleaning of materials, while Trace Select Ultra 65 % $HNO_3$ from Sigma-Aldrich (St. Louis, MO, USA) was used for the final stage of the cleaning procedure. Optima $HNO_3$ from Fisher Chemicals (Waltham, MA, USA) was used for the preparation of standards and samples.

All work, except for the pre-concentration procedure, was carried out in a metal-free class-10 clean lab facility at Ghent University. The pre-concentration procedure was accomplished in a class-100 laminar flow area at the University of Genoa.

### 7.2.2 Standard reference materials

Isotopic reference materials for Pb (NIST SRM 981) and Tl (NIST SRM 997), acquired from the National Institute for Standards and technology (NIST, Gaithersburg, MD, USA), were used for correction for the bias introduced by instrument mass discrimination. A solution containing 10 ng/mL of both elements in 0.05 % ultrapure $HNO_3$ matrix was prepared for that purpose. The values used for the mass bias correction were $^{207}Pb/^{206}Pb = 0.914\,64 \pm 0.000\,33$; $^{208}Pb/^{206}Pb = 2.1681 \pm 0.0008$; $^{208}Pb/^{207}Pb = 2.370\,40 \pm 0.000\,49$ and $^{203}Tl/^{205}Tl = 0.418\,922 \pm 0.000\,028$, as reported on the certificates released by NIST.

A 10 ng/mL in-house isotopic standard was prepared by serial dilution of a commercially available 1 mg/mL stock solution (Inorganic Ventures, Christiansburg, VD, USA; lot G2-PB03044) and is further referred to as "A&MS-Pb". Lead isotope ratios for this solution are $^{207}Pb/^{206}Pb = 0.904\,13 \pm 0.000\,02$; $^{208}Pb/^{206}Pb = 2.153\,31 \pm 0.000\,03$; $^{208}Pb/^{207}Pb = 2.381\,67 \pm 0.000\,03$ (average ± 95 % confidence interval; $n = 15$; determined at 100 ngPb/mL using a conventional sample introduction system working at sample uptake rate of 200 µL/min).

### 7.2.3 Instrument and measurements

Pb isotope ratios were measured using a Thermo Scientific (Bremen, Germany) Neptune MC-ICP-MS instrument, operating at low mass resolution. The solutions were introduced into the plasma by means of a PFA nebuliser, operating in self-aspiration mode at a flow rate of 20 µL/min, mounted onto the TISIS chamber. The system required 0.2 mL of solution for each analysis. The instrument settings and data acquisition parameters are summarized in table 7.1. All sample and standard solutions were prepared in 0.05 % ultrapure $HNO_3$ doped with 10 ng/mL of Tl (NIST SRM 997) and the correction for the bias introduced by instrument mass discrimination was performed offline by internal calibration with Tl as calibrant element (section 2.2), using the method proposed by Woodhead (2002) and further refined by Baxter et al. (2006). With this method, a regression line in ln–ln space is determined by measuring both the isotope ratio for Tl (NIST SRM 997) and that selected for Pb (NIST SRM 981) in a series of standard solutions. Based on the regression line thus obtained and the Tl isotope ratio measured for NIST SRM 997 Tl, admixed to the sample, the mass bias is corrected for.

The A&MS-Pb solution was analysed as a quality control sample every five samples, whereas a full procedural blank was analysed for every analytical batch.

Table 7.1. Thermo Scientific Neptune instrument settings and data acquisition parameters used for the determination of Pb isotope ratios by MC-ICP-MS.

| Instrument parameters | |
|---|---|
| Sample uptake rate (µL/min) | 20 |
| Plasma gas flow rate (L/min) | 15 |
| Auxiliary gas flow rate (L/min) | 0.90 |
| Nebuliser gas flow rate (L/min) | 0.72 |
| Sheating gas flow rate (L/min)[a] | 0.35 |
| Temperature of the chamber (°C)[a] | 150 |
| RF power (W) | 1200 |
| Sampling cone | Ni; 1.1 mm Ø orifice |
| Skimmer | Ni; H-type; 0.8 mm Ø orifice |
| Lens settings | Optimised for maximum Pb signal intensity |
| Resolution mode | Low |
| **Data acquisition parameters** | |
| Scan type | Static; multi-collection |
| Number of blocks | 7 |
| Number of cycle/blocks | 6 |
| Integration time (s) | 8.4 |
| Magnet settling time (s) | 0 |
| Idle time (s) | 3 |
| Cup configuration[b] | L3: $^{202}$Hg; L2: $^{203}$Tl; L1: $^{204}$Pb, $^{204}$Hg; C: $^{205}$Tl; H1: $^{206}$Pb; H2: $^{207}$Pb; H3: $^{208}$Pb |
| Resistivity of the pre-amplifier | C, L1, L2, L3: $10^{11}$ ; H1, H2, H3: $10^{12}$ |

[a] Parameters of the TISIS chamber
[b] As a result of the low isotopic abundance of $^{204}$Pb and the spectral overlap from $^{204}$Hg, Pb isotope ratios including this Pb isotope were not considered.

### 7.2.4 Sample collection and analysis

Antarctic snow samples were collected with a monthly resolution at Dome C (East Antarctic Plateau) during the 2006 and 2010 campaigns. In order to prevent contamination during sampling, the scientists taking the samples wore clean room garment and approached the sampling site upwind. The samples were collected in acid-cleaned 50 mL PP graduated tubes (Kartell, Milan, Italy), sealed inside double polyethylene bags and stored at −20 °C until analysis. Following a previously developed procedure (Grotti et al. 2008), samples were first allowed to melt in their closed tubes. Subsequently, 20 g aliquots were transferred into acid-cleaned 50 mL PP graduated tubes, acidified with 100 µL of $HNO_3$ and refrozen. Then, the samples were freeze-dried, re-dissolved in 0.2 mL of 0.05 % $HNO_3$ solution containing 10 ng/mL of Tl (NIST SRM 997) and analysed using MC-ICP-MS.

## 7.3 *Results and discussion*

### 7.3.1 Sensitivity and stability of the signal

Instrument sensitivity strongly depended on the combination of both nebuliser and sheathing gas flow rates, resulting in a behaviour similar to that described earlier for different instrument set-ups (Grotti et al. 2013a; Paredes et al. 2013a). Under optimum

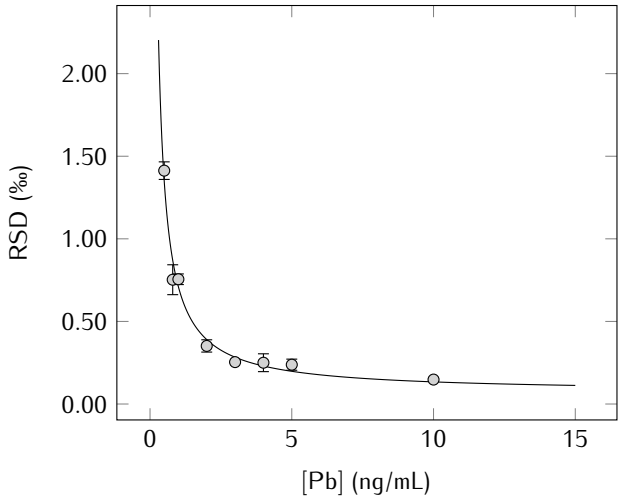


Figure 7.1. variation of the $^{207}Pb/^{206}Pb$ isotope ratio repeatability (internal precision) with the Pb concentration. The solid line is the best-fitting curve through the experimental data and the error bars represent the standard deviation of the average repeatability ($n = 3$).

conditions, 10 ng/mL of Pb (NIST SRM 981) gave rise to a signal of about 0.4 V for $^{208}Pb$ with a variation <2 % RSD over a period of more than six hours of analysis.

The signal produced by the reagents blank (0.05 % of ultrapure $HNO_3$) was about $10^{-5}$ V for $^{208}Pb$ and was stable during approximately six hours of analysis. After this period of time, signal spikes usually started to appear, necessitating the analysis to be stopped. In such an event, the TISIS chamber was thoroughly cleaned by immersion in a bath of hot $HNO_3$ (about 10 % v/v) for several hours. This phenomenon was already described by Paredes et al. (2011) and is likely due to the re-nebulisation of dry analyte particles from the nebuliser tip and the spray chamber walls.

### 7.3.2 Repeatability and intermediate precision

The repeatability or internal precision (RSD for 42 successive measurements) was studied in a concentration range from 0.5 to 10 ng/mL of Pb (NIST SRM 981), equivalent to a total Pb amount from 0.1 to 2 ng. In figure 7.1, the RSD for the $^{207}Pb/^{206}Pb$ ratio is reported, showing values below 1.5 ‰ in the entire concentration range studied. At 10 ng/mL of Pb, the RSD was 0.16 ± 0.03 ‰ (average ± 95 %-confidence interval). This value is more than an order of magnitude better than that reported in chapter 3 using the same sample introduction system, but using a quadrupole-based ICP-MS instrument with ammonia as a damping gas for smoothing the fluctuations of the ion beam intensity for Pb isotope ratio measurements.

The intermediate or external precision was assessed by measuring the $^{207}Pb/^{206}Pb$ ratio in a solution with 10 ng/mL of Pb (NIST SRM 981) over a period of more than three months and was 0.11 ‰ (0.914 65 ± 0.000 05, $n = 73$) when expressed as twice the relative standard deviation of the ratios (not the standard error of the mean). This result is very similar to that obtained by Cocherie and Robert (2007), who reported a value of 0.1 ‰ using a similar MC-ICP-MS instrument and a sample uptake rate of 50 µL/min. Similar values have also been reported by Kuritani and Nakamura (2002) (0.13 ‰) Amelin and Davis (2006) (0.07 ‰) for isotopic analysis of absolute amounts of Pb of 1 and 2 ng by TIMS and double-spike TIMS, respectively. On the other hand, Makishima and Nakamura (2010) reported a reproducibility down to 0.03 ‰ in the isotopic analysis of 1 ng

of Pb at a sample uptake rate of 50 µL/min (0.2 mL total sample consumption) when using an Aridus II aerosol desolvation system and a Neptune MC-ICP-MS instrument equipped with a Jet-type skimmer cone (also termed X-type), characterised by enhanced transport efficiency. Finally, Thirlwall (2002) reported an external precision of 0.06–0.18 ‰ (2SD) for isotopic analysis of ∼7 ng of Pb using double-spike MC-ICP-MS and the Aridus desolvation system.

When reducing the Pb concentration to 0.5 ng/mL, the intermediate precision deteriorated to 0.31 ‰ (0.914 38 ± 0.000 28, $n = 3$) for the $^{207}Pb/^{206}Pb$ ratio.

### 7.3.3 Validation of the measurement results

The validity of the Pb isotope ratios determined via the newly developed method was evaluated by analysing the in-house A&MS-Pb standard, previously characterized using the standard MC-ICP-MS procedure. The average biases and their accompanying 95 % confidence intervals for $^{207}Pb/^{206}Pb$ measurement were 0.06 ± 0.03 ‰ ($n = 25$) and 0.25 ± 0.08 ‰ ($n = 3$) at 10 and 0.5 ng/mL, respectively. The reported biases are within the range defined by the intermediate precision calculated in the previous section, thus the method provides accurate lead isotope ratios over the range of Pb concentration from 0.5 to 10 ng/mL.

#### Procedural blanks

The instrumental performance reported on so far deemed suitable for the accurate determination of $^{207}Pb/^{206}Pb$, $^{208}Pb/^{206}Pb$ and $^{208}Pb/^{207}Pb$ ratios at concentration levels from 0.5 to 10 ng/mL, using 0.2 mL mL of solution only and, therefore, requiring 0.1 to 2 ng of total Pb only. In order to further decrease the lowest concentration feasible, a simple pre-concentration procedure relying on freeze-drying was used for sample pre-treatment. The corresponding blank contribution was estimated on the basis of 5 synthetic samples, obtained by pouring 20 g of ultrapure water (the same mass as for the snow samples) in acid-cleaned tubes that were subsequently submitted to the entire analytical procedure.

The Pb concentration was estimated by comparing the Pb intensity observed for the blanks to that of the bracketing standards at 10 ng/mL (NIST SRM 981), resulting in a concentration of 0.5 ± 0.3 pg/g (or an absolute amount of 10 ± 6 pg of Pb) and a Pb isotopic composition characterized by $^{207}Pb/^{206}Pb = 0.868 \pm 0.008$ and $^{208}Pb/^{206}Pb = 2.103 \pm 0.020$. Taking these results into account, the blank can induce variations in the isotopic composition ranging from 0.1 to 0.2 % in snow samples with a Pb concentration of 5 pg/g, the lowest Pb concentration encountered in the snow samples analysed. A bias of this magnitude is relatively small compared to the natural variation in the isotopic composition of Pb as measured in Antarctic snow and ice (Vallelonga et al. 2005; Van de Velde et al. 2005).

### 7.3.4 Uncertainty estimation

In order to discriminate different isotope ratios and hence, apply the results of isotopic analysis to environmental studies, a realistic estimation of the uncertainty is needed. The total uncertainty was calculated by combining the different single contributions, according to the GUM guidelines (BIPM et al. 1995). The contributions considered are related to

- the instrument precision in measuring the Pb isotope ratios in the samples ($r_x$);
- the precision in measuring the Tl isotope ratio ($r_s$);
- the error associated to the reference values for NIST SRM 981 ($R_c$);

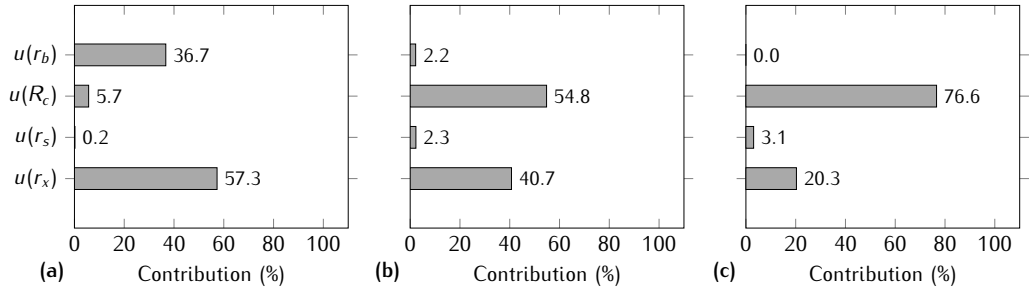


Figure 7.2. contribution to the combined uncertainty of the measurement precision for the Pb isotope ratio in the sample ($r_x$); the measurement precision for the Tl isotope ratio ($r_s$); the uncertainty associated to the certified value for NIST SRM 981 ($R_c$), and the blank ($r_b$). In sub-figures **(a)**, **(b)** and **(c)** samples with a Pb concentration of 5, 23 and 700 pg/g are considered.

- the error due to the blank subtraction ($r_b$).

The relative contributions for the first three effects were estimated and propagated according to equation (7.1), previously reported by Baxter et al. (2006) and based on the assumption that the input quantities are not correlated:

$$\frac{u_c^2(R_{x,f})}{R_{x,f}^2} = \frac{s_m^2(r_x)}{r_x^2} + \frac{s_m^2(r_s)}{r_s^2} b^2 + s_m^2(b) \left[ \ln \left( \frac{r_s}{\rho_{s,SRM}} \right) \right]^2 + \frac{s_m^2(R_c)}{R_c^2} \tag{7.1}$$

here $b$ is the estimated slope of the regression line used for the mass-bias correction, $\rho$ denotes the means of the uncorrected ratios for the analyte and $s_m^2(r_i)$ is the standard error of the mean for a generic ratio $r_i$ measured within the blocks. Due to the low influence of $s_m^2(b)$ (<1 % of the total uncertainty budget), it was merged with $s_m^2(r_s)$.

The relative contribution from the blank was estimated as the difference in the combined uncertainty calculated before and after the subtraction of the intensity of the blank.

Finally, the expanded uncertainty was calculated by multiplying the combined uncertainty, $u_c(R_{x,f})$, with a coverage factor $k = 2$.

In figure 7.2, the different contributions to the combined uncertainty are visualized at concentrations of 5, 23 and 700 pg/g, corresponding to the minimum, median and maximum concentration found in the Antarctic snow samples analysed (see section 7.3.5). In the first case, the major contributions came from the instrument precision (57 %) and the blank (37 %), whereas the contribution from the uncertainty on the NIST SRM 981 certified value accounted for 6 % only. On the other hand, at higher concentrations, 55–77 % of the uncertainty is attributed to the uncertainty of the certified value, 20–41 % is stemming from the Pb isotope ratio measurement precision, while the contribution to the uncertainty coming from the blank is lower than 2 %.

Despite the increased influence of the blank at low concentrations, it did not appear to be the main effect in the range of concentrations from 5 to 700 pg/g. The contribution from the uncertainty on the certified value was found to become dominant at concentrations above 20 pg/g. A better precision can be achieved when using the literature data obtained for NIST SRM 981 by double spike techniques (Baker et al. 2004; Makishima and Nakamura 2010; Taylor et al. 2015; Thirlwall 2002) instead of the NIST certified values, but it could be argued that the confidence in these data cannot be as high as in the certified values. At Pb concentrations below 20 pg/g, the uncertainty associated to the Pb isotope ratios can be reduced by up to 40% by increasing the instrument sensitivity. Additionally, lowering the blank level could result in reducing the uncertainty by more than 20 % for samples with Pb concentrations below 10 pg/g.

Table 7.2. Pb isotope ratios measured in the snow collected at Dome C in the 2006 and 2010 campaigns. Uncertainties are reported as ±95 % confidence interval.

| Date | Pb (ng) | $^{207}Pb/^{206}Pb$ | U | $^{208}Pb/^{206}Pb$ | U | $^{208}Pb/^{207}Pb$ | U |
|---|---|---|---|---|---|---|---|
| 2006 | | | | | | | |
| Dec-05 | 2.5 | 0.8650 | 0.0002 | 2.1048 | 0.0006 | 2.4333 | 0.0008 |
| Jan-06 | 0.2 | 0.8630 | 0.0010 | 2.0984 | 0.0016 | 2.4317 | 0.0014 |
| Feb-06 | – | – | – | – | – | – | – |
| Mar-06 | 0.5 | 0.8685 | 0.0002 | 2.1057 | 0.0005 | 2.4244 | 0.0004 |
| Apr-06 | 0.5 | 0.8747 | 0.0002 | 2.1160 | 0.0005 | 2.4190 | 0.0004 |
| May-06 | 0.8 | 0.8700 | 0.0002 | 2.1082 | 0.0005 | 2.4233 | 0.0004 |
| Jun-06 | 0.5 | 0.8691 | 0.0002 | 2.1070 | 0.0005 | 2.4242 | 0.0004 |
| Jul-06 | 0.4 | 0.8629 | 0.0002 | 2.1020 | 0.0008 | 2.4360 | 0.0007 |
| Aug-06 | 0.2 | 0.8455 | 0.0011 | 2.0727 | 0.0016 | 2.4513 | 0.0017 |
| Sep-06 | 0.3 | 0.8542 | 0.0004 | 2.0914 | 0.0007 | 2.4484 | 0.0006 |
| Oct-06 | 1.1 | 0.8445 | 0.0002 | 2.0692 | 0.0005 | 2.4503 | 0.0005 |
| Nov-06 | 0.1 | 0.8469 | 0.0009 | 2.0774 | 0.0014 | 2.4529 | 0.0013 |
| Dec-06 | – | – | – | – | – | – | – |
| 2010 | | | | | | | |
| Jan-10 | 0.2 | 0.8616 | 0.0020 | 2.0971 | 0.0035 | 2.4340 | 0.0025 |
| Feb-10 | 2.0 | 0.8661 | 0.0002 | 2.1046 | 0.0004 | 2.4299 | 0.0004 |
| Mar-10 | 1.4 | 0.8626 | 0.0002 | 2.0979 | 0.0004 | 2.4321 | 0.0003 |
| Apr-10 | 1.0 | 0.8650 | 0.0002 | 2.1041 | 0.0004 | 2.4324 | 0.0003 |
| May-10 | 14 | 0.8701 | 0.0002 | 2.1108 | 0.0006 | 2.4259 | 0.0007 |
| Jun-10 | 0.4 | 0.8596 | 0.0002 | 2.0939 | 0.0005 | 2.4358 | 0.0005 |
| Jul-10 | 0.6 | 0.8596 | 0.0003 | 2.0945 | 0.0006 | 2.4367 | 0.0007 |
| Aug-10 | 0.2 | 0.8606 | 0.0004 | 2.0969 | 0.0008 | 2.4364 | 0.0008 |
| Sep-10 | 1.3 | 0.8640 | 0.0005 | 2.1006 | 0.0008 | 2.4312 | 0.0012 |
| Oct-10 | 0.3 | 0.8591 | 0.0004 | 2.0956 | 0.0007 | 2.4393 | 0.0007 |
| Nov-10 | 0.1 | 0.8499 | 0.0005 | 2.0799 | 0.0014 | 2.4473 | 0.0019 |
| Dec-10 | 0.4 | 0.8608 | 0.0002 | 2.0974 | 0.0006 | 2.4365 | 0.0006 |

### 7.3.5 Pb isotope ratios measured in recent Antarctic snow with monthly resolution

$^{207}Pb/^{206}Pb$, $^{208}Pb/^{206}Pb$ and $^{208}Pb/^{207}Pb$ isotopes ratios were determined in recent snow samples, collected on a monthly basis during the 2006 and 2010 campaigns. Snow from inland Antarctica is a very simple matrix, not requiring any Pb isolation step. Indeed, the most abundant specie is Na, the concentration of which is typically below 100 ng/mL (Grotti et al. 2015; Udisti et al. 2004). Therefore, the Na concentration after the sample preparation step (<10 µg/mL) was well below the concentration (400 µg/mL) for which Cocherie and Robert (2007) reported a 0.09 ‰ bias in the MC-ICP-MS $^{207}Pb/^{206}Pb$ measurement.

The analytical procedure required 20 g of snow and about 10 minutes for each isotope ratio measurement. The Pb concentration was estimated by comparison of the Pb intensity observed for the sample to that of the closest standards (NIST SRM 981 at 10 ng/mL) and it ranged from 5 to 707 pg/g (0.1 to 14.1 ng of Pb), with a median value of 23 pg/g (0.5 ng of Pb). The estimated Pb amount, the ratios obtained and their uncertainties (95 % confidence interval) are reported in table 7.2.

At 5 pg/g Pb concentration, the uncertainty on the $^{207}Pb/^{206}Pb$ ratio ($n = 2$) was assessed to be ~0.08 %. This result is almost a factor of 5 better than that calculated for the data reported by Vallelonga et al. (2010) (0.39 %, $n = 7$) at 10 pg/g of Pb, using ID-TIMS and 10 g of snow.

In figure 7.3, the data are presented in a three-isotope plot. The Pb isotope ratios plotted on a straight line and are in agreement with data reported in literature (Planchon et al. 2003). Particularly, data lie between the natural and the anthropogenic end-members reported by Van de Velde et al. (2005) and the actual values are similar to those measured at the Hercules Névé for the period 1986–1994. The same authors pointed out that the natural end-member is the result of a mixing of volcanic and crustal inputs, whereas the anthropogenic end-member was governed by both South American and Australian industrial emissions. Also Pb isotope ratios measured in the coastal area of East Antarctica (table 6.4 and Bazzano et al. 2015) are included in figure 7.3. These values are closer to the anthropogenic end-member than those measured on the Plateau, possibly indicating a larger anthropogenic input for the coastal area.

The time-series obtained for the years 2006 and 2010 are reported in figure 7.4. The first year showed a strong seasonal variation of the $^{208}Pb/^{207}Pb$ ratio, characterised by lower values from March to July 2006, and higher values from both December 2005 to January 2006, and from September to November 2006. Particularly, the ratios measured during spring showed values similar to those of the pelagic sediments and South Sandwich volcanic rock (Van de Velde et al. 2005), thus suggesting a predominance of crustal Pb for this period. This result partly contradicts that reported by Burn-Nunes et al. (2011) who found a maximum of both anthropogenic and mineral dust occurring during spring and autumn in the late 1880s. On the other hand, Planchon et al. (2003) reported evidence for close-to-radiogenic values for the $^{206}Pb/^{207}Pb$ ratio occurring in spring/summer during maxima of dust deposition, likely originating from South America.

On the contrary, no clear seasonal trend was apparent in the Pb isotope ratios recorded for the 2010 samples, showing just minor fluctuations around the average value ($^{208}Pb/^{207}Pb = 2.435 \pm 0.005$). The absence of a regular seasonal pattern was also reported by other authors, suggesting that the transport of aerosols and their deposition on the Antarctic ice sheet are complex and may vary from year to year (Planchon et al. 2002b; Van de Velde et al. 2005). To improve the understanding of this variability and to highlight possible correlation with meteorological patterns, the analysis of more years and the use of additional chemical markers is clearly required.

## 7.4 *Conclusions*

The method developed allowed for MC-ICP-MS Pb isotopic analysis at concentrations as low as 0.5 ng/mL, using 0.2 mL of sample solution only. The intermediate precision of the $^{207}Pb/^{206}Pb$ measurement was 0.11 ‰ RSD ($n = 73$) and 0.31 ‰ RSD ($n = 3$) at 10 and 0.5 ng/mL, respectively.

The low sample consumption allowed us to combine the method with a simple analyte pre-concentration procedure consisting of freeze-drying of 20 g samples of snow, thus providing accurate ratios at Pb concentration levels down to 5 pg/g. The mean concentration of the blanks ($0.5 \pm 0.3$ pg/g) was sufficiently low to obtain reliable Pb isotope ratios in this range of concentrations. Particularly, at 5 pg/g, the uncertainty associated to the blank subtraction accounted for about 38 % of the total uncertainty budget, thus still not representing the major contribution.

The analytical protocol developed was applied to the measurement of Pb isotope ratios in recent snow samples collected at Dome C (Antarctic Plateau) during the 2006 and 2010 campaigns. These are the first data of Pb isotope ratios measured in the Antarctic snow using MC-ICP-MS. The relative uncertainty of the ratios measured at 5 pg/g turned out to be competitive with that reported in literature for ID-TIMS. Moreover, the data provided some preliminary insights into the complex pattern of the transport of Pb towards Antarctica and its deposition on the ice sheet.

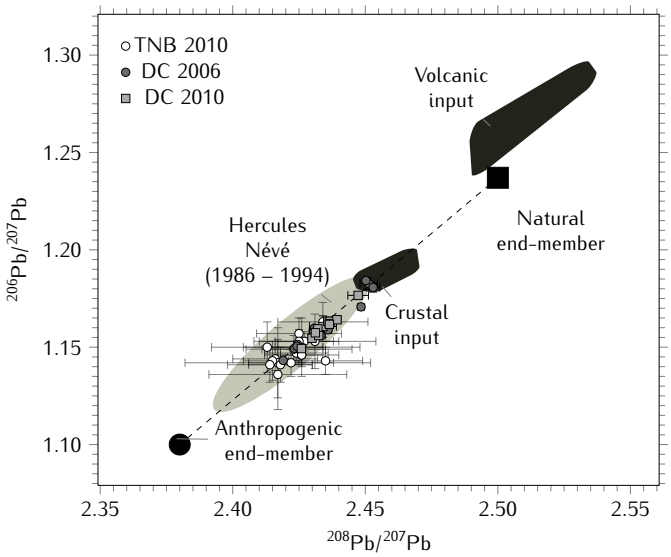


Figure 7.3. three-isotopes plot showing the results obtained for the Antarctic snow samples collected at Dome C during the 2006 (•) and 2010 (■) campaigns, respectively. For comparison, data from table 6.4 determined in particulate matter from Terra Nova Bay (Coastal Antarctica) are also reported (○), while the shaded areas are from Van de Velde et al. (2005). All the error bars represent 95 % confidence intervals.

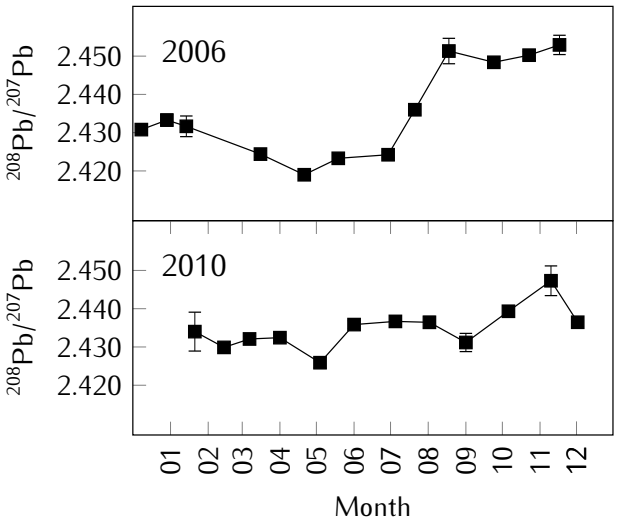


Figure 7.4. annual variation of the $^{208}Pb/^{207}Pb$ ratio at Dome C during 2006 and 2010. Error bars represent 95 % confidence intervals.

*References*

Amelin, Y. and Davis, W. J., 2006. Isotopic analysis of lead in sub-nanogram quantities by TIMS using a $^{202}$Pb-$^{205}$Pb spike. *Journal of Analytical Atomic Spectrometry*, **21**, 1053–1061. DOI: 10.1039/b606842a

Ardini, F., Grotti, M., Sánchez, R., and Todolí, J.-L., 2012. Improving the analytical performances of ICP-AES by using a high-temperature single-pass spray chamber and segmented-injections micro-sample introduction for the analysis of environmental samples. *Journal of Analytical Atomic Spectrometry*, **27**, 1400–1404. DOI: 10.1039/c2ja30152k

Baker, J., Peate, D., Waight, T., and Meyzen, C., 2004. Pb isotopic analysis of standards and samples using a $^{207}$Pb-$^{204}$Pb double spike and thallium to correct for mass bias with a double-focusing MC-ICP-MS. *Chemical Geology*, **211**, 275–303. DOI: 10.1016/j.chemgeo.2004.06.030

Baxter, D. C., Rodushkin, I., Engström, E., and Malinovsky, D., 2006. Revised exponential model for mass bias correction using an internal standard for isotope abundance ratio measurements by multi-collector inductively coupled plasma mass spectrometry. *Journal of Analytical Atomic Spectrometry*, **21**, 427–430. DOI: 10.1039/b517457k

Bazzano, A. and Grotti, M., 2014. Determination of lead isotope ratios in environmental matrices by quadrupole ICP-MS working at low sample consumption rates. *Journal of Analytical Atomic Spectrometry*, **29**, 926–933. DOI: 10.1039/c3ja50388g

Bazzano, A., Ardini, F., Becagli, S., Traversi, R., Udisti, R., Cappelletti, D., and Grotti, M., 2015. Source assessment of atmospheric lead measured at Ny-Ålesund, Svalbard. *Atmospheric Environment*, **113**, 20–26. DOI: 10.1016/j.atmosenv.2015.04.053

BIPM, IEC, IFCC, ISO, IUPAC, IUPAP, and OIML, 1995. *Guide to the expression of uncertainty in measurement*. Joint Committee for Guides in Metrology (JCGM)

Burn-Nunes, L. J., Vallelonga, P., Loss, R. D., Burton, G. R., Moy, A., Curran, M., Hong, S., Smith, A. M., Edwards, R., Morgan, V. I., and Rosman, K. J. R., 2011. Seasonal variability in the input of lead, barium and indium to Law Dome, Antarctica. *Geochimica et Cosmochimica Acta*, **75**, 1–20. DOI: 10.1016/j.gca.2010.09.037

Chisholm, W., Rosman, K., Boutron, C., Candelone, J., and Hong, S., 1995. Determination of lead isotopic ratios in Greenland and Antarctic snow and ice at picogram per gram concentrations. *Analytica Chimica Acta*, **311**, 141–151. DOI: 10.1016/0003-2670(95)00181-X

Cocherie, A. and Robert, M., 2007. Direct measurement of lead isotope ratios in low concentration environmental samples by MC-ICP-MS and multi-ion counting. *Chemical Geology*, **243**, 90–104. DOI: 10.1016/j.chemgeo.2007.05.011

Grotti, M., Soggia, F., and Luis Todolì, J.-L., 2008. Ultratrace analysis of Antarctic snow samples by reaction cell inductively coupled plasma mass spectrometry using a total-consumption micro-sample-introduction system. *Analyst*, **133**, 1388–1394. DOI: 10.1039/b804043e

Grotti, M., Ardini, F., and Todolì, J.-L., 2013a. Total introduction of microsamples in inductively coupled plasma mass spectrometry by high-temperature evaporation chamber with a sheathing gas stream. *Analytica Chimica Acta*, **767**, 14–20. DOI: 10.1016/j.aca.2013.01.017

Grotti, M., Soggia, F., Ardini, F., Magi, E., Becagli, S., Traversi, R., and Udisti, R., 2015. Year-round record of dissolved and particulate metals in surface snow at Dome Concordia (East Antarctica). *Chemosphere*, **138**, 916–923. DOI: 10.1016/j.chemosphere.2014.10.094

Kuritani, T. and Nakamura, E., 2002. Precise isotope analysis of nanogram-level Pb for natural rock samples without use of double spikes. *Chemical Geology*, **186**, 31–43. DOI: 10.1016/S0009-2541(02)00004-9

Lagomarsino, C., Grotti, M., Todolì, J.-L., and Mermet, J.-M., 2007. Study of the absence of recondensation with low liquid delivery rates by using a cavity sheathing gas in inductively coupled plasma-atomic emission spectrometry. *Journal of Analytical Atomic Spectrometry*, **22**, 523. DOI: 10.1039/b618487a

Makishima, A. and Nakamura, E., 2010. Precise isotopic determination of Hf and Pb at sub-nano gram levels by MC-ICP-MS employing a newly designed sample cone and a pre-amplifier with a 1012 ohm register. *Journal of Analytical Atomic Spectrometry*, **25**, 1712–1716. DOI: 10.1039/c0ja00015a

Paredes, E., Grotti, M., Mermet, J.-M., and Todolí, J.-L., 2009. Heated-spray chamber-based low sample consumption system for inductively coupled plasma spectrometry. *Journal of Analytical Atomic Spectrometry*, **24**, 903–910. DOI: 10.1039/b904002a

Paredes, E., Asfaha, D. G., Ponzevera, E., Brach-Papa, C., Van Bocxstaele, M., Todolí, J.-L., and Quétel, C. R., 2011. MC-ICPMS isotope ratio measurements using an ultra-low flow sample introduction system. *Journal of Analytical Atomic Spectrometry*, **26**, 1372–1379. DOI: 10.1039/c0ja00254b

Paredes, E., Asfaha, D. G., and Quétel, C. R., 2013a. Isotope ratio measurements by MC-ICPMS below 10 µL/min under continuous sample flow conditions. Exploring the limits with strontium. *Journal of Analytical Atomic Spectrometry*, **28**, 320–326. DOI: 10.1039/c2ja30209h

Paredes, E., Todoli, J.-L., and Quétel, C. R., 2013b. Limitations of the exponential model for the correction for mass discrimination effects during isotope ratio measurements by MC-ICPMS. Demonstration with Sr at 5–15 µL/min continuous liquid flow rates. *Journal of Analytical Atomic Spectrometry*, **28**, 327–333. DOI: 10.1039/c3ja30210e

Planchon, F. A. M., Boutron, C. F., Barbante, C., Cozzi, G., Gaspari, V., Wolff, E. W., Ferrari, C. P., and Cescon, P., 2002b. Short-term variations in the occurrence of heavy metals in Antarctic snow from Coats Land since the 1920s. *Science of the Total Environment*, **300**, 129–142. DOI: 10.1016/S0048-9697(02)00277-2

Planchon, F. A. M., van de Velde, K., Rosman, K. J. R., Wolff, E. W., Ferrari, C. P., and Boutron, C. F., 2003. One hundred fifty–year record of lead isotopes in Antarctic snow from Coats Land. *Geochimica et Cosmochimica Acta*, **67**, 693–708. DOI: 10.1016/S0016-7037(02)01136-5

Rosman, K. J. R., Chisholm, W., Boutron, C. F., Candelone, J.-P., and Patterson, C. C., 1994. Anthropogenic lead isotopes in Antarctica. *Geophysical Research Letters*, **21**, 2669–2672. DOI: 10.1029/94GL02603

Rosman, K. J. R., Chisholm, W., Boutron, C. F., Candelone, J.-P., Jaffrezo, J.-L., and Davidson, C. I., 1998. Seasonal variations in the origin of lead in snow at Dye 3, Greenland. *Earth and Planetary Science Letters*, **160**, 383–389. DOI: 10.1016/S0012-821X(98)00098-3

Taylor, R. N., Ishizuka, O., Michalik, A., Milton, J. A., and Croudace, I. W., 2015. Evaluating the precision of Pb isotope measurement by mass spectrometry. *Journal of Analytical Atomic Spectrometry*, **30**, 198–213. DOI: 10.1039/C4JA00279B

Thirlwall, M. F., 2002. Multicollector ICP-MS analysis of Pb isotopes using a 207pb-204pb double spike demonstrates up to 400 ppm/amu systematic errors in TI-normalization. *Chemical Geology*, **184**, 255–279. DOI: 10.1016/S0009-2541(01)00365-5

Udisti, R., Becagli, S., Benassai, S., Castellano, E., Fattori, I., Innocenti, M., Migliori, A., and Traversi, R., 2004. Atmosphere-snow interaction by a comparison between aerosol and uppermost snow-layers composition at Dome C, East Antarctica. *Annals of Glaciology*, **39**, 53–61. DOI: 10.3189/172756404781814474

Vallelonga, P., Van de Velde, K., Candelone, J. P., Morgan, V. I., Boutron, C. F., and Rosman, K. J. R., 2002. The lead pollution history of Law Dome, Antarctica, from

isotopic measurements on ice cores: 1500 AD to 1989 AD. *Earth and Planetary Science Letters*, **204**, 291–306. DOI: 10.1016/S0012-821X(02)00983-4

Vallelonga, P., Gabrielli, P., Rosman, K. J. R., Barbante, C., and Boutron, C. F., 2005. A 220 kyr record of Pb isotopes at Dome C Antarctica from analyses of the EPICA ice core. *Geophysical Research Letters*, **32** (L01706), 1–4. DOI: 10.1029/2004GL021449

Vallelonga, P., Gabrielli, P., Balliana, E., Wegner, A., Delmonte, B., Turetta, C., Burton, G., Vanhaecke, F., Rosman, K. J. R., Hong, S., Boutron, C. F., Cescon, P., and Barbante, C., 2010. Lead isotopic compositions in the EPICA Dome C ice core and Southern Hemisphere Potential Source Areas. *Quaternary Science Reviews*, **29**, 247–255. DOI: 10.1016/j.quascirev.2009.06.019

Van de Velde, K., Vallelonga, P., Candelone, J. P., Rosman, K. J. R., Gaspari, V., Cozzi, G., Barbante, C., Udisti, R., Cescon, P., and Boutron, C. F., 2005. Pb isotope record over one century in snow from Victoria Land, Antarctica. *Earth and Planetary Science Letters*, **232**, 95–108. DOI: 10.1016/j.epsl.2005.01.007

Woodhead, J., 2002. A simple method for obtaining highly accurate Pb isotope data by MC-ICP-MS. *Journal of Analytical Atomic Spectrometry*, **17**, 1381–1385. DOI: 10.1039/b205045e

# 8 Sr isotopic analysis at sub ng-level by multi-collector ICP-MS

## 8.1 *Introduction*

Similarly to Pb, the determination of Sr isotope ratios in snow and ice from polar areas can help to identify sources of atmospheric particulate matter and reconstruct how these changed over time. Using this approach, Delmonte et al. (2004, 2010) and Revel-Rolland et al. (2006) demonstrated the contribution of South American and Australian sources of dust to the East Antarctic plateau during glacial and interglacial stages, respectively. However, due to the low Sr concentration in snow and ice, typically a few tens of pg/g (Grotti et al. 2011, 2015; Ikegawa et al. 1999), large sample volumes are required in order to obtain precise isotope ratio values, thus preventing the identification of short time-scales events.

TIMS was used extensively for Sr isotopic the analysis of polar snow and ice (*e.g.* Basile et al. 1997; Burton et al. 2002, 2007). Indeed, because of the direct loading of the sample onto the source filament, without the need of solvent or low-efficiency sample introduction systems, TIMS is the method of choice for the determination of the $^{87}Sr/^{86}Sr$ ratio in samples with low Sr amount (Lin et al. 2015). However, recent improvements in the sensitivity of MC-ICP-MS instruments, based on the use of a desolvating nebuliser system coupled with a modified interface capable of a better ion transmission (Breton et al. 2015), open interesting possibilities for the accurate and precise determination of $^{87}Sr/^{86}Sr$ ratios using limited Sr amounts.

In this chapter, a method for the determination of $^{87}Sr/^{86}Sr$ ratios in solutions containing 0.4 and 0.8 ng/mL of Sr was optimised. Such concentration range mimics that obtained by evaporating or freeze-drying 30 g of Antarctic snow with a Sr concentration of 10–60 pg/g, as reported for recent snow samples collected at Dome C station, on the Antarctic plateau (Grotti et al. 2015).

## 8.2 *Materials and method*

### 8.2.1 Reagents

All solutions were prepared with ultrapure water (resistivity $\geq$18.2 MΩ cm), obtained from a Milli-Q Element water purification system (Millipore, Mollsheim, France). HCl and $HNO_3$ purified in-house by sub-boiling distillation were used for the cleaning of materials (see section 8.2.2), while Optima ultrapure (UP) $HNO_3$ from Fisher Chemicals (Waltham, MA, USA) was used for the final stage of the cleaning procedure and for the preparation of standards, samples and procedural blanks.

Table 8.1. cleaning procedure for plastic labware used for the determination of $^{87}Sr/^{86}Sr$ by MC-ICP-MS.

| Stage | Reagent | Duration | Temperature |
|---|---|---|---|
| 1 | HCl (50 % sub-boiled) | 24 h | 110 °C |
| 2 | $HNO_3$ (50 % sub-boiled) | 24 h | 110 °C |
| 3 | $HNO_3$ (1 % UP) | 24 h | 110 °C |
| 4 | $HNO_3$ (0.1 % UP) | 24 h | 110 °C |
| 5 | $HNO_3$ 0.01 % UP) | up to analysis | ambient |

Table 8.2. elution sequence used for the Sr isolation.

| Step | Reagents |
|---|---|
| Wash | 4 × 5 mL $H_2O$ (Milli-Q) |
| | 4 mL $HNO_3$ (0.3% UP) |
| | 1 mL HCl (50 % sub-boiled) |
| | 4 × 5 mL $H_2O$ (Milli-Q) |
| Conditioning | 2 mL $HNO_3$ (50 % UP) |
| Loading sample | |
| Matrix removal | 2 × 2.5 mL $HNO_3$ (50 % UP) |
| Elution | 6 mL $HNO_3$ (0.3 % UP) |

### 8.2.2 Cleaning of the labware

Sr is not particularly prone to contamination but, because of the low analyte concentration, care was required to avoid potential sources of Sr contamination during the sample preparation.

All work was carried out in a metal-free class-10 clean lab facility at Ghent University. PFA screwcap beakers (Savillex Corp., Minneapolis, USA) and polyethylene 1 mL columns were cleaned following the procedure outlined in table 8.1, whereas pipette tips were cleaned applying only steps 3 and 4 of the same procedure. The resin used for the isolation (Sr-Spec, SR_B50-A 100–150 µm from Triskem International) was stored in an acid-cleaned polyethylene vial filled with Milli-Q water to aid cleaning. The solution was discharged after 24 h and the vial re-filled with fresh Milli-Q water. This procedure was repeated 5 times before using the resin.

### 8.2.3 Sr isolation by column chemistry

In order to avoid spectral overlap of the signals from the isobaric nuclides $^{87}Sr$ and $^{87}Rb$, Sr was isolated by extraction chromatography using 400 µL of a Sr-specific resin with a crown ether as the active component and the elution sequence summarised in table 8.2. 1 mL of sample ($HNO_3$ 50 % UP) was loaded onto the column and, after elution, the solution was concentrated to dryness on a hotplate. Before the analysis, the sample was dissolved in 1 mL of $HNO_3$ (0.3 % UP) and transferred into pre-cleaned 2 mL poly-propylene vials (Eppendorf AG, Hamburg, Germany). The recovery of the whole procedure was $71.2 \pm 0.4$ % ($n = 5$), in accordance to previous literature data (Charlier et al. 2006).

Table 8.3. Thermo Scientific Neptune instrument settings and data acquisition parameters used for the determination of $^{87}Sr/^{86}Sr$.

| Instrumental parameters | |
|---|---|
| Sample uptake rate (µL/min) | 100 |
| Plasma gas flow rate (L/min) | 15 |
| Auxiliary gas flow rate (L/min) | 0.6–0.7[b] |
| Nebuliser gas flow rate (L/min) | 0.9–1.1[b] |
| Ar sweep gas (L/min)[a] | 6.2 |
| $N_2$ additional gas (mL/min)[a] | 3.0 |
| Spray chamber temperature (°C)[a] | 110 |
| Membrane oven temperature (°C)[a] | 160 |
| RF power (W) | 1200 |
| Sampling cone | Ni; Jet-type; 1.1 mm Ø orifice |
| Skimmer | Ni; X-type; 0.8 mm Ø orifice |
| Resolution mode | Low |
| **Data acquisition parameters** | |
| Scan type | Static, multi-collection |
| Number of blocks | 6 |
| Number of cycle/blocks | 5 |
| Integration time (s) | 4 |
| Magnet settling time (s) | 0 |
| Idle time (s) | 3 |
| Cup configuration | L4: $^{82}Kr$; L3: $^{83}Kr$; L2: $^{84}Sr$, $^{84}Kr$; L1: $^{85}Rb$ C:$^{86}Sr$, $^{84}Kr$; H1: $^{87}Sr$, $^{87}Rb$; H2: $^{88}Sr$ |
| Resistivity of the pre-amplifier | L1, L2, L3, L4: $10^{11}$ ; C, H1, H2: $10^{12}$ |

[a] Parameters of the Aridus II membrane nebuliser desolvating system;
[b] Optimised daily for maximum Sr intensity.

### 8.2.4 Instrument and measurements

Sr isotope ratios were measured using a Thermo Scientific (Bremen, Germany) Neptune MC-ICP-MS instrument, operating at low mass resolution. The solutions were introduced into the plasma by means of a PFA nebuliser, operating in self-aspiration mode at a flow rate of 100 µL/min, mounted onto the Aridus II membrane nebuliser desolvating system (Cetac Technologies, Omaha, NE, USA). The system required 0.4 mL of solution for each analysis. The instrument settings and data acquisition parameters are summarized in table 8.3.

The potential contribution of remaining Rb at mass-to-charge ratio 87 was calculated by monitoring the signal of $^{85}Rb^+$ and using the ratio $^{87}Rb/^{85}Rb = 0.385617$. Similarly, contribution from $^{84}Kr^+$ and $^{86}Kr^+$ were calculated on the basis of the signal intensity for $^{8e}Kr^+$ and using $^{84}Kr/^{83}Kr$ and $^{86}Kr/^{83}Kr$ of 4.955 391 and 1.502 522, respectively. For both corrections, the effect of mass discrimination on these isotope ratios was taken into account using the Russell's law:

$$K = \frac{R_t}{R_o} = \left(\frac{m_1}{m_2}\right)^{\beta} \tag{8.1}$$

where $R_t$ is the true isotope ratio, $R_o$ the measured isotope ratio, $m_1$ and $m_2$ the mass of the two isotopes monitored and $\beta$ the mass discrimination factor. In this approach, the

calibration of the measured isotope ratio can be realised by using another known ratio either of the target element itself or of another, admixed element (according to section 2.2, these approaches are named internal calibration with the target element and internal calibration with a calibrant element, respectively). In this work, the mass discrimination factor $\beta$ was calculated assuming a constant $^{88}Sr/^{86}Sr$ ratio (8.375 209) and using the Sr signals obtained after correction for isobaric interference which, in turn, allowed a better correction for the isobaric overlap. This iterative process was repeated eight times (Rich et al. 2012). Finally, standard solutions prepared from the isotopic reference material SRM 987 $SrCO_3$ from NIST (Gaithersburg, MD, USA) were run in a sample-standard bracketing sequence, enabling an additional external bracketing calibration using the certified value $^{87}Sr/^{86}Sr = 0.710\,34 \pm 0.000\,26$.

## 8.3 *Results and discussion*

### 8.3.1 Sensitivity and stability of the signal

Instrument sensitivity was enhanced using the Aridus II sample introduction system described in section 2.3.2, a high-performance interface pump and an high-efficiency skimmer (X-type). Under optimal conditions a solution containing 0.8 ng/mL of Sr resulted above 1 V for $^{88}Sr$ with a $<2$ % RSD within a single measurement and $<5$ % RSD over a 5-hour measurement session.

The signal for a solution of 0.3 % UP $HNO_3$ was about 5 mV during the whole analytical session. The wash-out time, required to reach this baseline signal after the analysis of 1 ng/mL Sr solutions, was below 1 minute.

### 8.3.2 Repeatability and intermediate precision

The repeatability (RSD for 30 successive replicates) was studied at 0.8 and 0.4 ng/mL of Sr (NIST SRM 987), equivalent to a total Sr amount of 320 and 160 pg. At 0.8 ng/mL the RSD was $0.31 \pm 0.03$ ‰ (average ±95 % confidence interval), whereas the relative standard error (RSE) was $0.05 \pm 0.01$ ‰. Ratios measured at 0.4 ng/mL were accompanied by a higher uncertainty, resulting in $0.67 \pm 0.24$ and $0.12 \pm 0.09$ ‰ RSD and RSE, respectively. These results are slightly worse than those reported from Harlou et al. (2009) who obtained $0.04 \pm 0.01$ and $0.08 \pm 0.04$ ‰ RSE for 300 and 100 pg of Sr (NIST SRM 987), measured by TIMS.

The intermediate precision was assessed by repeated measurements at 0.8 and 0.4 ng/mL of Sr (NIST SRM 987) over a period of two months, resulting in values of 0.17 ($0.710\,35 \pm 0.000\,06$, $n = 14$) and 0.19 ‰ ($0.710\,36 \pm 0.000\,10$, $n = 7$), respectively. This value is better than the 0.25 ‰ precision reported by Burton et al. (2002) for the analysis of 1 ng of Sr by TIMS but it is about 6 times worse in comparison to the precision of 0.03 ‰ reported by Harlou et al. (2009) and Koornneef et al. (2014) for TIMS measurements of sub-ng samples.

In figure 8.1, the precision of the method is compared with the variability of $^{87}Sr/^{86}Sr$ measured in ice cores from East Antartica (Delmonte et al. 2004) and potential source areas in South America (Delmonte et al. 2010; Gaiero et al. 2007) and Australia (Revel-Rolland et al. 2006). Both at 0.8 and 0.4 ng/mL, the precision of the method is lower than both the variability within the single sources and the difference among the isotopic signatures of the potential source areas. Therefore, the method can discriminate among the different sources influencing the Sr isotopic signature at the Antarctic plateau.

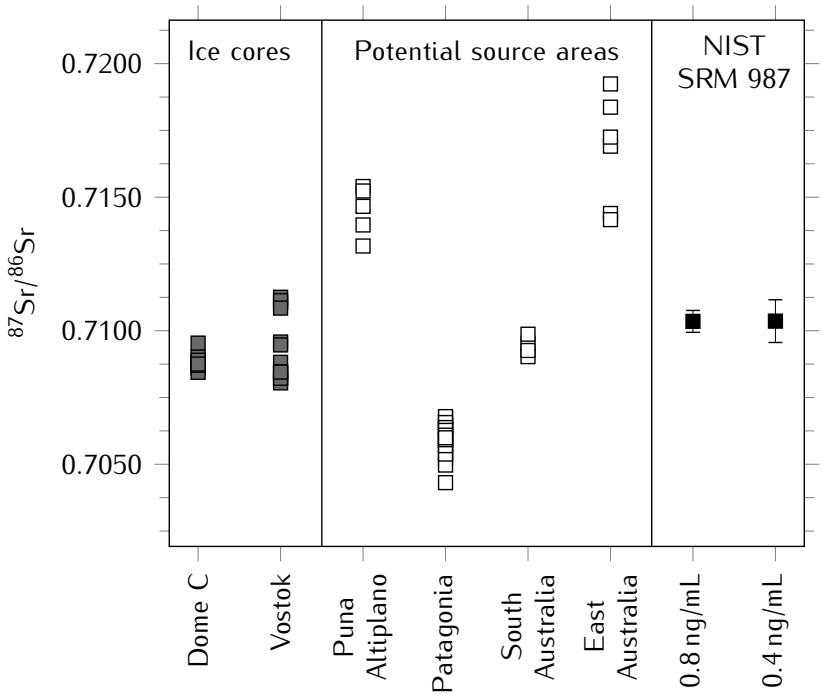


Figure 8.1. precision of the MC-ICP-MS method is compared to the variability of $^{87}Sr/^{86}Sr$ in Antarctic ice cores (Delmonte et al. 2004) and different potential source areas (Delmonte et al. 2010; Gaiero et al. 2007; Revel-Rolland et al. 2006). The error bars are expressed as 2 standard deviation.

### 8.3.3 Procedural blanks and accuracy

Procedural blank is an important factor limiting the accuracy of isotope ratios measured on small amounts of analyte. The procedural blank was $6.3 \pm 1.2$ pg/mL, equivalent to a total Sr amount of $6.3 \pm 1.2$ pg ($n = 8$). This value comprises all the contributions from Sr isolation to sample analysis and is in accordance with previous data reported in literature, using similar Sr isolation procedures (Harlou et al. 2009; Li et al. 2005).

The effect of the blank on the $^{87}Sr/^{86}Sr$ ratio was assessed comparing the results obtained at different Sr concentrations (NIST SRM 987) without and with the isolation procedure. Isotope ratios measured in the solutions submitted to column chemistry were not significantly different from those determined without Sr isolation (figure 8.2) and their error in comparison to the certificate value was $0.04 \pm 0.10$ ($n = 6$) and $0.05 \pm 0.17$ ‰ ($n = 3$) for 0.8 and 0.4 ng/mL, respectively.

## 8.4 *Conclusions*

The MC-ICP-MS method developed allowed $^{87}Sr/^{86}Sr$ determination at concentrations as low as 0.4 ng/mL, using 0.4 mL of sample solution. The intermediate precision was 0.17 ‰ RSD ($n = 14$) and 0.19 ‰ RSD ($n = 7$) at 0.8 and 0.4 ng/mL, respectively. Although these figures of merit are about 6 times worse than those reported for TIMS analysis of similar equivalent Sr amounts (Harlou et al. 2009; Koornneef et al. 2014), the method precision is high enough to allow the discrimination among different source areas potentially influencing the Sr isotopic signature at the Antarctic plateau.

The procedural blank was $6.3 \pm 1.2$ pg/mL and it did not significantly affect the measured ratios at a concentration as low as 0.4 ng/mL. At this concentration, the

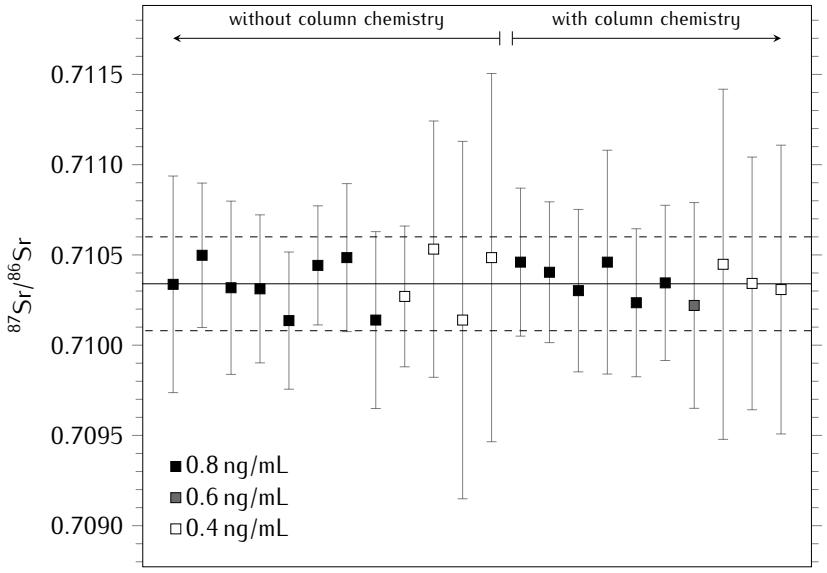


Figure 8.2. $^{87}Sr/^{86}Sr$ ratio measured at different Sr concentrations without and with Sr isolation. The certificate value for NIST SRM 987 and its uncertainty are reported as solid and dashed lines, respectively.

relative error measured for the certified value of NIST SRM 987 was $0.05 \pm 0.17$ ‰ ($n = 3$).

Combining the method with a simple analyte pre-concentration procedure consisting of evaporating or freeze-drying 30 g of snow, accurate $^{87}Sr/^{86}Sr$ ratios at concentrations as low as 10 pg/g would be possible.

*References*

Basile, I., Grousset, F. E., Revel, M., Petit, J. R., Biscaye, P. E., and Barkov, N. I., 1997. Patagonian origin of glacial dust deposited in East Antarctica (Vostok and Dome C) during glacial stages 2, 4 and 6. *Earth and Planetary Science Letters*, **146**, 573–589. DOI: 10.1016/S0012-821X(96)00255-5

Breton, T., Lloyd, N. S., Trinquier, A., Bouman, C., and Schwieters, J. B., 2015. Improving Precision and Signal/Noise Ratios for MC-ICP-MS. *Procedia Earth and Planetary Science*, 11th Applied Isotope Geochemistery Conference AIG-11 **13**, 240–243. DOI: 10.1016/j.proeps.2015.07.056

Burton, G. R., Morgan, V. I., Boutron, C. F., and Rosman, K. J. R., 2002. High-sensitivity measurements of strontium isotopes in polar ice. *Analytica Chimica Acta*, **469**, 225–233. DOI: 10.1016/S0003-2670(02)00720-1

Burton, G. R., Rosman, K. J. R., Candelone, J.-P., Burn, L. J., Boutron, C. F., and Hong, S., 2007. The impact of climatic conditions on Pb and Sr isotopic ratios found in Greenland ice, 7–150 ky BP. *Earth and Planetary Science Letters*, **259**, 557–566. DOI: 10.1016/j.epsl.2007.05.015

Charlier, B. L. A., Ginibre, C., Morgan, D., Nowell, G. M., Pearson, D. G., Davidson, J. P., and Ottley, C. J., 2006. Methods for the microsampling and high-precision analysis of strontium and rubidium isotopes at single crystal scale for petrological and geochronological applications. *Chemical Geology*, **232**, 114–133. DOI: 10.1016/j.chemgeo.2006.02.015

Delmonte, B., Basile-Doelsch, I., Petit, J.-R., Maggi, V., Revel-Rolland, M., Michard, A., Jagoutz, E., and Grousset, F., 2004. Comparing the Epica and Vostok dust records during the last 220,000 years: stratigraphical correlation and provenance in glacial periods. *Earth-Science Reviews*, **66**, 63–87. DOI: 10.1016/j.earscirev.2003.10.004

Delmonte, B., Andersson, P., Schöberg, H., Hansson, M., Petit, J., Delmas, R., Gaiero, D., Maggi, V., and Frezzotti, M., 2010. Geographic provenance of aeolian dust in East Antarctica during Pleistocene glaciations: preliminary results from Talos Dome and comparison with East Antarctic and new Andean ice core data. *Quaternary Science Reviews*, **29**, 256–264. DOI: 10.1016/j.quascirev.2009.05.010

Gaiero, D. M., Brunet, F., Probst, J.-L., and Depetris, P. J., 2007. A uniform isotopic and chemical signature of dust exported from Patagonia: Rock sources and occurrence in southern environments. *Chemical Geology*, **238**, 107–120. DOI: 10.1016/j.chemgeo.2006.11.003

Grotti, M., Soggia, F., Ardini, F., and Magi, E., 2011. Major and trace element partitioning between dissolved and particulate phases in Antarctic surface snow. *Journal of Environmental Monitoring*, **13**, 2511–2520. DOI: 10.1039/c1em10215j

Grotti, M., Soggia, F., Ardini, F., Magi, E., Becagli, S., Traversi, R., and Udisti, R., 2015. Year-round record of dissolved and particulate metals in surface snow at Dome Concordia (East Antarctica). *Chemosphere*, **138**, 916–923. DOI: 10.1016/j.chemosphere.2014.10.094

Harlou, R., Pearson, D. G., Nowell, G. M., Ottley, C. J., and Davidson, J. P., 2009. Combined Sr isotope and trace element analysis of melt inclusions at sub-ng levels using micro-milling, TIMS and ICPMS. *Chemical Geology*, **260**, 254–268. DOI: 10.1016/j.chemgeo.2008.12.020

Ikegawa, M., Kimura, M., Honda, K., Akabane, I., Makita, K., Motoyama, H., Fujii, Y., and Itokawa, Y., 1999. Geographical variations of major and trace elements in East Antarctica. *Atmospheric Environment*, **33**, 1457–1467. DOI: 10.1016/S1352-2310(98)00243-X

Koornneef, J. M., Bouman, C., Schwieters, J. B., and Davies, G. R., 2014. Measurement of small ion beams by thermal ionisation mass spectrometry using new $10^{13}\,\Omega$ resistors. *Analytica Chimica Acta*, **819**, 49–55. DOI: 10.1016/j.aca.2014.02.007

Li, Q., Chen, F., Wang, X., Li, X., and Li, C., 2005. Ultra-low procedural blank and the single-grain mica Rb-Sr isochron dating. *Chinese Science Bulletin*, **50**, 2861–2865. DOI: 10.1360/982005-984

Lin, J., Liu, Y., Chen, H., Zhou, L., Hu, Z., and Gao, S., 2015. Review of High-Precision Sr Isotope Analyses of Low-Sr Geological Samples. *Journal of Earth Science*, **26**, 763–774. DOI: 10.1007/s12583-015-0593-0

Revel-Rolland, M., De Deckker, P., Delmonte, B., Hesse, P., Magee, J., Basile-Doelsch, I., Grousset, F., and Bosch, D., 2006. Eastern Australia: A possible source of dust in East Antarctica interglacial ice. *Earth and Planetary Science Letters*, **249**, 1–13. DOI: 10.1016/j.epsl.2006.06.028

Rich, S., Manning, S. W., Degryse, P., Vanhaecke, F., and Lerberghe, K. V., 2012. Strontium isotopic and tree-ring signatures of Cedrus brevifolia in Cyprus. *Journal of Analytical Atomic Spectrometry*, **27**, 796–806. DOI: 10.1039/C2JA10345A

# 9 Conclusions

The determination of isotope ratios can provide valuable information in various research topics spanning from cosmochemistry to physiology. In environmental sciences, the determination of Pb and Sr isotope ratios can help to identify different sources and to constrain their possible geographic origins. However, insufficient instrument precision and the presence of significant biases can easily jeopardise the results, leading to wrong conclusions. In particular, obtaining precise isotope ratios for samples with a low amount of the target element or limited sample volume is often an issue.

In this dissertation different approaches were used in order to reduce the amount of target element required to obtain precise and accurate Pb and Sr isotope ratios. Two different strategies were investigated for the determination of $^{208}Pb/^{207}Pb$ and $^{206}Pb/^{207}Pb$ by single-collector ICP-MS using a limited sample amount. In the first approach Pb isotope ratios were determined using a PFA micro-nebuliser working at 150 µL/min, whereas in the second approach the TISIS, working at 20 µL/min, was used. Both methods used a 10 s integration time and $NH_3$ as damping gas to improve the precision. Repeatability for the $^{206}Pb/^{207}Pb$ ratio was $0.12 \pm 0.03$ and $0.17 \pm 0.04$ % RSD at 150 and 20 µL/min, respectively, whereas the error for the analysis of $^{208}Pb/^{207}Pb$ and $^{206}Pb/^{207}Pb$ ratios in lichen reference material CRM 482 was $<1$ h.

The developed methods were successfully applied in the context of polar research, along with well-established atomic spectrometry methods for elemental analysis. In particular, atmospheric particulate matter ($PM_{10}$) collected at Ny-Ålesund (Svalbard Islands, Norwegian Arctic) during spring and summer from 2010 to 2014 was analysed for Pb content, enrichment factors and isotopic composition. Spring samples were characterised by higher content of Pb compared to summer, whereas enrichment factors indicated a dominant input of anthropogenic sources in both seasons. The determination of $^{208}Pb/^{207}Pb$ and $^{206}Pb/^{207}Pb$ ratios revealed a different isotopic composition of the anthropogenic sources influencing the two seasons. In spring most of Pb reaching Ny-Ålesund showed an isotopic composition compatible with emission related to mining activities in the region of the Rudny Altai (at the Russian-Kazakh border), whereas in summer industrial emissions in north eastern North America appeared the main source of the atmospheric Pb. During 2013 the described seasonal transition was not apparent and the influence of the Eurasian source was observed also in summer. Results obtained by Pb isotopic composition were further corroborated by back-trajectories cluster analysis of air masses reaching the sampling site.

The analytical method for measuring Pb isotope ratios by single-collector ICP-MS also proved very useful in the investigation of the coastal marine environment of Kongsfjorden (Svalbard Islands), allowing to assess the natural and anthropogenic sources of particulate trace elements. It was found that Al, Co, Fe, K, Ti and V were mainly influenced by natural input from the glaciers, whereas Ba, Cr, Cu, Mn, Mo, Ni, Pb and Zn were of anthropogenic origin and reached the fjord through the intrusion

of Atlantic waters. Pb isotopic composition of suspended particulate matter associated to Atlantic waters was similar to those measured in $PM_{10}$ collected at NyÅlesund, revealing an important role of atmospheric deposition for anthropogenic Pb entering the Kongsfjorden.

In the framework of the Antarctic research, the study was focused on the understanding of sources and transport pathways of metals associated to the atmospheric particulate and surface snow. In particular, size-segregated atmospheric particulate matter collected during 2010–2011 austral summer at a coastal Antarctic site (Terra Nova Bay, Victoria Land) were analysed for major, trace elements and Pb isotopic composition. Al, Co, Fe, Li, Mn, Rb, Y and V were dominated by crustal inputs, Li, Mg, Na and Rb were related to marine inputs, whereas Cr, Cu, Mo and Pb were influenced by an anthropogenic source. Both crustal and anthropogenic elements appeared related to air masses carried by the katabatic wind from the inland, whereas the marine input was higher when the sea-ice extent was reduced. Pb isotope ratios suggested that 50–70 % of the measured Pb was likely related to anthropogenic sources from South America and Australia.

Simultaneous measurements of different isotopic signals by MC-ICP-MS resulted in very precise isotope ratio values. Coupling this technique with the TISIS sample introduction system, the repeatability was 0.16 ‰ RSD for $^{207}Pb/^{206}Pb$ measured at 10 ng/mL and using 0.2 mL of solution. This value is about one order of magnitude better than that obtained using a single-collector ICP-MS. Accurate and precise determinations of Pb isotope ratios were possible at concentrations as low as 0.5 ng/mL (total Pb amount: 100 pg). This concentration range was further extended downwards by using a 100-fold analyte element preconcentration via freeze-drying of 20 g of snow. Pb concentration in procedural blanks was $0.5 \pm 0.3$ pg/g, enabling the determination of Pb isotope ratios in snow samples containing down to 5 pg/g of Pb. The procedure was applied to surface snow samples collected at Dome C (East Antarctic Plateau) on a monthly basis during the 2006 and 2010 campaigns, revealing a seasonal variation in the Pb isotope ratios occurring during 2006 and a strong inter-annual variation between the two campaigns.

MC-ICP-MS was also used in combination with a membrane nebuliser desolvating system (Aridus II) for the determination of precise $^{87}Sr/^{86}Sr$ ratios. Isobaric interference by $^{87}Rb^+$ was avoided by isolation of Sr using column chemistry, whereas the interference from $^{86}Kr^+$ was mathematically corrected measuring the signal intensity for $^{83}Kr^+$. The intermediate precision was 0.17 and 0.19 ‰ RSD at Sr concentrations of 0.8 and 0.4 ng/mL, respectively. Sr concentration in procedural blanks was $6.3 \pm 1.2$ pg/mL and it did not significantly affect the measured ratios at concentration as low as 0.4 ng/mL. At this concentration, the error in comparison to NIST SRM 987 was $0.05 \pm 0.17$ ‰.

In conclusion, the use of efficient sample introduction systems in combination with ICP-MS provided accurate and precise Pb and Sr isotopic analysis of several kind of environmental matrices, significantly supporting different polar research studies. The achieved figures of merits were always fit-for-purpose and, when using MC-ICP-MS, comparable to those obtained by TIMS, that nowadays, is still the method of choice for the determination of isotope ratios using low amounts of the target elements. However, further improvements in this field will help to fill the gap between the two techniques. In addition, the use of efficient sample introduction systems and ICP-MS can provide unique advantages over TIMS for the determination of precise and accurate isotope ratios working with small amount of elements with a high ionisation potentials, such as Hf, or very volatile, such as Hg.

# Bibliography


Åberg, G., 1995. The use of natural strontium isotopes as tracers in environmental studies. *Water, Air, and Soil Pollution*, **79**, 309–322. DOI: 10.1007/BF01100444

Ahn, I. Y., Chung, K. H., and Choi, H. J., 2004. Influence of glacial runoff on baseline metal accumulation in the Antarctic limpet Nacella concinna from King George Island. *Marine Pollution Bulletin*, **49**, 119–127. DOI: 10.1016/j.marpolbul.2004.03.008

Albarède, F. and Beard, B., 2004. Analytical methods for non-traditional isotopes. *Reviews in Mineralogy and Geochemistry*, **55**, 113–152. DOI: 10.2138/gsrmg.55.1.113

Aliani, S., Bartholini, G., Degl'innocenti, F., Delfanti, R., Galli, C., Lazzoni, E., Lorenzelli, R., Malaguti, A., Meloni, R., Papucci, C., Salvi, S., and Zaborska, A., 2004. Multidisciplinary investigations in the marine environment of the inner Kongsfiord, Svalbard islands (September 2000 and 2001). *Chemistry and Ecology*, **20** (sup1), S19–S28. DOI: 10.1080/02757540410001655396

AMAP, 2005. *AMAP Assessment 2002: Heavy Metals in the Arctic*. Oslo, Norway: Arctic Monitoring and Assessment Programme, xvi + 265 pp.

Amelin, Y. and Davis, W. J., 2006. Isotopic analysis of lead in sub-nanogram quantities by TIMS using a $^{202}$Pb-$^{205}$Pb spike. *Journal of Analytical Atomic Spectrometry*, **21**, 1053–1061. DOI: 10.1039/b606842a

Ardini, F., Grotti, M., Sánchez, R., and Todolí, J.-L., 2012. Improving the analytical performances of ICP-AES by using a high-temperature single-pass spray chamber and segmented-injections micro-sample introduction for the analysis of environmental samples. *Journal of Analytical Atomic Spectrometry*, **27**, 1400–1404. DOI: 10.1039/c2ja30152k

Argentini, S., Del Buono, P., Della Vedova, A., and Mastrantonio, G., 1995. A statistical analysis of wind in Terra Nova Bay, Antarctica, for the austral summers 1988 and 1989. *Atmospheric Research*, **39**, 145–156. DOI: 10.1016/0169-8095(95)00009-G

Bacon, J. R., 2002. Isotopic characterisation of lead deposited 1989–2001 at two upland Scottish locations. *Journal of Environmental Monitoring*, **4**, 291–299. DOI: 10.1039/b109731h

Baker, J., Peate, D., Waight, T., and Meyzen, C., 2004. Pb isotopic analysis of standards and samples using a $^{207}$Pb-$^{204}$Pb double spike and thallium to correct for mass bias with a double-focusing MC-ICP-MS. *Chemical Geology*, **211**, 275–303. DOI: 10.1016/j.chemgeo.2004.06.030

Balcaen, L. I. L., De Schamphelaere, K. A. C., Janssen, C. R., Moens, L., and Vanhaecke, F., 2008. Development of a method for assessing the relative contribution of waterborne and dietary exposure to zinc bioaccumulation in Daphnia magna by using isotopically enriched tracers and ICP-MS detection. *Analytical and Bioanalytical Chemistry*, **390**, 555–569. DOI: 10.1007/s00216-007-1620-5

Bandura, D. R., Baranov, V. I., and Tanner, S. D., 2000. Effect of collisional damping and reactions in a dynamic reaction cell on the precision of isotope ratio measurements. *Journal of Analytical Atomic Spectrometry*, **15**, 921–928. DOI: 10.1039/B000285M

Bandura, D. R., Baranov, V. I., and Tanner, S. D., 2002. Inductively coupled plasma mass spectrometer with axial field in a quadrupole reaction cell. *Journal of American Society for Mass Spectrometry*, **13**, 1176–1185. DOI: 10.1016/S1044-0305(02)00435-X

Barrie, L. A., 1986. Arctic air pollution: An overview of current knowledge. *Atmospheric Environment*, **20**, 643–663. DOI: 10.1016/0004-6981(86)90180-0

Basile, I., Grousset, F. E., Revel, M., Petit, J. R., Biscaye, P. E., and Barkov, N. I., 1997. Patagonian origin of glacial dust deposited in East Antarctica (Vostok and Dome C) during glacial stages 2, 4 and 6. *Earth and Planetary Science Letters*, **146**, 573–589. DOI: 10.1016/S0012-821X(96)00255-5

Baxter, D. C., Rodushkin, I., Engström, E., and Malinovsky, D., 2006. Revised exponential model for mass bias correction using an internal standard for isotope abundance ratio measurements by multi-collector inductively coupled plasma mass spectrometry. *Journal of Analytical Atomic Spectrometry*, **21**, 427–430. DOI: 10.1039/b517457k

Bazzano, A. and Grotti, M., 2014. Determination of lead isotope ratios in environmental matrices by quadrupole ICP-MS working at low sample consumption rates. *Journal of Analytical Atomic Spectrometry*, **29**, 926–933. DOI: 10.1039/c3ja50388g

Bazzano, A., Rivaro, P., Soggia, F., Ardini, F., and Grotti, M., 2014. Anthropogenic and natural sources of particulate trace elements in the coastal marine environment of Kongsfjorden, Svalbard. *Marine Chemistry*, **163**, 28–35. DOI: 10.1016/j.marchem.2014.04.001

Bazzano, A., Ardini, F., Becagli, S., Traversi, R., Udisti, R., Cappelletti, D., and Grotti, M., 2015. Source assessment of atmospheric lead measured at Ny-Ålesund, Svalbard. *Atmospheric Environment*, **113**, 20–26. DOI: 10.1016/j.atmosenv.2015.04.053

Beard, B., Johnson, C. M., Skulan, J. L., Nealson, K. H., Cox, L., and Sun, H., 2003. Application of Fe isotopes to tracing the geochemical and biological cycling of Fe. *Chemical Geology*, Isotopic records of microbially mediated processes **195**, 87–117. DOI: 10.1016/S0009-2541(02)00390-X

Becagli, S., Scarchilli, C., Traversi, R., Dayan, U., Severi, M., Frosini, D., Vitale, V., Mazzola, M., Lupi, A., Nava, S., and Udisti, R., 2012. Study of present-day sources and transport processes affecting oxidised sulphur compounds in atmospheric aerosols at Dome C (Antarctica) from year-round sampling campaigns. *Atmospheric Environment*, **52**, 98–108. DOI: 10.1016/j.atmosenv.2011.07.053

Bentley, R. A., 2006. Strontium isotopes from the Earth to the archaeological skeleton: a review. *Journal of Archaeological Method and Theory*, **13**, 135–187. DOI: 10.1007/s10816-006-9009-x

Beszczynska-Moller, A., Weslawski, J. M., Walczowski, W., and Zajaczkowski, M., 1997. Estimation of glacial meltwater discharge into Svalbard coastal waters. *Oceanologia*, **39**, 289–298

Biancato, D., Ceccato, D., Chiminello, F., and Mittner, P., 2006. Micro-PIXE and principal component analysis in a study of internal mixing phenomena in Antarctic coastal aerosol. *Nuclear Instruments and Methods in Physics Research Section B: Beam Interactions with Materials and Atoms*, **249**, 561–565. DOI: 10.1016/j.nimb.2006.03.053

Bindler, R., 2011. Contaminated lead environments of man: Reviewing the lead isotopic evidence in sediments, peat, and soils for the temporal and spatial patterns of atmospheric lead pollution in Sweden. *Environmental Geochemistry and Health*, **33**, 311–329. DOI: 10.1007/s10653-011-9381-7

BIPM, IEC, IFCC, ISO, IUPAC, IUPAP, and OIML, 1995. *Guide to the expression of uncertainty in measurement*. Joint Committee for Guides in Metrology (JCGM)

BIPM, 2012. International Vocabulary of Metrology - Basic and general concept and associated terms (VIM)

Blanckenburg, F. v., Oelze, M., Schmid, D. G., Zuilen, K. v., Gschwind, H.-P., Slade, A. J., Stitah, S., Kaufmann, D., and Swart, P., 2014. An iron stable isotope comparison between human erythrocytes and plasma. *Metallomics*, **6**, 2052–2061. DOI: 10.1039/C4MT00124A

Bodhaine, B. A., Barrie, L. A., Schnell, R. C., Shaw, G. E., and Mckie, J. K., 1992. Symposium on the tropospheric chemistry of the Antarctic Region. *Tellus B*. Vol. 44, 250–251. DOI: 10.1034/j.1600-0889.1992.t01-3-00002.x

Bollhöfer, A. and Rosman, K. J. R., 2000. Isotopic source signatures for atmospheric lead: the Southern Hemisphere. *Geochimica et Cosmochimica Acta*, **64**, 3251–3262. DOI: 10.1016/S0016-7037(00)00436-1

Bollhöfer, A. and Rosman, K. J. R., 2001a. Isotopic source signatures for atmospheric lead: The Northern Hemisphere. *Geochimica et Cosmochimica Acta*, **65**, 1727–1740. DOI: 10.1016/S0016-7037(00)00630-X

Bollhöfer, A. and Rosman, K. J. R., 2001b. Lead isotopic ratios in European atmospheric aerosols. *Physics and Chemistry of the Earth, Part B: Hydrology, Oceans and Atmosphere*, **26**, 835–838. DOI: 10.1016/S1464-1909(01)00094-6

Bollhöfer, A. and Rosman, K. J. R., 2002. The temporal stability in lead isotopic signatures at selected sites in the Southern and Northern Hemispheres. *Geochimica et Cosmochimica Acta*, **66**, 1375–1386. DOI: 10.1016/S0016-7037(01)00862-6

Bollhöfer, A., Rosman, K. J. R., Dick, A. L., Chisholm, W., Burton, G. R., Loss, R. D., and Zahorowski, W., 2005. Concentration, isotopic composition, and sources of lead in Southern Ocean air during 1999/2000, measured at the Cape Grim Baseline Air Pollution Station, Tasmania. *Geochimica et Cosmochimica Acta*, **69**, 4747–4757. DOI: 10.1016/j.gca.2005.06.024

Bory, A. J.-M., Biscaye, P. E., and Grousset, F. E., 2003. Two distinct seasonal Asian source regions for mineral dust deposited in Greenland (NorthGRIP). *Geophysical Research Letters*, **30**, 1167. DOI: 10.1029/2002GL016446

Bourdon, B., Turner, S., Henderson, G. M., and Lundstrom, C. C., 2003. Introduction to U-series Geochemistry. *Reviews in Mineralogy and Geochemistry*, **52**, 1–21. DOI: 10.2113/0520001

Boutron, C. F., Görlach, U., Candelone, J.-P. J. P., Bolshov, M. A., and Delmas, R. J., 1991. Decrease in anthropogenic lead, cadmium and zinc in Greenland snows since the late 1960s. *Nature*, **353**, 153–156

Box, G. E. P., Hunter, J. S., and Hunter, W. G., 2005. *Statistics for experimenters: design, innovation, and discovery*. Wiley series in probability and statistics. Wiley-Interscience

Breton, T., Lloyd, N. S., Trinquier, A., Bouman, C., and Schwieters, J. B., 2015. Improving Precision and Signal/Noise Ratios for MC-ICP-MS. *Procedia Earth and Planetary Science*, 11th Applied Isotope Geochemistery Conference AIG-11 **13**, 240–243. DOI: 10.1016/j.proeps.2015.07.056

Bromwich, D. H., 1989. Satellite analyses of Antarctic katabatic wind behavior. *Bulletin American Meteorological Society*, **70**, 738–749. DOI: 10.1175/1520-0477(1989)070<0738:SAOAKW>2.0.CO;2

Browner, R. F. and Boorn, A. W., 1984. Sample Introduction: The Achilles' Heel of Atomic Spectroscopy? *Analytical Chemistry*, **56**, 786A–798A. DOI: 10.1021/ac00271a718

Burn-Nunes, L. J., Vallelonga, P., Loss, R. D., Burton, G. R., Moy, A., Curran, M., Hong, S., Smith, A. M., Edwards, R., Morgan, V. I., and Rosman, K. J. R., 2011. Seasonal variability in the input of lead, barium and indium to Law Dome, Antarctica. *Geochimica et Cosmochimica Acta*, **75**, 1–20. DOI: 10.1016/j.gca.2010.09.037

Burton, G. R., Morgan, V. I., Boutron, C. F., and Rosman, K. J. R., 2002. High-sensitivity measurements of strontium isotopes in polar ice. *Analytica Chimica Acta*, **469**, 225–233. DOI: 10.1016/S0003-2670(02)00720-1

Burton, G. R., Rosman, K. J. R., Candelone, J.-P., Burn, L. J., Boutron, C. F., and Hong, S., 2007. The impact of climatic conditions on Pb and Sr isotopic ratios found in Greenland ice, 7–150 ky BP. *Earth and Planetary Science Letters*, **259**, 557–566. DOI: 10.1016/j.epsl.2007.05.015

Carignan, J. and Gariépy, C., 1995. Isotopic composition of epiphytic lichens as a tracer of the sources of atmospheric lead emissions in southern Québec, Canada. *Geochimica et Cosmochimica Acta*, **59**, 4427–4433. DOI: 10.1016/0016-7037(95)00302-G

Carignan, J., Simonetti, A., and Gariépy, C., 2002. Dispersal of atmospheric lead in northeastern North America as recorded by epiphytic lichens. *Atmospheric Environment*, **36**, 3759–3766. DOI: 10.1016/S1352-2310(02)00294-7

Charlier, B. L. A., Ginibre, C., Morgan, D., Nowell, G. M., Pearson, D. G., Davidson, J. P., and Ottley, C. J., 2006. Methods for the microsampling and high-precision analysis of strontium and rubidium isotopes at single crystal scale for petrological and geochronological applications. *Chemical Geology*, **232**, 114–133. DOI: 10.1016/j.chemgeo.2006.02.015

Chavent, M., Guégan, H., Kuentz, V., Patouille, B., and Saracco, J., 2009. PCA- and PMF-based methodology for air pollution sources identification and apportionment. *Environmetrics*, **20**, 928–942. DOI: 10.1002/env.963

Chisholm, W., Rosman, K., Boutron, C., Candelone, J., and Hong, S., 1995. Determination of lead isotopic ratios in Greenland and Antarctic snow and ice at picogram per gram concentrations. *Analytica Chimica Acta*, **311**, 141–151. DOI: 10.1016/0003-2670(95)00181-X

Cloquet, C., Carignan, J., and Libourel, G., 2006. Atmospheric pollutant dispersion around an urban area using trace metal concentrations and Pb isotopic compositions in epiphytic lichens. *Atmospheric Environment*, **40**, 574–587. DOI: 10.1016/j.atmosenv.2005.09.073

Cocherie, A. and Robert, M., 2007. Direct measurement of lead isotope ratios in low concentration environmental samples by MC-ICP-MS and multi-ion counting. *Chemical Geology*, **243**, 90–104. DOI: 10.1016/j.chemgeo.2007.05.011

Cottier, F., Tverberg, V., Inall, M., Svendsen, H., Nilsen, F., and Griffiths, C., 2005. Water mass modification in an Arctic fjord through cross-shelf exchange: The seasonal hydrography of Kongsfjorden, Svalbard. *Journal of Geophysical Research, C: Oceans*, **110** (C12), 1–18. DOI: 10.1029/2004JC002757

De Deckker, P., Norman, M., Goodwin, I. D., Wain, A., and Gingele, F. X., 2010. Lead isotopic evidence for an Australian source of aeolian dust to Antarctica at times over the last 170,000 years. *Palaeogeography, Palaeoclimatology, Palaeoecology*, **285**, 205–223. DOI: 10.1016/j.palaeo.2009.11.013

De Muynck, D., Cloquet, C., and Vanhaecke, F., 2008. Development of a new method for Pb isotopic analysis of archaeological artefacts using single-collector ICP-dynamic reaction cell-MS. *Journal of Analytical Atomic Spectrometry*, **23**, 62–71. DOI: 10.1039/b709461b

Degerlund, M. and Eilertsen, H. C., 2009. Main species characteristics of phytoplankton spring blooms in NE Atlantic and Arctic waters (68–80 °N). *Estuaries and Coasts*, **33**, 242–269. DOI: 10.1007/s12237-009-9167-7

Degryse, P., Muynck, D. D., Delporte, S., Boyen, S., Jadoul, L., Winne, J. D., Ivaneanu, T., and Vanhaecke, F., 2012. Strontium isotopic analysis as an experimental auxiliary technique in forensic identification of human remains. *Analytical Methods*, **4**, 2674–2679. DOI: 10.1039/C2AY25035G

Delmonte, B., Basile-Doelsch, I., Petit, J.-R., Maggi, V., Revel-Rolland, M., Michard, A., Jagoutz, E., and Grousset, F., 2004. Comparing the Epica and Vostok dust records during the last 220,000 years: stratigraphical correlation and provenance in glacial periods. *Earth-Science Reviews*, **66**, 63–87. DOI: 10.1016/j.earscirev.2003.10.004

Delmonte, B., Andersson, P., Schöberg, H., Hansson, M., Petit, J., Delmas, R., Gaiero, D., Maggi, V., and Frezzotti, M., 2010. Geographic provenance of aeolian dust in East Antarctica during Pleistocene glaciations: preliminary results from Talos Dome and comparison with East Antarctic and new Andean ice core data. *Quaternary Science Reviews*, **29**, 256–264. DOI: 10.1016/j.quascirev.2009.05.010

Draxler, R. and Rolph, G., 2014. *HYSPLIT (HYbrid Single-Particle Lagrangian Integrated Trajectory) Model access via NOAA ARL READY Website.* URL: http://ready.arl.noaa.gov/HYSPLIT_ash.php (visited on 03/03/2016)

Ehrlich, S., Gavrieli, I., Dor, L.-B., and Halicz, L., 2001. Direct high-precision measurements of the $^{87}Sr/^{86}Sr$ isotope ratio in natural water, carbonates and related materials by multiple collector inductively coupled plasma mass spectrometry (MC-ICP-MS). *Journal of Analytical Atomic Spectrometry*, **16**, 1389–1392. DOI: 10.1039/B107996B

Eichler, A., Tobler, L., Eyrikh, S., Gramlich, G., Malygina, N., Papina, T., and Schwikowski, M., 2012. Three centuries of Eastern European and Altai lead emissions recorded in a Belukha ice core. *Environmental Science and Technology*, **46**, 4323–4330. DOI: 10.1021/es2039954

Encinar, J. R., Garcia Alonso, J. I., Sanz-Medel, A., Main, S., and Turner, P. J., 2001. A comparison between quadrupole, double focusing and multicollector ICP-MS. Part II. Evaluation of total combined uncertainty in the determination of lead in biological matrices by isotope dilution. *Journal of Analytical Atomic Spectrometry*, **16**, 322–326. DOI: 10.1039/b006147f

Engvall, A.-C., Krejci, R., Ström, J., Treffeisen, R., Scheele, R., Hermansen, O., and Paatero, J., 2007. Changes in aerosol properties during spring-summer period in the Arctic troposphere. *Atmospheric Chemistry and Physics Discussions*, **7**, 1215–1260. DOI: 10.5194/acpd-7-1215-2007

Erel, Y., Dubowski, Y., Halicz, L., Erez, J., and Kaufman, A., 2001. Lead concentrations and isotopic ratios in the sediments of the Sea of Galilee. *Environmental Science and Technology*, **35**, 292–299

Farmer, J. G., Eades, L. J., Graham, M. C., and Bacon, J. R., 2000. The changing nature of the $^{206}Pb/^{207}Pb$ isotopic ratio of lead in rainwater, atmospheric particulates, pine needles and leaded petrol in Scotland, 1982-1998. *Journal of Environmental Monitoring*, **2**, 49–57. DOI: 10.1039/a907558e

Fattori, I., Becagli, S., Bellandi, S., Castellano, E., Innocenti, M., Mannini, A., Severi, M., Vitale, V., and Udisti, R., 2005. Chemical composition and physical features of summer aerosol at Terra Nova Bay and Dome C, Antarctica. *Journal of Environmental Monitoring*, **7**, 1265–1274. DOI: 10.1039/b507327h

Faure, G. and Mensing, T. M., 2007. *Introduction to Planetary Science*. Dordrecht: Springer Netherlands

Fisher, J. A., Jacob, D. J., Wang, Q., Bahreini, R., Carouge, C. C., Cubison, M. J., Dibb, J. E., Diehl, T., Jimenez, J. L., Leibensperger, E. M., Lu, Z., Meinders, M. B., Pye, H. O., Quinn, P. K., Sharma, S., Streets, D. G., van Donkelaar, A., and Yantosca, R. M., 2011. Sources, distribution, and acidity of sulfate–ammonium aerosol in the Arctic in winter–spring. *Atmospheric Environment*, **45**, 7301–7318. DOI: 10.1016/j.atmosenv.2011.08.030

Gaiero, D. M., 2007. Dust provenance in Antarctic ice during glacial periods: From where in southern South America? *Geophysical Research Letters*, **34**, L17707. DOI: 10.1029/2007GL030520

Gaiero, D. M., Brunet, F., Probst, J.-L., and Depetris, P. J., 2007. A uniform isotopic and chemical signature of dust exported from Patagonia: Rock sources and occurrence in southern environments. *Chemical Geology*, **238**, 107–120. DOI: 10.1016/j.chemgeo.2006.11.003

Gallon, C., Aggarwal, J., and Flegal, A. R., 2008. Comparison of mass discrimination correction methods and sample introduction systems for the determination of lead isotopic composition using a Multicollector Inductively Coupled Plasma Mass Spectrometer. *Analytical Chemistry*, **80**, 8355–8363. DOI: 10.1021/ac800554k

Garrett, T. J., Zhao, C., and Novelli, P. C., 2010. Assessing the relative contributions of transport efficiency and scavenging to seasonal variability in Arctic aerosol. *Tellus Series B*, **62**, 190–196. DOI: 10.1111/j.1600-0889.2010.00453.x

Gassó, S., Stein, A., Marino, F., Castellano, E., Udisti, R., and Ceratto, J., 2010. A combined observational and modeling approach to study modern dust transport from the Patagonia desert to East Antarctica. *Atmospheric Chemistry and Physics*, **10**, 8287–8303. DOI: 10.5194/acp-10-8287-2010

Geng, H., Ryu, J., Jung, H. J., Chung, H., Ahn, K. H. O., and Ro, C. U. N., 2010. Single-particle characterization of summertime arctic aerosols collected at Ny-Ålesund, Svalbard. *Environmental Science and Technology*, **44**, 2348–2353. DOI: 10.1021/es903268j

Gill, R., 2014. *Modern Analytical Geochemistry: An Introduction to Quantitative Chemical Analysis Techniques for Earth, Environmental and Materials Scientists*. Routledge. 342 pp.

Gray, A. L., Williams, J. G., Ince, A. T., and Liezers, M., 1994. Communication. Noise sources in inductively coupled plasma mass spectrometry: an investigation of their importance to the precision of isotope ratio measurements. *Journal of Analytical Atomic Spectrometry*, **9**, 1179–1181. DOI: 10.1039/ja9940901179

Grotti, M., Soggia, F., Abelmoschi, M. L., Rivaro, P., Magi, E., and Frache, R., 2001. Temporal distribution of trace metals in Antarctic coastal waters. *Marine Chemistry*, **76**, 189–209. DOI: 10.1016/S0304-4203(01)00063-9

Grotti, M., Soggia, F., and Luis Todolì, J.-L., 2008. Ultratrace analysis of Antarctic snow samples by reaction cell inductively coupled plasma mass spectrometry using a total-consumption micro-sample-introduction system. *Analyst*, **133**, 1388–1394. DOI: 10.1039/b804043e

Grotti, M., Soggia, F., Ardini, F., and Magi, E., 2011. Major and trace element partitioning between dissolved and particulate phases in Antarctic surface snow. *Journal of Environmental Monitoring*, **13**, 2511–2520. DOI: 10.1039/c1em10215j

Grotti, M., Ardini, F., and Todolì, J.-L., 2013a. Total introduction of microsamples in inductively coupled plasma mass spectrometry by high-temperature evaporation chamber with a sheathing gas stream. *Analytica Chimica Acta*, **767**, 14–20. DOI: 10.1016/j.aca.2013.01.017

Grotti, M., Soggia, F., Ianni, C., Magi, E., and Udisti, R., 2013b. Bioavailability of trace elements in surface sediments from Kongsfjorden, Svalbard. *Marine Pollution Bulletin*, **77**, 367–374. DOI: 10.1016/j.marpolbul.2013.10.010

Grotti, M., Soggia, F., Ardini, F., Magi, E., Becagli, S., Traversi, R., and Udisti, R., 2015. Year-round record of dissolved and particulate metals in surface snow at Dome Concordia (East Antarctica). *Chemosphere*, **138**, 916–923. DOI: 10.1016/j.chemosphere.2014.10.094

Grousset, F. E. and Biscaye, P. E., 2005. Tracing dust sources and transport patterns using Sr, Nd and Pb isotopes. *Chemical Geology*, **222**, 149–167. DOI: 10.1016/j.chemgeo.2005.05.006

Halliday, A. N., Lee, D.-C., Christensen, J. N., Rehkämper, M., Yi, W., Luo, X., Hall, C. M., Ballentine, C. J., Pettke, T., and Stirling, C., 1998. Applications of Multiple Collector-ICPMS to cosmochemistry, geochemistry, and paleoceanography. *Geochimica et Cosmochimica Acta*, **62**, 919–940. DOI: 10.1016/S0016-7037(98)00057-X

Halliday, A. N., 2000. Hf-W Chronometry and Inner Solar System Accretion Rates. *Space Science Reviews*, **92**, 355–370. DOI: 10.1023/A:1005280220751

Hansen, H. P. and Koroleff, F., 1999. Determination of nutrients. *Methods of Seawater Analysis*. Ed. by Grasshoff, K., Kremling, K., and Ehrhardt, n. Wiley-VCH Verlag GmbH, 159–228

Harlou, R., Pearson, D. G., Nowell, G. M., Ottley, C. J., and Davidson, J. P., 2009. Combined Sr isotope and trace element analysis of melt inclusions at sub-ng levels using micro-milling, TIMS and ICPMS. *Chemical Geology*, **260**, 254–268. DOI: 10.1016/j.chemgeo.2008.12.020

Hegseth, E. N. and Tverberg, V., 2013. Effect of Atlantic water inflow on timing of the phytoplankton spring bloom in a high Arctic fjord (Kongsfjorden, Svalbard). *Journal of Marine Systems*, **113–114**, 94–105. DOI: 10.1016/j.jmarsys.2013.01.003

Heumann, K. G., Gallus, S. M., Rädlinger, G., and Vogl, J., 1998. Precision and accuracy in isotope ratio measurements by plasma source mass spectrometry. *Journal of Analytical Atomic Spectrometry*, **13**, 1001–1008. DOI: 10.1039/A801965G

Hong, S., Candelone, J.-P., Patterson, C. C., and Boutron, C. F., 1994. Greenland ice evidence of hemispheric lead pollution two millennia ago by Greek and Roman civilizations. *Science*, **265**, 1841–1843. DOI: 10.1126/science.265.5180.1841

Hopper, J. F., Ross, H. B., Sturges, W. T., and A., B. L., 1991. Regional source discrimination of atmospheric aerosols in Europe using the isotopic composition of lead. *Tellus Series B*, **43**, 45–60. DOI: 10.1034/j.1600-0889.1991.00004.x

Iizuka, T. and Hirata, T., 2005. Improvements of precision and accuracy in in situ Hf isotope microanalysis of zircon using the laser ablation-MC-ICPMS technique. *Chemical Geology*, **220**, 121–137. DOI: 10.1016/j.chemgeo.2005.03.010

Ikegawa, M., Kimura, M., Honda, K., Akabane, I., Makita, K., Motoyama, H., Fujii, Y., and Itokawa, Y., 1999. Geographical variations of major and trace elements in East Antarctica. *Atmospheric Environment*, **33**, 1457–1467. DOI: 10.1016/S1352-2310(98)00243-X

Jackson, B. P., Winger, P. V., and Lasier, P. J., 2004. Atmospheric lead deposition to Okefenokee Swamp, Georgia, USA. *Environmental Pollution*, **130**, 445–451. DOI: 10.1016/j.envpol.2003.12.019

Jourdain, B. and Legrand, M., 2002. Year-round records of bulk and size-segregated aerosol composition and HCl and $HNO_3$ levels in the Dumont d'Urville (coastal Antarctica) atmosphere: Implications for sea-salt aerosol fractionation in the winter and summer. *Journal of Geophysical Research, D: Atmospheres*, **107** (D22), 4645. DOI: 10.1029/2002JD002471

Jourdain, B., Preunkert, S., Cerri, O., Castebrunet, H., Udisti, R., and Legrand, M., 2008. Year-round record of size-segregated aerosol composition in central Antarctica (Concordia station): Implications for the degree of fractionation of sea-salt particles. *Journal of Geophysical Research, D: Atmospheres*, **113** (D14), D14308. DOI: 10.1029/2007JD009584

Klonecki, A., Hess, P., Emmons, L., Smith, L., Orlando, J., and Blake, D., 2003. Seasonal changes in the transport of pollutants into the Arctic troposphere-model study. *Journal of Geophysical Research, D: Atmospheres*, **108** (D4), 8367. DOI: 10.1029/2002JD002199

Koornneef, J. M., Bouman, C., Schwieters, J. B., and Davies, G. R., 2014. Measurement of small ion beams by thermal ionisation mass spectrometry using new $10^{13}\,\Omega$ resistors. *Analytica Chimica Acta*, **819**, 49–55. DOI: 10.1016/j.aca.2014.02.007

Krachler, M., Le Roux, G., Kober, B., and Shotyk, W., 2004. Optimising accuracy and precision of lead isotope measurement ($^{206}$Pb, $^{207}$Pb, $^{208}$Pb) in acid digests of peat with ICP-SMS using individual mass discrimination correction. *Journal of Analytical Atomic Spectrometry*, **19**, 354–361. DOI: 10.1039/b314956k

Kuritani, T. and Nakamura, E., 2002. Precise isotope analysis of nanogram-level Pb for natural rock samples without use of double spikes. *Chemical Geology*, **186**, 31–43. DOI: 10.1016/S0009-2541(02)00004-9

Kylander, M. E., Klaminder, J., Bindler, R., and Weiss, D. J., 2010. Natural lead isotope variations in the atmosphere. *Earth and Planetary Science Letters*, **290**, 44–53. DOI: 10.1016/j.epsl.2009.11.055

Lagomarsino, C., Grotti, M., Todolì, J.-L., and Mermet, J.-M., 2007. Study of the absence of recondensation with low liquid delivery rates by using a cavity sheathing gas in inductively coupled plasma-atomic emission spectrometry. *Journal of Analytical Atomic Spectrometry*, **22**, 523. DOI: 10.1039/b618487a

Law, K. S. and Stohl, A., 2007. Arctic Air Pollution: Origins and Impacts. *Science*, **315**, 1537–1540. DOI: 10.1126/science.1137695

Li, Q., Chen, F., Wang, X., Li, X., and Li, C., 2005. Ultra-low procedural blank and the single-grain mica Rb-Sr isochron dating. *Chinese Science Bulletin*, **50**, 2861–2865. DOI: 10.1360/982005-984

Lin, J., Liu, Y., Chen, H., Zhou, L., Hu, Z., and Gao, S., 2015. Review of High-Precision Sr Isotope Analyses of Low-Sr Geological Samples. *Journal of Earth Science*, **26**, 763–774. DOI: 10.1007/s12583-015-0593-0

Liu, X., Jiang, S., Zhang, P., and Xu, L., 2012. Effect of recent climate change on Arctic Pb pollution: A comparative study of historical records in lake and peat sediments. *Environmental Pollution*, **160**, 161–168. DOI: 10.1016/j.envpol.2011.09.019

Longerich, H. P., Fryer, B. J., and Strong, D. F., 1987. Determination of lead isotope ratios by inductively coupled plasma-mass spectrometry (ICP-MS). *Spectrochimica Acta, Part B: Atomic Spectroscopy*, **42**, 39–48. DOI: 10.1016/0584-8547(87)80048-4

Lorenzen, C. J., 1967. Determination of Chlorophyll and Pheo-Pigments: Spectrophotometric Equations1. *Limnology and Oceanography*, **12**, 343–346. DOI: 10.4319/lo.1967.12.2.0343

Lu, Z., Cai, M., Wang, J., Yin, Z., and Yang, H., 2013. Levels and distribution of trace metals in surface sediments from Kongsfjorden, Svalbard, Norwegian Arctic. *Environmental Geochemistry and Health*, **35**, 257–269. DOI: 10.1007/s10653-012-9481-z

Macdonald, R. W., Barrie, L. A., Bidleman, T. F., Diamond, M. L., Gregor, D. J., Semkin, R. G., Strachan, W. M. J., Li, Y. F., Wania, F., Alaee, M., Alexeeva, L. B., Backus, S. M., Bailey, R., Bewers, J. M., Gobeil, C., Halsall, C. J., Harner, T., Hoff, J. T., Jantunen, L. M. M., Lockhart, W. L., Mackay, D., Muir, D. C. G., Pudykiewicz, J., Reimer, K. J., Smith, J. N., Stern, G. A., Schroeder, W. H., Wagemann, R., and Yunker, M. B., 2000. Contaminants in the Canadian Arctic: 5 years of progress in understanding sources, occurrence and pathways. *Science of the Total Environment*, **254**, 93–234. DOI: 10.1016/S0048-9697(00)00434-4

Maenhaut, W., Zoller, W. H., Duce, R. A., and Hoffman, G. L., 1979. Concentration and size distribution of particulate trace elements in the south polar atmosphere. *Journal of Geophysical Research, D: Atmospheres*, **84** (C5), 2421. DOI: 10.1029/JC084iC05p02421

Makishima, A. and Nakamura, E., 2010. Precise isotopic determination of Hf and Pb at sub-nano gram levels by MC-ICP-MS employing a newly designed sample cone and a pre-amplifier with a 1012 ohm register. *Journal of Analytical Atomic Spectrometry*, **25**, 1712–1716. DOI: 10.1039/c0ja00015a

Maréchal, C. N., Télouk, P., and Albarède, F., 1999. Precise analysis of copper and zinc isotopic compositions by plasma-source mass spectrometry. *Chemical Geology*, **156**, 251–273. DOI: 10.1016/S0009-2541(98)00191-0

Massolo, S., Messa, R., Rivaro, P., and Leardi, R., 2009. Annual and spatial variations of chemical and physical properties in the Ross Sea surface waters (Antarctica). *Continental Shelf Research*, **29**, 2333–2344. DOI: 10.1016/j.csr.2009.10.003

Matsumoto, A. and Hinkley, T. K., 2001. Trace metal suites in Antarctic pre-industrial ice are consistent with emissions from quiescent degassing of volcanoes worldwide. *Earth and Planetary Science Letters*, **186**, 33–43. DOI: 10.1016/S0012-821X(01)00228-X

Mazzera, D. M., Lowenthal, D. H., Chow, J. C., Watson, J. G., and Grubisíc, V., 2001. PM10 measurements at McMurdo Station, Antarctica. *Atmospheric Environment*, **35**, 1891–1902. DOI: 10.1016/S1352-2310(00)00409-X

Mermet, J.-M., 2006. Fundamental Principles of Inductively Coupled Plasmas. *Inductively Coupled Plasma Spectrometry and its Applications*. Ed. by Hill, S. J. Blackwell Publishing Ltd, 27–60

Mitchell, B. G. and Holm-Hansen, O., 1991. Observations of modeling of the Antartic phytoplankton crop in relation to mixing depth. *Deep Sea Research Part A: Oceanographic Research Papers*, **38**, 981–1007. DOI: 10.1016/0198-0149(91)90093-U

Monna, F., Loizeau, J.-L., Thomas, B. A., Guéguen, C., and Favarger, P.-Y., 1998. Pb and Sr isotope measurements by inductively coupled plasma–mass spectrometer: efficient time management for precision improvement. *Spectrochimica Acta, Part B: Atomic Spectroscopy*, **53**, 1317–1333. DOI: 10.1016/S0584-8547(98)00164-5

Muir, D. C. G., Wagemann, R., Hargrave, B. T., Thomas, D. J., Peakall, D. B., and Norstrom, R. J., 1992. Arctic marine ecosystem contamination. *Science of the Total Environment*, **122**, 75–134. DOI: 10.1016/0048-9697(92)90246-O

Muir, D. C. G., Braune, B., DeMarch, B., Norstrom, R., Wagemann, R., Lockhart, L., Hargrave, B., Bright, D., Addison, R., Payne, J., and Reimer, K., 1999. Spatial and temporal trends and effects of contaminants in the Canadian Arctic marine ecosystem: a review. *Science of the Total Environment*, **230**, 83–144. DOI: 10.1016/S0048-9697(99)00037-6

Mukai, H., Machida, T., Tanaka, A., Vera, Y. P., and Uematsu, M., 2001a. Lead isotope ratios in the urban air of eastern and central Russia. *Atmospheric Environment*, **35**, 2783–2793. DOI: 10.1016/S1352-2310(00)00341-1

Mukai, H., Tanaka, A., Fujii, T., Zeng, Y., Hong, Y., Tang, J., Guo, S., Xue, H., Sun, Z., Zhou, J., Xue, D., Zhao, J., Zhai, G., Gu, J., and Zhai, P., 2001b. Regional characteristics of sulfur and lead isotope ratios in the atmosphere at several Chinese urban sites. *Environmental Science and Technology*, **35**, 1064–1071. DOI: 10.1021/es001399u

Murozumi, M., Chow, T. J., and Patterson, C., 1969. Chemical concentrations of pollutant lead aerosols, terrestrial dusts and sea salts in Greenland and Antarctic snow strata. *Geochimica et Cosmochimica Acta*, **33**, 1247–1294. DOI: 10.1016/0016-7037(69)90045-3

Négrel, P. and Deschamps, P., 1996. Natural and anthropogenic budgets of a small watershed in the massif central (France): Chemical and strontium isotopic characterization of water and sediments. *Aquatic Geochemistry*, **2**, 1–27. DOI: 10.1007/BF00240851

Nelms, S. M., Quétel, C. R., Prohaska, T., Vogl, J., and Taylor, P. D. P., 2001. Evaluation of detector dead time calculation models for ICP-MS. *Journal of Analytical Atomic Spectrometry*, **16**, 333–338. DOI: 10.1039/b007913h

Nies, D. H., 1999. Microbial heavy-metal resistance. *Applied Microbiology and Biotechnology*, **51**, 730–750

Norris, G., Duvall, R., Brown, S., and Bai, S., 2015. *EPA Positive Matrix Factorization (PMF) 5.0 Fundamentals and User Guide*. Version 5.0. URL:

http://www.epa.gov/heasd/documents/PMF_5.0_User_Guide.pdf (visited on 03/03/2016)

Nriagu, J. O., 1983. Occupational exposure to lead in ancient times. *Science of the Total Environment*, **31**, 105–116. DOI: 10.1016/0048-9697(83)90063-3

Nukiyama, S. and Tanasawa, Y., 1939. Experiments on the atomization of liquids in an air stream. *Japanese Society of Mechanical Engineering*, **5**, 68–75

Paatero, P. and Tapper, U., 1994. Positive matrix factorization: A non-negative factor model with optimal utilization of error estimates of data values. *Environmetrics*, **5**, 111–126. DOI: 10.1002/env.3170050203

Pacyna, J. and Pacyna, E., 2001. An assessment of global and regional emissions of trace metals to the atmosphere from anthropogenic sources worldwide. *Environmental Reviews*, **9**, 269–298. DOI: 10.1139/er-9-4-269

Paredes, E., Grotti, M., Mermet, J.-M., and Todolí, J.-L., 2009. Heated-spray chamber-based low sample consumption system for inductively coupled plasma spectrometry. *Journal of Analytical Atomic Spectrometry*, **24**, 903–910. DOI: 10.1039/b904002a

Paredes, E., Asfaha, D. G., Ponzevera, E., Brach-Papa, C., Van Bocxstaele, M., Todolí, J.-L., and Quétel, C. R., 2011. MC-ICPMS isotope ratio measurements using an ultra-low flow sample introduction system. *Journal of Analytical Atomic Spectrometry*, **26**, 1372–1379. DOI: 10.1039/c0ja00254b

Paredes, E., Asfaha, D. G., and Quétel, C. R., 2013a. Isotope ratio measurements by MC-ICPMS below 10 µL/min under continuous sample flow conditions. Exploring the limits with strontium. *Journal of Analytical Atomic Spectrometry*, **28**, 320–326. DOI: 10.1039/c2ja30209h

Paredes, E., Todoli, J.-L., and Quétel, C. R., 2013b. Limitations of the exponential model for the correction for mass discrimination effects during isotope ratio measurements by MC-ICPMS. Demonstration with Sr at 5–15 µL/min continuous liquid flow rates. *Journal of Analytical Atomic Spectrometry*, **28**, 327–333. DOI: 10.1039/c3ja30210e

Parish, T. R. and Bromwich, D. H., 1991. Continental-scale simulation of the Antarctic katabatic wind regime. *Journal of Climate*, **4**, 135–146. DOI: 10.1175/1520-0442(1991)004<0135:CSSOTA>2.0.CO;2

Patterson, C., 1956. Age of meteorites and the earth. *Geochimica et Cosmochimica Acta*, **10**, 230–237. DOI: 10.1016/0016-7037(56)90036-9

Planchon, F. A. M., Boutron, C. F., Barbante, C., Cozzi, G., Gaspari, V., Wolff, E. W., Ferrari, C. P., and Cescon, P., 2002a. Changes in heavy metals in Antarctic snow from Coats Land since the mid-19th to the late-20th century. *Earth and Planetary Science Letters*, **200**, 207–222. DOI: 10.1016/S0012-821X(02)00612-X

Planchon, F. A. M., Boutron, C. F., Barbante, C., Cozzi, G., Gaspari, V., Wolff, E. W., Ferrari, C. P., and Cescon, P., 2002b. Short-term variations in the occurrence of heavy metals in Antarctic snow from Coats Land since the 1920s. *Science of the Total Environment*, **300**, 129–142. DOI: 10.1016/S0048-9697(02)00277-2

Planchon, F. A. M., van de Velde, K., Rosman, K. J. R., Wolff, E. W., Ferrari, C. P., and Boutron, C. F., 2003. One hundred fifty–year record of lead isotopes in Antarctic snow from Coats Land. *Geochimica et Cosmochimica Acta*, **67**, 693–708. DOI: 10.1016/S0016-7037(02)01136-5

Prohaska, T., Irrgeher, J., Zitek, A., and Jakubowski, N., 2014. *Sector Field Mass Spectometry for Elemental and Isotopic Analysis*. Royal Society of Chemistry. 666 pp.

Quétel, C. R., Thomas, B., Donard, O. F., and Grousset, F. E., 1997. Factorial optimization of data acquisition factors for lead isotope ratio determination by inductively coupled plasma mass spectrometry. *Spectrochimica Acta, Part B: Atomic Spectroscopy*, **52**, 177–187. DOI: 10.1016/S0584-8547(96)01587-X

Quinn, P. K., Shaw, G., Andrews, E., Dutton, E. G., Ruoho-Airola, T., and Gong, S. L., 2007. Arctic haze: Current trends and knowledge gaps. *Tellus Series B*, **59**, 99–114. DOI: 10.1111/j.1600-0889.2006.00238.x

R Core Team, 2015. *R: A Language and Environment for Statistical Computing*. URL: http://www.r-project.org/ (visited on 03/03/2016)

Rehkämper, M. and Halliday, A. N., 1998. Accuracy and long-term reproducibility of lead isotopic measurements by multiple-collector inductively coupled plasma mass spectrometry using an external method for correction of mass discrimination. *International Journal of Mass Spectrometry*, **181**, 123–133. DOI: 10.1016/S1387-3806(98)14170-2

Rehkämper, M., Schönbächler, M., and Stirling, C. H., 2001. Multiple Collector ICP-MS: introduction to instrumentation, measurement techniques and analytical capabilities. *Geostandards Newsletter: The Journal of Geostandards and Geoanalysis*, **25**, 23–40. DOI: 10.1111/j.1751-908X.2001.tb00785.x

Resano, M., Marzo, P., Pérez-Arantegui, J., Aramendía, M., Cloquet, C., and Vanhaecke, F., 2008. Laser ablation-inductively coupled plasma-dynamic reaction cell-mass spectrometry for the determination of lead isotope ratios in ancient glazed ceramics for discriminating purposes. *Journal of Analytical Atomic Spectrometry*, **23**, 1182–1191. DOI: 10.1039/b802266f

Revel-Rolland, M., De Deckker, P., Delmonte, B., Hesse, P., Magee, J., Basile-Doelsch, I., Grousset, F., and Bosch, D., 2006. Eastern Australia: A possible source of dust in East Antarctica interglacial ice. *Earth and Planetary Science Letters*, **249**, 1–13. DOI: 10.1016/j.epsl.2006.06.028

Rich, S., Manning, S. W., Degryse, P., Vanhaecke, F., and Lerberghe, K. V., 2012. Strontium isotopic and tree-ring signatures of Cedrus brevifolia in Cyprus. *Journal of Analytical Atomic Spectrometry*, **27**, 796–806. DOI: 10.1039/C2JA10345A

Riley, G. H. and Compston, W., 1962. Theoretical and technical aspects of Rb-Sr geochronology. *Geochimica et Cosmochimica Acta*, **26**, 1255–1281. DOI: 10.1016/0016-7037(62)90055-8

Rosman, K. J. R., Chisholm, W., Boutron, C. F., Candelone, J.-P., and Patterson, C. C., 1994. Anthropogenic lead isotopes in Antarctica. *Geophysical Research Letters*, **21**, 2669–2672. DOI: 10.1029/94GL02603

Rosman, K. J. R., Chisholm, W., Boutron, C. F., Candelone, J.-P., Jaffrezo, J.-L., and Davidson, C. I., 1998. Seasonal variations in the origin of lead in snow at Dye 3, Greenland. *Earth and Planetary Science Letters*, **160**, 383–389. DOI: 10.1016/S0012-821X(98)00098-3

Rudge, J. F., Reynolds, B. C., and Bourdon, B., 2009. The double spike toolbox. *Chemical Geology*, **265**, 420–431. DOI: 10.1016/j.chemgeo.2009.05.010

Russ III, G. P., 1989. Isotope ratio measurements using ICP-MS. *Applications of inductively coupled plasma mass spectrometry*

Saha, M. N., 1920. Ionization in the solar chromosphere. *Philosophical Magazine A*, **40**, 472–488. DOI: 10.1080/14786441008636148

Sangster, D. F., Outridge, P. M., and Davis, W. J., 2000. Stable lead isotope characteristics of lead ore deposits of environmental significance. *Environmental Reviews*, **8**, 115–147. DOI: 10.1139/a00-008

Schlitzer, R., 2015. *Ocean Data View*. URL: http://odv.awi.de (visited on 03/03/2016)

Schoene, B., 2014. U–Th–Pb Geochronology. *Treatise on Geochemistry*. Ed. by Karl K. Turekian and Holland, H. Second Edition. Vol. 4. The crust. 16 vols. Oxford: Elsevier, 341–378

Sherman, L. S., Blum, J. D., Dvonch, J. T., Gratz, L. E., and Landis, M. S., 2015. The use of Pb, Sr, and Hg isotopes in Great Lakes precipitation as a tool for pollution source

attribution. *Science of the Total Environment*, **502**, 362–374. DOI: 10.1016/j.scitotenv.2014.09.034

Shirahata, H., Elias, R. W., Patterson, C. C., and Koide, M., 1980. Chronological variations in concentrations and isotopic compositions of anthropogenic atmospheric lead in sediments of a remote subalpine pond. *Geochimica et Cosmochimica Acta*, **44**, 149–162. DOI: 10.1016/0016-7037(80)90127-1

Simonetti, A., Gariépy, C., and Carignan, J., 2000. Pb and Sr isotopic compositions of snowpack from québec, canada: inferences on the sources and deposition budgets of atmospheric heavy metals. *Geochimica et Cosmochimica Acta*, **64**, 5–20. DOI: 10.1016/S0016-7037(99)00207-0

Simonetti, A., Gariépy, C., Banic, C. M., Tanabe, R., and Wong, H. K., 2004. Pb isotopic investigation of aircraft-sampled emissions from the Horne smelter (Rouyn, Québec): Implications for atmospheric pollution in northeastern North America1. *Geochimica et Cosmochimica Acta*, **68**, 3285–3294. DOI: 10.1016/j.gca.2004.02.008

Steinnes, E., Berg, T., and Uggerud, H. T., 2011. Three decades of atmospheric metal deposition in Norway as evident from analysis of moss samples. *Science of the Total Environment*, **412-413**, 351–8. DOI: 10.1016/j.scitotenv.2011.09.086

Stohl, A., 1998. Computation, accuracy and applications of trajectories - a review and bibliography. *Atmospheric Environment*, Developments in Environmental Science **32**, 947–966. DOI: 10.1016/S1474-8177(02)80024-9

Stohl, A., 2006. Characteristics of atmospheric transport into the Arctic troposphere. *Journal of Geophysical Research, D: Atmospheres*, **111** (D11), D11306. DOI: 10.1029/2005JD006888

Sturges, W. T. and Barrie, L. A., 1987. Lead 206/207 isotope ratios in the atmosphere of North America as tracers of US and Canadian emissions. *Nature*, **329**, 144–146. DOI: 10.1038/329144a0

Sturges, W. T. and Barrie, L. A., 1989. Stable lead isotope ratios in arctic aerosols: evidence for the origin of arctic air pollution. *Atmospheric Environment*, **23**, 2513–2519. DOI: 10.1016/0004-6981(89)90263-1

Sturges, W. T., Hopper, J. F., Barrie, L. A., and Schnell, R. C., 1993. Stable lead isotope ratios in Alaskan arctic aerosols. *Atmospheric EnvironmentPart A General Topics*, **27**, 2865–2871. DOI: 10.1016/0960-1686(93)90317-R

Svendsen, H., Beszczynska-Møller, A., Hagen, J. O., Lefauconnier, B., Tverberg, V., Gerland, S., Ørbøk, J. B., Bischof, K., Papucci, C., Zajaczkowski, M., Azzolini, R., Bruland, O., Wiencke, C., Winther, J. G., and Dallmann, W., 2002. The physical environment of Kongsfjorden-Krossfjorden, and Arctic fjord system in Svalbard. *Polar Research*, **21**, 133–166. DOI: 10.1111/j.1751-8369.2002.tb00072.x

Tanner, S. D. and Baranov, V. I., 1999. Theory, design, and operation of a dynamic reaction cell for ICP-MS. *Atomic Spectroscopy*, **20**, 45–52

Tanner, S. D., Baranov, V. I., and Vollkopf, U., 2000. A dynamic reaction cell for inductively coupled plasma mass spectrometry (ICP-DRC-MS). Part III. Optimization and analytical performance. *Journal of Analytical Atomic Spectrometry*, **15**, 1261–1269. DOI: 10.1039/B002604M

Taylor, R. N., Ishizuka, O., Michalik, A., Milton, J. A., and Croudace, I. W., 2015. Evaluating the precision of Pb isotope measurement by mass spectrometry. *Journal of Analytical Atomic Spectrometry*, **30**, 198–213. DOI: 10.1039/C4JA00279B

Thirlwall, M. F., 2002. Multicollector ICP-MS analysis of Pb isotopes using a 207pb-204pb double spike demonstrates up to 400 ppm/amu systematic errors in TI-normalization. *Chemical Geology*, **184**, 255–279. DOI: 10.1016/S0009-2541(01)00365-5

Todolì, J.-L. and Mermet, J.-M., 2002a. New torch design with an in-built chamber for liquid sample analysis by ICP-AES. *Journal of Analytical Atomic Spectrometry*, **17**, 345–351. DOI: 10.1039/b111416f

Todolì, J.-L. and Mermet, J.-M., 2002b. Study of matrix effects using an adjustable chamber volume in a torch-integrated sample introduction system (TISIS) in ICP-AES. *Journal of Analytical Atomic Spectrometry*, **17**, 913–921. DOI: 10.1039/b201881k

Todolì, J.-L. and Mermet, J.-M., 2003. Optimization of the evaporation cavity in a torch integrated sample introduction system based ICP-AES system. Applications to matrix and transient effects, analysis of microsamples and analysis of certified solid samples. *Journal of Analytical Atomic Spectrometry*, **18**, 1185–1191. DOI: 10.1039/b212698b

Toscano, G., Gambaro, A., Moret, I., Capodaglio, G., Turetta, C., and Cescon, P., 2005. Trace metals in aerosol at Terra Nova Bay, Antarctica. *Journal of Environmental Monitoring*, **7**, 1275–1280. DOI: 10.1039/b507337p

Townsend, A. T. and Snape, I., 2008. Multiple Pb sources in marine sediments near the Australian Antarctic Station, Casey. *Science of the Total Environment*, **389**, 466–474. DOI: 10.1016/j.scitotenv.2007.09.022

Tunved, P., Ström, J., and Krejci, R., 2013. Arctic aerosol life cycle: linking aerosol size distributions observed between 2000 and 2010 with air mass transport and precipitation at Zeppelin station, Ny-Ålesund, Svalbard. *Atmospheric Chemistry and Physics*, **13**, 3643–3660. DOI: 10.5194/acp-13-3643-2013

Turekian, K. K., 1968. *Oceans*. Ed. by Prentice-Hall. 2nd editio. Englewood Cliffs, NJ. 120 pp.

Udisti, R., Becagli, S., Benassai, S., Castellano, E., Fattori, I., Innocenti, M., Migliori, A., and Traversi, R., 2004. Atmosphere-snow interaction by a comparison between aerosol and uppermost snow-layers composition at Dome C, East Antarctica. *Annals of Glaciology*, **39**, 53–61. DOI: 10.3189/172756404781814474

Udisti, R., Dayan, U., Becagli, S., Busetto, M., Frosini, D., Legrand, M., Lucarelli, F., Preunkert, S., Severi, M., Traversi, R., and Vitale, V., 2012. Sea spray aerosol in central Antarctica. Present atmospheric behaviour and implications for paleoclimatic reconstructions. *Atmospheric Environment*, **52**, 109–120. DOI: 10.1016/j.atmosenv.2011.10.018

UNI 14902, 2005. *Ambient air quality-Standard method for the measurement of Pb, Cd, As and Ni in the $PM_{10}$ fraction of suspended particulate matter*

Vallelonga, P., Van de Velde, K., Candelone, J. P., Morgan, V. I., Boutron, C. F., and Rosman, K. J. R., 2002. The lead pollution history of Law Dome, Antarctica, from isotopic measurements on ice cores: 1500 AD to 1989 AD. *Earth and Planetary Science Letters*, **204**, 291–306. DOI: 10.1016/S0012-821X(02)00983-4

Vallelonga, P., Gabrielli, P., Rosman, K. J. R., Barbante, C., and Boutron, C. F., 2005. A 220 kyr record of Pb isotopes at Dome C Antarctica from analyses of the EPICA ice core. *Geophysical Research Letters*, **32** (L01706), 1–4. DOI: 10.1029/2004GL021449

Vallelonga, P., Gabrielli, P., Balliana, E., Wegner, A., Delmonte, B., Turetta, C., Burton, G., Vanhaecke, F., Rosman, K. J. R., Hong, S., Boutron, C. F., Cescon, P., and Barbante, C., 2010. Lead isotopic compositions in the EPICA Dome C ice core and Southern Hemisphere Potential Source Areas. *Quaternary Science Reviews*, **29**, 247–255. DOI: 10.1016/j.quascirev.2009.06.019

Van de Velde, K., Vallelonga, P., Candelone, J. P., Rosman, K. J. R., Gaspari, V., Cozzi, G., Barbante, C., Udisti, R., Cescon, P., and Boutron, C. F., 2005. Pb isotope record over one century in snow from Victoria Land, Antarctica. *Earth and Planetary Science Letters*, **232**, 95–108. DOI: 10.1016/j.epsl.2005.01.007

Vanhaecke, F., Moens, L., Dams, R., and Taylor, P., 1996. Precise seasurement of isotope ratios with a double-focusing magnetic sector ICP mass spectrometer. *Analytical Chemistry*, **68**, 567–569. DOI: 10.1021/ac9507247

Vanhaecke, F., Moens, L., Dams, R., Allen, L., and Georgitis, S., 1999. Evaluation of the isotope ratio performance of an axial time-of-flight ICP mass spectrometer. *Analytical Chemistry*, **71**, 3297–3303. DOI: 10.1021/ac990016b

Vanhaecke, F., Balcaen, L., Deconinck, I., De Schrijver, I., Marisa Almeida, C., and Moens, L., 2003. Mass discrimination in dynamic reaction cell (DRC)-ICP-mass spectrometry. *Journal of Analytical Atomic Spectrometry*, **18**, 1060–1065. DOI: 10.1039/b303528j

Vanhaecke, F. and Moens, L., 2003. Overcoming spectral overlap in isotopic analysis via single- and multi-collector ICP–mass spectrometry. *Analytical and Bioanalytical Chemistry*, **378**, 232–240. DOI: 10.1007/s00216-003-2175-8

Vanhaecke, F. and Degryse, P., 2012. *Isotopic Analysis: Fundamentals and Applications Using ICP-MS*. Wiley

Véron, A. J., Church, T. M., Rivera-Duarte, I., and Flegal, A. R., 1999. Stable lead isotopic ratios trace thermohaline circulation in the subarctic North Atlantic. *Deep Sea Research Part II: Topical Studies in Oceanography*, **46**, 919–935. DOI: 10.1016/S0967-0645(99)00009-0

Von Storch, H., Costa-Cabral, M., Hagner, C., Feser, F., Pacyna, J., Pacyna, E., and Kolb, S., 2003. Four decades of gasoline lead emissions and control policies in Europe: a retrospective assessment. *Science of the Total Environment*, **311**, 151–176. DOI: 10.1016/S0048-9697(03)00051-2

Walder, A. J. and Freedman, P. A., 1992. Communication. Isotopic ratio measurement using a double focusing magnetic sector mass analyser with an inductively coupled plasma as an ion source. *Journal of Analytical Atomic Spectrometry*, **7**, 571–575. DOI: 10.1039/JA9920700571

Wedepohl, K. H., 1995. The composition of the continental crust. *Geochimica et Cosmochimica Acta*, **58A**, 959–960. DOI: 10.1180/minmag.1994.58A.2.234

Weyer, S. and Schwieters, J. B., 2003. High precision Fe isotope measurements with high mass resolution MC-ICPMS. *International Journal of Mass Spectrometry*, **226**, 355–368. DOI: 10.1016/S1387-3806(03)00078-2

Weyer, S., Anbar, A. D., Gerdes, A., Gordon, G. W., Algeo, T. J., and Boyle, E. A., 2008. Natural fractionation of 238U/235U. *Geochimica et Cosmochimica Acta*, **72**, 345–359. DOI: 10.1016/j.gca.2007.11.012

White, W. M., Albarède, F., and Télouk, P., 2000. High-precision analysis of Pb isotope ratios by multi-collector ICP-MS. *Chemical Geology*, **167**, 257–270. DOI: 10.1016/S0009-2541(99)00182-5

Williams, H. M., Peslier, A. H., McCammon, C., Halliday, A. N., Levasseur, S., Teutsch, N., and Burg, J.-P., 2005. Systematic iron isotope variations in mantle rocks and minerals: The effects of partial melting and oxygen fugacity. *Earth and Planetary Science Letters*, **235**, 435–452. DOI: 10.1016/j.epsl.2005.04.020

Woodhead, J., 2002. A simple method for obtaining highly accurate Pb isotope data by MC-ICP-MS. *Journal of Analytical Atomic Spectrometry*, **17**, 1381–1385. DOI: 10.1039/b205045e

Woods, G. and McCurdy, E., 2013. Triple-quadrupole ICP-MS provides improved performance for difficult polyatomic and isobaric overlaps on lead isotopes. *Spectroscopy*, **28**, s28–s34

Yang, L., 2009. Accurate and precise determination of isotopic ratios by MC-ICP-MS: A review. *Mass Spectrometry Reviews*, **28**, 990–1011. DOI: 10.1002/mas.20251

Zaborska, A., Pempkowiak, J., and Papucci, C., 2006. Some sediment characteristics and sedimentation rates in an Arctic Fjord (Kongsfjorden, Svalbard). *Annual Environmental Protection*, **8**, 79–96

Zajaczkowski, M., 2008. Sediment supply and fluxes in glacial and outwash fjords, Kongsfjorden and Adventfjorden, Svalbard. *Polish Polar Research*, **29**, 59–72

Zreda-Gostynska, G., Kyle, P. R., Finnegan, D., and Prestbo, K. M., 1997. Volcanic gas emissions from Mount Erebus and their impact on the Antarctic environment. *Journal of Geophysical Research, D: Atmospheres*, **102** (B7), 15039–15055. DOI: 10.1029/97JB00155